DESIGN OF TRANSPIRATION COOLED THERMAL PROTECTION SYSTEMS

E. Eugene Callens, Jr.
Robert F. Vinet

Mechanical Engineering
Louisiana Tech University
P.O. Box 10348
Ruston LA 71272-0046

March 1999

Technical Report

Contract No. 32-4136-58019
and NASA(1997)-Stennis-17
and NAS13-580

Prepared for:
National Aeronautics and Space Administration
John C. Stennis Space Center
Stennis Space Center, MS 39529-6000

ABSTRACT

This study explored three approaches for the utilization of transpiration cooling in thermal protection systems. One model uses an impermeable wall with boiling water heat transfer at the backface (Model I). A second model uses a permeable wall with a boiling water backface and additional heat transfer to the water vapor as it flows in channels toward the exposed surface (Model II). The third model also uses a permeable wall, but maintains a boiling condition at the exposed surface of the material (Model III). The governing equations for the models were developed in non-dimensional form and a comprehensive parametric investigation of the effects of the independent variables on the important dependent variables was performed. In addition, detailed analyses were performed for selected materials to evaluate the practical limitations of the results of the parametric study.

It was found that for sufficiently thin walls using Model I, even materials with low critical temperatures might be used in very high temperature environments. However, in many practical engineering applications, the thin walls do not provide adequate structural strength. Realization of the maximum theoretical gains for Model II requires small diameter channels, larger material thickness, and higher environmental temperatures. Small diameter channels typically have substantial problems with fouling which will limit their applicability. Above an environmental temperature of 3,600 K, it was found Model III requires only moderately more water than the impermeable wall model (Model I). The maximum difference is approximately 19 percent at 5,000 K. Model III is the better design choice in this temperature range since a relative strong, ductile, and inexpensive material such as steel can be used. In the range below 3,600 K, Model III requires an increase in mass flow rate from 50 – 80 percent over niobium carbide. In this region, Model I using niobium carbide or some other suitable ceramic is a reasonable design alternative

For the severe thermal environments such as the flame buckets of rocket engine test facilities, the boiling water exposed surface model (Model III) is recommended in the impingement regions. The impermeable wall model (Model I) with a layered combination of a ceramic, such as niobium carbide for the exposed material and steel or aluminum as the support material, is recommended in the peripheral areas. For thermal protection of personnel and equipment under conventional fire conditions, Model I with steel or aluminum as the wall material is recommended. The use of the impermeable wall with heat transfer to the vapor in the channels (Model II) should be limited to a restricted range of design requirements as its disadvantages outweigh its advantages for most materials and environmental conditions.

TABLE OF CONTENTS

Page

Appendix

LIST OF FIGURES

Page

Page

LIST OF TABLES

NOMENCLATURE

A	Area
Bi	Biot Number, Eqn. (10)
C_1	Eqn. (49)
C_2	Eqn. (48)
C_3	Eqn. (47)
C_p	Specific Heat at Constant Pressure
h	Heat Transfer Coefficient
h_{fg}	Latent Heat of Vaporization
H_{bf}	Eqn. (24)
H_{vI}	Eqn. (25)
H_{vII}	Eqn. (58)
k	Thermal Conductivity
L	Material Thickness
$\dot{m}$	Mass Flow Rate
P	Perimeter of Flow Channel
q	Heat Transfer Rate
Q_L	Eqn. (23)
T	Temperature
x	Direction Normal to Wall Surface

Subscripts

bf	Backface Condition
cond	Conduction
conv	Convection
e	Environmental
f	Flame
h	Environmental Convection Condition
rad	Radiation
s	Surface
trans	Transpiration
v	Vapor
w	Wall

Superscript

*	Dimensionless Parameter

Greek Symbols

α	Eqn. (32)
β_I	Eqn. (18)
β_{II}	Eqn. (59)
γ	Eqn. (31)
ε	Emissivity
λ_2	Eqn. (45)
λ_3	Eqn. (46)
Λ	Eqn. (9)
σ	Stefan-Boltzman Constant

CHAPTER 1

INTRODUCTION

Background

Experience in the protection of reentry vehicle nosetips utilizing transpiration cooling can be applied to the development of transpiration cooled thermal protection systems for personnel and equipment. The high heat of vaporization of water permits protection against very large heat transfer rates with modest transpiration flow rates. The reentry vehicle designs that utilize this concept are able to protect metallic nosetips with an on-board water supply during the entire reentry trajectory for high reentry angles and, consequently, extremely high heat rates. If the system is designed to provide boiling at the surface, the temperature of the protected surface is limited to the boiling temperature of the water at the given pressure. It is easy to provide insulation for this relatively low temperature. The heat rates and exposure times that can be tolerated are limited only by the ability of the system to deliver the required flow rates.

The most efficient model for using transpiration cooling is a thermal protection system design where the surface temperature is maintained at the maximum allowable operating temperature of the material. This permits the water to absorb the maximum heat for the thermal constraints as sensible heat in the liquid phase, latent heat in the phase change, and sensible heat in the vapor phase. Water has been found to be the most effective liquid for use as the coolant because of its relatively high heat capacity and heat of vaporization. In order to achieve this design goal, the outer protective layer must have a relatively high density of flow channels (high porosity) to provide sufficient area for the required heat transfer to the water within the material.

Potential applications of transpiration cooled thermal protection systems at NASA-SSC include cooling of flame buckets; protection of fire fighters and their equipment; shields to permit rocket engine test and diagnostic equipment to be located near the high temperature exhaust plumes; and firewalls or shields to protect personnel and equipment from high temperature environments.

The current and future planned use of existing rocket engine test facilities for ground testing of various size engines necessitates development of improved concepts for satisfying the cooling requirements for the flame deflectors. Research efforts are directed at providing a basic design methodology that includes materials and required flow rates for specific thermal environments. The basic design data can be utilized to predict system requirements for specific applications. One goal is to reduce the amount of water used, and the associated cost, during testing.

Previous Work

Previous work at Louisiana Tech University in the use of transpiration cooling in thermal protection systems includes three unpublished senior design projects and one master's thesis (Ref. 1). The senior design projects include both experimental and theoretical studies of concepts based on transpiration cooling to provide protection for personnel and equipment in domestic fire environments.

In the two experimental studies, the basic design consisted of flexible, transpiration cooled material that could be used as clothing for personnel or covering for equipment. Many material combinations were investigated with the most effective being an inner waterproof layer of aluminized Kevlar and an outer porous layer of Hexel fiberglass. Water was supplied at a controlled pressure to the interface between the materials. This design was tested in an oven at temperatures up to 550 ºC (1022 ºF). It was found that the maximum steady-state temperature for the water in the interface region at the maximum environmental temperature tested (550 ºC) was 46 ºC (115 ºF). It was concluded that this design would provide adequate protection for personnel and materials in domestic fire environments for extended periods of time.

The other senior design project involved the design of a specific piece of fire-fighting equipment, namely, a transpiration cooled fire fighter's glove. It was found in interviews with firemen that, using current gloves, their hands often become excessively hot and limit the amount of time that they can stay near certain fires. Major components in the design included two pressurized aluminum cylinders for water storage, tubing and insulation to transport the water to the glove and to distribute the water throughout the glove, and a transpiration medium to absorb water and allow the water to evaporate. It was found that in an environment with a 1300 ºC (2372 ºF) flame temperature and a 700 ºC (1292 ºF) environmental temperature, 1.8 kg (4 lbm) of water is required for a 30 minute exposure time. This is approximately 0.5 gallon or 2 liters of water which can easily be stored in a self-contained vessel and transported by a fireman.

The objective of the master's thesis by Gamblin (Ref. 1) was to investigate the potential use of thermal protection coatings, single tiles, and layered insulation systems to protect the walls of the flame buckets used in the testing of the Space Shuttle Main Engine (SSME) at NASA-SSC. The physical behavior of the hypothetical system was modeled by a plane wall boundary value problem with a convective frontface condition and a boiling water backface condition. The principal recommendations and conclusions follow:

1. Presently available thermal coatings were not recommended because of their lack of durability under severe thermal conditions.

2. Metals were not recommended as the exposed tile material because of their relatively low melting temperatures or, in the case of tungsten, poor resistance to oxidation and brittleness.

3. Refractory metals were not recommended as the exposed tile material because of inadequate service temperatures and/or poor resistance to oxidation.

4. The recommended design was a two-layer composite with a ceramic material supported by a metal. The ceramics with the highest thermal performance were tantalum carbide, hafnium carbide, and niobium carbide, and the recommended metal support material was aluminum.

5. The recommended design options were partial replacements of the existing transpiration cooled system with the designated two-layer composite system, resulting in reductions in cooling water flowrate of 50 to 80 percent from the current value, depending on the magnitude of the replaced area in the flame buckets.

A search of the Compendex, INSPEC, and CARL Uncover databases reveal very few studies of the application of transpiration cooling to the design of thermal protection systems. The most directly applicable of these investigations to the current study is an experimental study by Yano, Ochi, and Enya (Ref. 2). They designed, built, and tested a room with transpiration cooled exterior walls. The room was intended to serve as a safe haven for people during a fire. They showed that the interior walls of the room remained at the initial room temperature for a flame temperature of 800 ºC (1472 ºF) for a test time of 25 minutes. All temperatures were at steady-state so it was expected that the transpiration walls would maintain the initial interior temperature indefinitely.

Approach of the Present Study

There are three approaches explored in the present study for the utilization of transpiration cooling for thermal protection. The first, entitled Model I, uses impermeable materials with water cooling of the inner surface of the system. Heat is absorbed by the water in the form of sensible heat to the liquid and latent heat to enable boiling, but the vapor is intentionally not superheated due to the reduction in the overall heat transfer coefficient associated with film-boiling. The temperature of the exposed surface is limited to the maximum operating temperature of the material.

The second approach, entitled Model II, specifies a permeable outer layer which is exposed to the high heat transfer environment. In this model, a boiling condition is maintained at the backside of the protective material, and heat is also added to the water vapor as it flows in channels toward the exposed surface. The heat is absorbed by the water as sensible heat to the liquid, latent heat to enable phase change, and sensible heat to the vapor. As in Model I, the surface temperature of the exposed surface can be as high as the maximum operating temperature for the material. Model II results in a lower heat transfer rate to the surface when compared to a transpiration model where the surface is maintained at the boiling temperature due to the reduced temperature difference between the environment and

the surface. It also utilizes the maximum heat absorption capability of the water for the system temperature limits.

The third approach, entitled Model III, maintains a boiling condition at the surface of the exposed material. Heat is transferred to the water in the form of sensible heat to the liquid and latent heat to enable phase change.

Model I is the same as Gamblin (Ref. 1) used in the flame bucket study. It is used here as a baseline model and applied to a range of environmental conditions from the domestic fires to the severe flame bucket thermal conditions. To this end, the model is developed in non-dimensional form and the influence of the dimensionless independent variables is studied parametrically.

The comparative advantage of Model II is that it minimizes the water flow rate required to maintain the exposed surface at or below its maximum operating temperature. The disadvantages are the additional cost of fabrication of the permeable materials and the operational problems of maintaining unrestricted flow of the water through the channels under all operating scenarios. The advantages of Model I are lower fabrication costs and reduced operational problems. The disadvantages are higher required water flow rates for a design surface temperature and additional insulation requirements for the boiling area in some applications. Model III has the advantage of avoiding problems associated with high surface temperature such as reduced structural strength and oxidation. It has the disadvantage of having the largest water flow rates of the three approaches. This study provides quantitative results which can be used as a basis for selection of the most suitable approach for a given application.

In both Model I and Model II the exposed surface temperature is maintained at or below the critical temperature for the material and the back face is maintained at a temperature 20 K above the boiling temperature of water. This corresponds to a boiling heat transfer coefficient of approximately 30 $kW/m^2 \cdot K$.

Also, all three models are steady-state since preliminary calculations show that steady-state is reached in less than two minutes for most conditions and materials of interest in this study. The thermal protection systems being considered here are envisioned to be used for extended periods in excess of 10 minutes.

CHAPTER 2

MODEL I DEVELOPMENT AND APPLICATION

Mathematical Model

In Model I, the material backface is maintained at the boiling condition. Heat is absorbed by the water in the form of sensible heat to the liquid and latent heat to enable boiling.

The schematic of Model I is presented in Fig. 1.

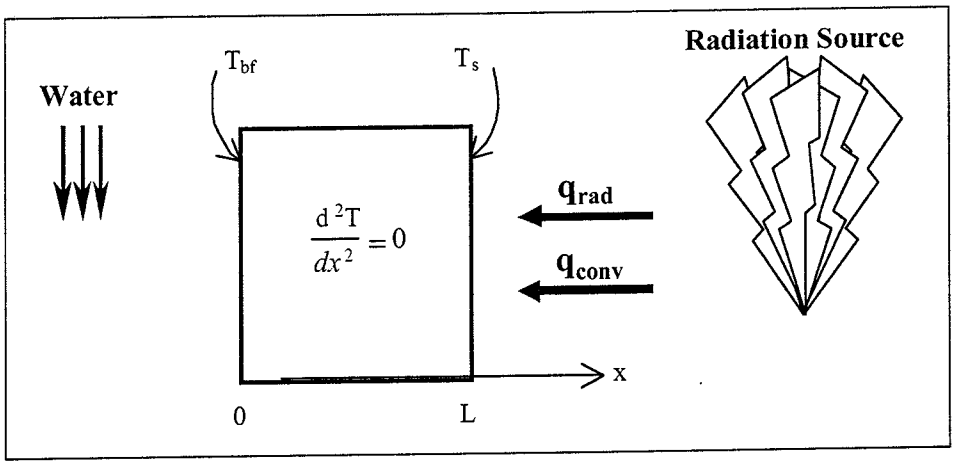

Figure 1. Schematic of Model I (Boiling Water Backface Model)

The governing equation for the temperature distribution in the wall is the steady state heat conduction equation

$$\frac{d^2T}{dx^2}=0 \tag{1}$$

with boundary conditions as follows:

At x = 0,

$$T(0)=T_{bf} \tag{2}$$

At x = L,

$$\frac{q_{rad}}{A}+\frac{q_{conv}}{A}=\frac{q_{cond}}{A} \tag{3}$$

$$\sigma\varepsilon(T_e^{\,4}-T_s^{\,4})+\bar{h}_e(T_h-T_s)=k_w\left.\frac{dT}{dx}\right|_{x=L} \tag{4}$$

$$\left.\frac{dT}{dx}\right|_{x=L}=\frac{\sigma\varepsilon}{k_w}(T_e^{\,4}-T_s^{\,4})+\frac{\bar{h}_e}{k_w}(T_h-T_s) \tag{5}$$

Applying the boundary conditions, the solution becomes

$$T(x)=\left[\frac{\sigma\varepsilon}{k_w}(T_e^{\,4}-T_s^{\,4})+\frac{\bar{h}_e}{k_w}(T_h-T_s)\right]x+T_{bf} \tag{6}$$

Find T_s by evaluating T(x) at x = L

$$T_s=\frac{\sigma\varepsilon L}{k_w}\left[T_e^{\,4}-T_s^{\,4}\right]+\frac{\bar{h}_e L}{k_w}(T_h-T_s)+T_{bf} \tag{7}$$

Normalize the equation by dividing by T_{bf}

$$\frac{T_s}{T_{bf}}=\frac{\sigma\varepsilon L T_{bf}^{\,3}}{k_w}\left[\left(\frac{T_e}{T_{bf}}\right)^4-\left(\frac{T_s}{T_{bf}}\right)^4\right]+\frac{\bar{h}_e L}{k_w}\left(\frac{T_h}{T_{bf}}-\frac{T_s}{T_{bf}}\right)+1 \tag{8}$$

Define

$$\Lambda=\frac{\sigma\varepsilon L T_{bf}^{\,3}}{k_w} \tag{9}$$

$$Bi = \frac{\bar{h}_e L}{k_w} \tag{10}$$

So that

$$\frac{T_s}{T_{bf}} = \Lambda\left[\left(\frac{T_e}{T_{bf}}\right)^4 - \left(\frac{T_s}{T_{bf}}\right)^4\right] + Bi\left(\frac{T_h}{T_{bf}} - \frac{T_s}{T_{bf}}\right) + 1 \tag{11}$$

At the backface

$$\frac{q_{cond}}{A} = \frac{q_{trans}}{A} \tag{12}$$

where

$$\frac{q_{cond}}{A} = k_w \left.\frac{dT}{dx}\right|_{x=0} = k_w \frac{\Delta T}{\Delta x} = k_w \frac{(T_s - T_{bf})}{L} \tag{13}$$

$$\frac{q_{trans}}{A} = \left[\frac{q_{latent}}{A}\right] + \left[\frac{q_{sensible}}{A}\right] = \left[\frac{\dot{m}}{A} h_{fg}\right] + \left[\frac{\dot{m}}{A} C_{p\,liquid}(T_{boil} - T_{initial}) + \frac{\dot{m}}{A} C_{p\,vapor}(T_{bf} - T_{boil})\right] \tag{14}$$

Therefore

$$k_w \frac{(T_s - T_{bf})}{L} = \frac{\dot{m}}{A}\left[h_{fg} + C_{p\,liquid}(T_{boil} - T_{initial}) + C_{p\,vapor}(T_{bf} - T_{boil})\right] \tag{15}$$

$$\frac{\dot{m}}{A} = \left[k_w \frac{(T_s - T_{bf})}{L}\right] \cdot \left[\frac{1}{h_{fg} + C_{p\,liquid}(T_{boil} - T_{initial}) + C_{p\,vapor}(T_{bf} - T_{boil})}\right] \tag{16}$$

Normalize the equation by multiplying through by $\frac{L}{k_w}\frac{h_{fg}}{T_{bf}}$

$$\frac{\dot{m}}{A}\frac{L}{k_w}\frac{h_{fg}}{T_{bf}} = \left(\frac{T_s}{T_{bf}} - 1\right) \cdot \left[\frac{h_{fg}}{h_{fg} + C_{p\,liquid}(T_{boil} - T_{initial}) + C_{p\,vapor}(T_{bf} - T_{boil})}\right] \tag{17}$$

Define

$$\beta_I = \left.\frac{\dot{m}}{A}\right)_I \frac{L}{k_w}\frac{h_{fg}}{T_{bf}} \tag{18}$$

so that

$$\beta_I = \left(\frac{T_s}{T_{bf}} - 1\right)\cdot\left[\frac{h_{fg}}{h_{fg} + C_{p_{liquid}}(T_{boil} - T_{initial}) + C_{p_{vapor}}(T_{bf} - T_{boil})}\right] \tag{19}$$

An alternate form is obtained by equating the heat transferred to the exposed surface to the heat transferred to the water

$$\frac{q_{rad}}{A} + \frac{q_{conv}}{A} = \frac{q_{trans}}{A} \tag{20}$$

so that

$$\frac{\dot{m}}{A} = \frac{\left[\sigma\varepsilon(T_e^{\,4} - T_s^{\,4}) + \bar{h}_e(T_h - T_s)\right]}{h_{fg} + C_{p_{liquid}}(T_{boil} - T_{initial}) + C_{p_{vapor}}(T_{bf} - T_{boil})} \tag{21}$$

Again, normalize the equation by multiplying through by $\frac{L}{k_w}\frac{h_{fg}}{T_{bf}}$

$$\frac{\dot{m}}{A}\frac{L}{k_w}\frac{h_{fg}}{T_{bf}} = \left[\frac{h_{fg}\cdot\left[\Lambda\left[\left(\frac{T_e}{T_{bf}}\right)^4 - \left(\frac{T_s}{T_{bf}}\right)^4\right] + Bi\left(\frac{T_h}{T_{bf}} - \frac{T_s}{T_{bf}}\right)\right]}{h_{fg} + Cp_{liquid}T_{bf}\left(\frac{T_{boil}}{T_{bf}} - \frac{T_{initial}}{T_{bf}}\right) + Cp_{vapor}T_{bf}\left(1 - \frac{T_{boil}}{T_{bf}}\right)}\right] \tag{22}$$

Define

$$Q_L = \Lambda\left[\left(\frac{T_e}{T_{bf}}\right)^4 - \left(\frac{T_s}{T_{bf}}\right)^4\right] + Bi\left(\frac{T_h}{T_{bf}} - \frac{T_s}{T_{bf}}\right) \tag{23}$$

$$H_{bf} = \frac{h_{fg} + C_{p\,liquid} T_{bf} \left(\frac{T_{boil}}{T_{bf}} - \frac{T_{initial}}{T_{bf}} \right)}{h_{fg}} \tag{24}$$

$$H_{vI} = \frac{C_{p\,vapor} T_{bf} \left(1 - \frac{T_{boil}}{T_{bf}} \right)}{h_{fg}} \tag{25}$$

so that

$$\beta_I = \frac{Q_L}{H_{bf} + H_{vI}} \tag{26}$$

The independent variables in the above equations are Λ, Bi, x, and T_e. The dependent variables are T(x), T_s, Q_L, and β_I. A parametric study is conducted in which the independent variables are varied over a range corresponding to typical materials and anticipated conditions. For the study, it is assumed that $T_h = T_e$ which is a worst-case condition for a given maximum environmental temperature. It is also assumed that the backface temperature is maintained at 20 K above the boiling temperature.

Parametric Study

There were six materials selected for use as either exposed or support layers as shown in Table 1. This table presents the material thermal conductivity, melting point, and critical or maximum operating temperature which is defined for this study as 75 percent of the melting temperature. These materials were selected because they are a good representation of the available range in thermal conductivity and maximum operating temperatures. The ranges of the dimensionless variables contained in the parametric studies below correspond to this set of materials. Other materials are easily studied using the computer codes provided with this report.

Table 1. Material Properties

Material	Description	k $\left(\frac{\text{BTU}}{\text{hr}\cdot\text{ft}\cdot^{\circ}\text{F}}\right)$	k $\left(\frac{\text{W}}{\text{m}\cdot\text{K}}\right)$	T_{mp} (°F)	T_{mp} (K)	$T_{critical}$ (K) $[0.75\cdot T_{mp}]$
Aluminum*	*6061-T6*	90	155.8	1080	855	642
Copper *	*pure*	227	392.9	1980	1355	1017
Steel *	*AISI C1020*	27	46.7	2750	1783	1337
Titanium †		12.65	21.9	3056	1953	1465
Tungsten †		100.54	174	6128	3660	2745
Ceramic **	*Niobium Carbide*	17.34	30	6542	3890	2917

* Ref. (3)
† Ref. (4)
** Ref. (1)

This study covers the range of expected environmental (flame) temperatures from ambient up to 5,000 K. Heat transfer coefficients vary from the value of 0.03 $kW/m^2\cdot K$ for a standard industrial fire to 10 $kW/m^2\cdot K$ for the maximum expected value in the flame buckets of the rocket test facilities.

In Fig. 2, the influence of Biot number on surface temperature is shown as a function of environmental temperature for four selected values of Λ, with the appropriate independent variable held constant. The non-dimensional parameter Λ may be thought of as a dimensionless material thickness and the Biot number as a dimensionless heat transfer coefficient. It is seen in Figs. 2a and 2b that at small material thickness and small heat transfer coefficients, the surface temperature is near the value of the backface temperature. However, as the heat transfer coefficient (Biot Number) increases, the surface temperature approaches the value of the environmental temperature. From Figs. 2c and 2d, it is observed that for larger material thickness, the surface temperature approaches the environmental temperature even for values of heat transfer coefficient near zero.

The conclusion is that for sufficiently thin walls using a boiling water backface, even materials with low critical temperatures like aluminum can be used in very high temperature environments. This concept is employed in a familiar Boy Scout demonstration where water is heated to boiling in a paper cup over hot coals. It is observed that the paper cup does not burn until all the water is boiled away because its surface temperature remains below the ignition temperature of the paper. It only works when the paper is sufficiently thin.

For very high environmental temperatures in more practical engineering applications, the thickness or more properly, thinness requirement, is often not achievable because of structural requirements.

Figure 2. Influence of Bi on T_s/T_{bf} as a function of T_e/T_{bf}

(a) $\Lambda = 0$

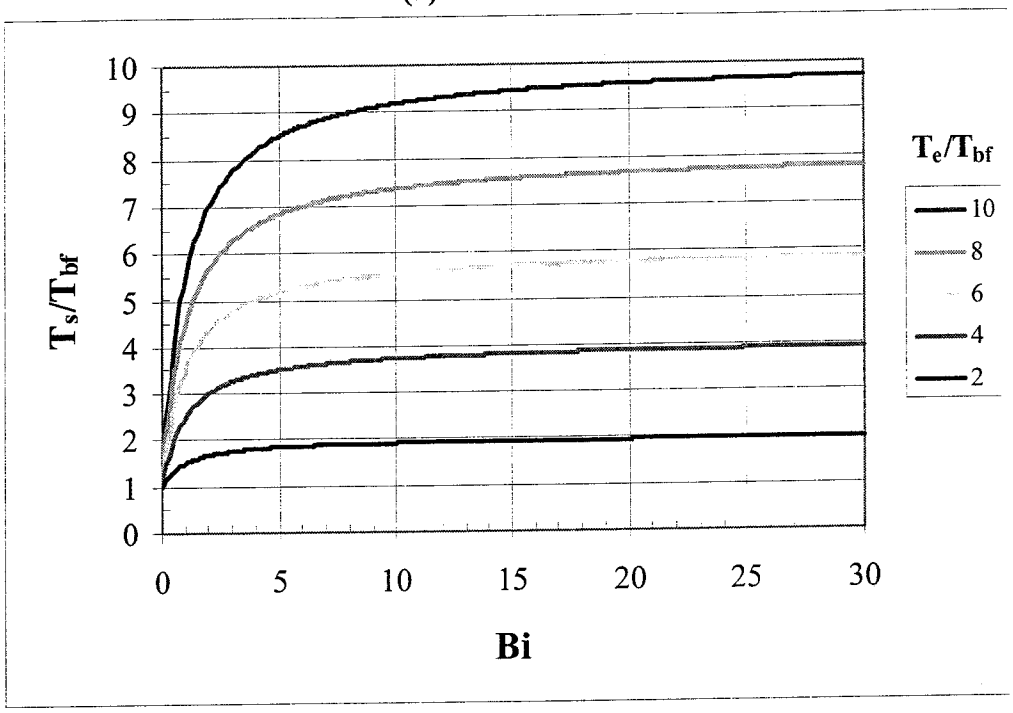

(b) $\Lambda = 0.0001$

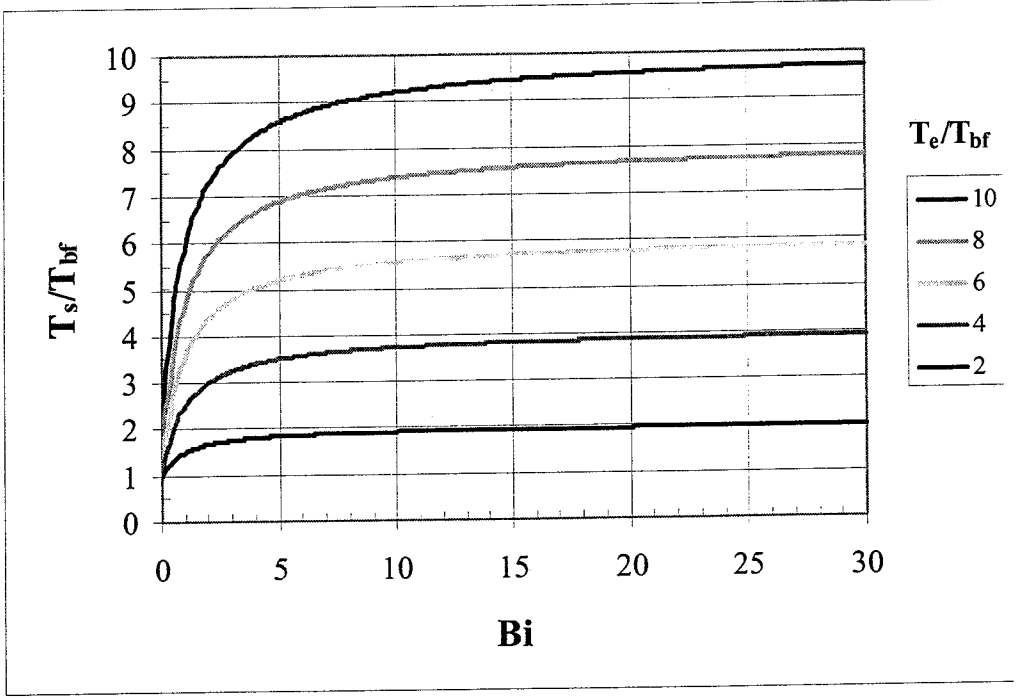

(c) $\Lambda = 0.001$

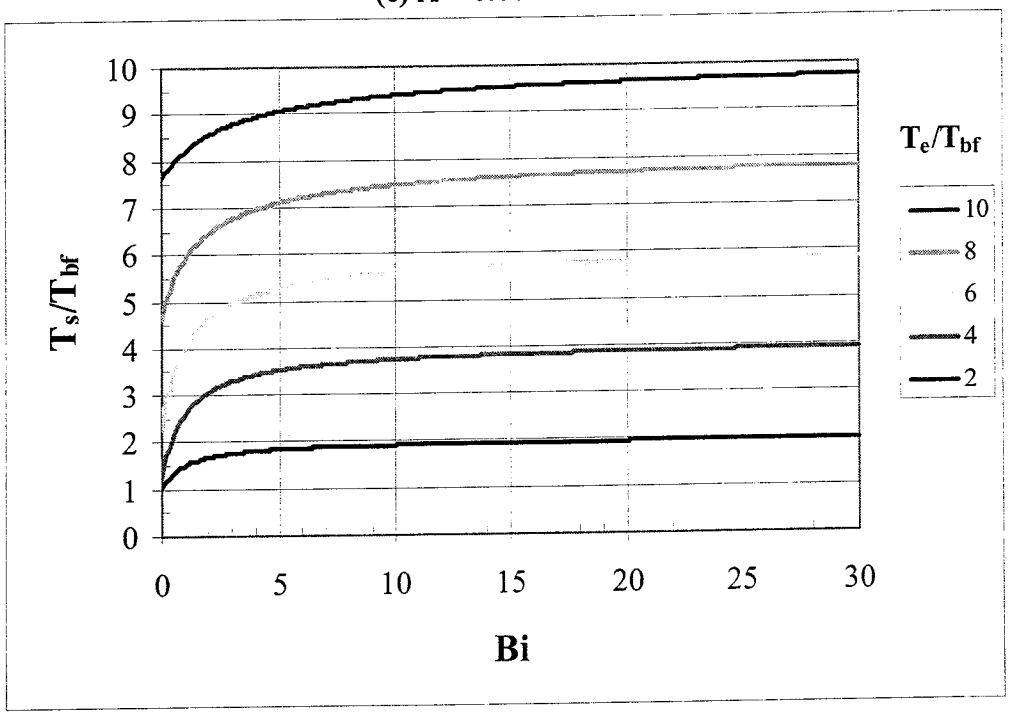

(d) $\Lambda = 0.01$

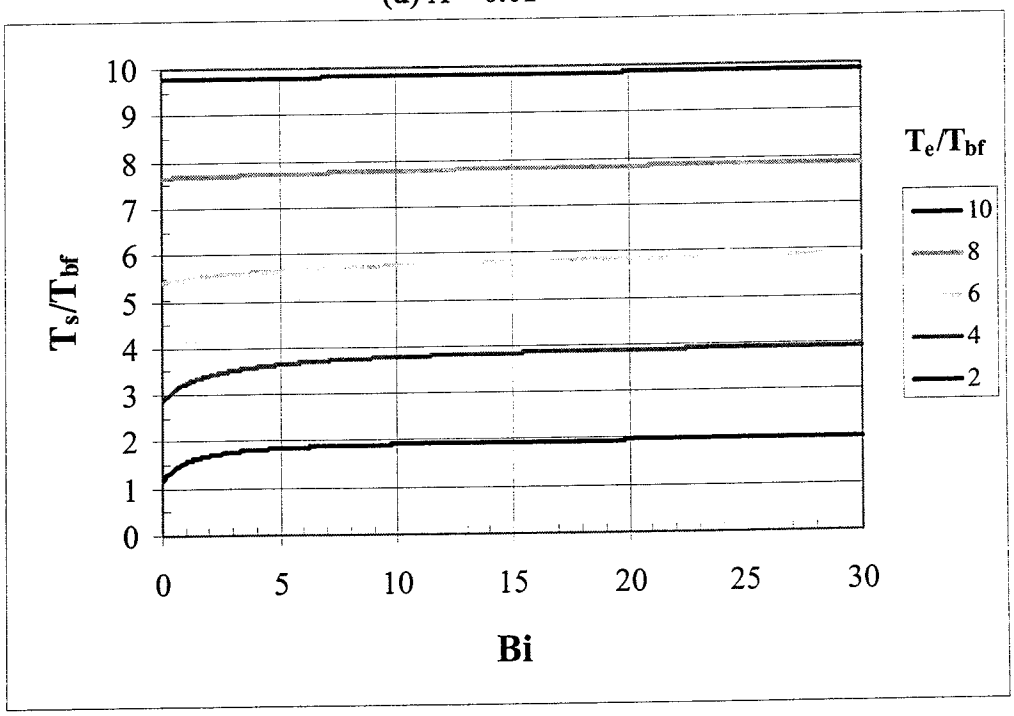

These same effects are shown from a different perspective by cross-plotting the independent variables as shown in Fig. 3 where the influence of T_e/T_{bf} on T_s/T_{bf} as a function of Bi for four different values of Λ is presented. As expected, it is seen in Fig. 2a that the surface temperature is equal to the backface temperature for all environmental temperatures when both the material thickness and heat transfer coefficient approach zero ($\Lambda = 0$ and $Bi = 0$). The curves tend to coalesce for large values of Bi corresponding to the asymptotic behavior observed in Fig. 2 for increasing Bi at constant T_e/T_{bf}. In Figs. 3c and d, it is seen that the curves tend to coalesce for all values of Bi when the material thickness becomes sufficiently large. This corresponds to the observation that all of the constant T_e/T_{bf} curves tend toward horizontal lines in Figs. 2c and d. Furthermore, for combinations of large material thickness and large heat transfer coefficient, the surface temperature approaches the environmental temperature as shown by the nearly 45 degree slope on the high Bi lines in Fig. 3d.

Figure 3. Influence of T_e/T_{bf} on T_s/T_{bf} as a function of Bi

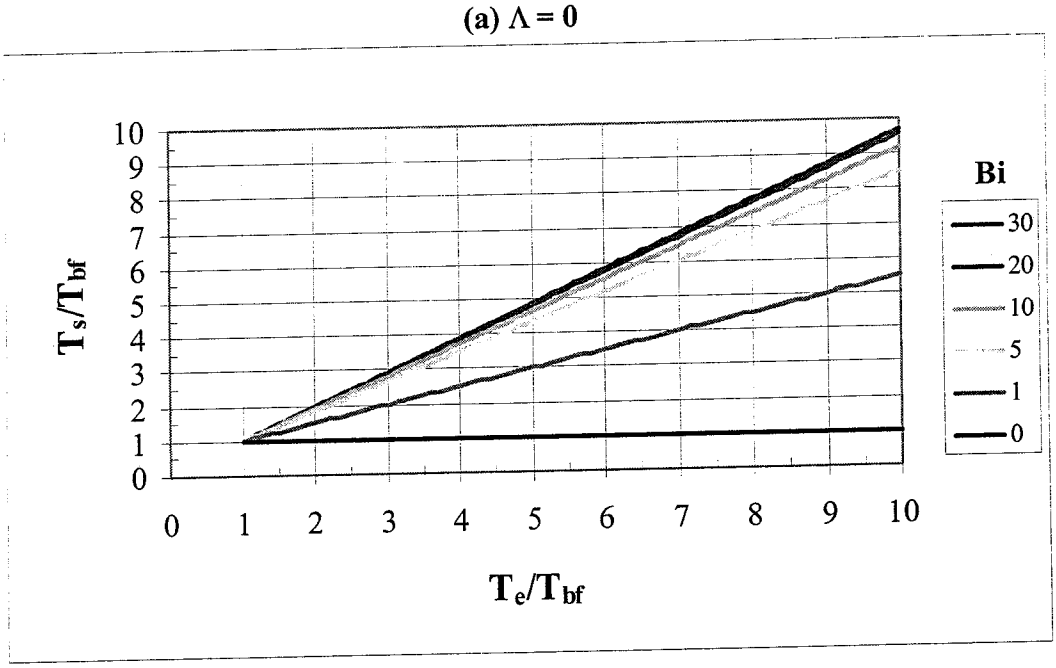

(b) $\Lambda = 0.0001$

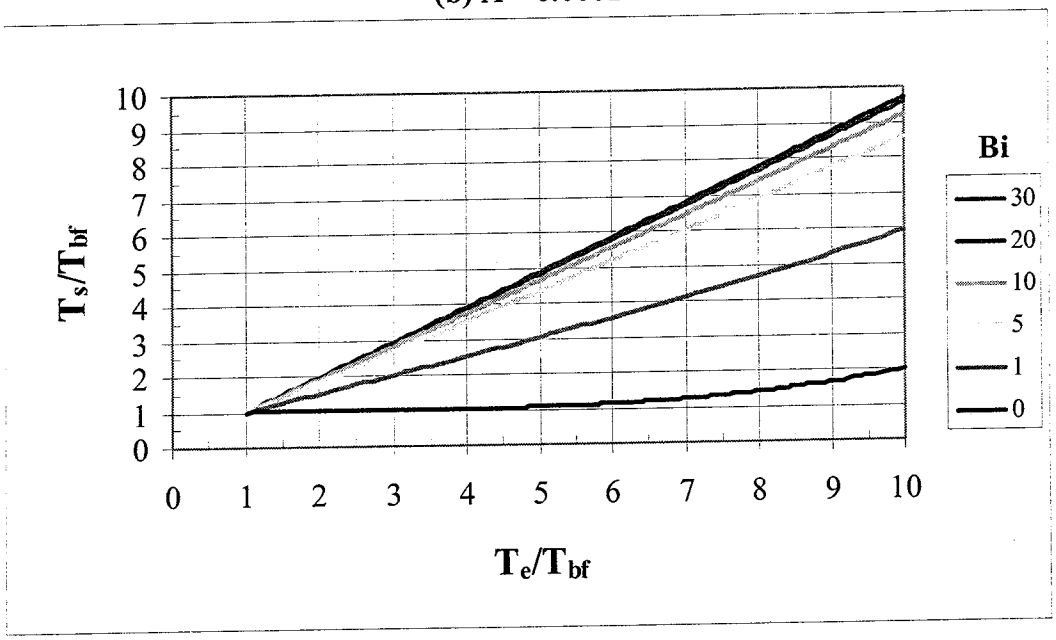

(c) $\Lambda = 0.001$

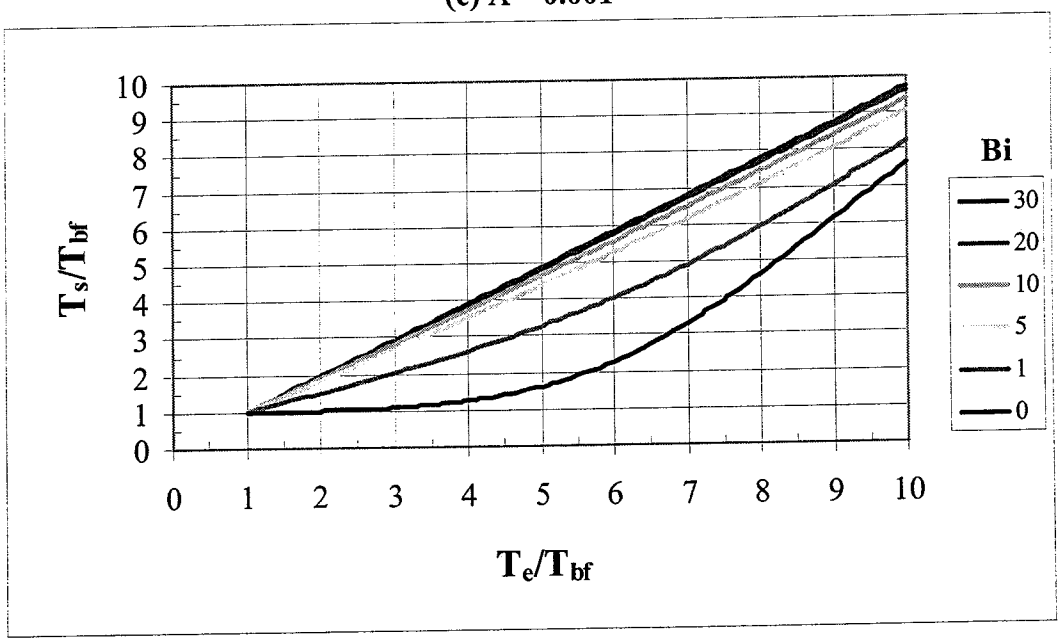

(d) $\Lambda = 0.01$

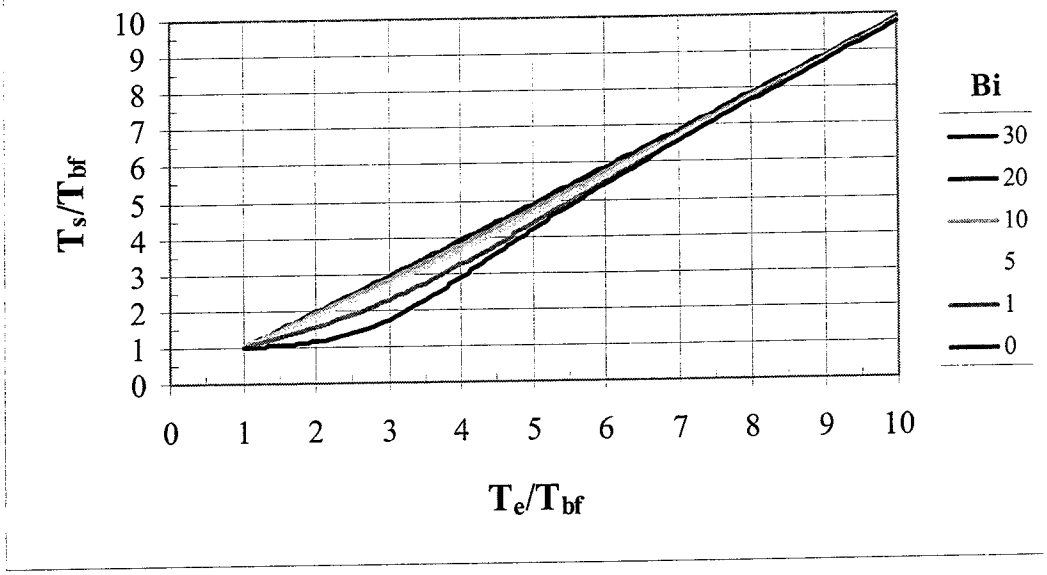

It is of interest to determine the maximum environmental temperature for which Model I can be used for specified values of material thickness and heat transfer coefficient. The maximum environmental temperature is obtained when the surface temperature is at its maximum or critical value. Fig. 4 shows the influence of heat transfer coefficient on $(T_e)_{max}$ as a function of material thickness. The curves are presented in a semi-log format to facilitate differentiation of material thickness effects at low values of heat transfer coefficient. As expected from the parametric results above, the highest allowable values of environmental temperature are associated with the combination of low values of material thickness and heat transfer coefficient. The maximum allowable environmental temperatures approaches the critical surface temperature as the heat transfer coefficient increases for all values of material thickness. The value of the heat transfer coefficient for which the material thickness curves converge increases only modestly for higher critical surface temperatures.

Figure 4. Influence of Bi on $(T_e/T_{bf})_{max}$ as a function of Λ

(a) Aluminum

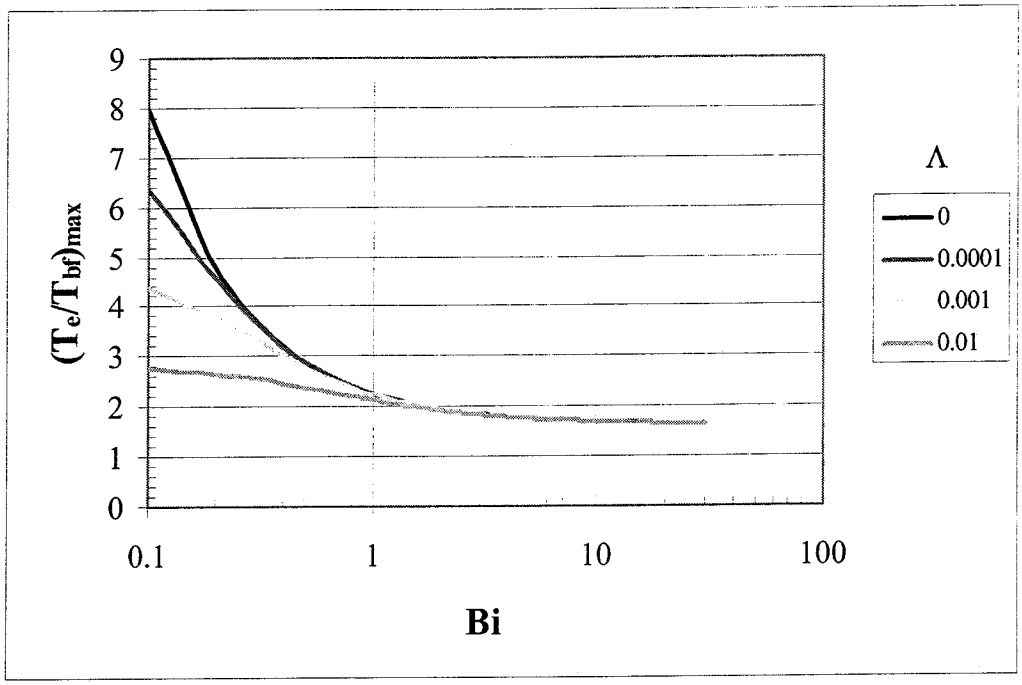

(b) Copper

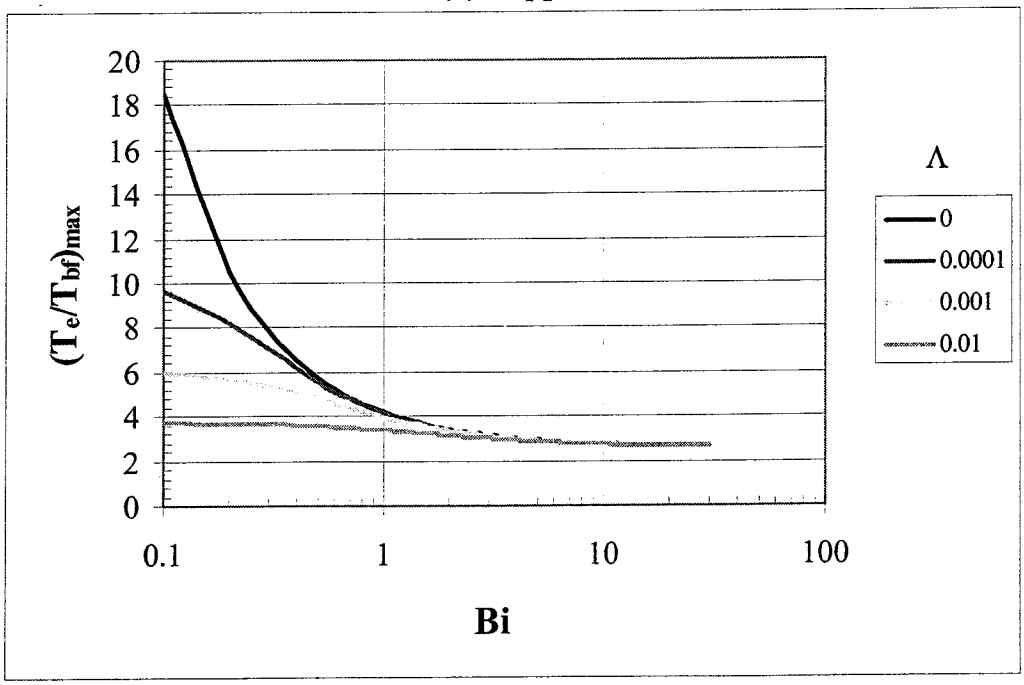

(c) Steel

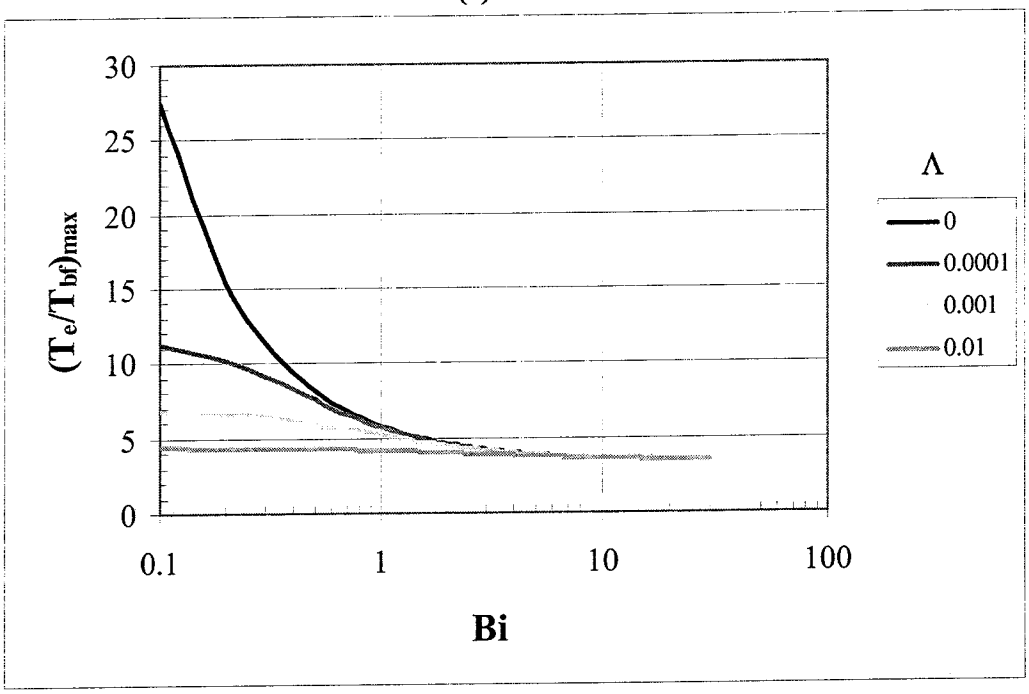

(d) Titanium

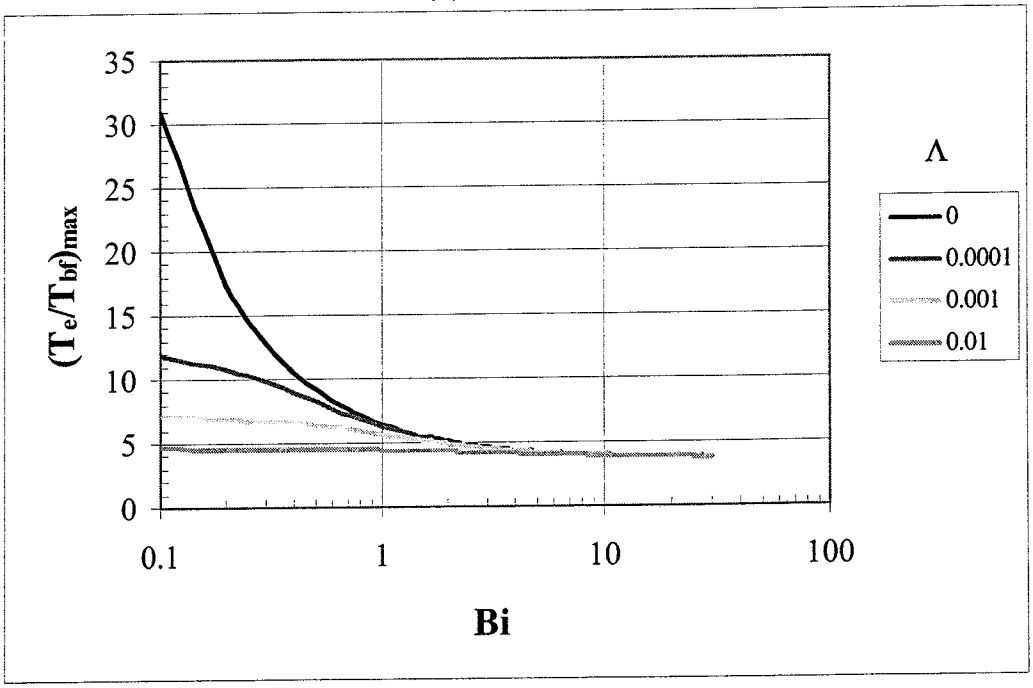

(e) Tungsten

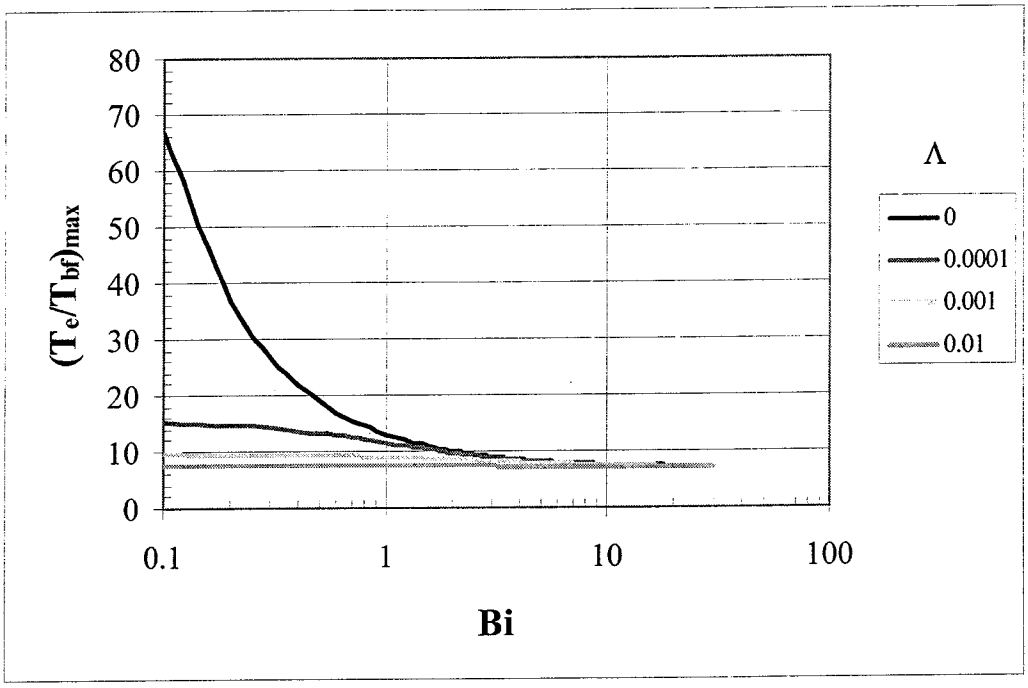

(f) Niobium Carbide

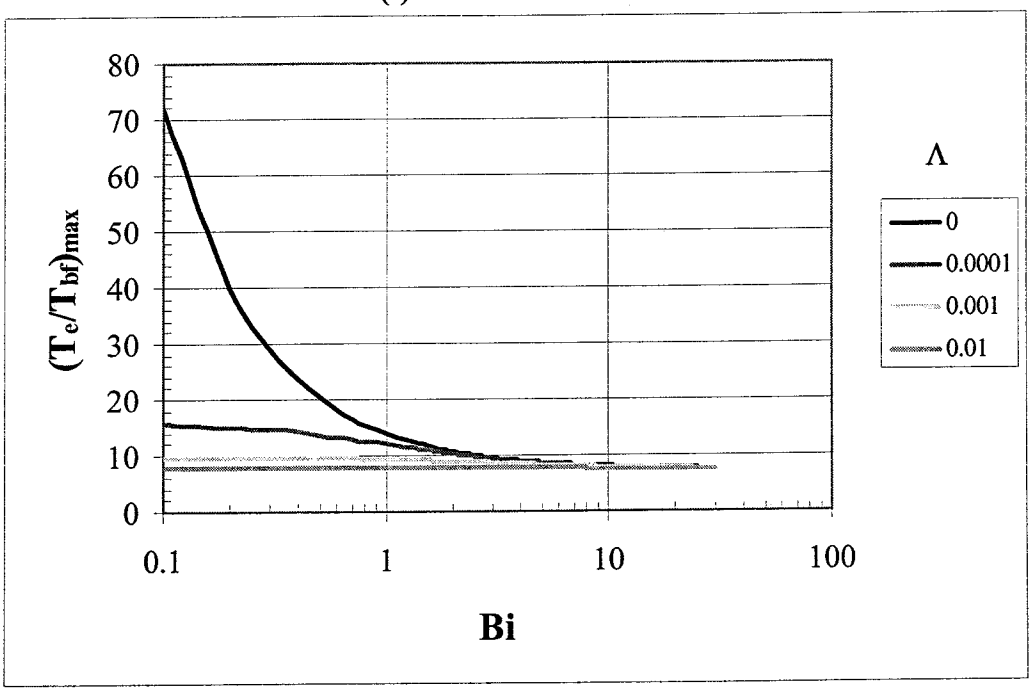

In Fig. 5, the two independent variables are reversed to show the same effects from a different perspective. For the higher values of heat transfer coefficient, all of the curves coalesce toward a single curve as the material thickness increases.

The conclusion from analyses of the results presented in Figs. 4 and 5 is that material selection for Model I is limited by the highest anticipated environmental temperature.

Figure 5. Influence of Λ on $(T_e/T_{bf})_{max}$ as a function of Bi

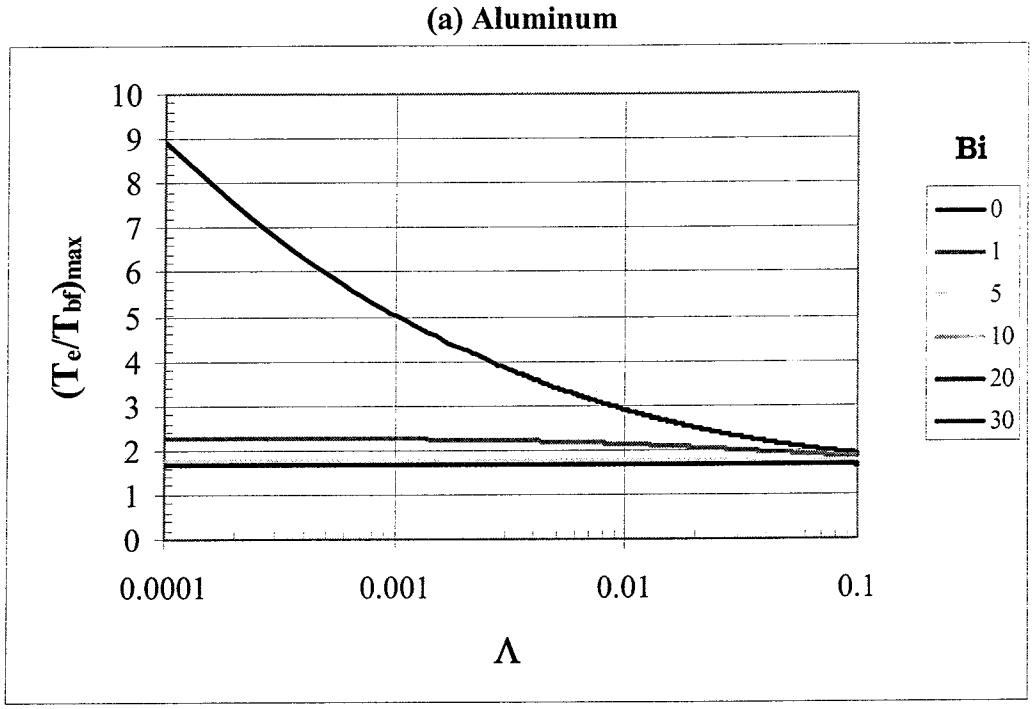

(b) Copper

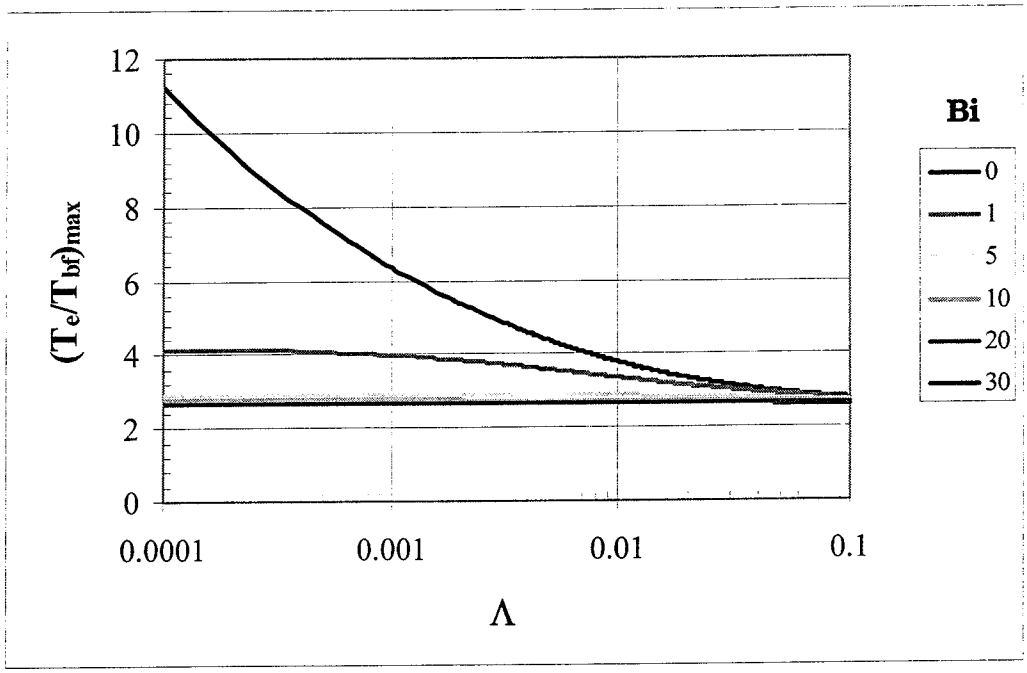

(c) Steel

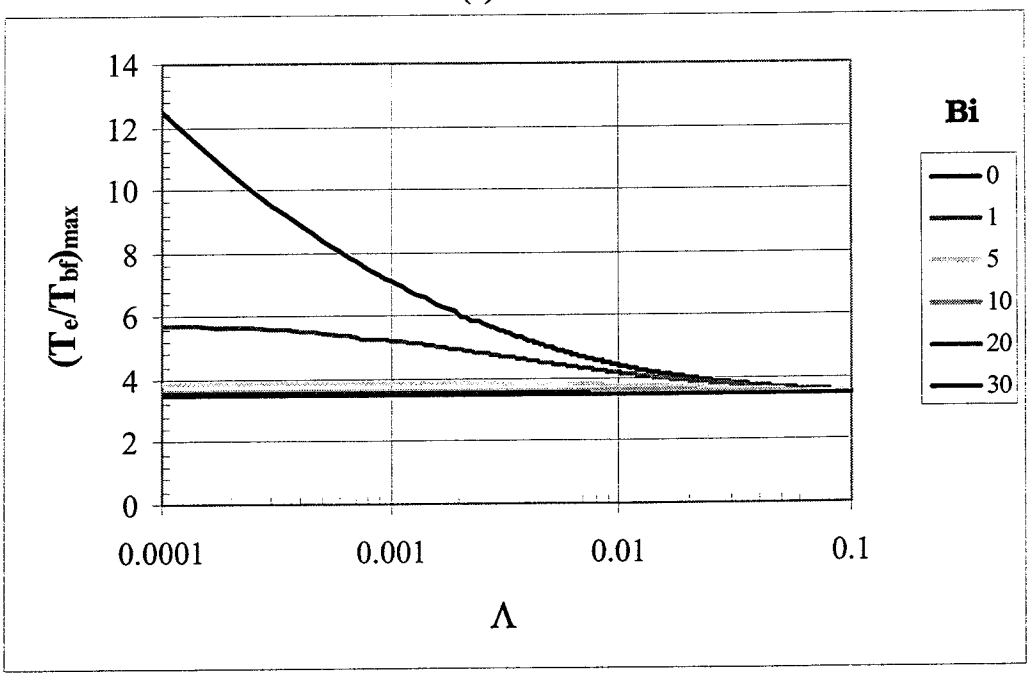

(d) Titanium

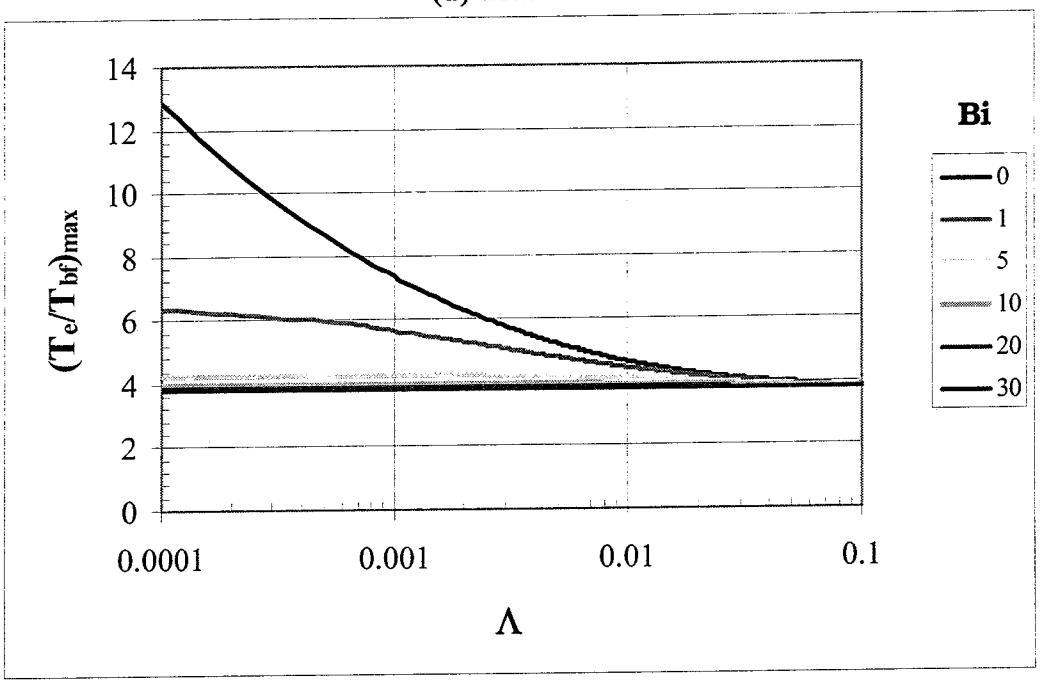

(e) Tungsten

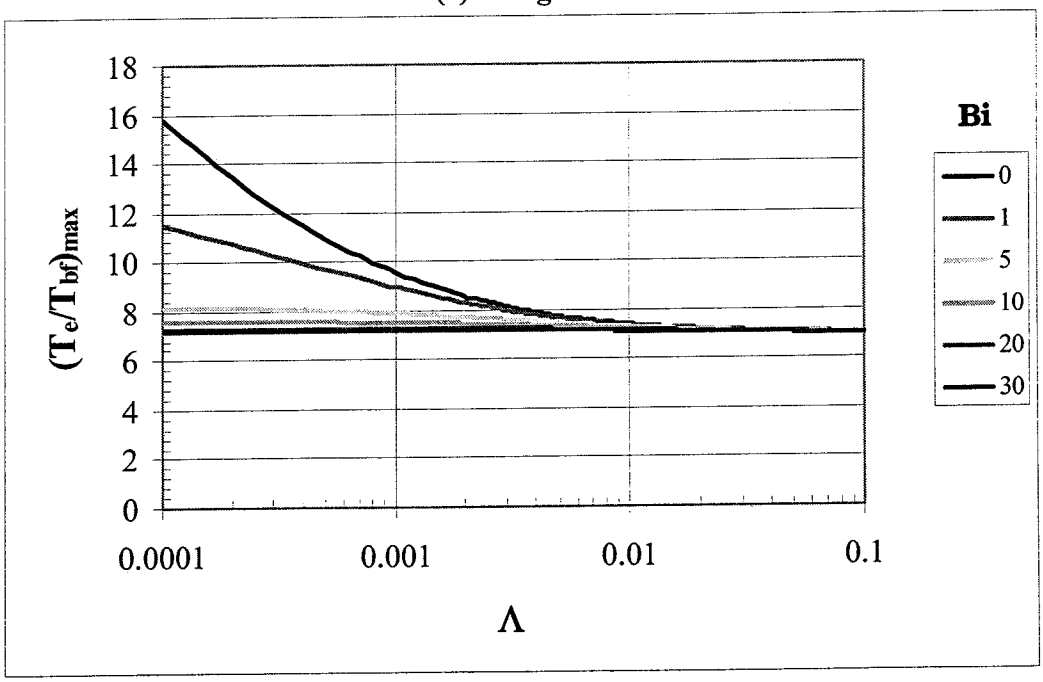

(f) Niobium Carbide

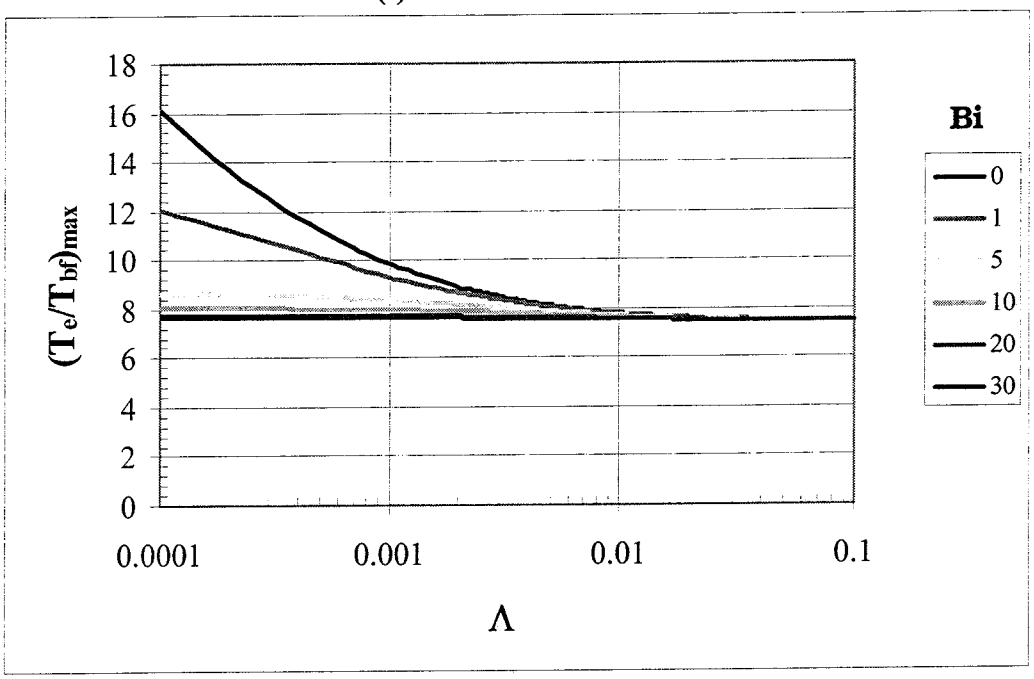

CHAPTER 3

MODEL II DEVELOPMENT AND APPLICATION

Mathematical Model

In Model II, the material backface is maintained at the boiling condition as in Model I. However, channels in the wall conduct the vapor through the wall where it continues to absorb heat and approach the wall temperature in the limit

The schematic of Model II is presented in Fig. 6.

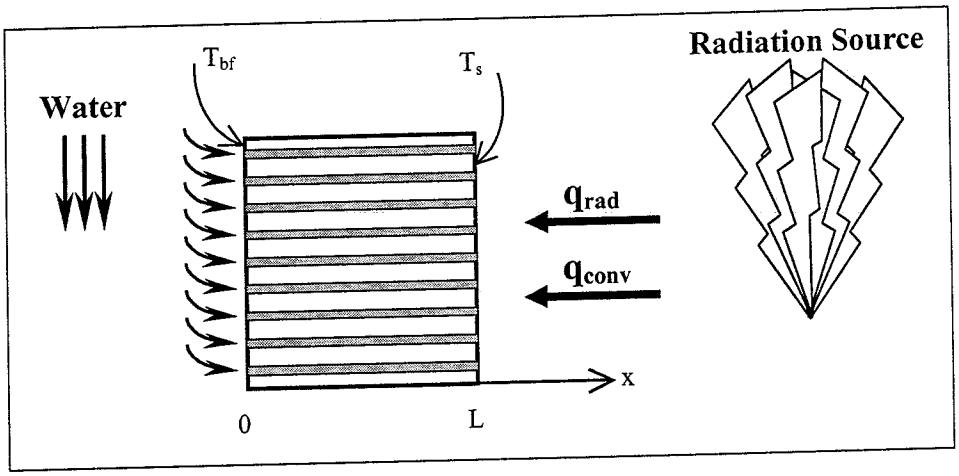

Figure 6. Schematic of Model II (Transpiration Model)

The governing equations for the temperature distributions in the wall and the vapor flow are obtained from a heat balance over the wall and vapor flow elements.

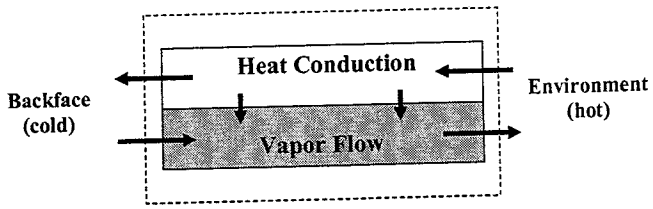

$$k_w A_w \frac{d^2 T_w}{dx^2} - \bar{h}_v P(T_w - T_v) = 0 \tag{27}$$

$$\dot{m}C_{p_v}\frac{dT_v}{dx}-\bar{h}_v P(T_w-T_v)=0 \tag{28}$$

Normalize the governing equations with $x^*=\frac{x}{L}$ and $T^*=\frac{T}{T_{bf}}$

$$\frac{d^2T_w^*}{dx^{*2}}-\frac{\bar{h}_v PL^2}{k_w A_w}\left(T_w^*-T_v^*\right)=0 \tag{29}$$

$$\frac{dT_v^*}{dx^*}-\frac{\bar{h}_v PL}{\dot{m}C_{p_v}}\left(T_w^*-T_v^*\right)=0 \tag{30}$$

Let

$$\gamma=\frac{\bar{h}_v PL^2}{k_w A_w} \tag{31}$$

$$\alpha=\frac{\bar{h}_v PL}{\dot{m}C_{p_v}} \tag{32}$$

so that

$$\frac{d^2T_w^*}{dx^{*2}}-\gamma T_w^*+\gamma T_v^*=0 \tag{33}$$

$$\frac{dT_v^*}{dx^*}-\alpha T_w^*+\alpha T_v^*=0 \tag{34}$$

Reduce the 2nd order ODE system to a coupled 1st order ODE system.

Let

$$z^*=\frac{dT_w^*}{dx^*} \tag{35}$$

Therefore

$$\frac{dT_w^*}{dx^*} = z^* \tag{36}$$

$$\frac{dT_v^*}{dx^*} = \alpha T_w^* - \alpha T_v^* \tag{37}$$

$$\frac{dz^*}{dx^*} = \gamma T_w^* - \gamma T_v^* \tag{38}$$

The boundary conditions follow:

$$\text{At } x^* = 0: \qquad T_w^* = 1 \text{ and } T_v^* = 1 \tag{39}$$

$$\text{At } x^* = 1: \qquad \frac{dT^*}{dx^*} = Q_L \tag{40}$$

where

$$Q_L = \frac{\sigma \varepsilon L T_{bf}^{\ 3}}{k_w}\left[\left(\frac{T_e}{T_{bf}}\right)^4 - \left(\frac{T_s}{T_{bf}}\right)^4\right] + \frac{\bar{h}_e L}{k_w}\left(\frac{T_e}{T_{bf}} - \frac{T_s}{T_{bf}}\right) \tag{41}$$

The solution is

$$T_w^* = C_1 + C_2 e^{\lambda_2 x^*} + C_3 e^{\lambda_3 x^*} \tag{42}$$

$$T_v^* = C_1 + \frac{\alpha}{\alpha + \lambda_2} C_2 e^{\lambda_2 x^*} + \frac{\alpha}{\alpha + \lambda_3} C_3 e^{\lambda_3 x^*} \tag{43}$$

$$\frac{dT_w^*}{dx^*} = \lambda_2 C_2 e^{\lambda_2 x^*} + \lambda_3 C_3 e^{\lambda_3 x^*} \tag{44}$$

where

$$\lambda_2 = \frac{-\alpha + \sqrt{\alpha^2 + 4\gamma}}{2} \tag{45}$$

$$\lambda_3 = \frac{-\alpha - \sqrt{\alpha^2 + 4\gamma}}{2} \tag{46}$$

$$C_3 = \frac{(\alpha + \lambda_3)Q_L}{\lambda_3\left(e^{\lambda_3}(\alpha + \lambda_3) - e^{\lambda_2}(\alpha + \lambda_2)\right)} \tag{47}$$

$$C_2 = -\frac{\lambda_3(\alpha + \lambda_2)}{\lambda_2(\alpha + \lambda_3)}C_3 \tag{48}$$

$$C_1 = 1 - C_2 - C_3 \tag{49}$$

An overall heat balance for the wall and coolant yields

$$\frac{q_{rad}}{A} + \frac{q_{conv}}{A} = \frac{q_{trans}}{A} \tag{50}$$

where

$$\frac{q_{rad}}{A} + \frac{q_{conv}}{A} = \sigma\varepsilon(T_e^{\,4} - T_s^{\,4}) + \bar{h}_e(T_h - T_s) \tag{51}$$

$$\frac{q_{trans}}{A} = \left[\frac{q_{latent}}{A}\right] + \left[\frac{q_{sensible}}{A}\right] = \left[\frac{\dot{m}}{A}h_{fg}\right] + \left[\frac{\dot{m}}{A}C_{p_{liquid}}(T_{boil} - T_{initial}) + \frac{\dot{m}}{A}C_{p_{vapor}}(T_{ve} - T_{boil})\right] \tag{52}$$

Therefore

$$\sigma\varepsilon(T_e^{\,4} - T_s^{\,4}) + \bar{h}_e(T_h - T_s) = \frac{\dot{m}}{A}\left[h_{fg} + C_{p\,liquid}(T_{boil} - T_{initial}) + C_{p\,vapor}(T_{ve} - T_{boil})\right] \tag{53}$$

$$\frac{\dot{m}}{A} = \left[\frac{\left[\sigma\varepsilon(T_e^{\,4} - T_s^{\,4}) + \bar{h}_e(T_h - T_s)\right]}{h_{fg} + C_{p\,liquid}(T_{boil} - T_{initial}) + C_{p\,vapor}(T_{ve} - T_{boil})}\right] \tag{54}$$

Normalize the equation by multiplying through by $\frac{L}{k_w}\frac{h_{fg}}{T_{bf}}$

$$\frac{\dot{m}}{A}\frac{L}{k_w}\frac{h_{fg}}{T_{bf}} = \left[\frac{h_{fg}\cdot\left[\Lambda\left[\left(\frac{T_e}{T_{bf}}\right)^4-\left(\frac{T_s}{T_{bf}}\right)^4\right]+Bi\left(\frac{T_e}{T_{bf}}-\frac{T_s}{T_{bf}}\right)\right]}{h_{fg}+Cp_{liquid}T_{bf}\left(\frac{T_{boil}}{T_{bf}}-\frac{T_{initial}}{T_{bf}}\right)+Cp_{vapor}T_{bf}\left(\frac{T_{ve}}{T_{bf}}-\frac{T_{boil}}{T_{bf}}\right)}\right] \tag{55}$$

Let

$$\beta_{II} = \frac{\dot{m}}{A}\Bigg)_{II}\frac{L}{k_w}\frac{h_{fg}}{T_{bf}} \tag{56}$$

$$H_{bf} = \frac{h_{fg}+C_{p\,liquid}T_{bf}\left(\frac{T_{boil}}{T_{bf}}-\frac{T_{initial}}{T_{bf}}\right)}{h_{fg}} \tag{57}$$

$$H_{vII} = \frac{C_{p\,vapor}T_{bf}\left(\frac{T_{ve}}{T_{bf}}-\frac{T_{boil}}{T_{bf}}\right)}{h_{fg}} \tag{58}$$

Therefore

$$\beta_{II} = \frac{Q_L}{H_{bf}+H_{vII}} \tag{59}$$

Model II requires the flow to be regulated so that all of the water is boiled at the backface and the vapor is superheated in the flow channels. This condition has the effect of coupling γ and α through β_{II} so that

$$\beta_{II} = \frac{\gamma}{\alpha}\left(\frac{h_{fg}}{T_{bf}C_{p_v}}\right) \tag{60}$$

The independent variables in the above equations are γ, α, Λ, Bi, x, and T_e. The dependent variables are $T_w(x)$, $T_v(x)$, T_s, T_{ve}, Q_L, and β_{II}.

Parametric Study

Similar to the Model I case, a parametric study is conducted in which the independent variables are varied over a range corresponding to typical materials and anticipated conditions. As before it is assumed that $T_h = T_e$. The baseline case for the parametric study is selected to be

$$\begin{aligned} T_e^* &= 6 \\ \Lambda &= 0.001 \\ Bi &= 5 \\ \gamma &= 2 \end{aligned} \tag{61}$$

Fig. 7 shows the axial temperature distribution through the wall and vapor for Model II and the linear axial temperature distribution through the wall for Model I, all at the baseline conditions. It is observed that the vapor flow reduces the temperature in the wall. The most efficient design that could be obtained for Model II is one in which the vapor exit temperature is equal to the wall surface temperature. This would correspond to a condition in which the full heat sink capacity of the vapor is realized for the existing temperature limits. The value of the vapor exit temperature relative to the surface temperature is a measure of efficiency rather than effectiveness since it is the actual exit temperature obtained compared to the maximum possible. In this sense, the difference between these temperatures at $x = L$ ($x^* = 1$) is indicative of the efficiency of Model II relative to Model I where a smaller difference corresponds to greater efficiency. The full parametric study of the wall and vapor temperature distributions is presented in the figures of Appendix A. The parametric study presents combinations of the following selected values of the independent variables:

$$\begin{aligned} T_e^* &= 2, 4, 6, 8 \\ \Lambda &= 10^{-5}, 10^{-4}, 10^{-3}, 10^{-2} \\ Bi &= 0, 1, 5, 20 \\ \gamma &= 1, 2, 3, 4 \end{aligned} \tag{62}$$

It is observed that conditions for which the vapor exit temperature is near the limiting value of the wall surface temperature is associated with high values of γ. Physically, γ represents the effectiveness of the channels in transferring heat from the wall to the water vapor.

Figure 7. Axial Wall and Vapor Temperature Distributions at the Baseline Conditions

T_e/T_{bf}=6, [$\Lambda=10^{-3}$], Bi=5, γ=2, α=1.9742

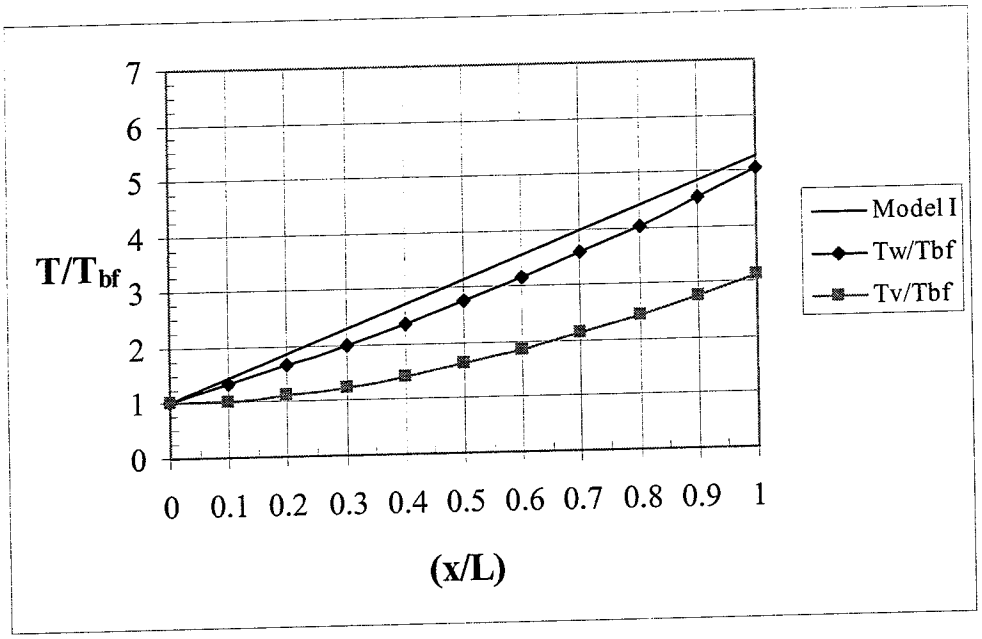

This effect is observed more directly in Fig. 8 where T_s/ T_{bf} and T_{ve}/ T_{bf} are plotted versus each of the independent variables with the remaining independent variables held constant at their baseline values. It is observed in Fig. 8d that the conditions associated with the higher efficiencies correspond to higher values of γ as previously noted. However, when the plausible ranges for the independent variables are calculated, it is noted that the maximum value of α is approximately 5 which corresponds to a value of γ of approximately 3.5 for these conditions. Therefore, the potential gain in efficiency suggested by Fig. 8d cannot be realized in practice for existing materials.

Fig. 8a shows that the efficiency of Model II decreases with increasing environmental temperature for these conditions. It is cautioned that observations for these conditions may not be valid for other reference conditions and should not be generalized. Fig. 8b suggests that the efficiency is nearly independent of Λ. In Fig. 8c, it is seen that lower values of Biot number are associated with higher efficiency which asymptotically approaches a constant value as Bi increases.

Figure 8. Variation of the Wall Surface Temperature and the Vapor Exit Temperature with Each Independent Variable

(a) Variation with Environmental Temperature
$\Lambda=10^{-3}$, Bi=5, γ=2

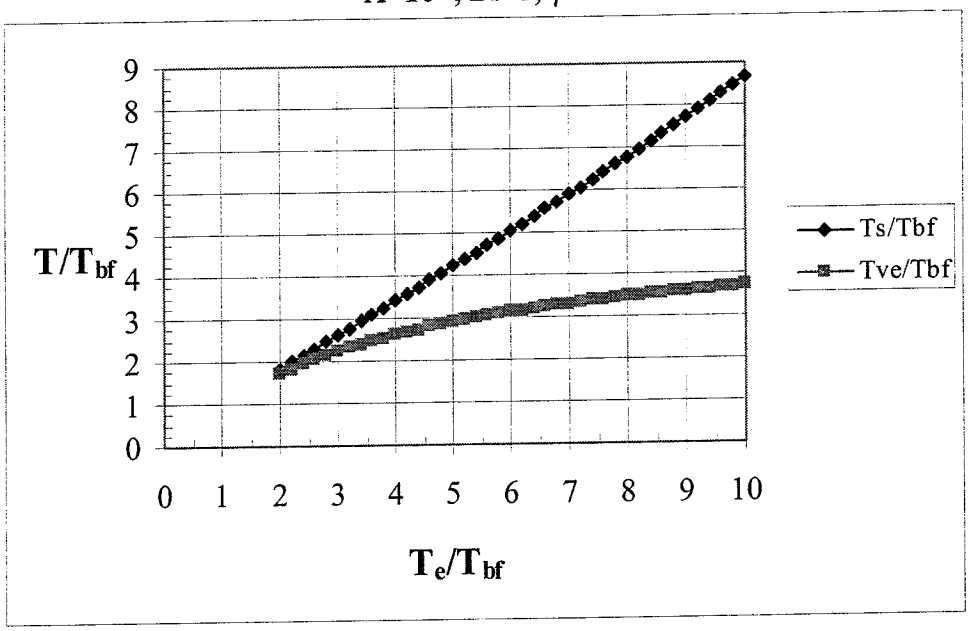

(b) Variation with Λ
T_e/T_{bf}=6, Bi=5, γ=2

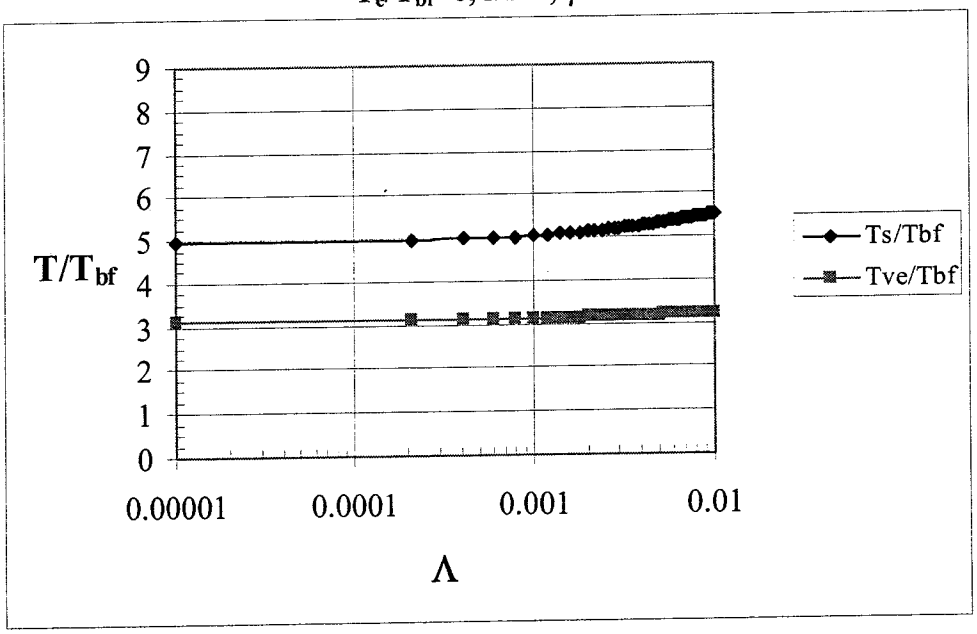

(c) Variation with Biot Number
$T_e/T_{bf}=6$, $\Lambda=10^{-3}$, $\gamma=2$

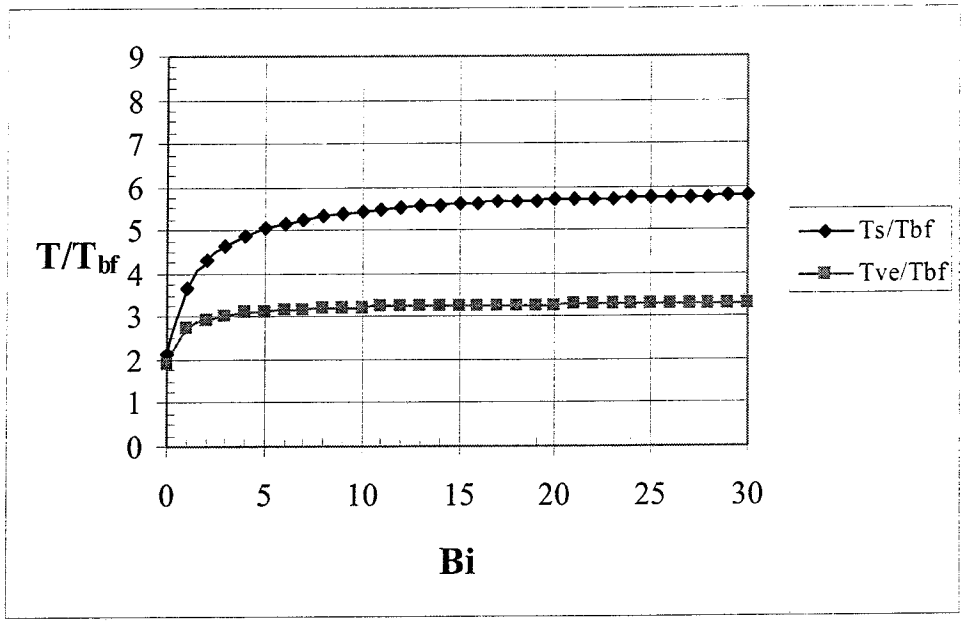

(d) Variation with γ
$T_e/T_{bf}=6$, $\Lambda=10^{-3}$, Bi=5

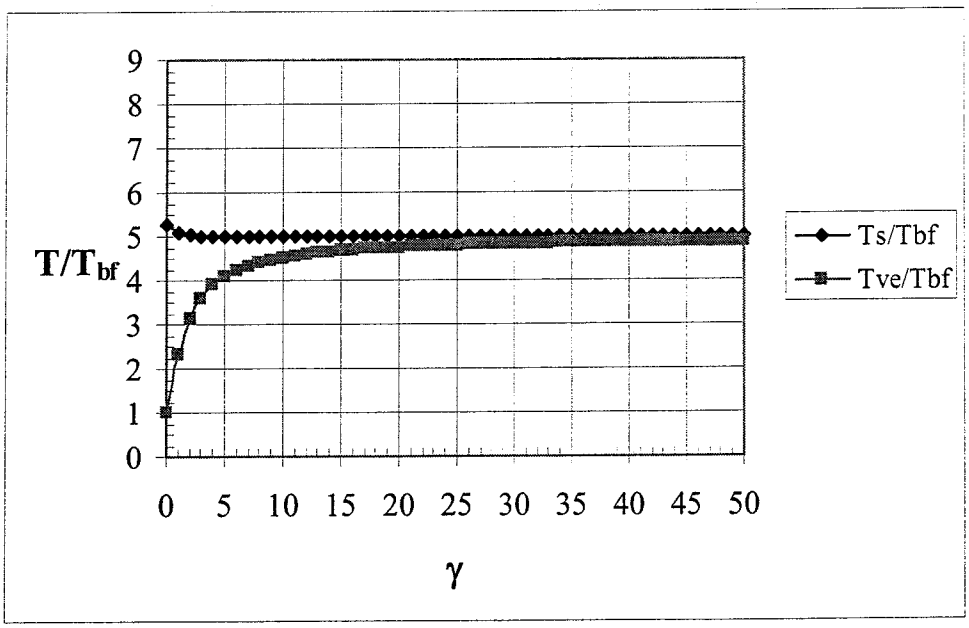

A more direct measure of the efficiency of Model II is found by plotting the ratio of the vapor exit temperature to the wall surface temperature versus the environmental temperature as shown in Fig. 9. In Fig. 9a the influence of Λ at the baseline conditions is illustrated. It is seen that efficiency decreases with increasing environmental temperature, and the effect of Λ is small. In Fig. 9b, higher efficiencies are observed to be associated with lower values of Biot number. The strong influence of higher values of γ is seen in Fig. 9c. These effects are further confirmed by the complete parametric variation of the independent variables at the baseline condition as presented in Appendix B.

Figure 9. Ratio of the Vapor Exit Temperature to the Wall Surface Temperature versus the Environmental Temperature

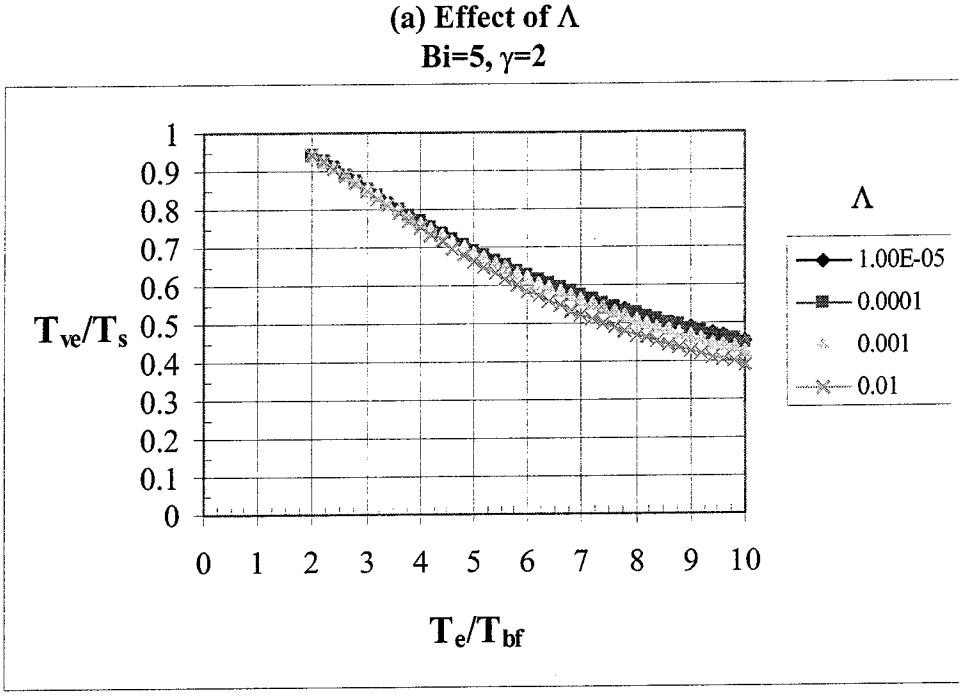

(b) Effect of Biot Number
$\Lambda=10^{-3}$, $\gamma=2$

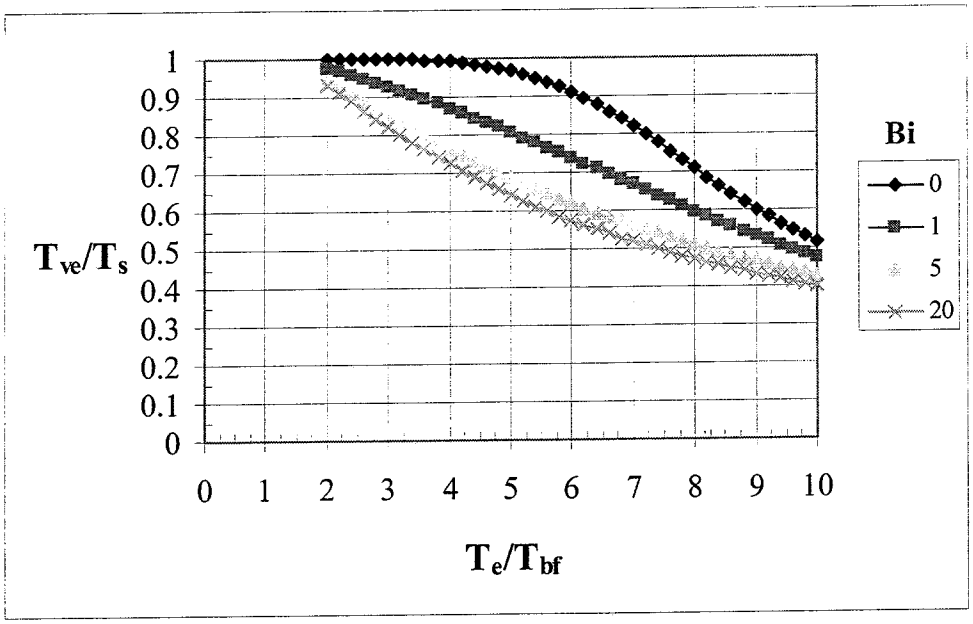

(c) Effect of γ
$\Lambda=10^{-3}$, Bi=5

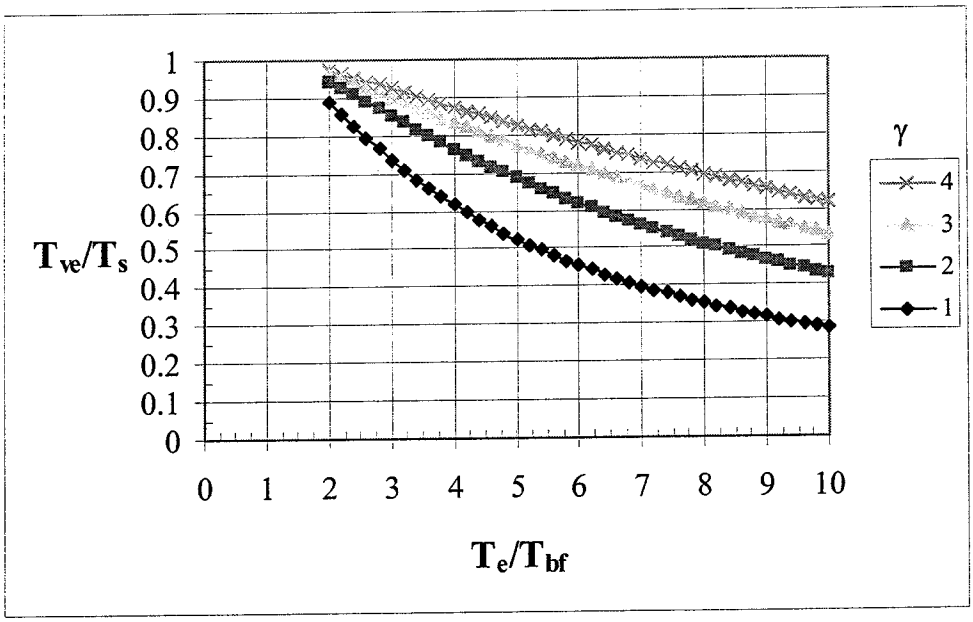

It is also of interest to study the heat transfer rate to the surface as a function of the various combinations of the independent variables. The dimensionless heat transfer rate for Model II, Q_{L2}, is presented in Fig. 10 as a function of environmental temperature for the selected values of the remaining independent variables. Fig. 10a shows the expected increase in heat transfer rate with increasing environmental temperature and a moderate increase in heat transfer rate with increasing Λ. In Fig. 10b the heat transfer rate increases significantly with increasing Biot number at all values of environmental temperature. A very important result is shown in Fig. 10c in that the heat transfer rate becomes nearly independent of γ for sufficiently high values of γ at all values of environmental temperature. This probably is responsible for the previously observed increasing efficiencies with increasing γ. The cross-plots for all the independent variables are shown in Appendix C.

Figure 10. Dimensionless Heat Transfer Rate, Q_{L2}, versus the Environmental Temperature

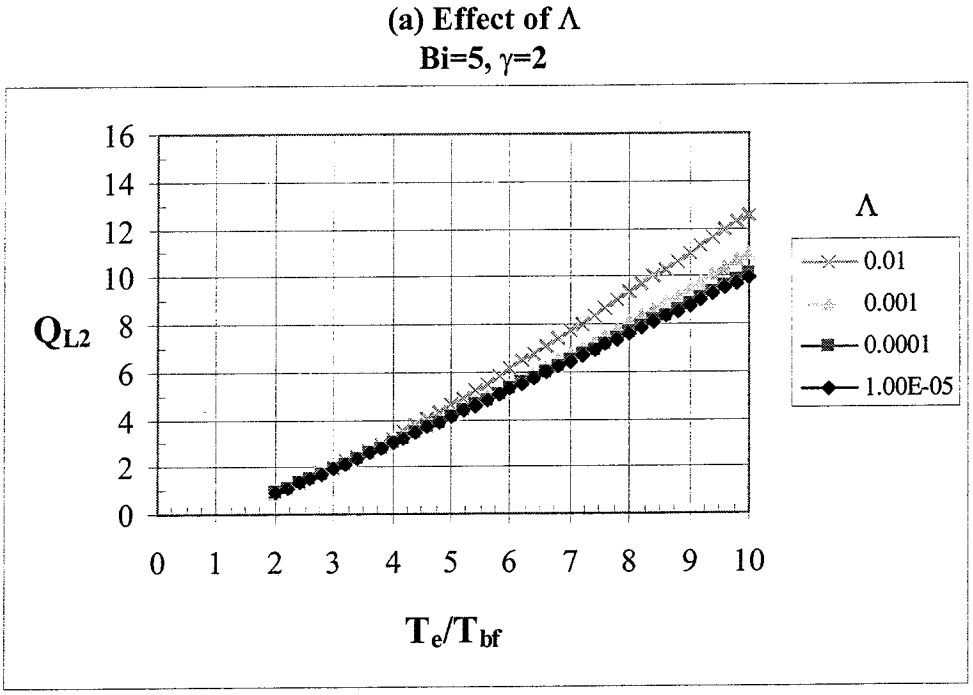

(b) Effect of Biot Number
$\Lambda=10^{-3}$, $\gamma=2$

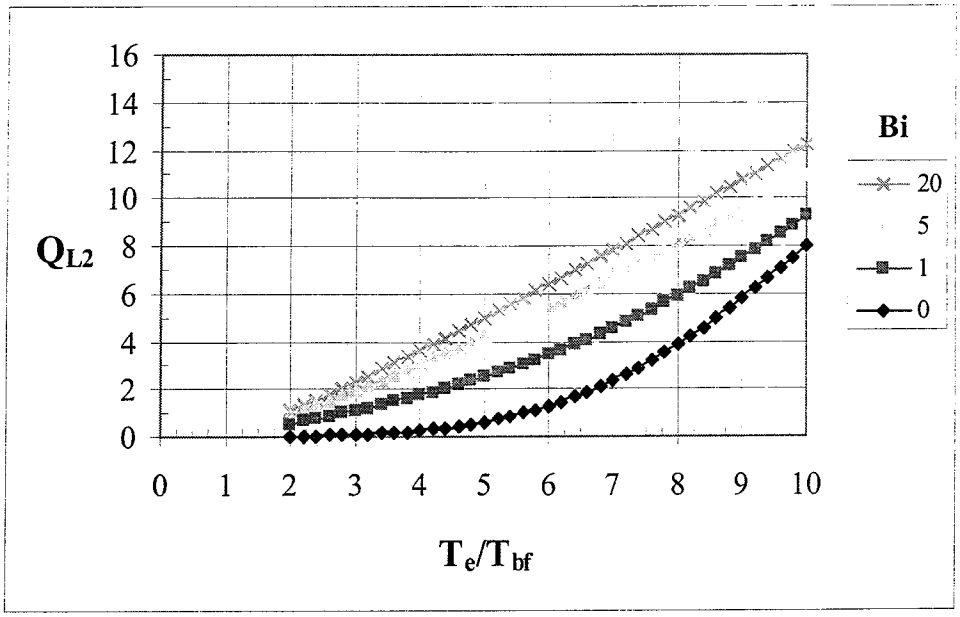

(c) Effect of γ
$\Lambda=10^{-3}$, Bi=5

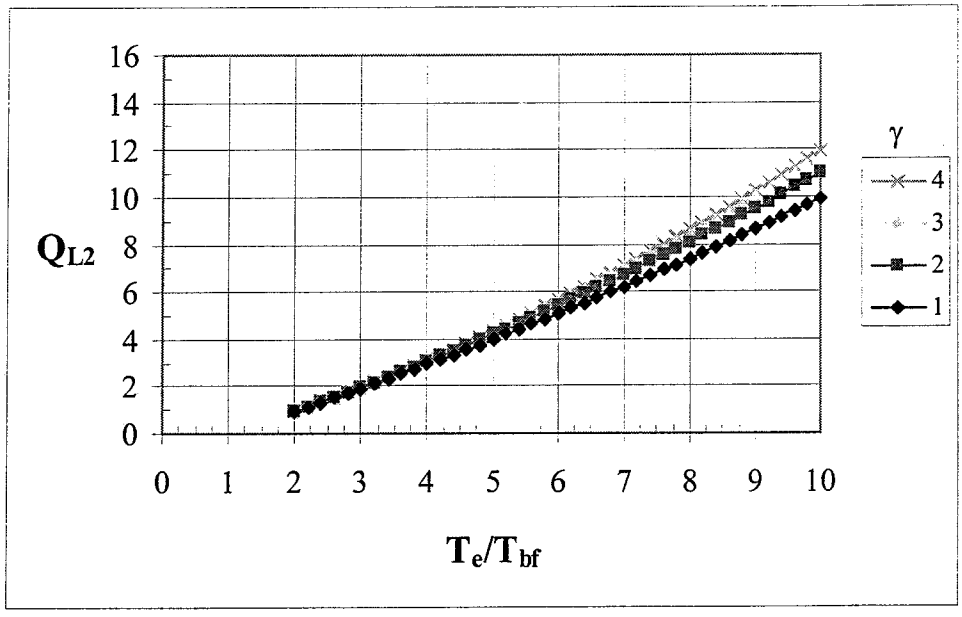

The heat transfer rate to the surface increases for Model II relative to Model I at the same environmental temperature due to the decreased wall surface temperature. This effect is shown in Fig. 11 as the ratio of the dimensionless heat transfer rate, Q_{L2}/ Q_{L1}, versus environmental temperature for the same selected values of the remaining independent variables as presented in Fig. 10. In Fig. 11a it is seen that the Model II heat transfer rate increases from approximately 5 to 40 percent over the Model I value as environmental temperature increases by a factor of 5. There is only a slight influence of Λ. In Fig. 10b the ratio of heat transfer rates increases moderately with increasing Biot number. The same near independence of γ for sufficiently high values of γ is observed in Fig 11c as was noted in Fig. 10c. The cross-plots of the ratio of heat transfer rates versus the other independent variables are shown in Appendix D.

Figure 11. Ratio of Dimensionless Heat Transfer Rate for Models II and I, Q_{L2}/ Q_{L1}, versus the Environmental Temperature

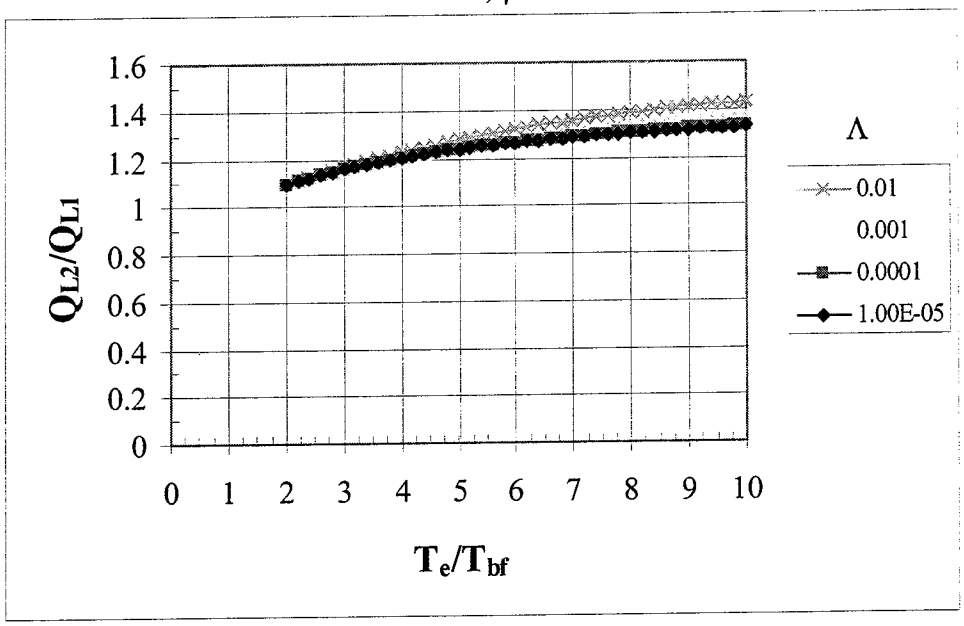

(b) Effect of Biot Number
$\Lambda=10^{-3}$, $\gamma=2$

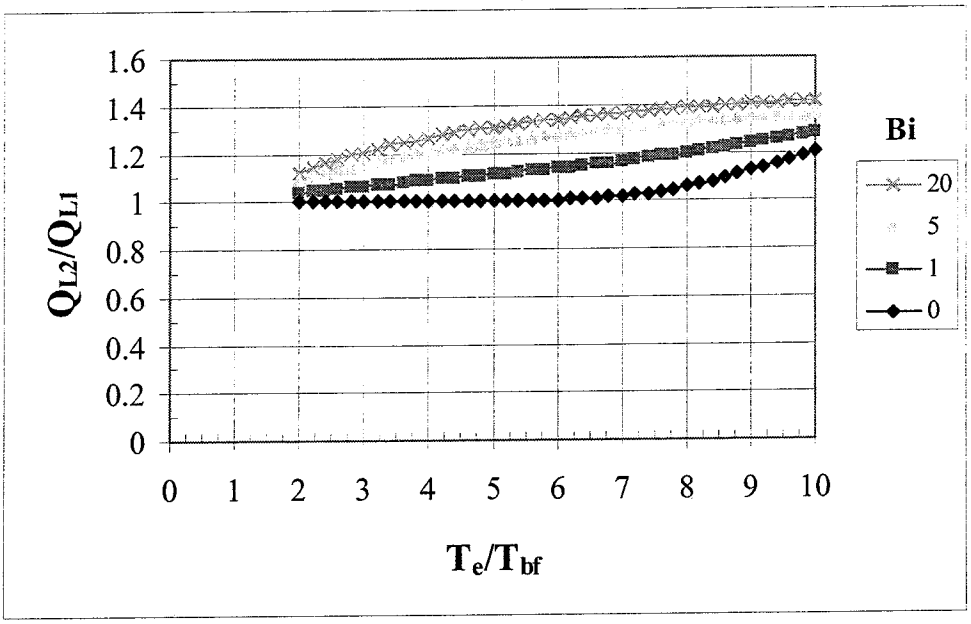

(c) Effect of γ
$\Lambda=10^{-3}$, Bi=5

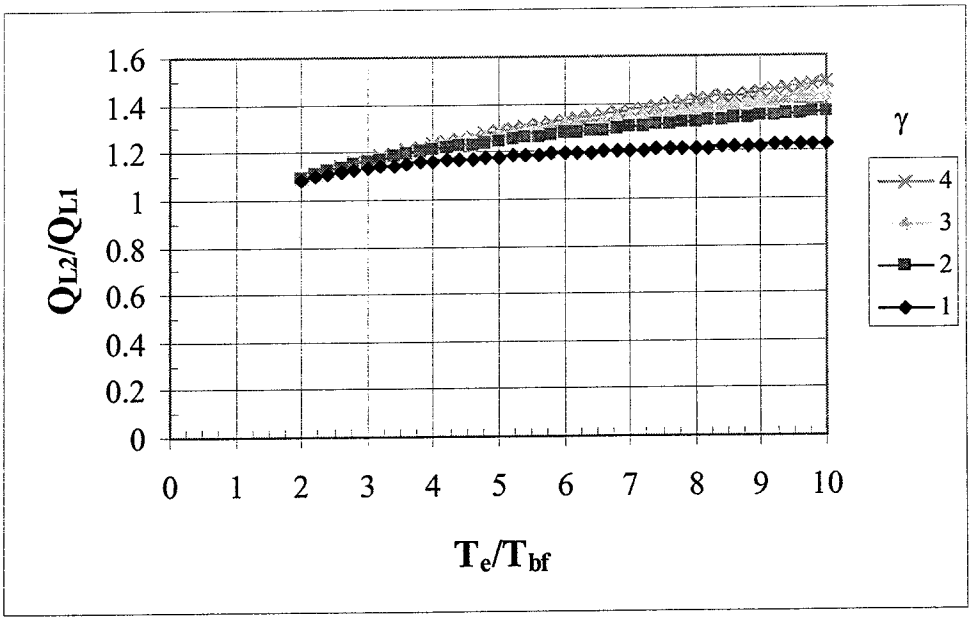

The most important of the output parameters for this study is the minimum mass flow rate required to maintain the backface temperature at its specified value. It is this flow rate that must be supplied by the thermal protection system for the given environmental conditions. In Fig. 12, the variation of the dimensionless parameter, β, with each independent variable is presented for Models I and II. The parameter, β, is proportional to the mass flow rate and is defined by Eqns. (18) and (56) as

$$\beta_I = \frac{\dot{m}}{A}\Big)_I \frac{L}{k_w}\frac{h_{fg}}{T_{bf}} \tag{18}$$

$$\beta_{II} = \frac{\dot{m}}{A}\Big)_{II} \frac{L}{k_w}\frac{h_{fg}}{T_{bf}} \tag{56}$$

It is observed in Fig. 12a that β increases with environmental temperature as expected, and the advantage of Model II over Model I (lower mass flow rate) also increases with increasing temperature. The parameter Λ, which is proportional to the material thickness, is seen to have only a small influence on β in Fig. 12b and the advantage of Model II remains approximately constant. It is observed in Fig. 12c that the value of the Bi has a significant influence on β for low values of Bi but above the value of approximately 5, β increases only slightly with increasing Bi. The channel heat transfer effectiveness parameter, γ, is seen to have a major effect on the advantage of Model II over Model I in Fig. 12d. The ability of any particular design to achieve high values of this parameter is critical to the selection of Model II or Model I.

Figure 12. Variation of Dimensionless Mass Flow Rate Parameter, β, for Models I and II with Each Independent Variable

(a) Variation with Environmental Temperature
$\Lambda=10^{-3}$, Bi=5, γ=2

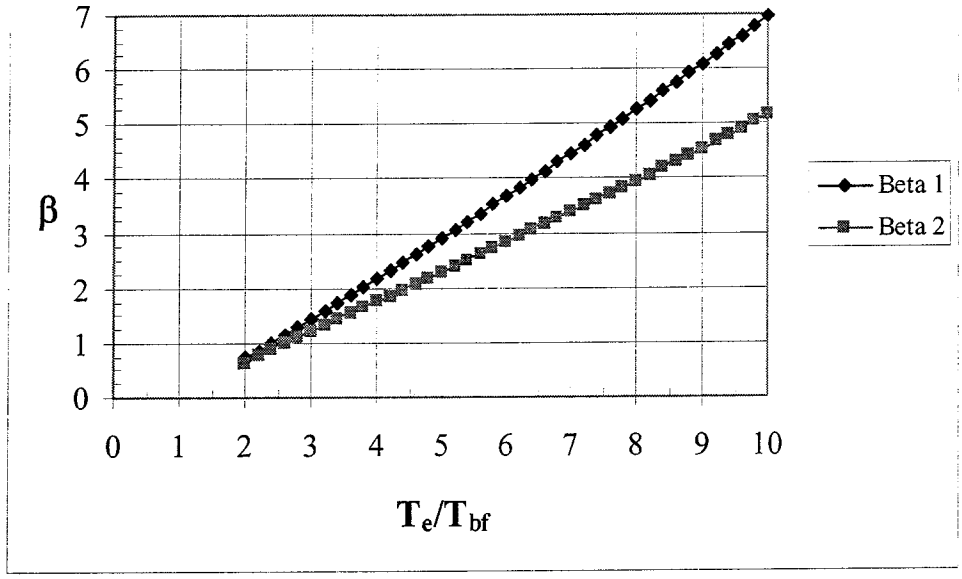

(b) Variation with Λ
T_e/T_{bf}=6, Bi=5, γ=2

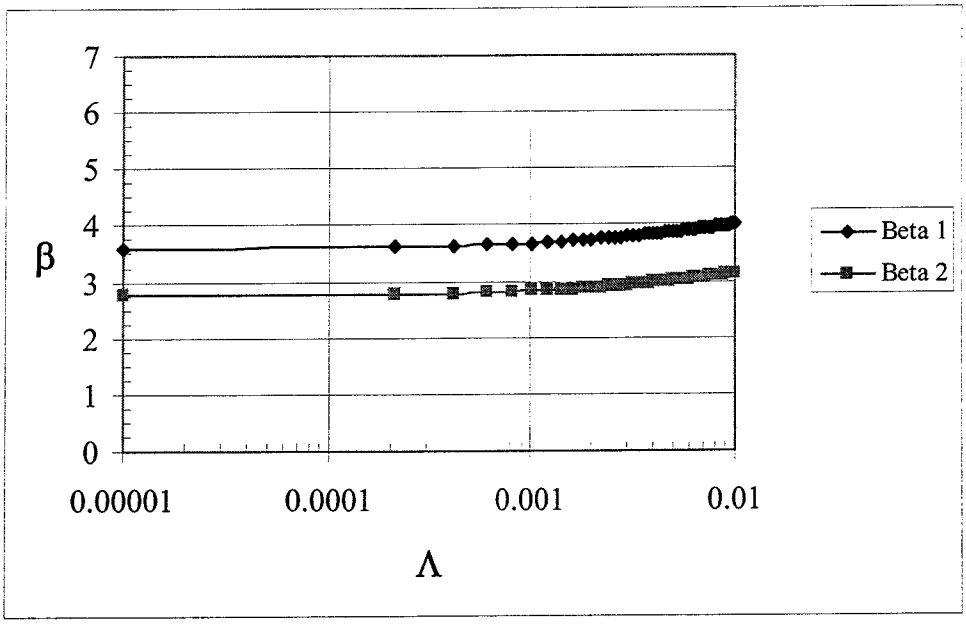

(c) Variation with Biot Number
$T_e/T_{bf}=6$, $\Lambda=10^{-3}$, $\gamma=2$

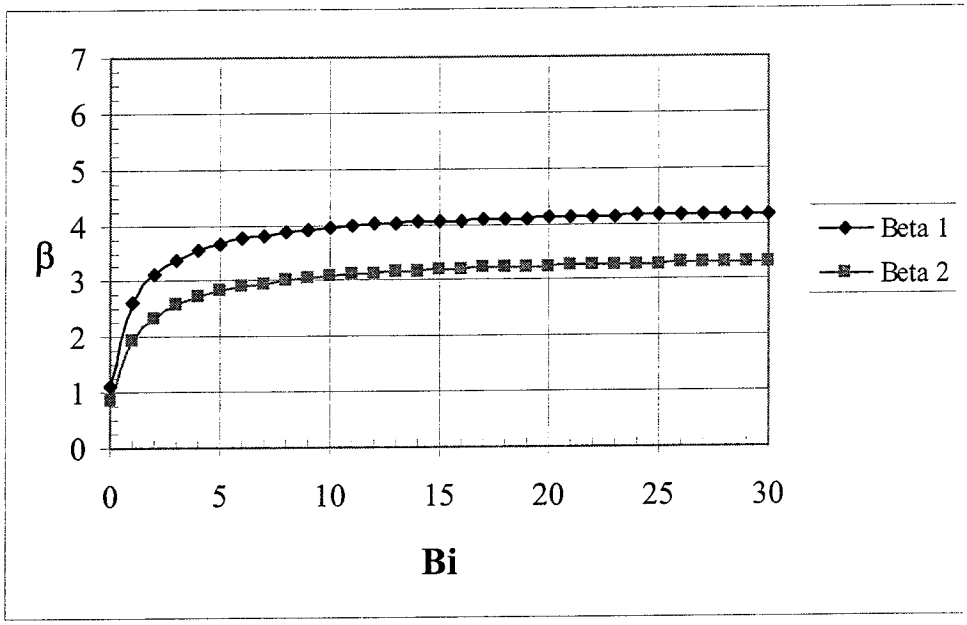

(d) Variation with γ
$T_e/T_{bf}=6$, $\Lambda=10^{-3}$, Bi=5

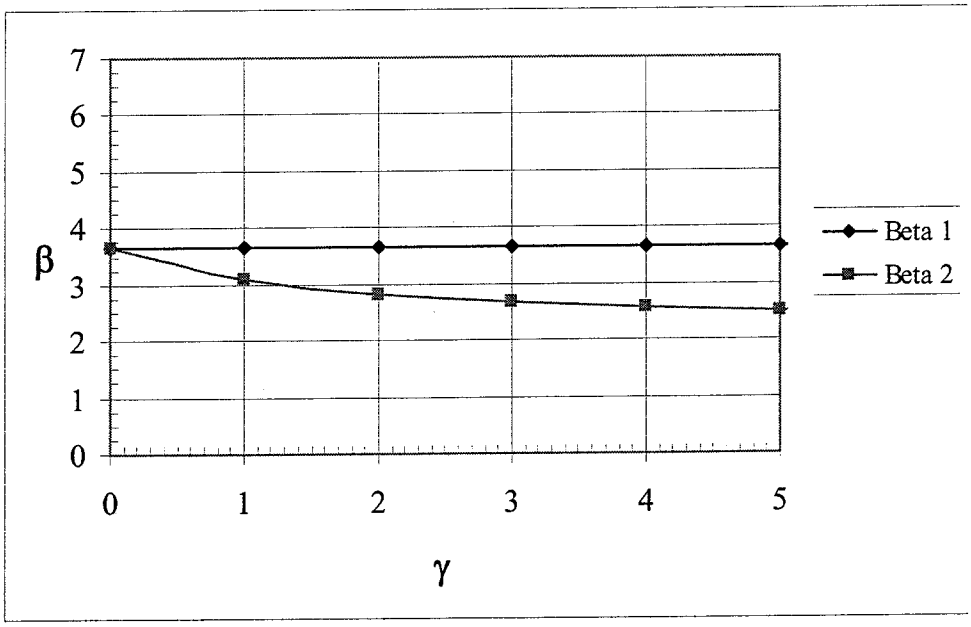

The potential advantage of Model II over Model I in terms of lower required mass flow rate is shown more directly in Fig. 13 where the ratio β_{II}/β_I is plotted versus the environmental temperature for selected values of the other independent variables. In Fig. 13a the potential advantage is seen to increase from approximately 10 percent at a temperature of twice the backface temperature to approximately 25 percent at a temperature of ten times the backface temperature. The parameter Λ has very little influence. A similar result is for the effect of Bi is observed in Fig. 13b. The crossover of the constant Bi curves is due to the fact that the convection heat transfer is more dominant at lower temperatures, and radiation is more dominant at higher temperatures. The strong influence of the parameter γ is shown in Fig. 13c where a potential advantage of approximately 35 percent is observed at a temperature ratio of ten. Again this shows the importance of being able to achieve high values of γ in a particular design.

The cross-plots of the independent variables are presented in Appendix E. The conclusion is that the greater advantages of Model II over Model I is achieved with combinations of high γ and high environmental temperatures with minor effects associated with Λ and Bi.

Figure 13. Ratio of Dimensionless Mass Flow Rate Parameter, β, for Models II and I versus the Environmental Temperature

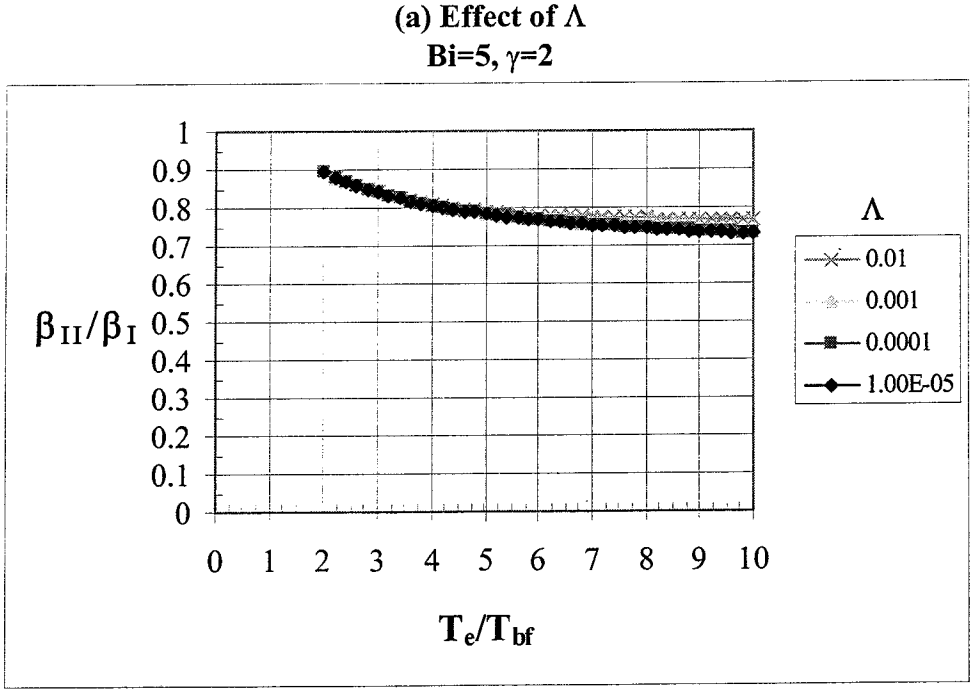

(b) Effect of Biot Number
$\Lambda=10^{-3}$, $\gamma=2$

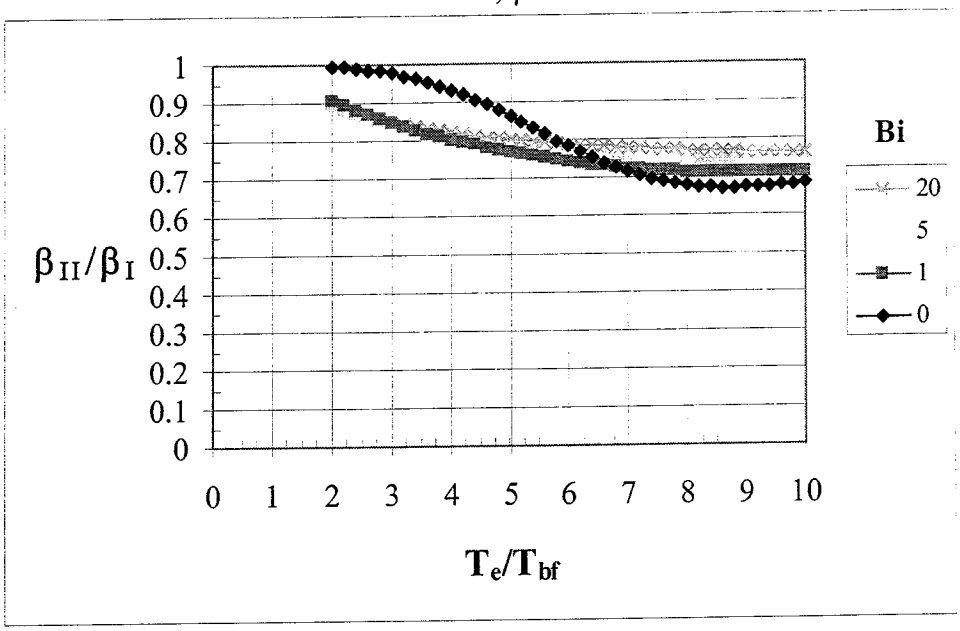

(c) Effect of γ
$\Lambda=10^{-3}$, Bi=5

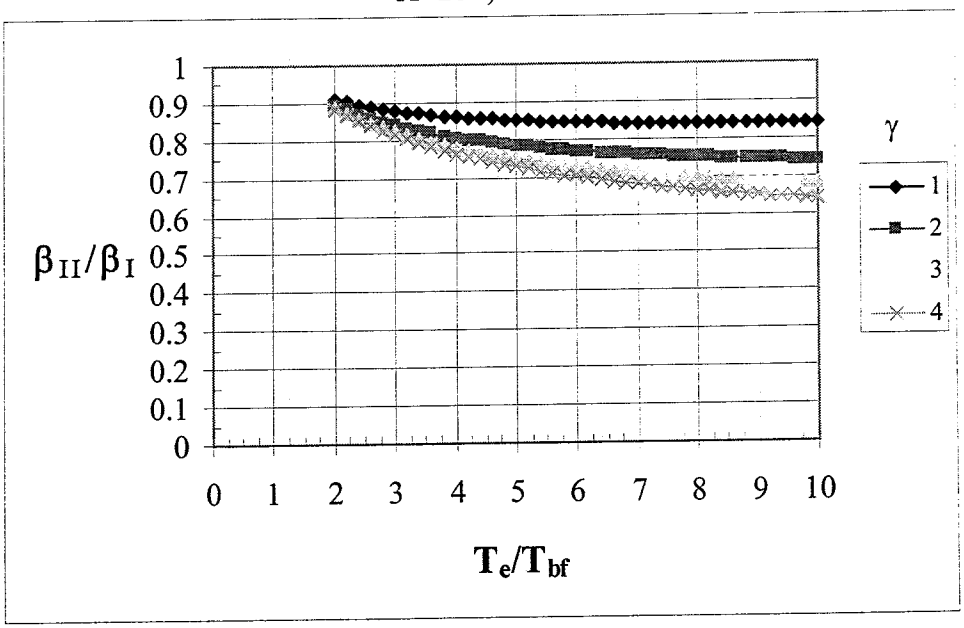

It is instructive to examine the actual values of maximum allowable environmental temperatures for the selected materials when the surface temperature is at the material's critical value. A baseline case was selected as follows:

$$\begin{aligned} T_e &= 0.5(T_{e_{max}} + 1) \\ L &= 12 \text{ mm} \\ d &= 3 \text{ mm} \\ h_e &= 1{,}000 \text{ W/m}^2\text{·K} \end{aligned} \tag{63}$$

In Fig. 14, two of these parameters are held at their baseline values while the other two are varied over their expected range. In Figs. 14a, b, c, and d it is seen that both material thickness and convection heat transfer coefficient have significant influence on the maximum allowable environmental temperature for aluminum, copper, steel, and titanium. The influence of the convection heat transfer coefficient on the maximum allowable temperature is observed to be small for both tungsten and niobium carbide in Figs. 14e and f. The influence of material thickness is only moderate for niobium carbide in Fig. 14f. The observed effects are further validated in the cross-plots of the independent variables presented in Appendix F.

Figure 14. Maximum Allowable Environmental Temperature for Model I as a Function of Material Thickness and Convection Heat Transfer Coefficient

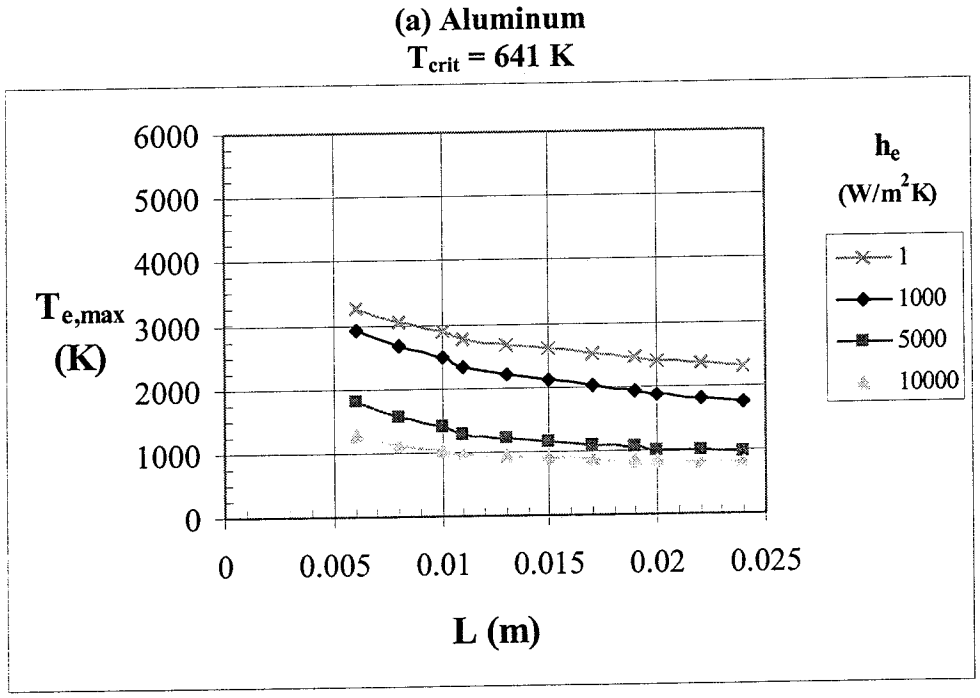

(b) Copper
T_{crit} = 1016 K

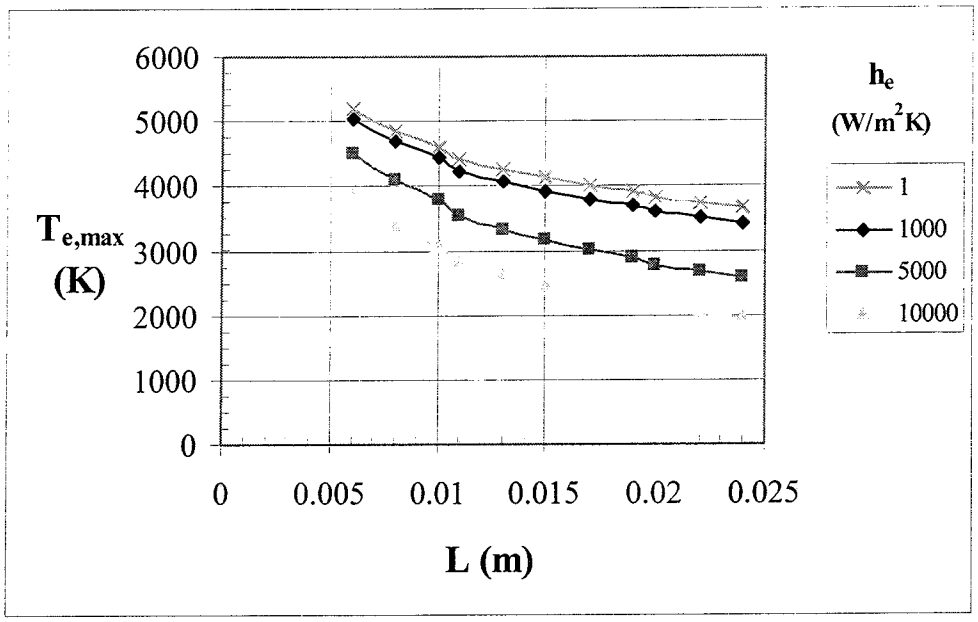

(c) Steel
T_{crit} = 1337 K

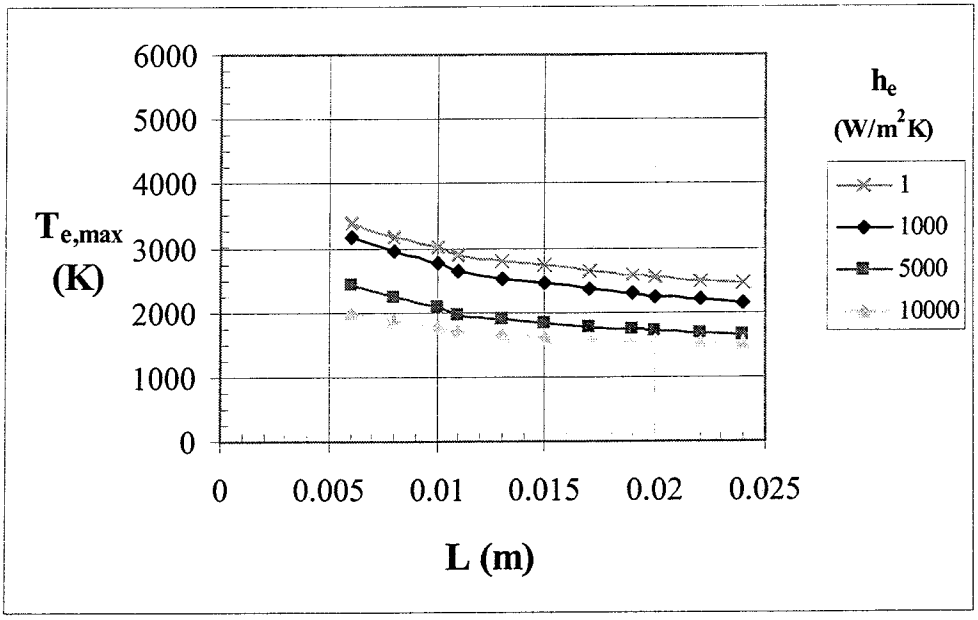

(d) Titanium
T_{crit} = 1464 K

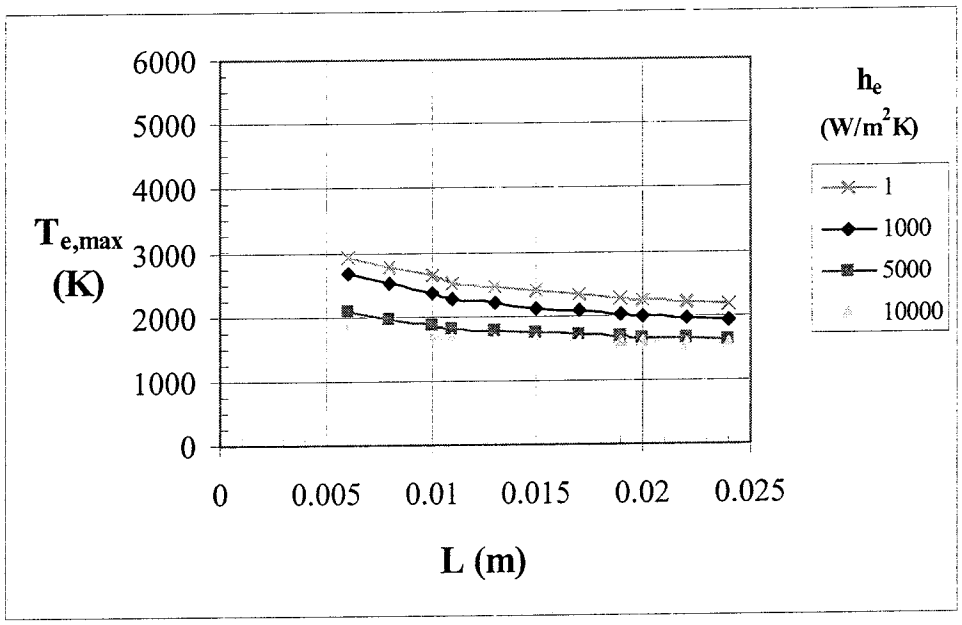

(e) Tungsten
T_{crit} = 2745 K

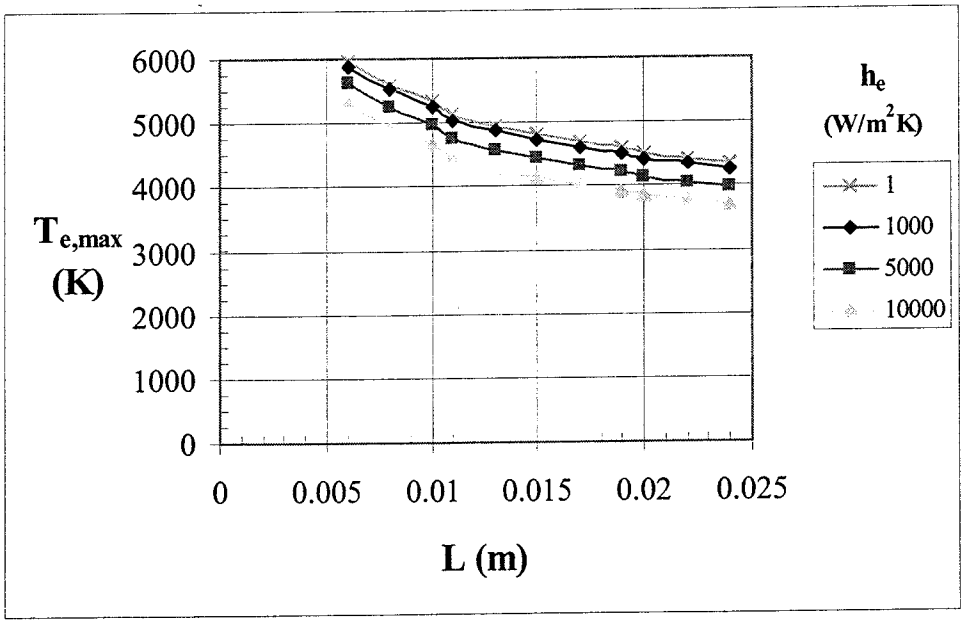

(f) Niobium Carbide
T_{crit} = 2917 K

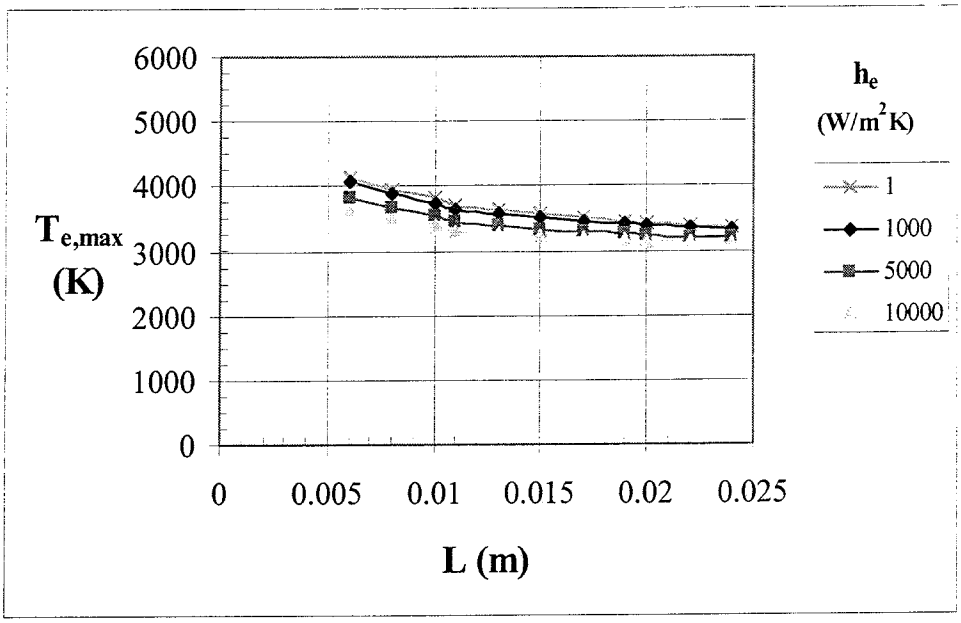

A direct comparison of the maximum environmental temperatures is presented in Fig. 15a for a specified value of convection heat transfer coefficient of 1,000 W/m^2·K. The ranking of these materials from highest to lowest is tungsten, copper, niobium carbide, steel, aluminum, and titanium. Copper ranks second in spite of its relatively low critical temperature because of its high thermal conductivity.

Another direct comparison of the maximum environmental temperatures is presented in Fig. 15b for a specified value of material thickness of 0.012m (0.47 in). The ranking of these materials is the same as in Fig. 15a except that the curves for copper and niobium carbide cross at high values of the heat transfer coefficient as do the curves for aluminum and tungsten.

When other important factors such as strength, weight, cost, and workability are considered, steel is an excellent choice among the metals for all but the most severe thermal conditions. The added weight, relatively high cost, and workability issues associated with tungsten limits its usability for most thermal environments. Since the ceramics are brittle and therefore not well suited for structural support, these results suggest that a layered combination of a ceramic such as niobium carbide for the exposed material and steel as the support material would be an effective design for severe thermal conditions.

Figure 15. Comparison of Maximum Allowable Environmental Temperature for Model I as a Function of Material Thickness and Convection Heat Transfer Coefficient

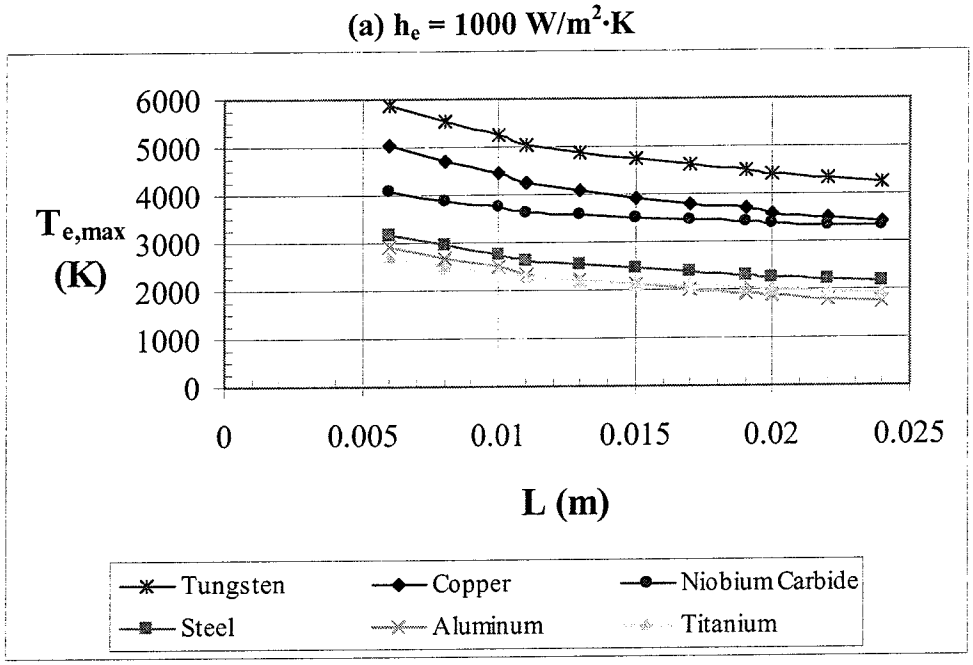

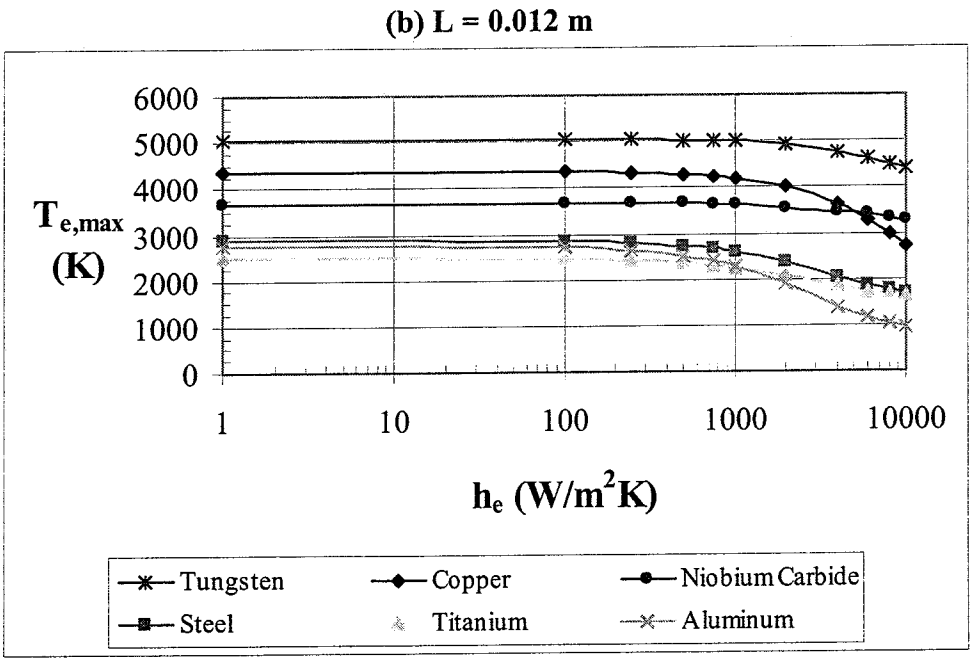

It is instructive to examine the actual values of the ratio β_{II}/β_I for the selected materials of this study when the surface temperature is at the material's critical value. The baseline case is the same as used in study of maximum allowable environmental temperature presented above, Eqn. (63).

Figs. 16, 17, and 18 show this ratio versus environmental temperature for selected values of the three remaining variables for each of the materials. The advantage of Model II over Model I is less than 10 percent for aluminum, copper, and tungsten for all combinations of environmental temperature and the other variables. Steel approaches an advantage of 20 percent and titanium 25 percent, with the greater advantages being at higher environmental temperature and material thickness. Niobium carbide also approaches an advantage of approximately 25 percent for higher temperature and larger thickness.

A comprehensive parametric study involving all combinations of the four independent variables is presented in Appendix G. The conclusions are as follows:

1. Aluminum and copper show advantages of Model II over Model I of less than 10 percent for all combinations of the design variables.

2. Tungsten shows advantages greater than 10 percent only for transpiration channels less than 2 mm in diameter.

3. Steel shows a maximum advantage of 20 percent.

4. Titanium and niobium carbide both show maximum advantages of approximately 30 percent.

Realization of these maximum gains requires small diameter channels, larger material thickness, and higher environmental temperatures. The added cost and complexity of Model II relative to Model I must be considered in selecting the final design.

Figure 16. Ratio of Dimensionless Mass Flow Rate Parameter, β, for Models II and I as a Function of Environmental Temperature and Material Thickness

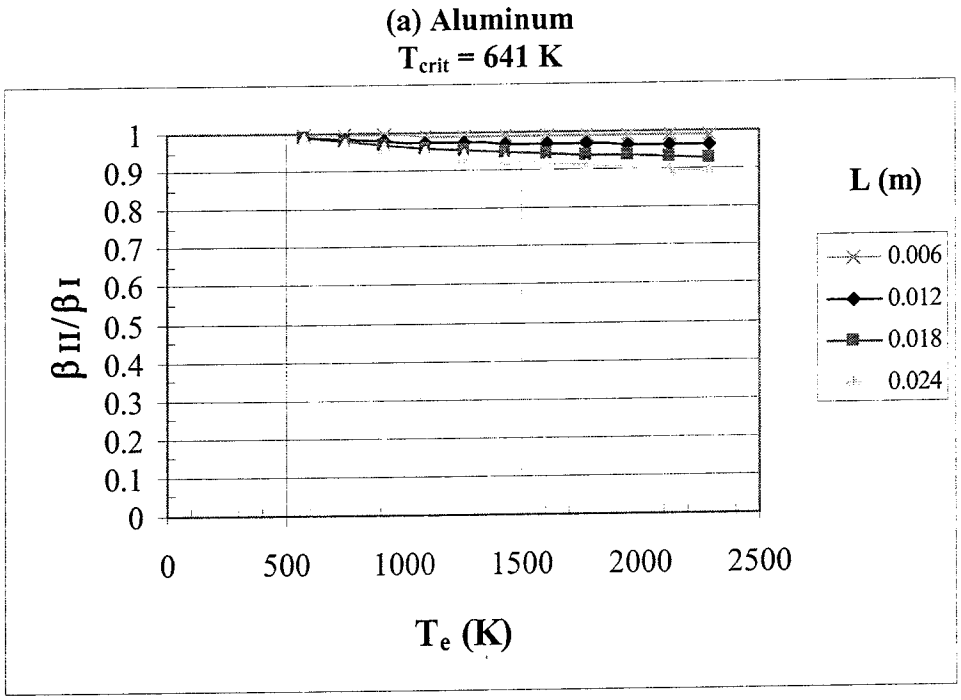

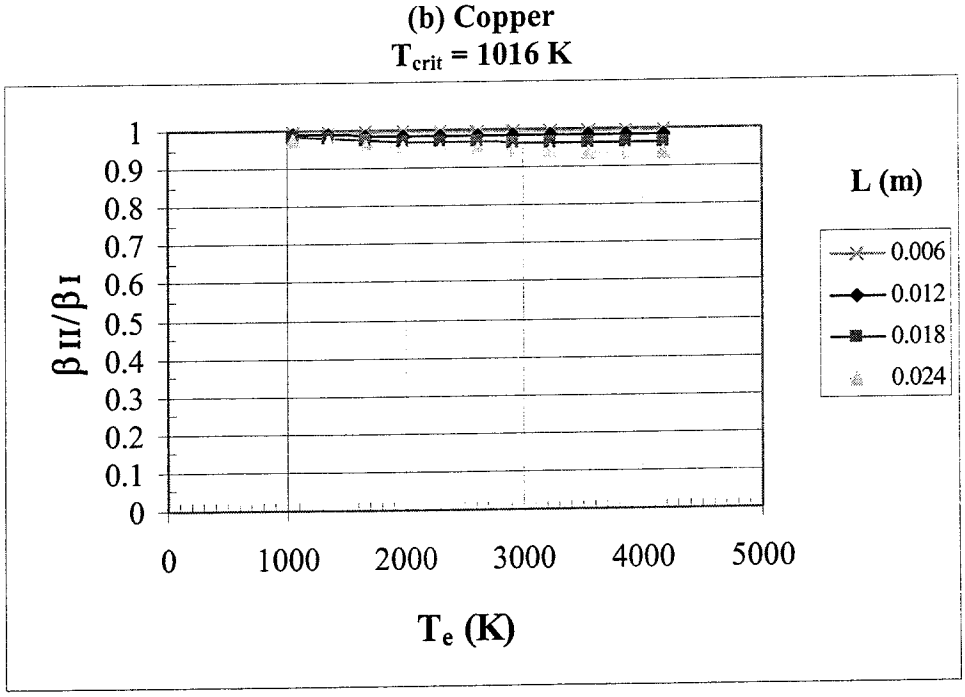

(c) Steel
T_{crit} = 1337 K

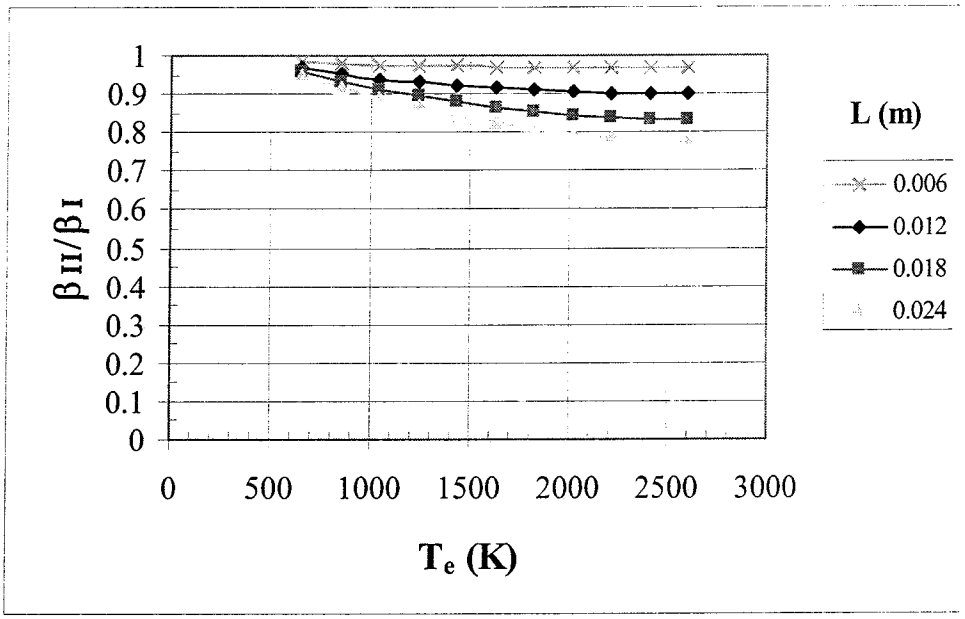

(d) Titanium
T_{crit} = 1464 K

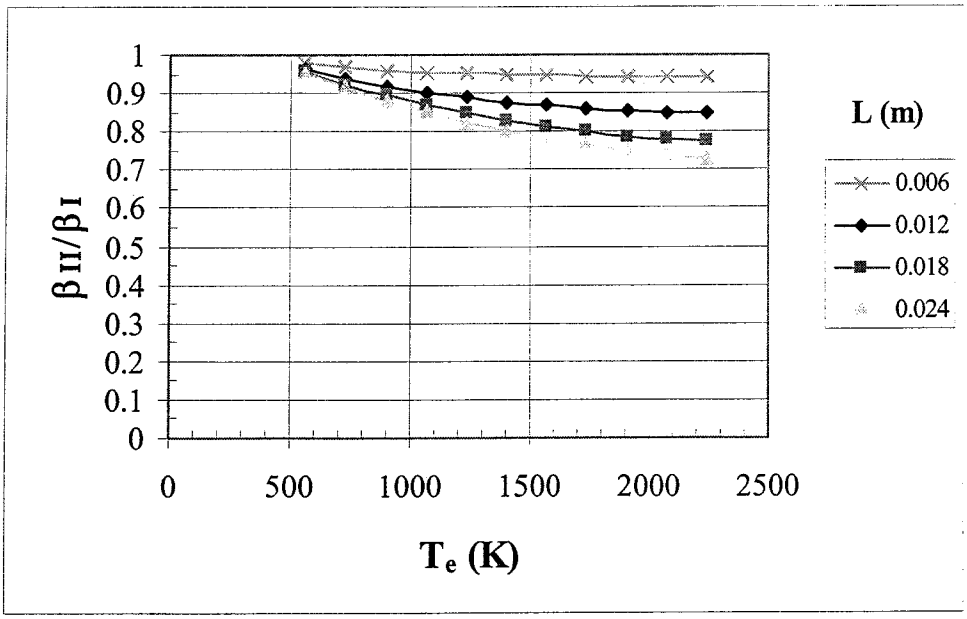

(e) Tungsten
T_{crit} = 2745 K

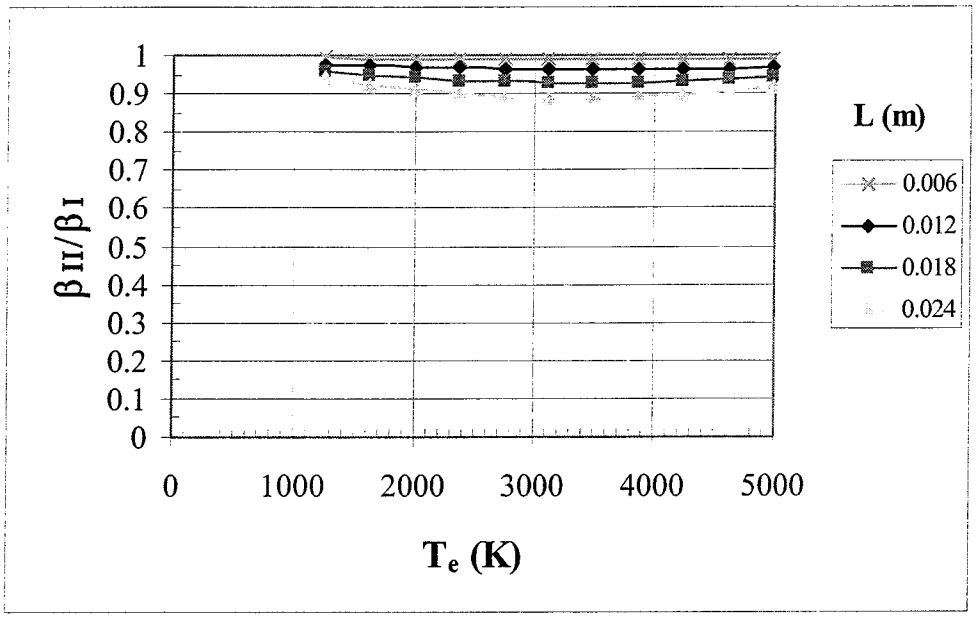

(f) Niobium Carbide
T_{crit} = 2917 K

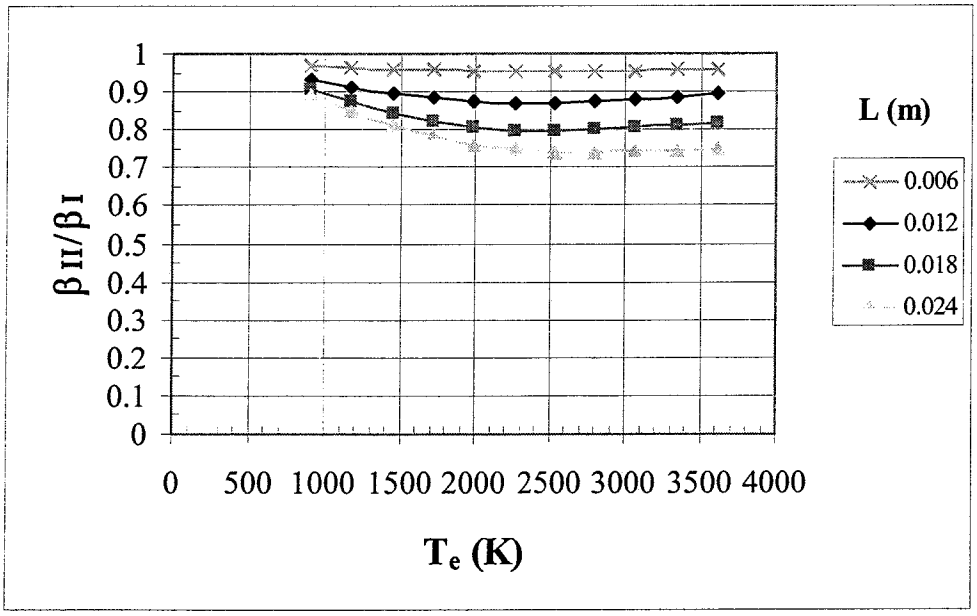

Figure 17. Ratio of Dimensionless Mass Flow Rate Parameter, β, for Models II and I as a Function of Environmental Temperature and Channel Diameter

(a) Aluminum
T_{crit} = 641 K

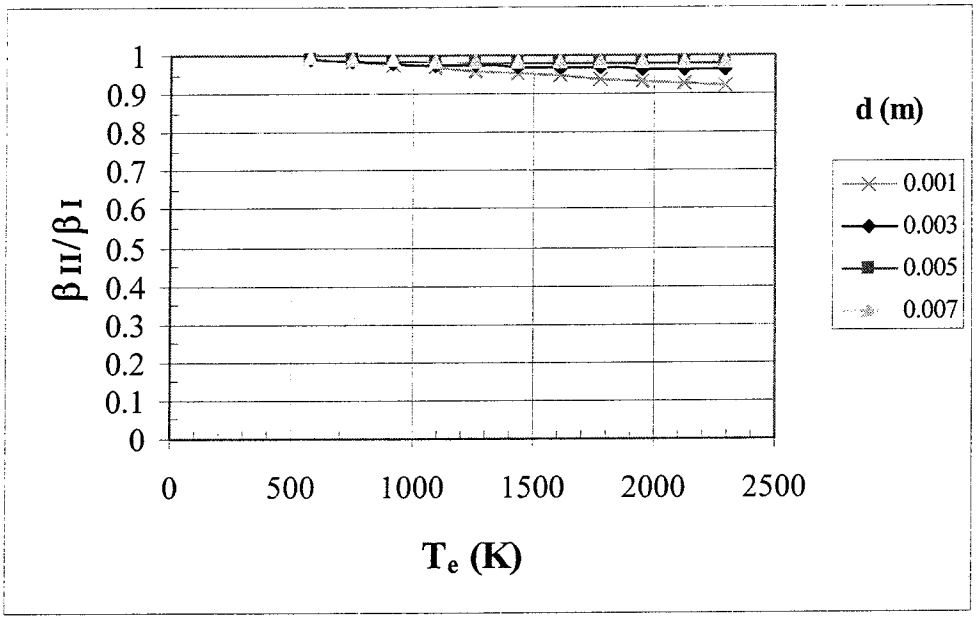

(b) Copper
T_{crit} = 1016 K

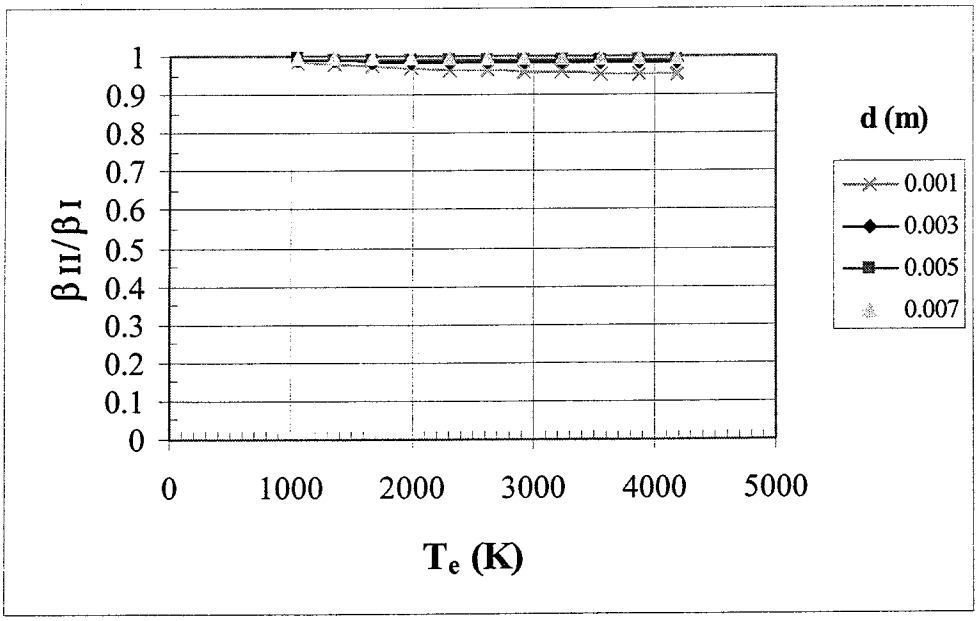

(c) Steel

T_{crit} = 1337 K

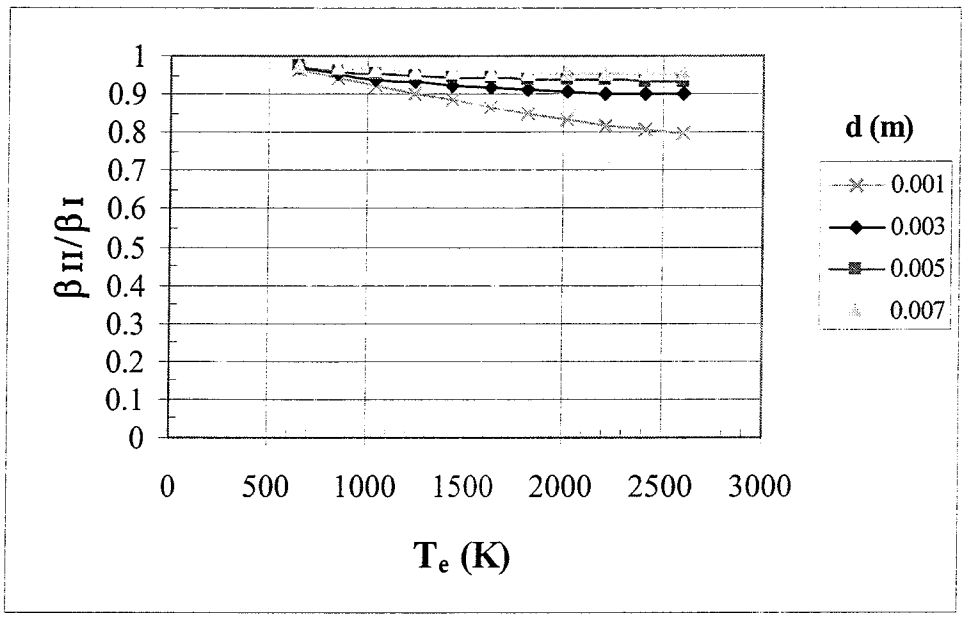

(d) Titanium

T_{crit} = 1464 K

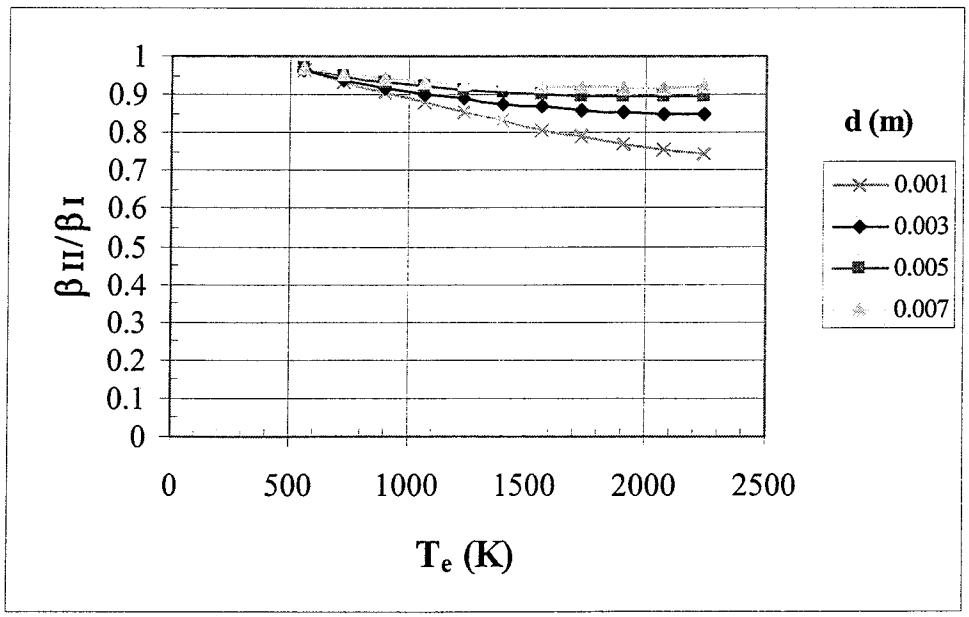

(e) Tungsten
T_{crit} = 2745 K

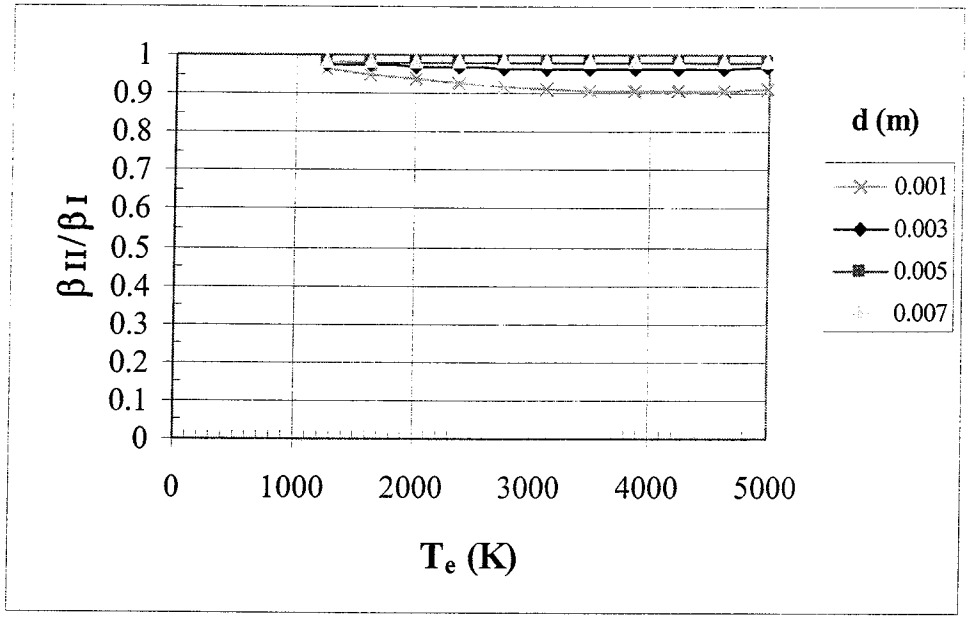

(f) Niobium Carbide
T_{crit} = 2917 K

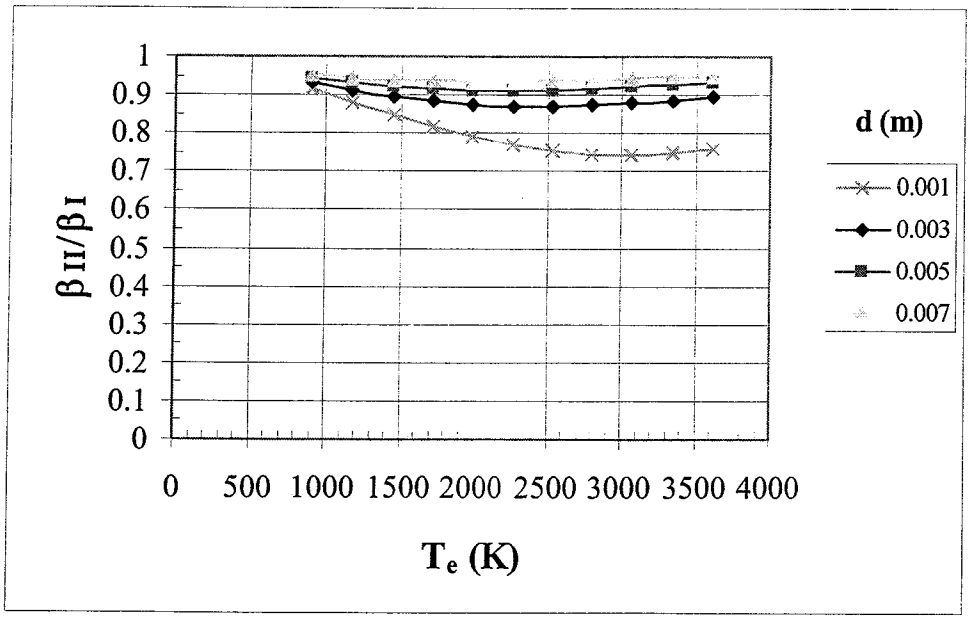

Figure 18. Ratio of Dimensionless Mass Flow Rate Parameter, β, for Models II and I as a Function of Environmental Temperature and Heat Transfer Coefficient

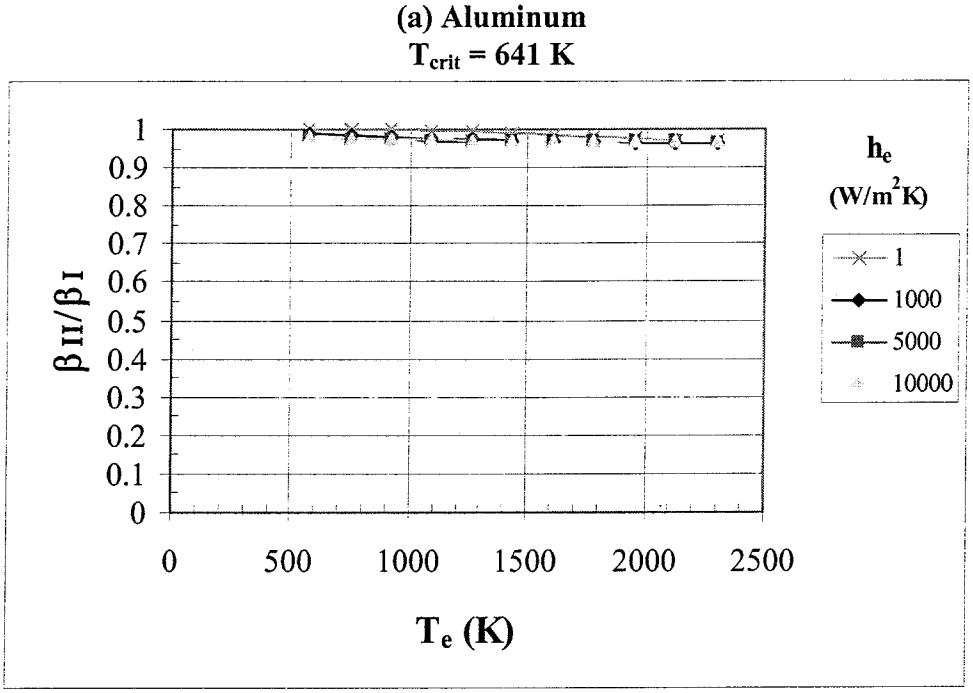

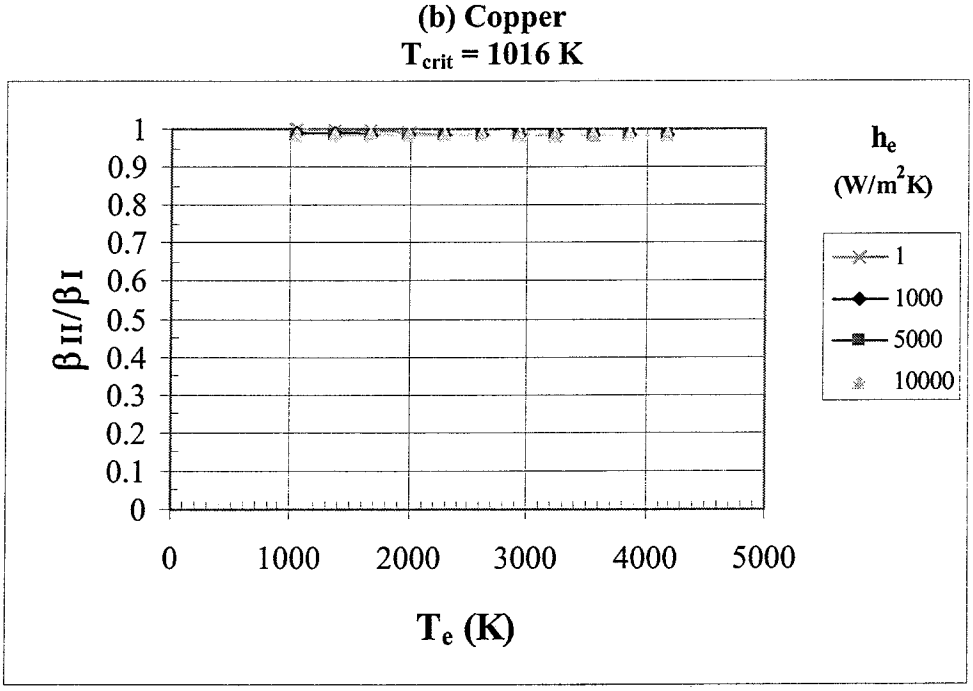

(c) Steel
T_{crit} = 2745 K

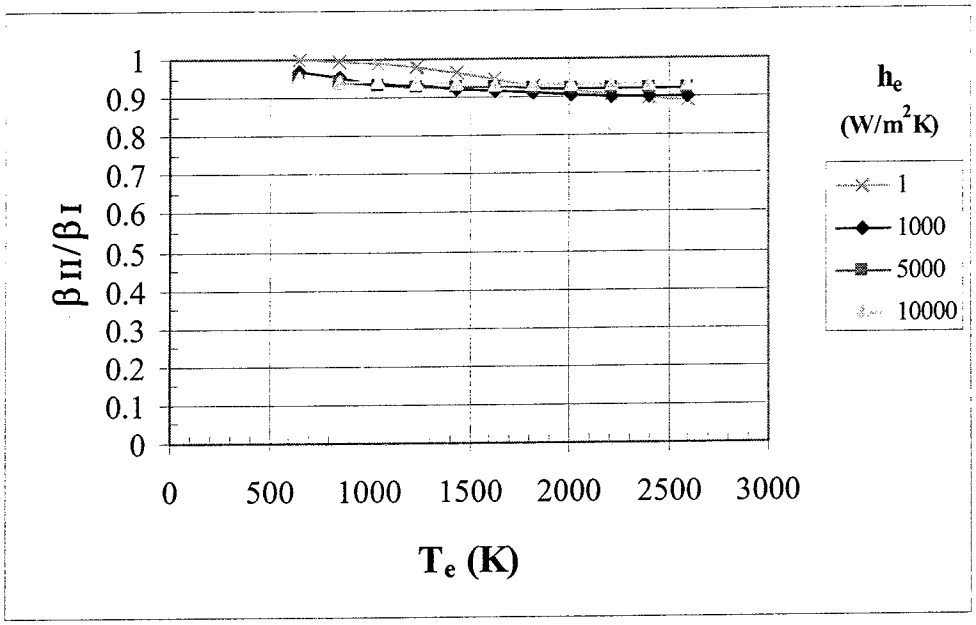

(d) Titanium
T_{crit} = 1464 K

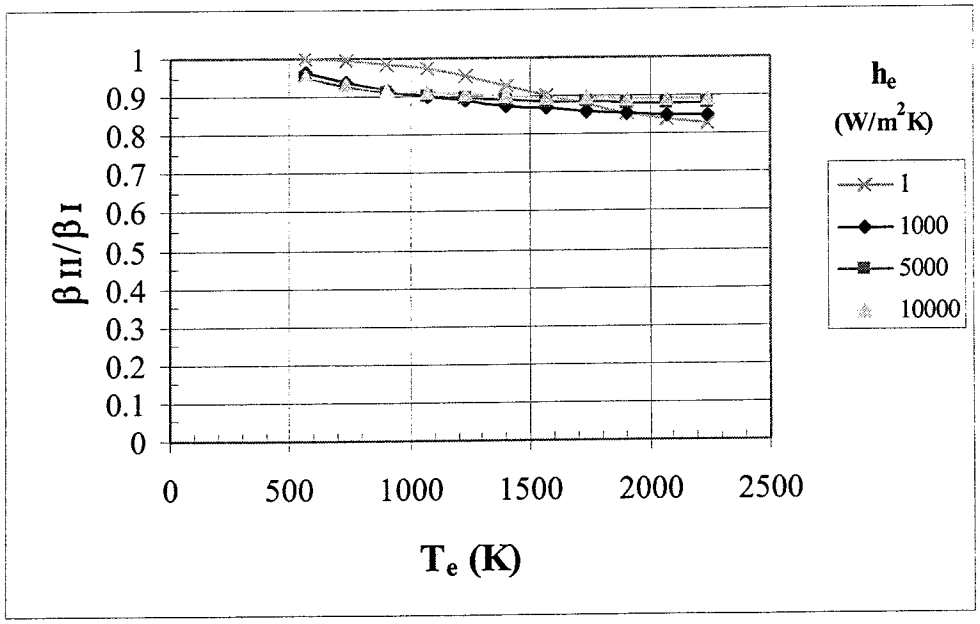

(e) Tungsten
T_{crit} = 2745 K

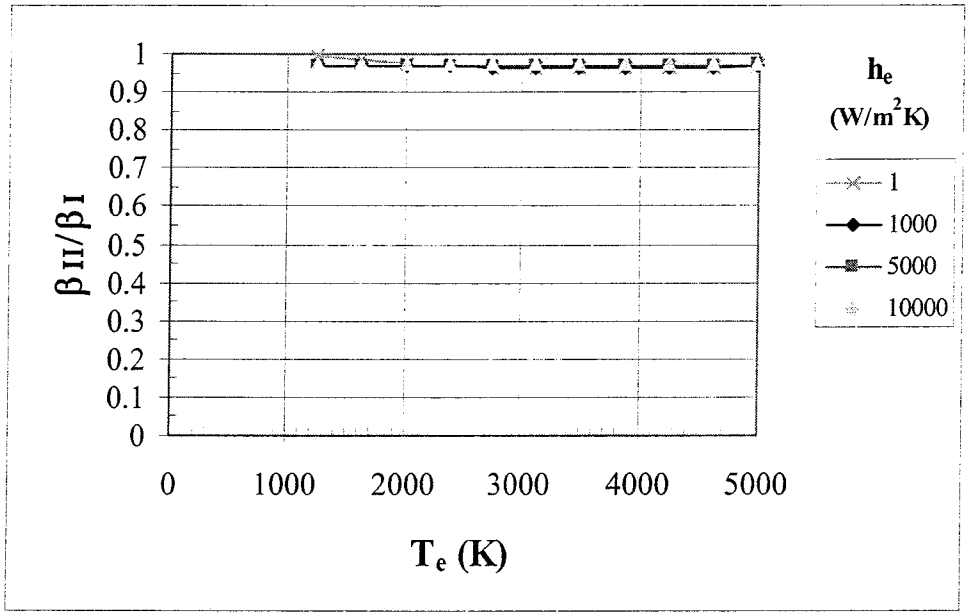

(f) Niobium Carbide
T_{crit} = 2917 K

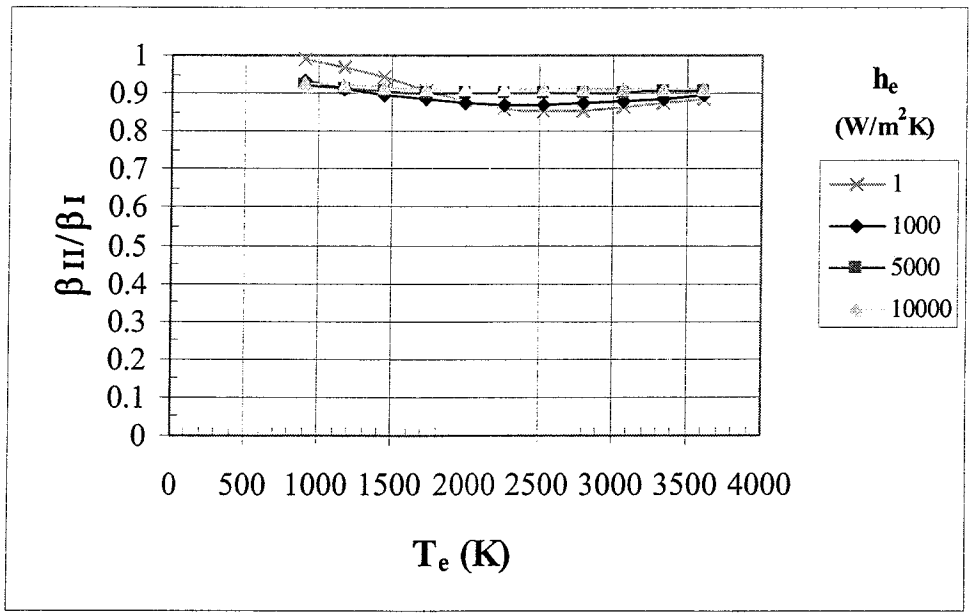

It is important to compare the dimensional mass flow rate per unit area as a function of environmental temperature for the selected materials as shown in Fig. 19. In these comparisons the surface temperature of each material is held at its critical value and the other independent variables are held at the baseline condition.

It is observed that there is little difference between Models I and II for any of the materials. Also, for environmental temperatures up to 2,200 K, the lowest mass flow rates are for titanium, niobium carbide, and steel – in that order. Niobium carbide and steel give the lowest values for temperatures between 2,300 – 2,600 K. For temperatures between 2,600 – 3,600 K, niobium carbide provides substantially lower flow rates than the other materials. Surprisingly, copper can handle temperatures between 3,600 – 4,200 K along with tungsten. From 4,200 – 5,000 K, tungsten is the only choice. However, as previously stated, tungsten has a severe oxidation problem that may preclude its selection.

A more complete parametric study is presented in Appendix H. The conclusion is that reductions of mass flow rate up to 20 percent may be achieved for some materials at combinations of thick walls, small diameter channels, and high environmental temperatures. However, small diameter channels typically have substantial problems with fouling which will limit their applicability.

Figure 19. Mass Flow Rate Per Unit Area for Models I and II as a Function of Environmental Temperature

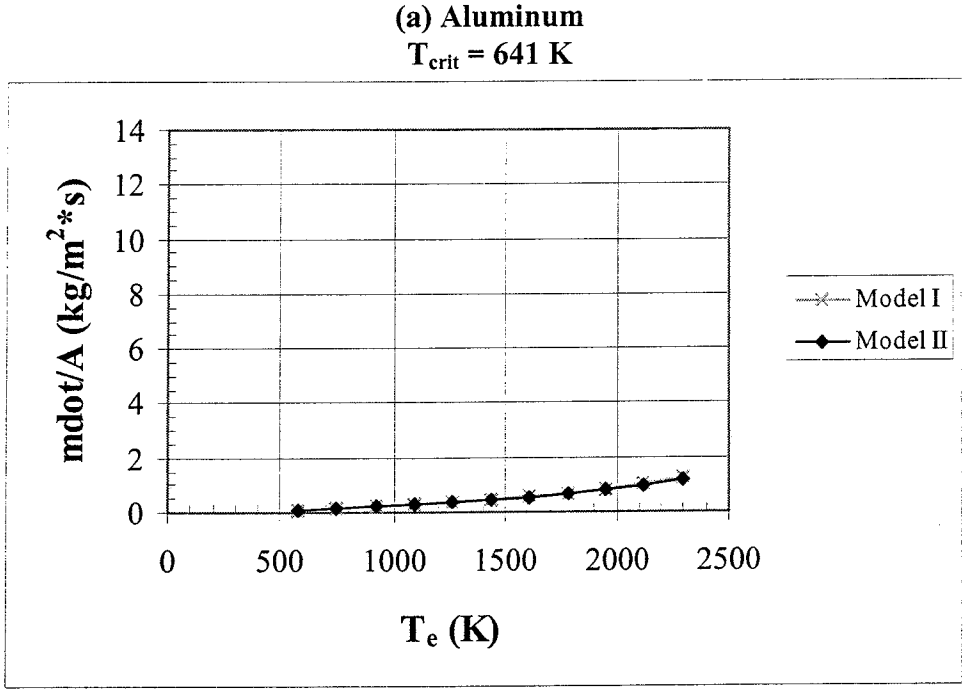

(b) Copper
T_{crit} = 1016 K

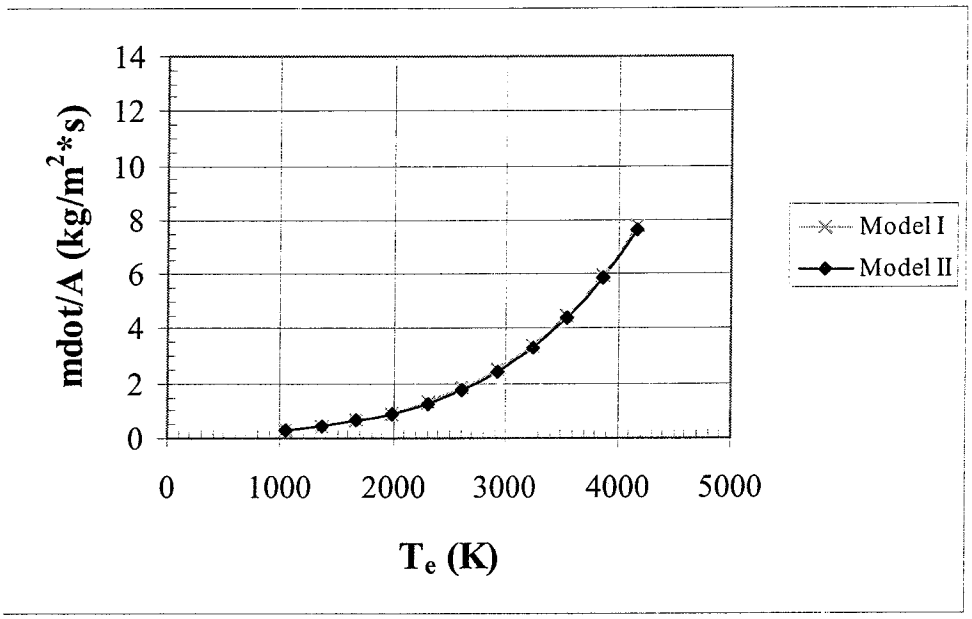

(c) Steel
T_{crit} = 1337 K

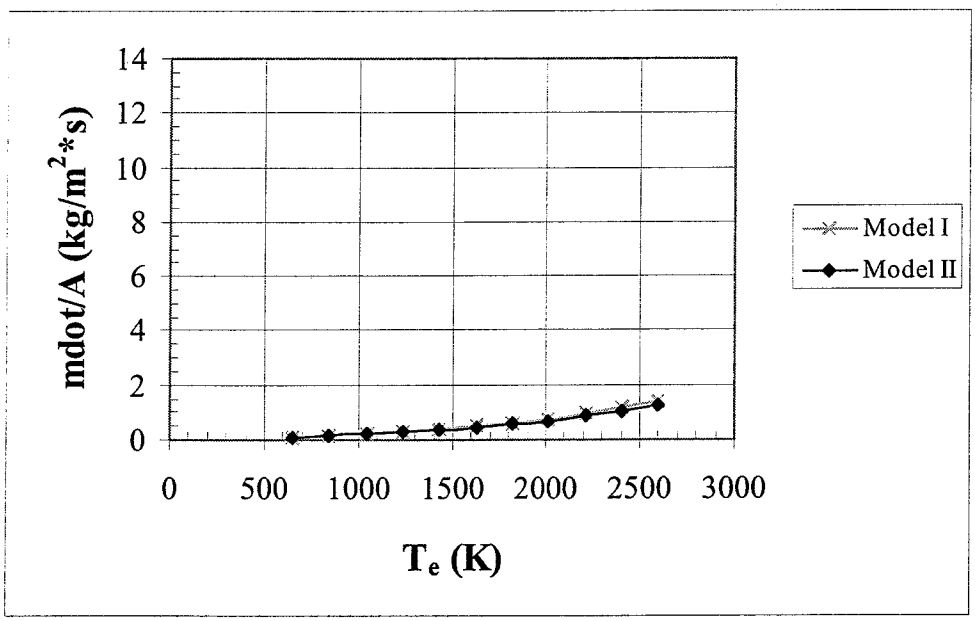

(d) Titanium
T_{crit} = 1464 K

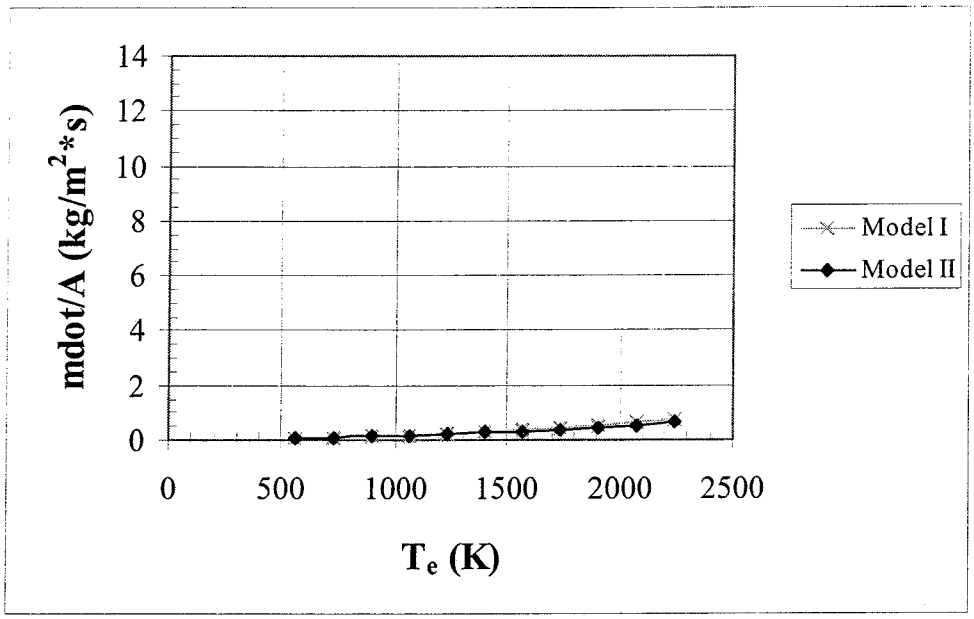

(e) Tungsten
T_{crit} = 2745 K

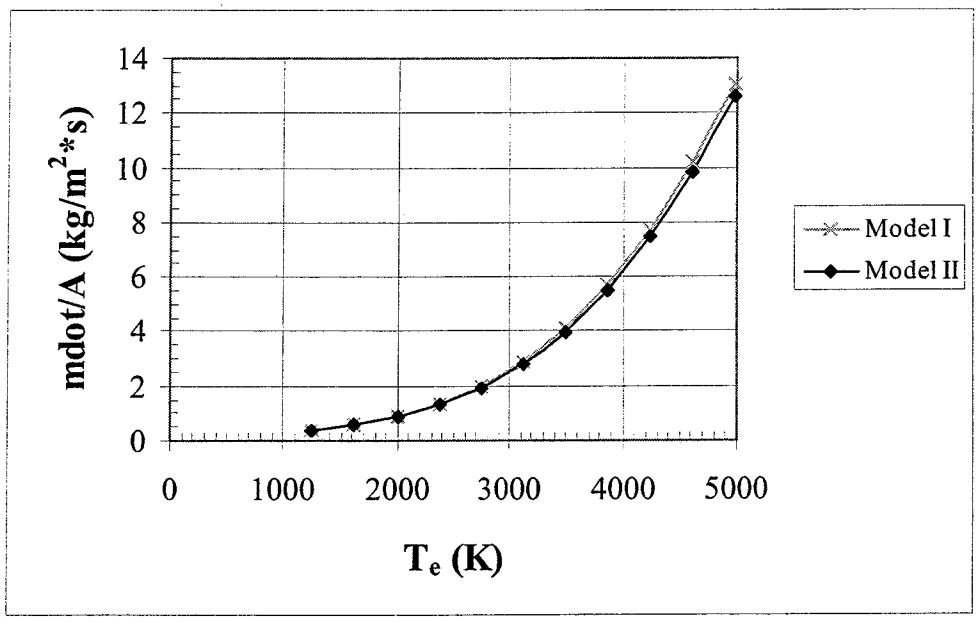

(f) Niobium Carbide
T_{crit} = 2917 K

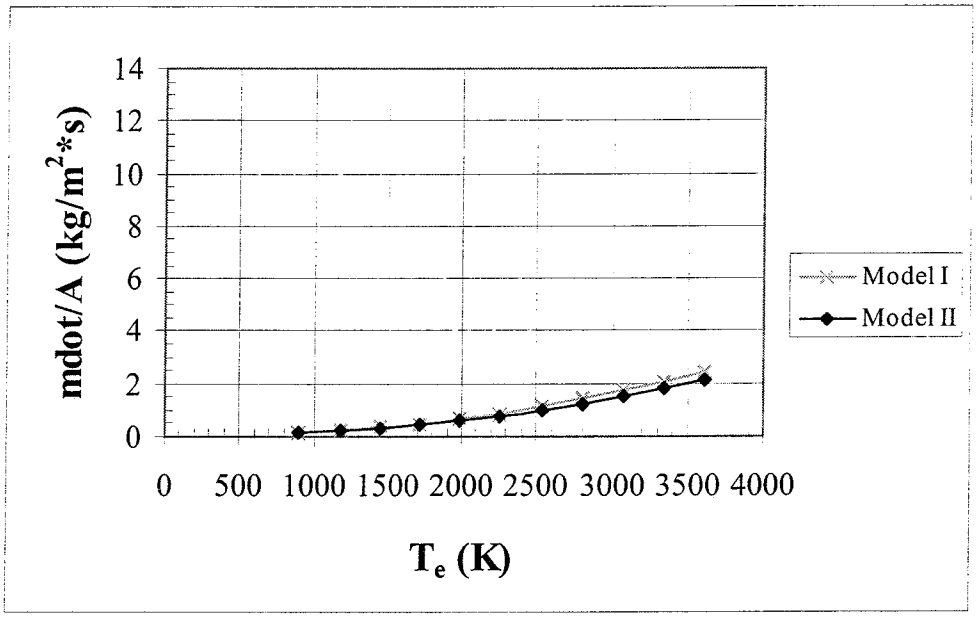

CHAPTER 4

MODEL III DEVELOPMENT AND APPLICATION

Mathematical Model

In Model III, there is sufficient flow in the channels to maintain the boiling condition at the exposed material surface. This avoids problems associated with a high surface temperature such as oxidation and loss of structural strength. However, there is a higher heat transfer rate from the environment due to the lower surface temperature and, therefore, more water flow is required. This chapter will explore the required increase in flow rate for Model III compared to Model I. The schematic of Model III is presented in Fig. 20.

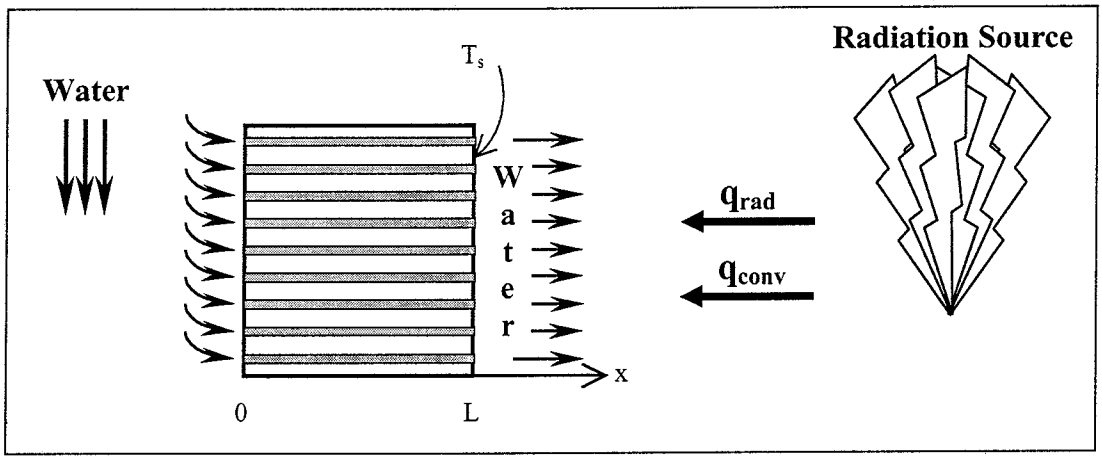

Figure 20. Schematic of Model III (Surface Transpiration Cooling)

The governing equation for the required mass flow rate to maintain boiling at the exposed surface is obtained from the heat balance between the radiation and convection from the environment to the water.

$$\frac{q_{rad}}{A} + \frac{q_{conv}}{A} = \frac{q_{trans}}{A} \tag{64}$$

where

$$\frac{q_{rad}}{A} + \frac{q_{conv}}{A} = \sigma\varepsilon(T_e^4 - T_s^4) + \bar{h}_e(T_e - T_s) \tag{65}$$

and

$$\frac{q_{trans}}{A} = \left[\frac{q_{latent}}{A}\right] + \left[\frac{q_{sensible}}{A}\right] = \left[\frac{\dot{m}}{A} h_{fg}\right] + \left[\frac{\dot{m}}{A} C_{p\,liquid}(T_{boil} - T_{initial})\right] \tag{66}$$

Therefore,

$$\sigma\varepsilon(T_e^{\,4} - T_s^{\,4}) + \bar{h}_e(T_e - T_s) = \frac{\dot{m}}{A}\left[h_{fg} + C_{p\,liquid}(T_{boil} - T_{initial})\right] \tag{67}$$

or

$$\frac{\dot{m}}{A} = \left[\sigma\varepsilon(T_e^{\,4} - T_s^{\,4}) + \bar{h}_e(T_e - T_s)\right] \cdot \left[\frac{1}{h_{fg} + C_{p\,liquid}(T_{boil} - T_{initial})}\right] \tag{68}$$

Comparison of Models I and III

The only independent variable in Eqn. (68) is the environmental temperature. It is assumed that the surface temperature is maintained 20 K above the boiling which is 393 K for the standard sea level condition. A comparison of the mass flow rate versus environmental temperature for Model III compared to Model I for the selected materials of this study is shown in Fig. 21. Model III is the same for all materials as no material properties appear in Eqn. (68). For Model I, all materials are at the baseline condition, Eqn. (63), and the surface temperature of each material is its critical temperature.

It is observed in Fig. 21a that above 3,600 K, Model III requires only moderately more water than copper or tungsten. The maximum difference is approximately 19 percent at 5,000 K. It is concluded that Model III is the better design choice in this temperature range since a relative strong, ductile, and inexpensive material such as steel can be used.

From Fig. 21b, it is observed that, in the range from 2,300 – 3,600 K, Model III requires an increase in mass flow rate from 50 – 80 percent over niobium carbide. In this region, Model I using niobium carbide or some other suitable ceramic may be a reasonable design alternative.

Finally, Fig. 21c indicates that, in the range below 2,300 K, Model III requires nominally 50 percent more mass flow than titanium or niobium carbide. Again, this is a sufficient difference to warrant consideration of Model I with either of these materials.

Figure 21. Comparison of Mass Flow Rate as a Function of Environmental Temperature for Model I and Model III

(a) Environmental Temperature 0 – 5000 K
$(T_s = T_{crit})_I$, $(T_s = 393\ K)_{III}$; $h_e = 1000\ W/m^2 \cdot K$; L = 0.012 m

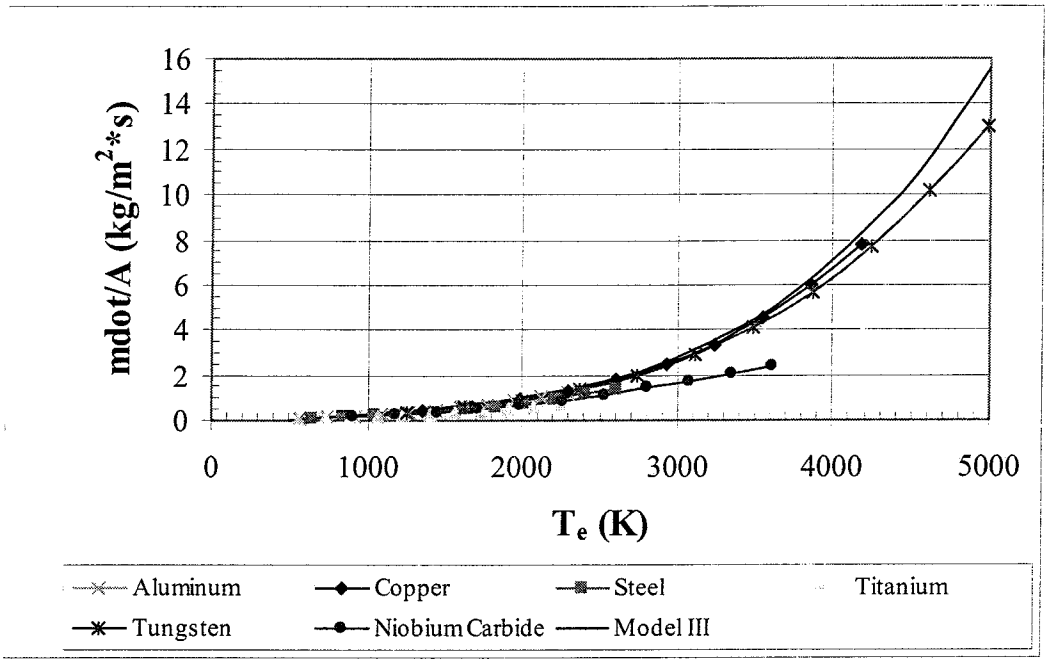

(b) Environmental Temperature 0 – 4000 K
$(T_s = T_{crit})_I$, $(T_s = 393\ K)_{III}$; $h_e = 1000\ W/m^2 \cdot K$; L = 0.012 m

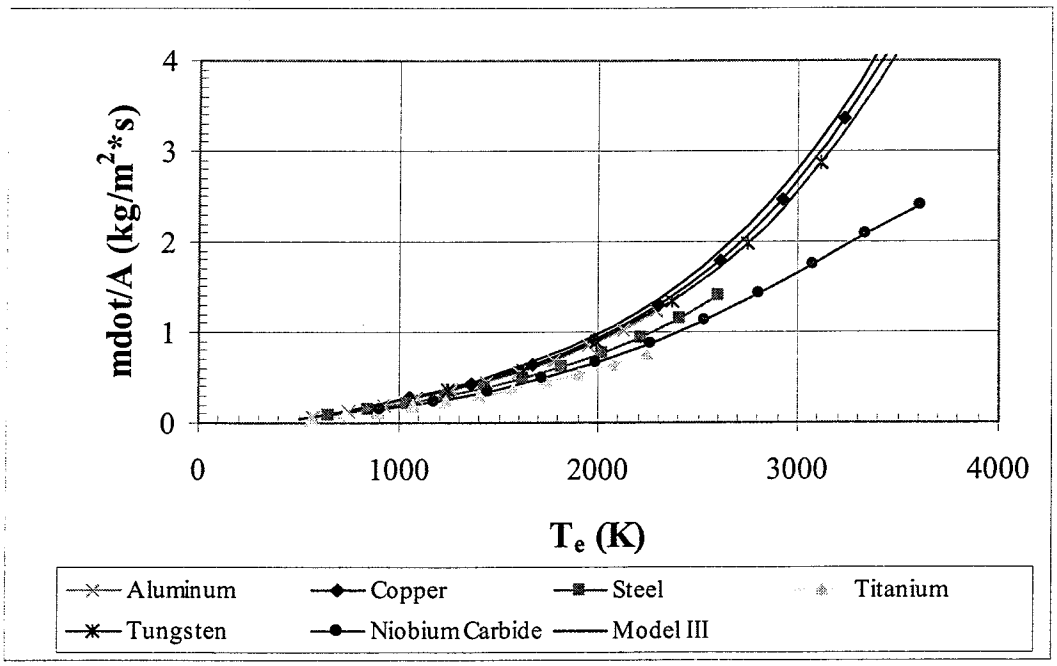

(c) Environmental Temperature 0 – 2000 K
($T_s = T_{crit})_I$, $(T_s = 393\ K)_{III}$; $h_e = 1000\ W/m^2 \cdot K$; L = 0.012 m

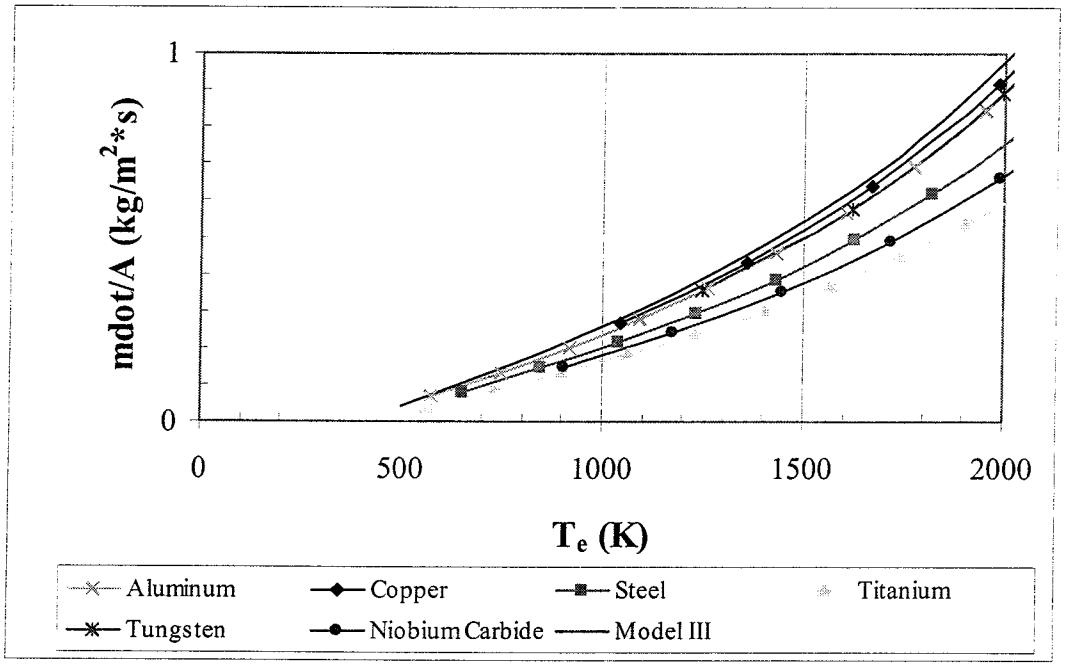

CHAPTER 5

CONCLUSIONS AND RECOMMENDATIONS

Summary of General Approach

There are three approaches explored in the present study for the utilization of transpiration cooling for thermal protection. They are summarized as follows:

- Model I has an impermeable wall with a boiling water backface. The temperature of the exposed surface is limited to the maximum operating temperature of the material.

- Model II has a permeable wall with a boiling water backface. However, in this model, heat is also added to the water vapor as it flows in channels toward the exposed surface. As in Model I, the temperature of the exposed surface can be as high as the maximum operating temperature of the material.

- Model III has a permeable wall with a boiling condition at the surface of the exposed material. The exposed surface is therefore maintained at a temperature 20 K above the boiling temperature of the water.

The comparative advantage of Model II is that it minimizes the water flow rate required to maintain the exposed surface at or below its maximum operating temperature. The disadvantages are the additional cost of fabrication of the permeable materials, the operational problems of maintaining unrestricted flow of the water through the channels under all operating scenarios, and problems associated with high surface temperature.

The advantages of Model I are lower fabrication costs and reduced operational problems. The disadvantages are higher required water flow rates for a design surface temperature, additional insulation requirements for the boiling area in some applications, and problems associated with high surface temperature.

Model III has the advantage of avoiding problems associated with high surface temperature such as reduced structural strength and oxidation. It has the disadvantage of having the largest water flow rates of the three approaches.

This study provides quantitative results, which can be used as a basis for selection of the most suitable approach for a given application. A computer program is provided with this report that allows the user to calculate the surface temperature and the water mass rate for any selected material properties and thermal conditions. The description of the program and user instructions are presented in Appendix I.

Conclusions

In this study, the governing equations for the models were developed in non-dimensional form and a comprehensive parametric investigation of the effects of the independent variables on the important dependent variables was performed. In addition, detailed analyses were performed for selected materials to evaluate the practical limitations of the results of the parametric study. The conclusions are classified by model type as follows:

Model I:

- For sufficiently thin walls using a boiling water backface, even materials with low critical temperatures like aluminum can be used in very high temperature environments. However, for very high environmental temperatures in more practical engineering applications, the thickness or more properly, thinness requirement, is often not achievable because of structural requirements.

- Material selection for Model I is limited by the highest anticipated environmental temperature. The ranking of these materials from highest to lowest is tungsten up to 5,000 K, copper up to 4,000 K, niobium carbide up to 3,800 K, steel up to 2,700 K, aluminum up to 2,300 K, and titanium up to 2,200 K. Copper ranks second in spite of its relatively low critical temperature because of its high thermal conductivity. In practice, the use of these materials at these temperatures may be limited by unacceptable oxidation.

Model II:

From the non-dimensional parametric analyses, the advantages of Model II over Model I in terms of reduction of required mass flow rate are summarized as follows:

- Aluminum and copper show advantages of Model II over Model I of less than 10 percent for all combinations of the design variables.

- Tungsten shows advantages greater than 10 percent only for transpiration channels less than 2 mm in diameter.

- Steel shows a maximum advantage of 20 percent.

- Titanium and niobium carbide both show maximum advantages of approximately 30 percent.

When the analyses were conducted for the selected materials over the entire range of anticipated environmental conditions, the following conclusions were reached:

- Realization of the above maximum gains requires small diameter channels, larger material thickness, and higher environmental temperatures. However, small diameter channels typically have substantial problems with fouling which will limit their applicability. The added cost and complexity of Model II relative to Model I must be considered in selecting the final design.

- When other important factors such as strength, weight, cost, and workability are considered, steel is an excellent choice among the metals for all but the most severe thermal conditions.

- The added weight, relatively high cost, and workability issues associated with tungsten limits its usability for most thermal environments.

- Since the ceramics are brittle and therefore not well suited for structural support, these results suggest that a layered combination of a ceramic such as niobium carbide for the exposed material and steel or aluminum as the support material would be an effective design for severe thermal conditions.

Model III:

In Model III, there is sufficient flow in the channels to maintain the boiling condition at the exposed material surface. This avoids problems associated with a high surface temperature such as oxidation and loss of structural strength. However, there is a higher heat transfer rate from the environment due to the lower surface temperature and, therefore, more water flow is required. This study established these water flow requirements as follows:

- Above 3,600 K, Model III requires only moderately more water than Model I. The maximum difference is approximately 19 percent at 5,000 K. It is concluded that Model III is the better design choice in this temperature range since a relative strong, ductile, and inexpensive material such as steel can be used.

- In the range from 2,300 – 3,600 K, Model III requires an increase in mass flow rate from 50 – 80 percent over niobium carbide. In this region, Model I using niobium carbide or some other suitable ceramic may be a reasonable design alternative.

- Below 2,300 K, Model III requires nominally 50 percent more mass flow than titanium or niobium carbide. Again, this is a sufficient difference to warrant consideration of Model I with either of these materials.

Models II and III have an additional potential advantage that was not evaluated in this study. When the water vapor is injected into the high temperature thermal environment, it will have a cooling effect. Specifically, this is expected to reduce the convection heat transfer coefficient. For large injection rates, this effect could be significant.

Recommendations

Based on the conclusions of this study, the following recommendations are made for application of these models to the NASA-SSC thermal protection problems:

- For the severe thermal environment of the flame buckets, Model III should be used in the impingement regions. Model I with a layered combination of a ceramic, such as niobium carbide for the exposed material and steel or aluminum as the support material, should be used in the peripheral areas.

- For thermal protection of personnel and equipment under conventional fire conditions, Model I should be used with steel or aluminum as the wall material.

The use of Model II should be limited to a restricted range of design requirements as its disadvantages outweigh its advantages for most materials and environmental conditions.

REFERENCES

1. Gamblin, Tonya Pleshette, "Thermal Insulation System for Large Flame Buckets," Master's Thesis, Louisiana Tech University, November 1996.

Also as

Callens, E. Eugene, Jr. and Tonya Pleshette Gamblin, "Thermal Insulation System for Large Flame Buckets," Final Report for NASA Stennis Space Center, Contract No. NASA (1995)-Stennis-06, Louisiana Tech University, October 1996.

2. Yano, Toshikazu, Masao Ochi, and Shintaro Enya, "Protection Against Fire and High Temperature by Using Porous Media and Water", ASME/JSME Thermal Engineering Proceedings, Volume 4, pp. 213-218, 1991.

3. Avallone, Eugene A. and Theodore Baumeister, III, eds., Marks' Standard Handbook for Mechanical Engineers, 10th Ed., McGraw-Hill, New York, 1996.

4. Incropera, Frank P. and David P. Dewitt, Fundamentals of Heat and Mass Transfer, 4th Ed., John Wiley & Sons, New York, 1996.

APPENDIX A

PARAMETRIC STUDY OF THE AXIAL WALL AND VAPOR TEMPERATURE DISTRIBUTIONS

Figure A1. Parametric Study of the Axial Wall and Vapor Temperature Distributions

(a) $[T_e/T_{bf}=2]$, $\Lambda=10^{-3}$, Bi=5, $\gamma=2$, $\alpha=8.6523$

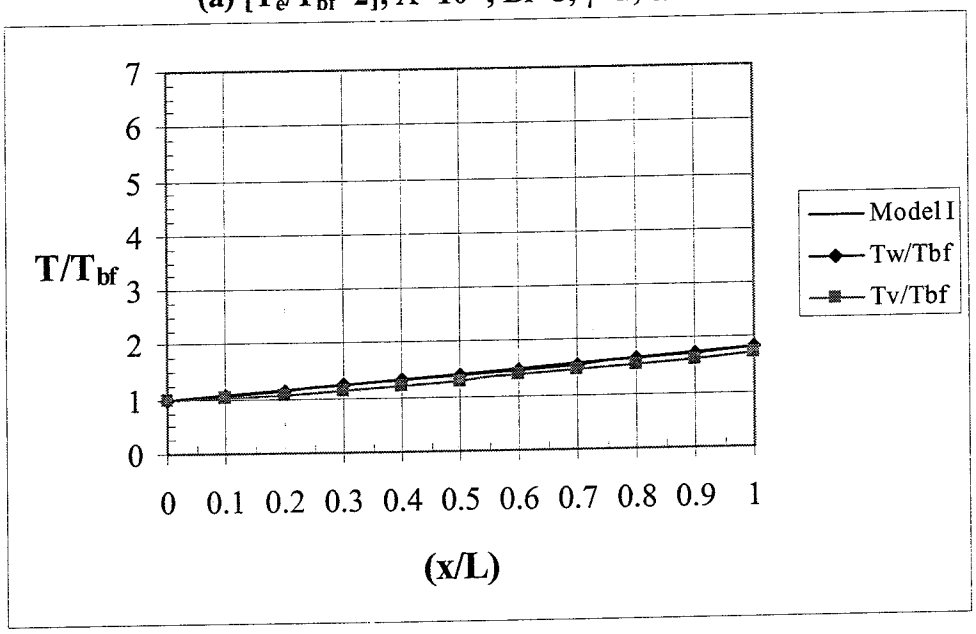

(b) $[T_e/T_{bf}=4]$, $\Lambda=10^{-3}$, Bi=5, $\gamma=2$, $\alpha=3.1823$

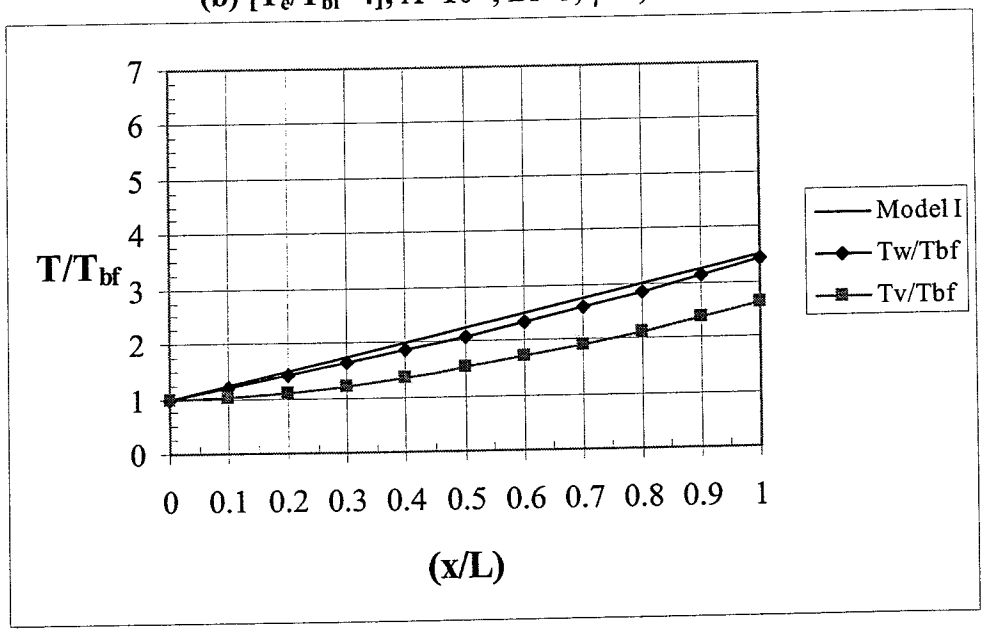

(c) $[T_e/T_{bf}=6]$, $\Lambda=10^{-3}$, Bi=5, $\gamma=2$, $\alpha=1.9742$

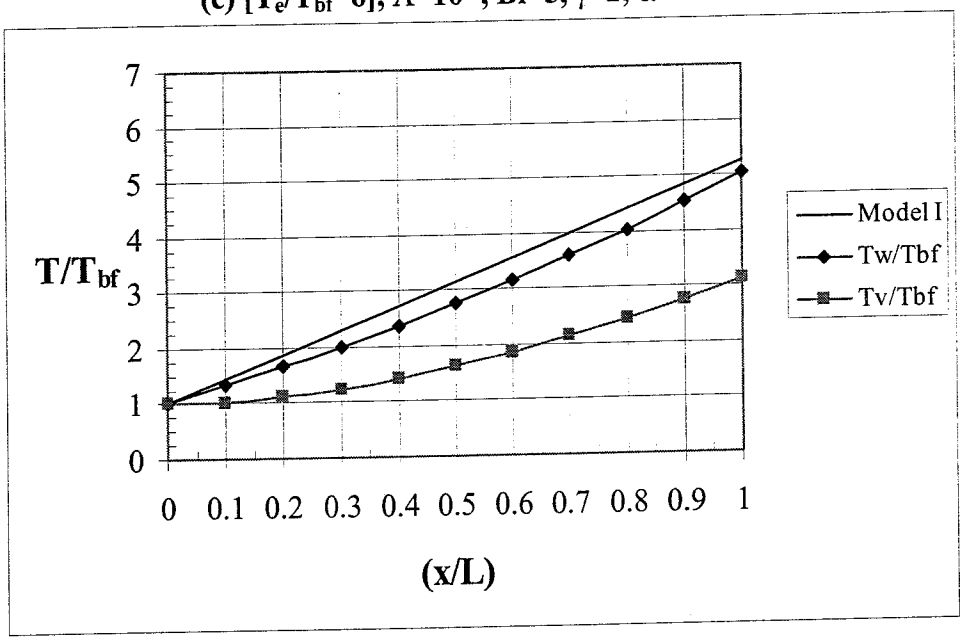

(d) $[T_e/T_{bf}=8]$, $\Lambda=10^{-3}$, Bi=5, $\gamma=2$, $\alpha=1.4125$

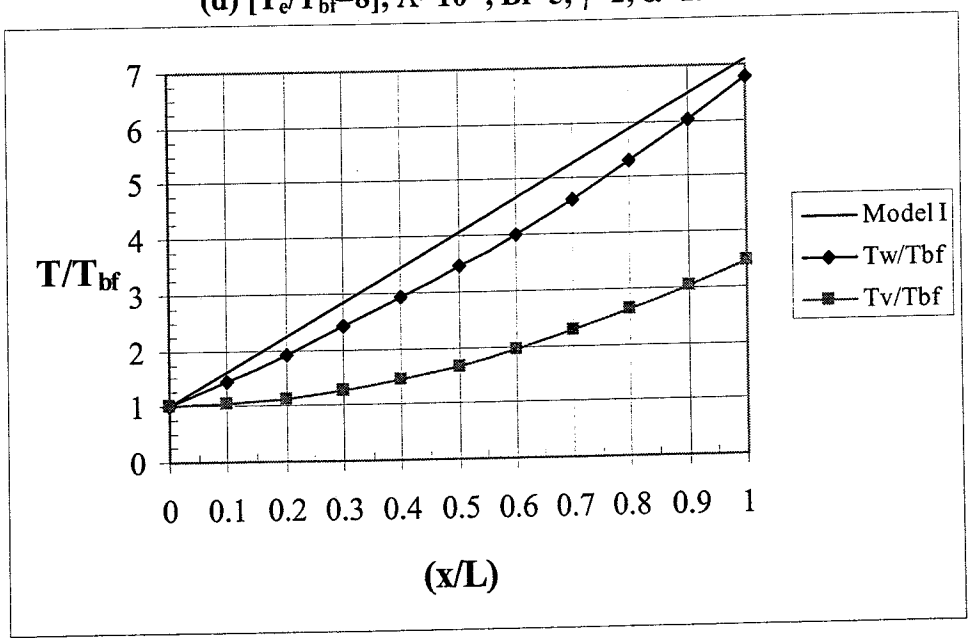

(e) $T_e/T_{bf}=6$, [$\Lambda=10^{-5}$], Bi=5, $\gamma=2$, $\alpha=2.0202$

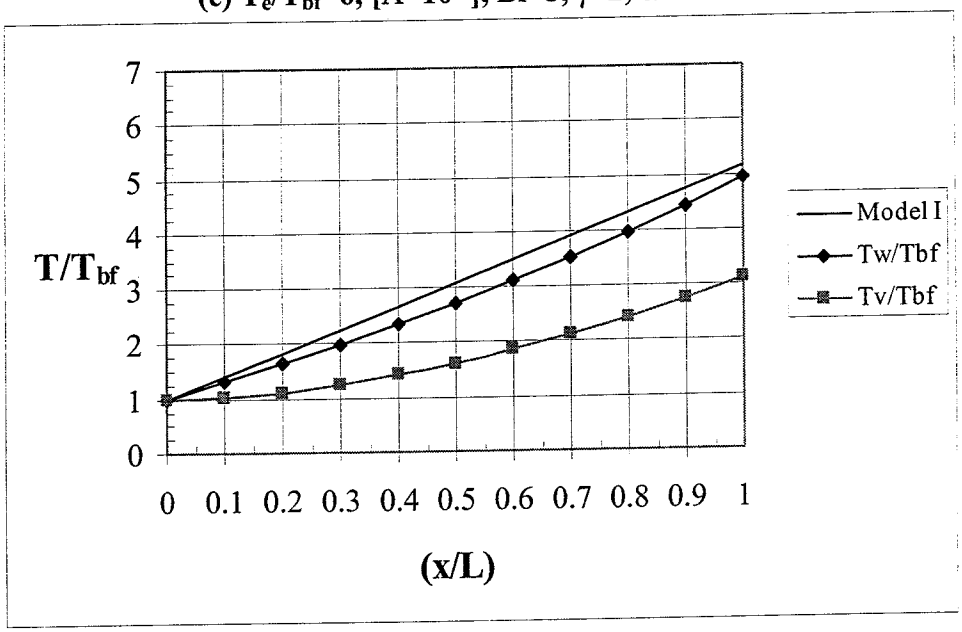

(f) $T_e/T_{bf}=6$, [$\Lambda=10^{-4}$], Bi=5, $\gamma=2$, $\alpha=2.0156$

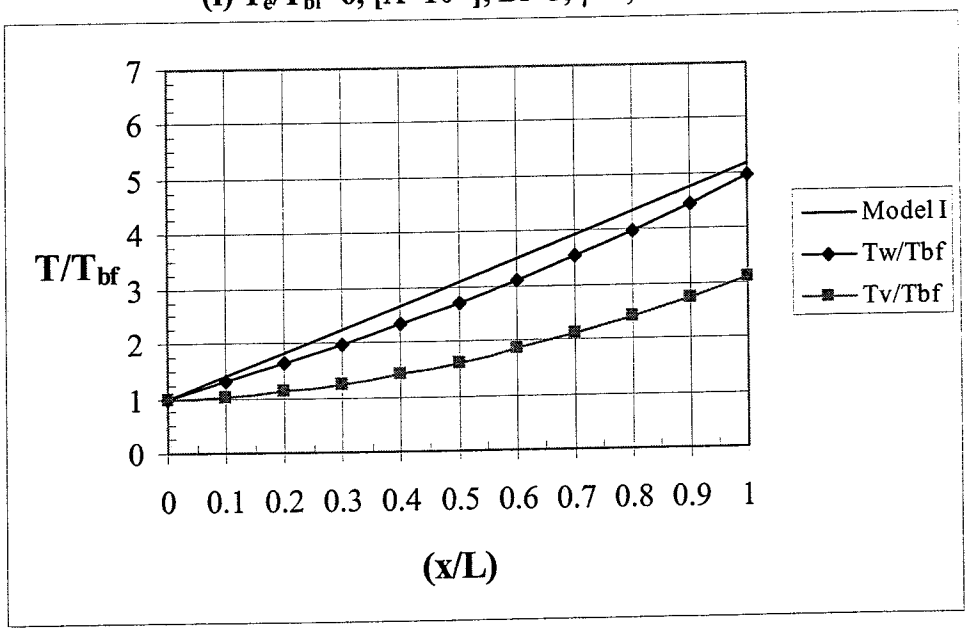

(g) T_e/T_{bf}=6, [$\Lambda=10^{-2}$], Bi=5, γ=2, α=1.7816

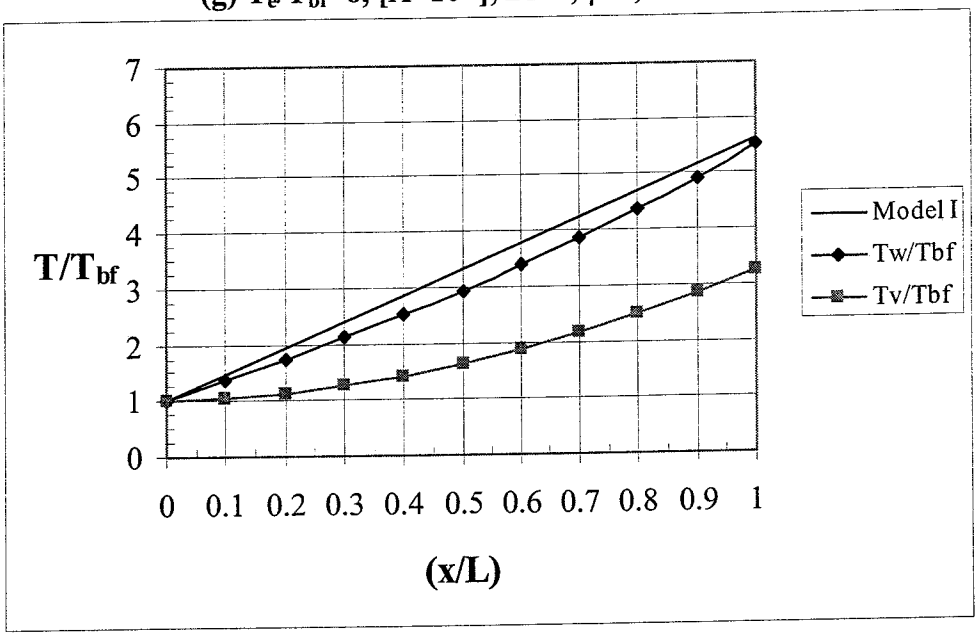

(h) T_e/T_{bf}=6, $\Lambda=10^{-3}$, [Bi=0], γ=2, α=6.5099

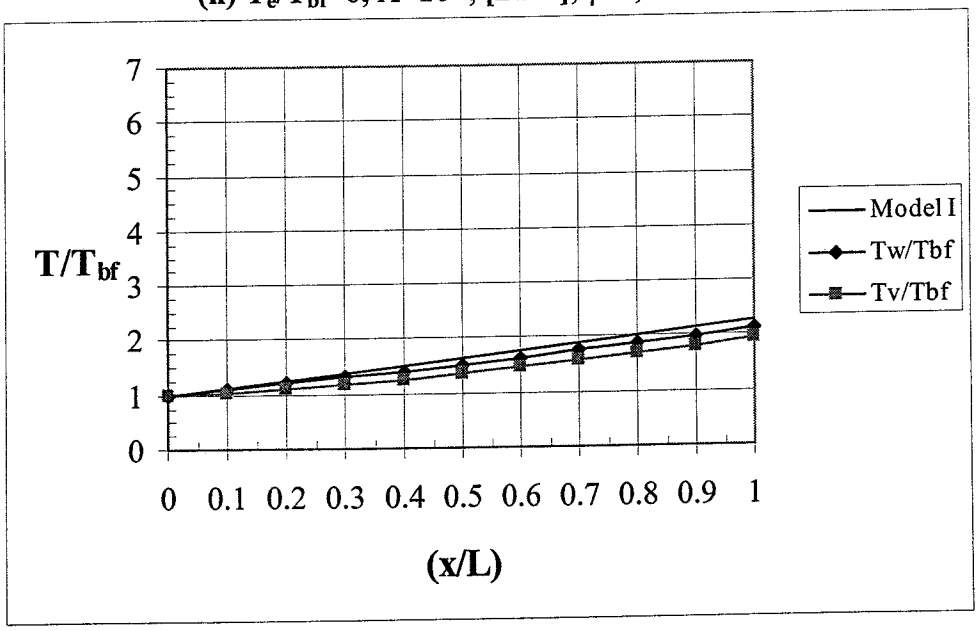

(i) $T_e/T_{bf}=6$, $\Lambda=10^{-3}$, [Bi=1], $\gamma=2$, $\alpha=2.8864$

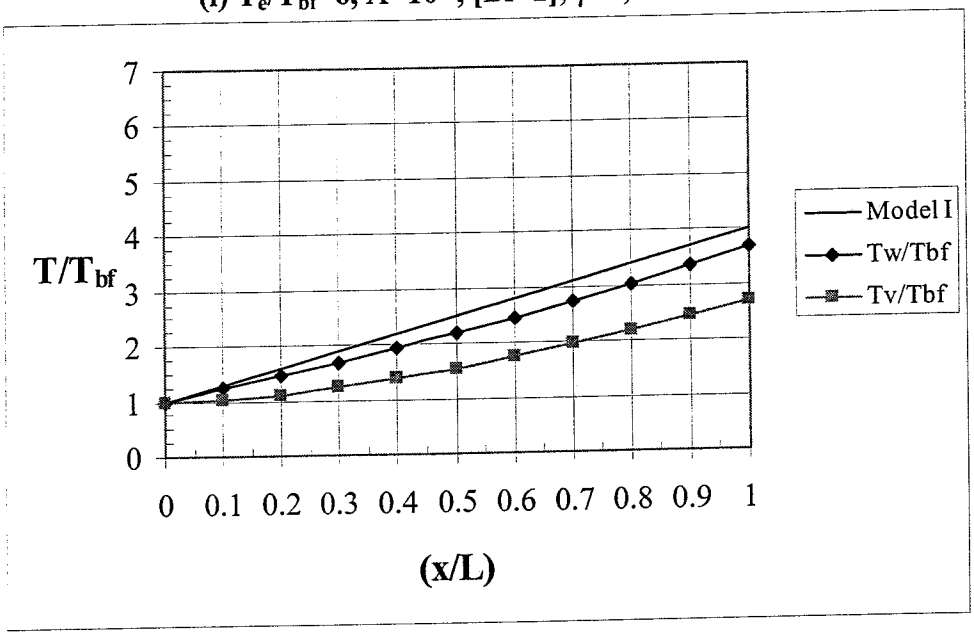

(j) $T_e/T_{bf}=6$, $\Lambda=10^{-3}$, [Bi=5], $\gamma=2$, $\alpha=1.9742$

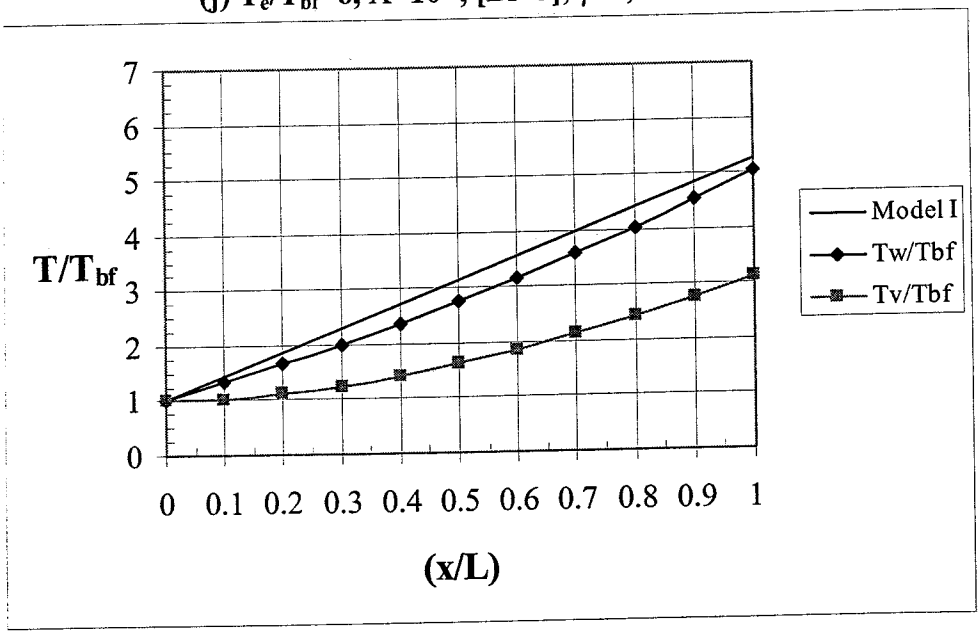

(k) T_e/T_{bf}=6, $\Lambda=10^{-3}$, [Bi=20], γ=2, α=1.7187

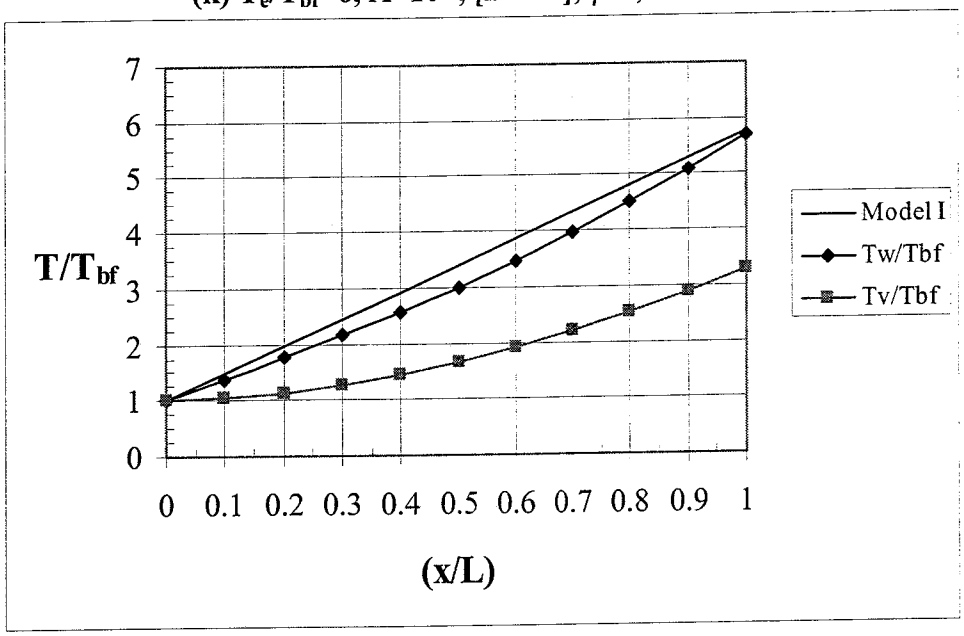

(i) T_e/T_{bf}=6, $\Lambda=10^{-3}$, Bi=5, [γ=1], α=0.8973

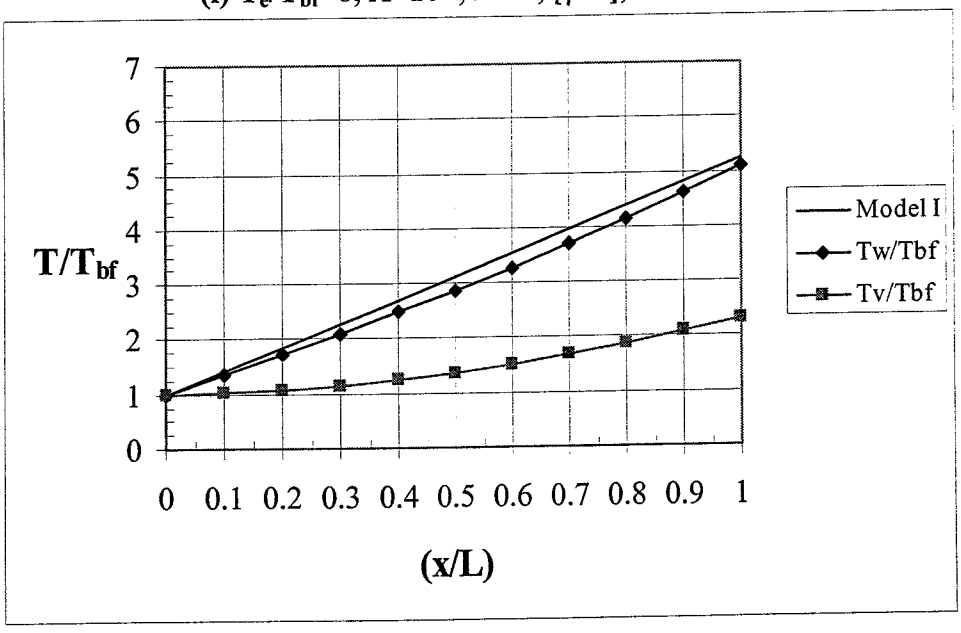

(m) $T_e/T_{bf}=6$, $\Lambda=10^{-3}$, Bi=5, [$\gamma=2$], $\alpha=1.9742$

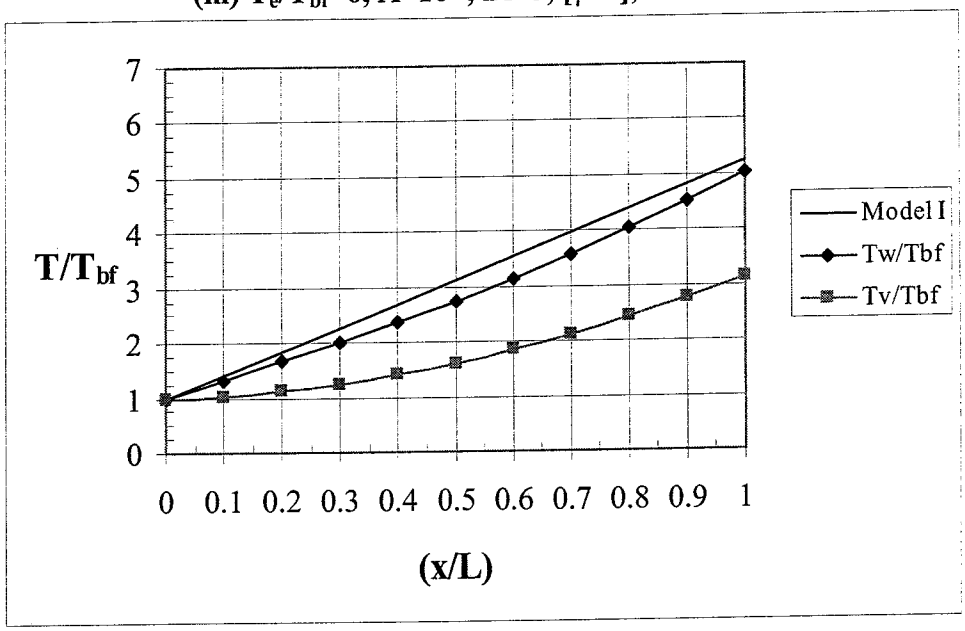

(n) $T_e/T_{bf}=6$, $\Lambda=10^{-3}$, Bi=5, [$\gamma=3$], $\alpha=3.1332$

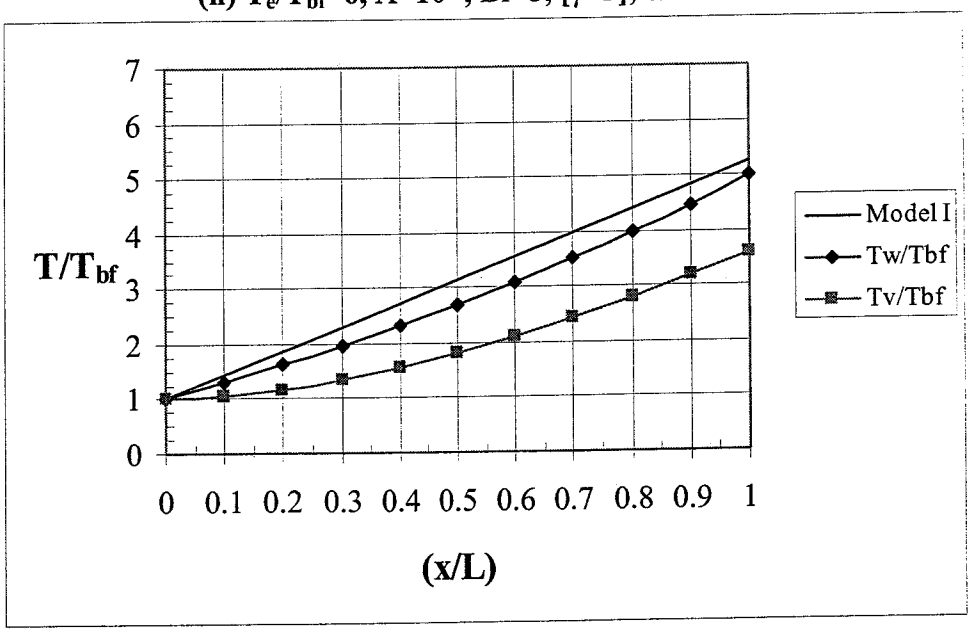

(o) $T_e/T_{bf}=6$, $\Lambda=10^{-3}$, Bi=5, [$\gamma=4$], $\alpha=4.3296$

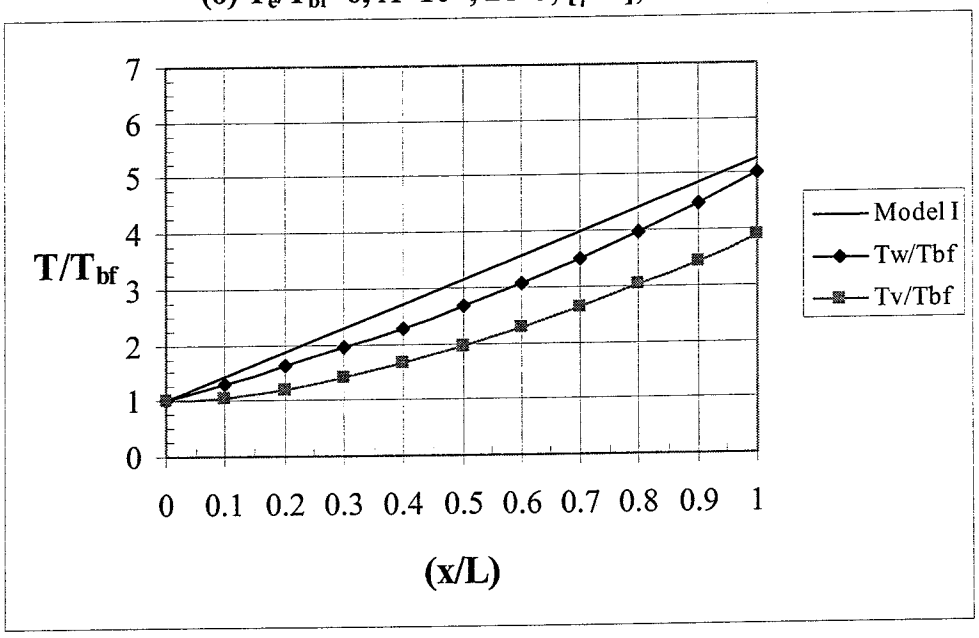

APPENDIX B

PARAMETRIC STUDY OF THE VARIATION OF THE RATIO OF THE VAPOR EXIT TEMPERATURE TO THE WALL SURFACE TEMPERATURE

Figure B1. Parametric Study of the Variation of the Ratio of the Vapor Exit Temperature to the Wall Surface Temperature

(a) Influence of Environmental Temperature and Λ
Bi=5, γ=2

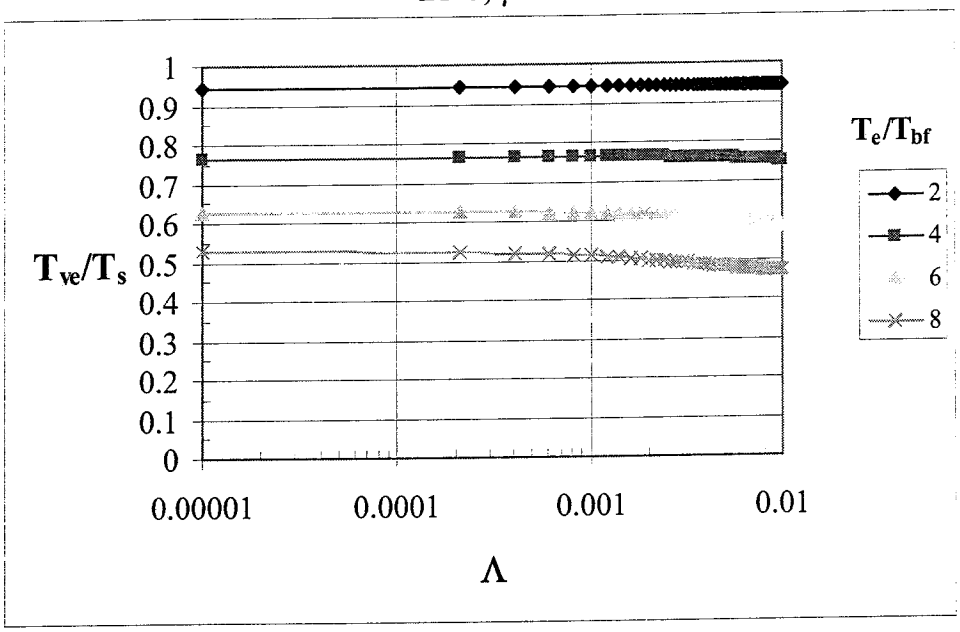

(b) Influence of Biot Number and Λ
T_e/T_{bf}=6, γ=2

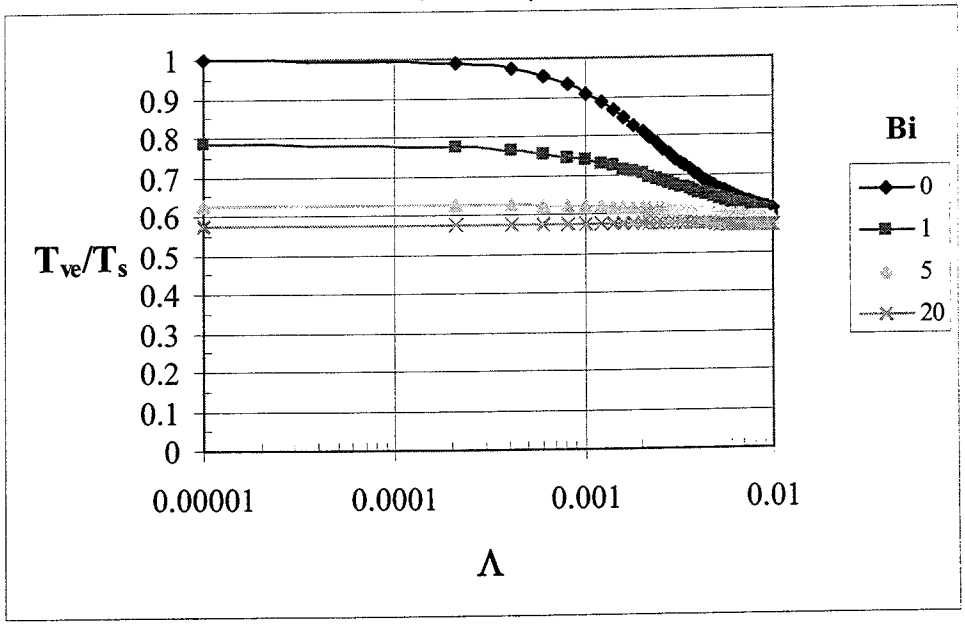

(c) Influence of γ and Λ
T_e/T_{bf}=6, Bi=5

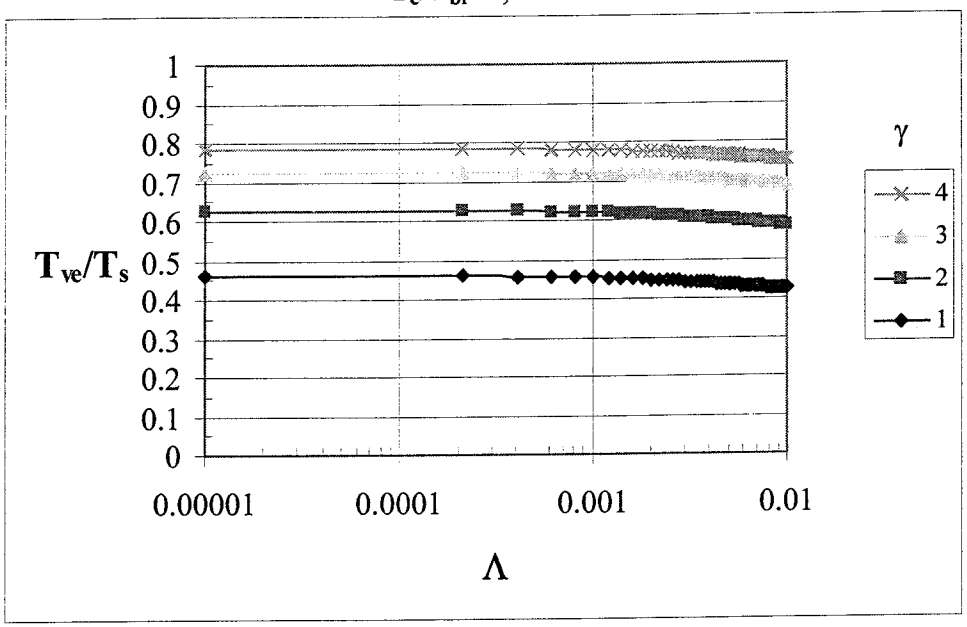

(d) Influence of Environmental Temperature and Biot Number
$\Lambda=10^{-3}$, γ=2

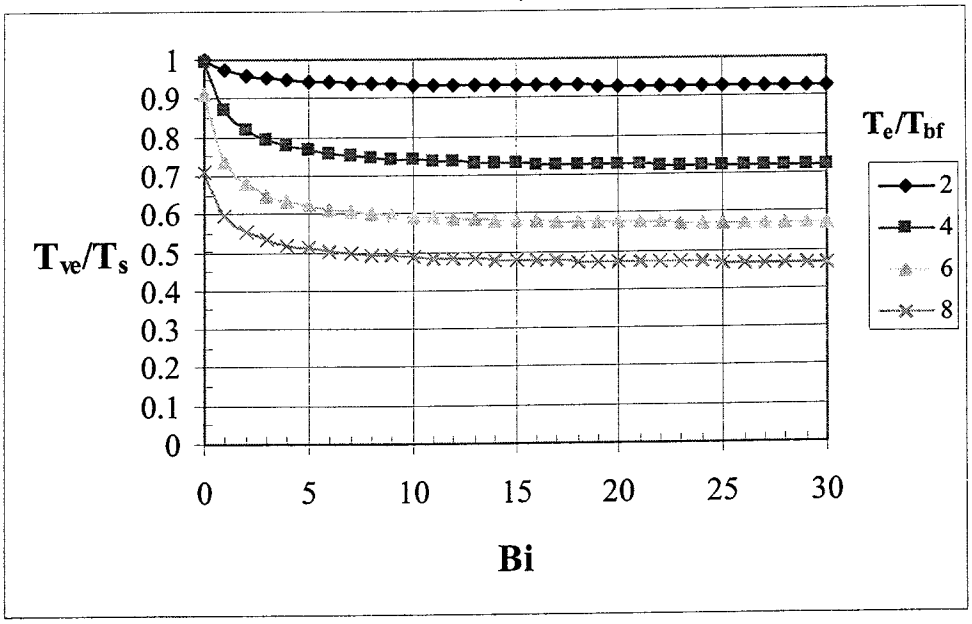

(e) Influence of Λ and Biot Number
T_e/T_{bf}=6, γ=2

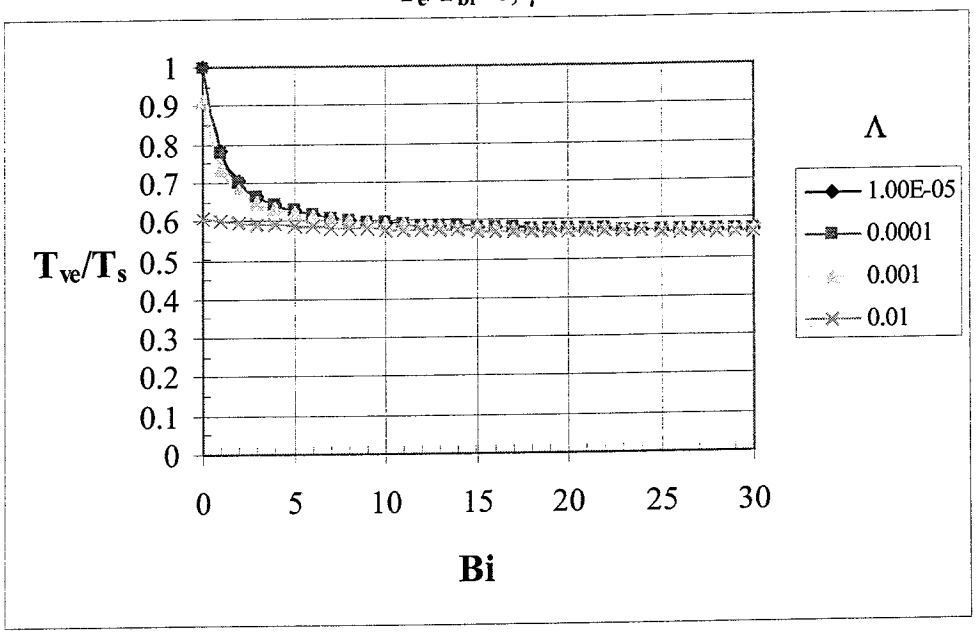

(f) Influence of γ and Biot Number
T_e/T_{bf}=6, Λ=10^{-3}

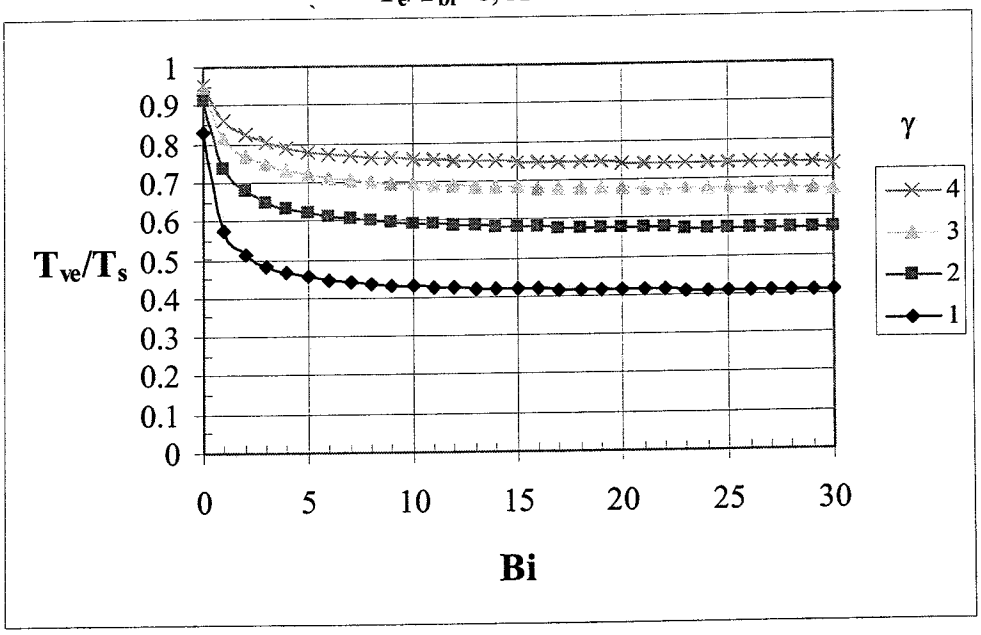

(g) Influence of Environmental Temperature and γ
$\Lambda=10^{-3}$, Bi=5

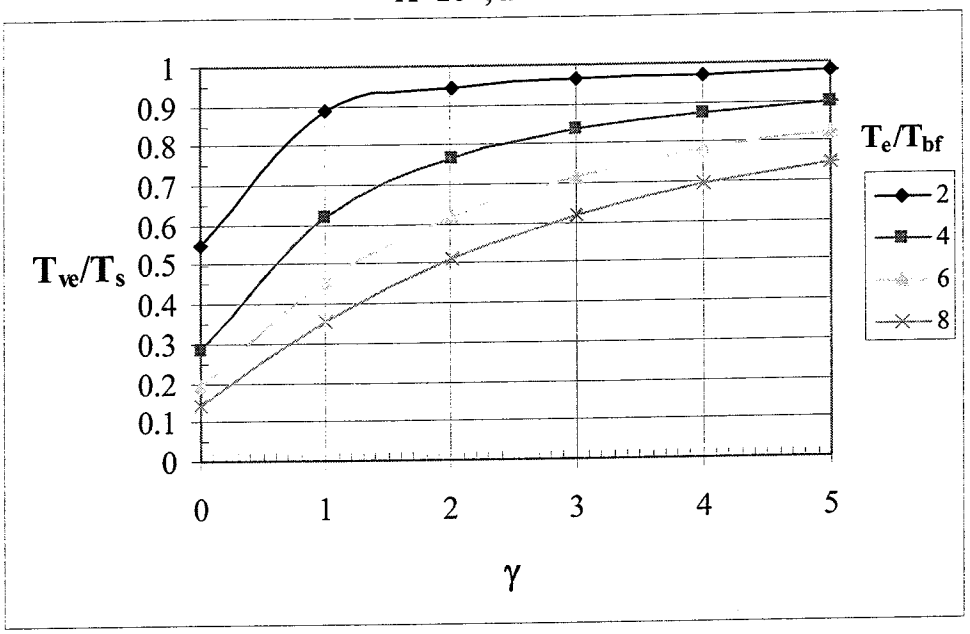

(h) Influence of Λ and γ
T_e/T_{bf}=6, Bi=5

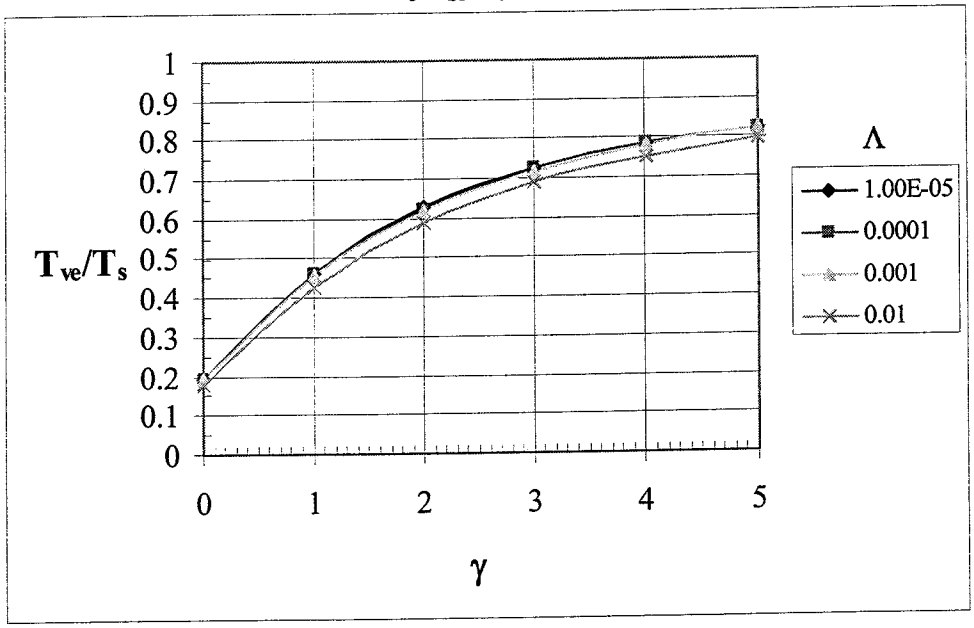

(i) Influence of Biot Number and γ

$T_e/T_{bf}=6$, $\Lambda=10^{-3}$

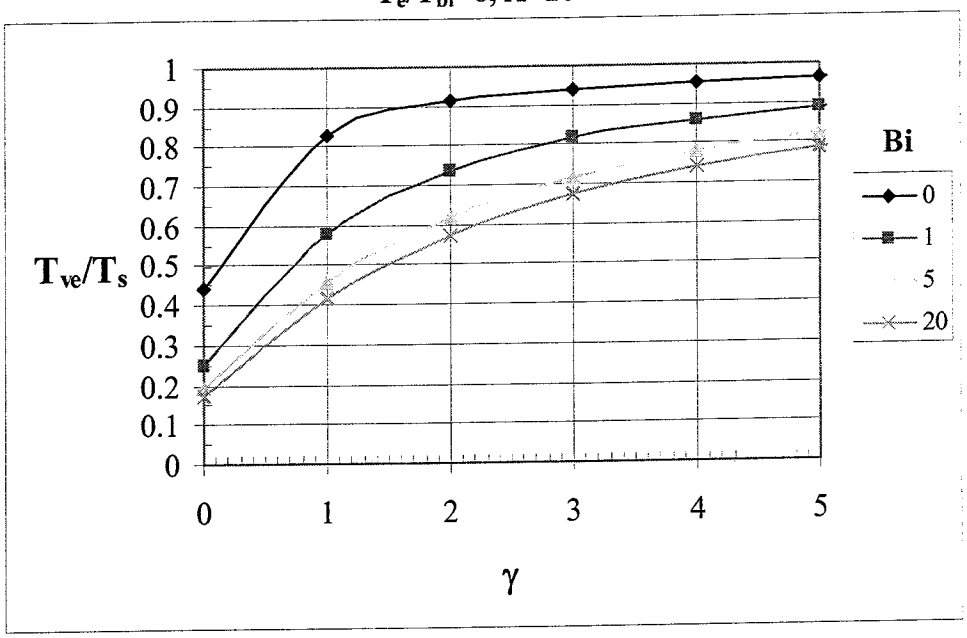

APPENDIX C

PARAMETRIC STUDY OF THE VARIATION OF THE DIMENSIONLESS HEAT TRANSFER RATE, Q_{L2}

Figure C1. Parametric Study of the Variation of the Dimensionless Heat Transfer Rate, Q_{L2}

(a) Influence of Environmental Temperature and Λ
Bi=5, γ=2

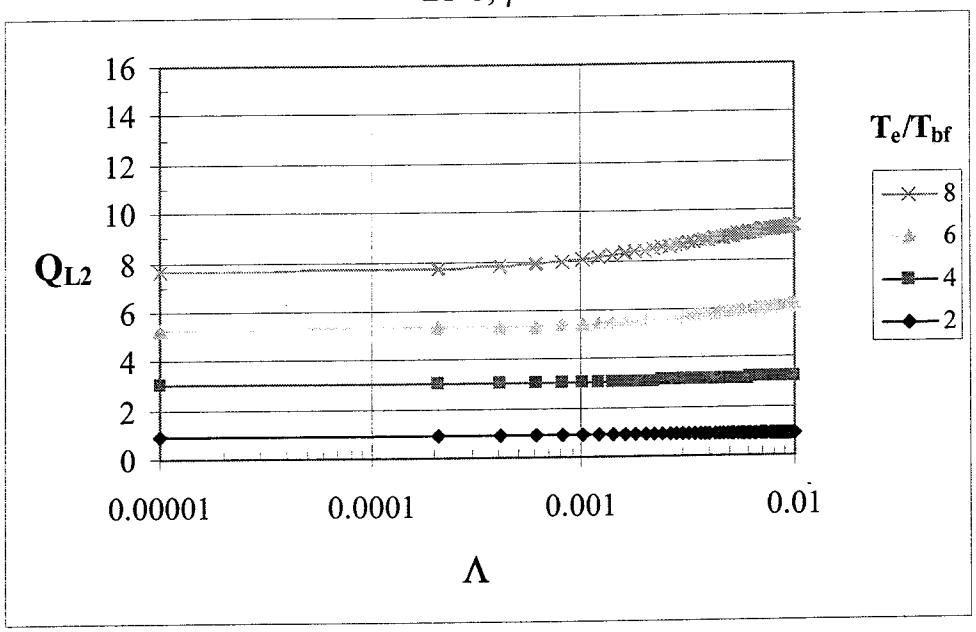

(b) Influence of Biot Number and Λ
T_e/T_{bf}=6, γ=2

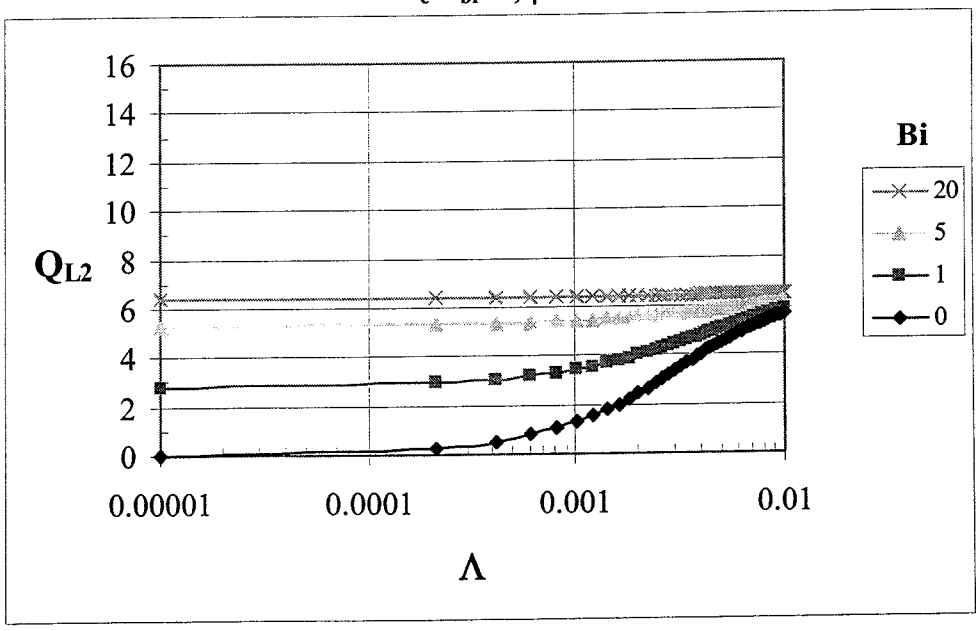

(c) Influence of γ and Λ
T_e/T_{bf}=6, Bi=5

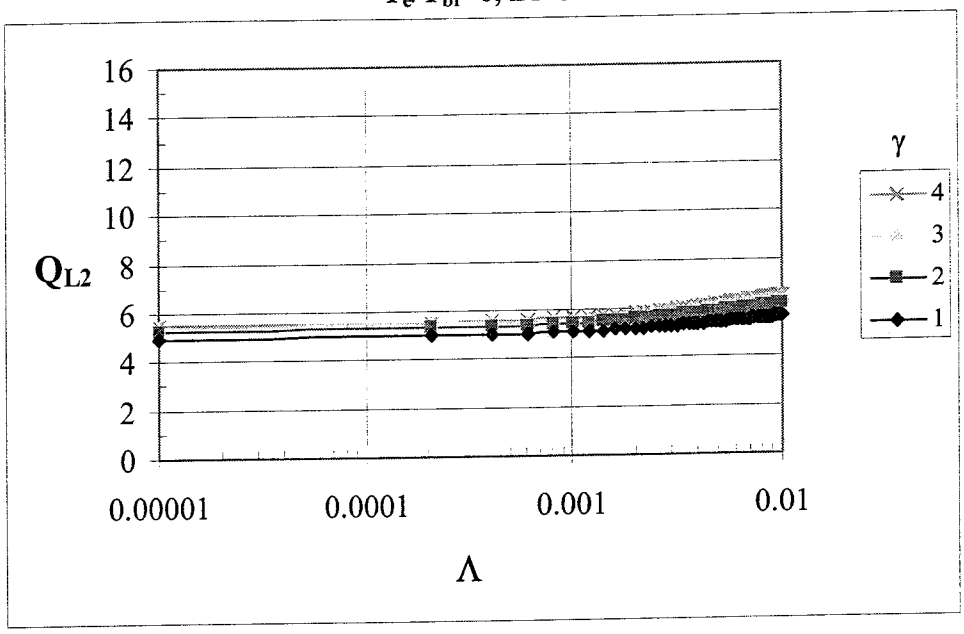

(d) Influence of Environmental Temperature and Biot Number
$\Lambda=10^{-3}$, γ=2

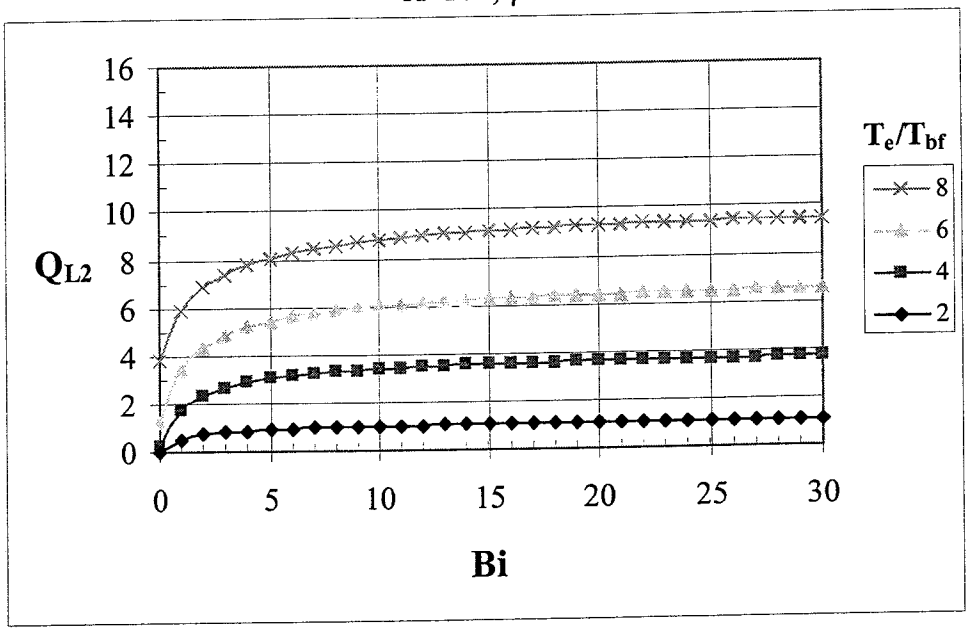

(e) Influence of Λ and Biot Number
T_e/T_{bf}=6, γ=2

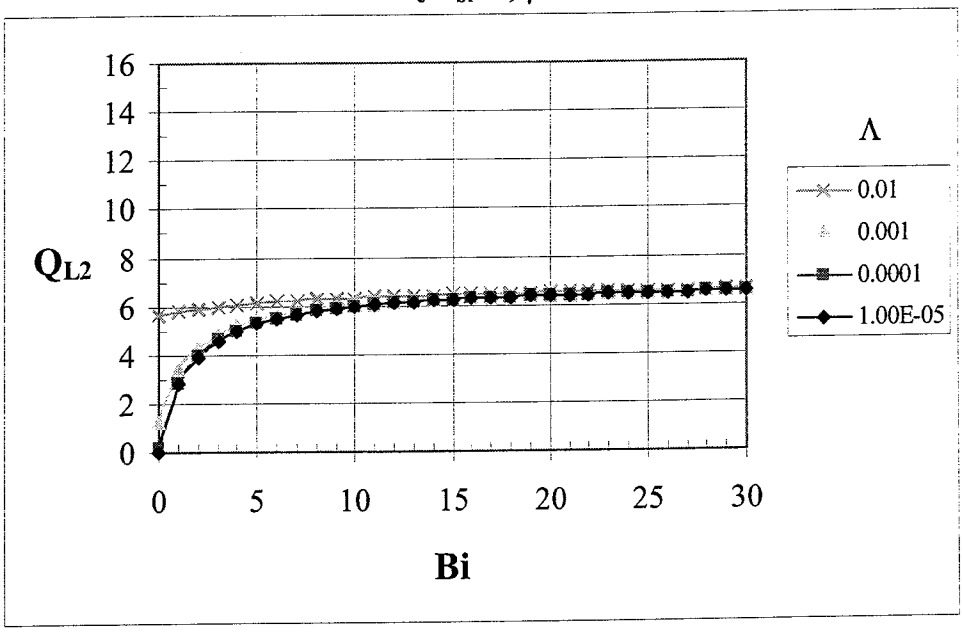

(f) Influence of γ and Biot Number
T_e/T_{bf}=6, Λ=10^{-3}

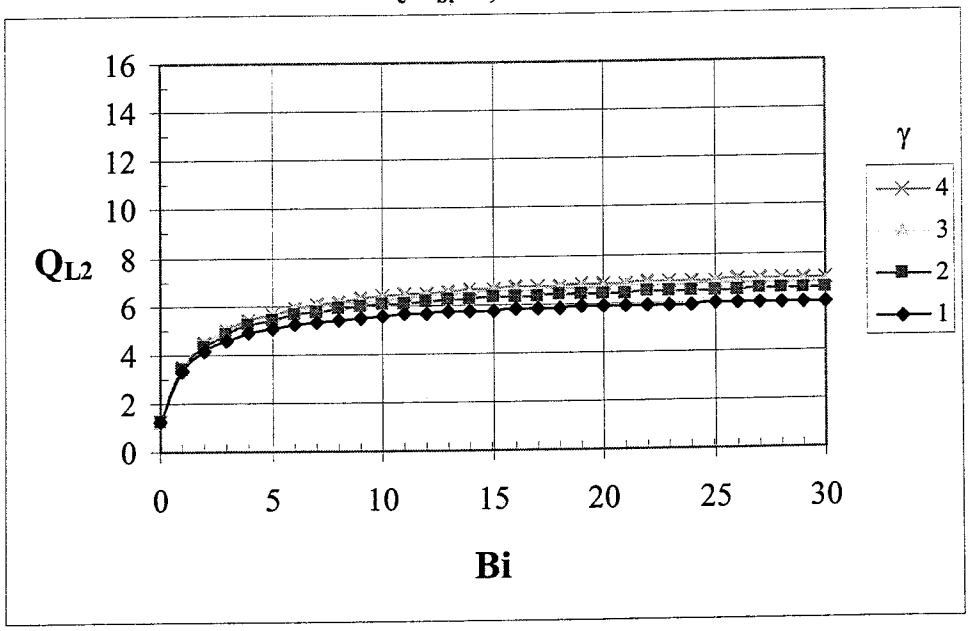

(g) Influence of Environmental Temperature and γ
$\Lambda=10^{-3}$, Bi=5

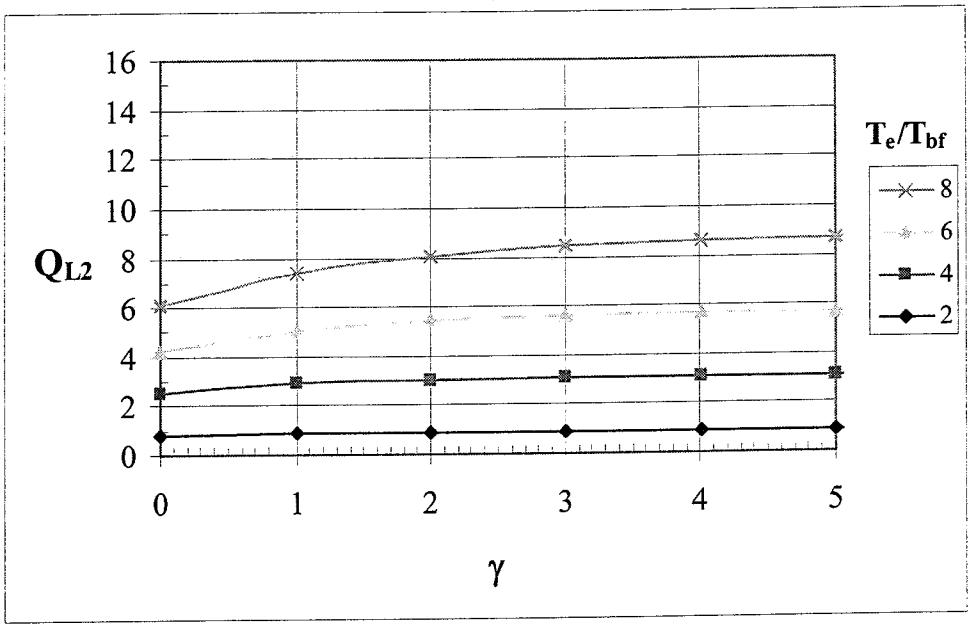

(h) Influence of Λ and γ
T_e/T_{bf}=6, Bi=5

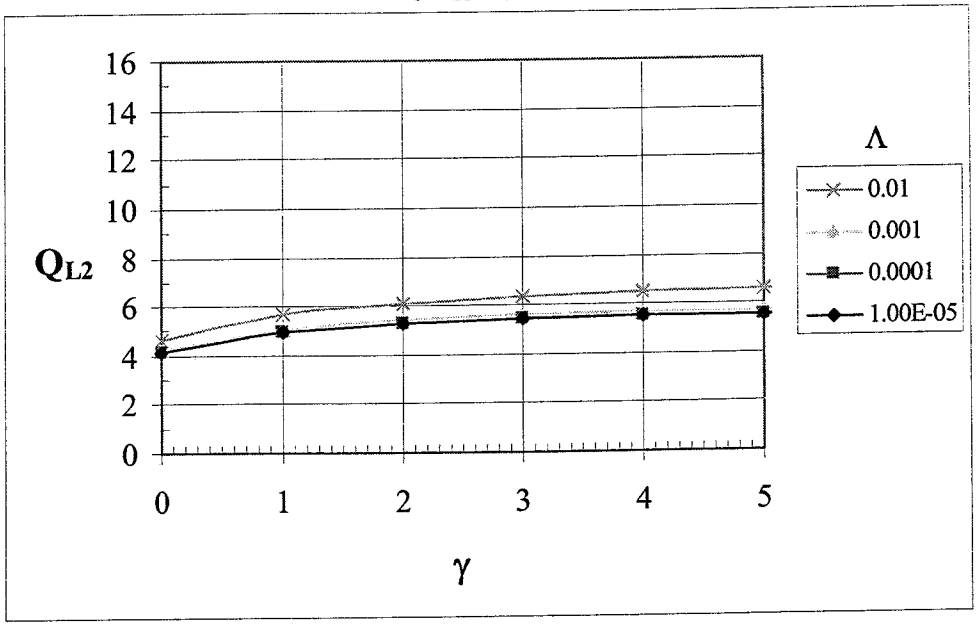

(i) Influence of Biot Number and γ

$T_e/T_{bf}=6$, $\Lambda=10^{-3}$

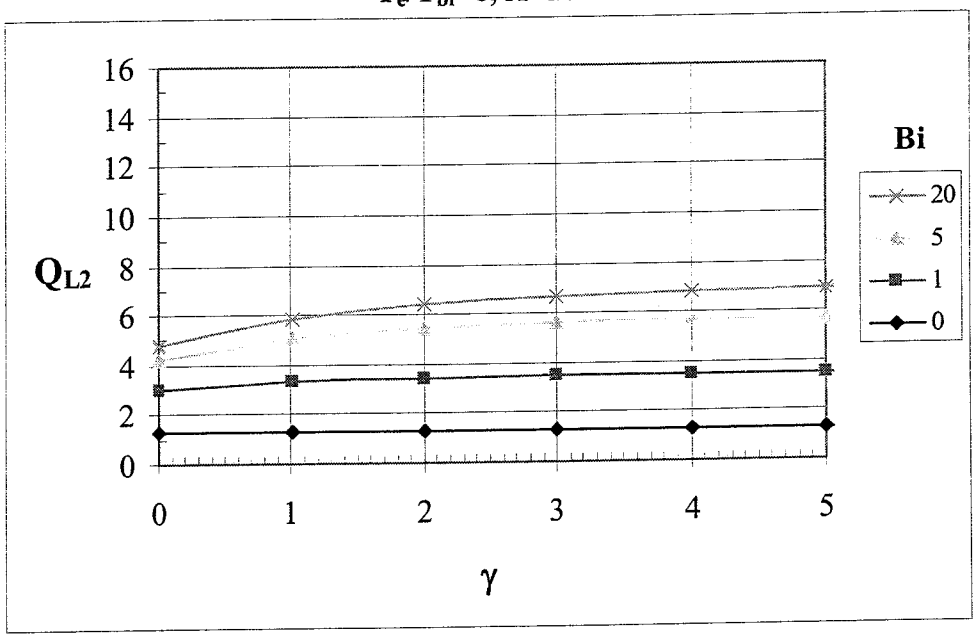

APPENDIX D

PARAMETRIC STUDY OF THE RATIO OF DIMENSIONLESS HEAT TRANSFER RATE FOR MODELS II AND I, Q_{L2}/ Q_{L1}

Figure D1. Parametric Study of the Ratio of Dimensionless Heat Transfer Rate for Models II and I, Q_{L2}/Q_{L1}

(a) Influence of Environmental Temperature and Λ
Bi=5, γ=2

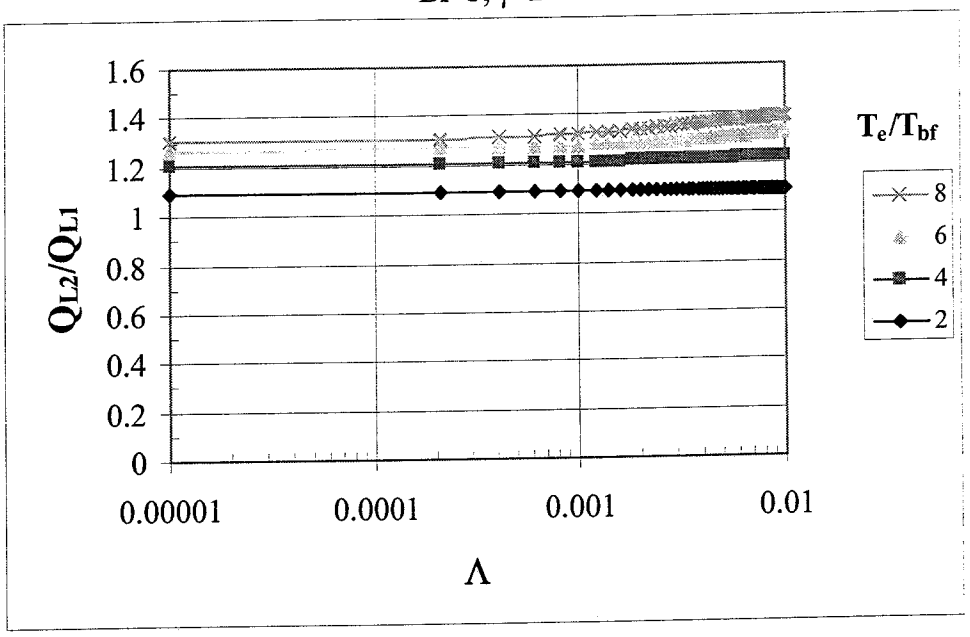

(b) Influence of Biot Number and Λ
T_e/T_{bf}=6, γ=2

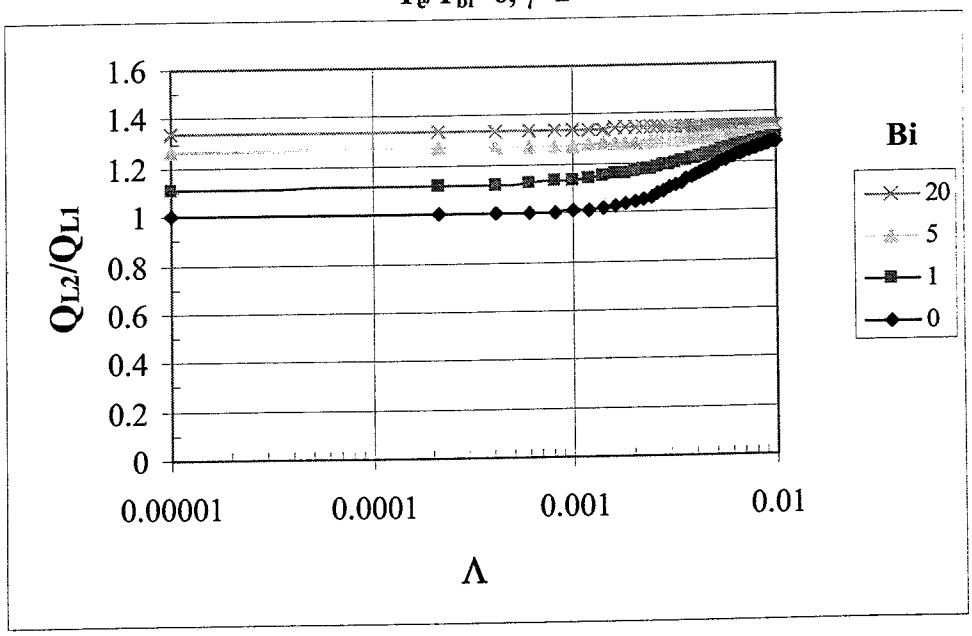

(c) Influence of γ and Λ
T_e/T_{bf}=6, Bi=5

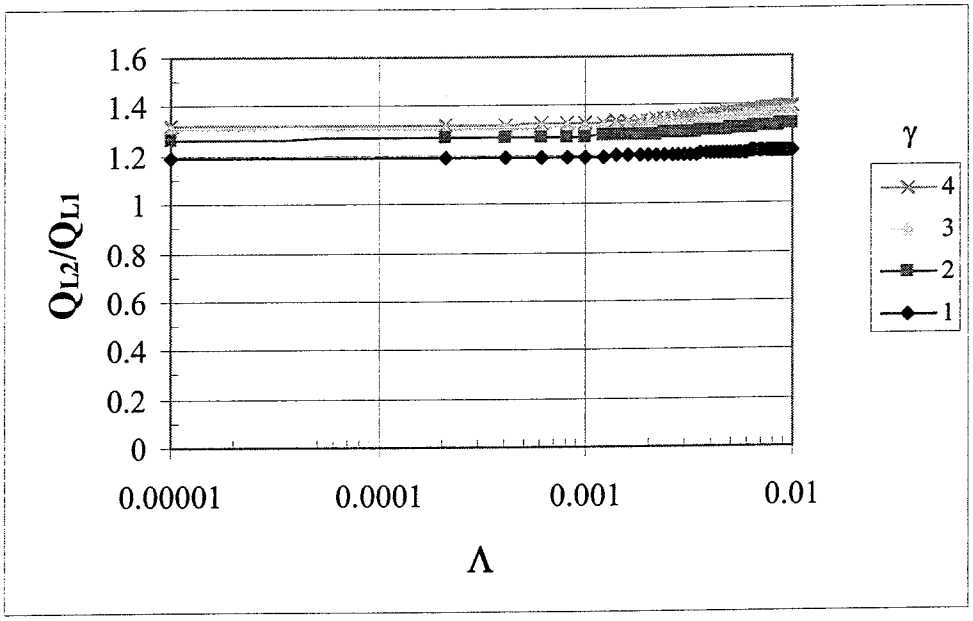

(d) Influence of Environmental Temperature and Biot Number
$\Lambda=10^{-3}$, γ=2

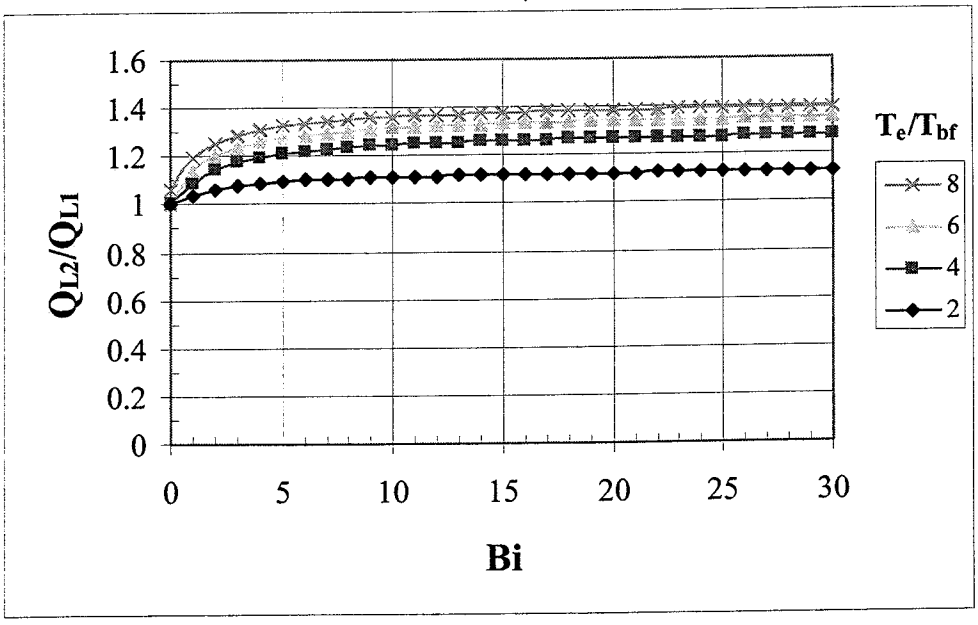

(e) Influence of Λ and Biot Number
T_e/T_{bf}=6, γ=2

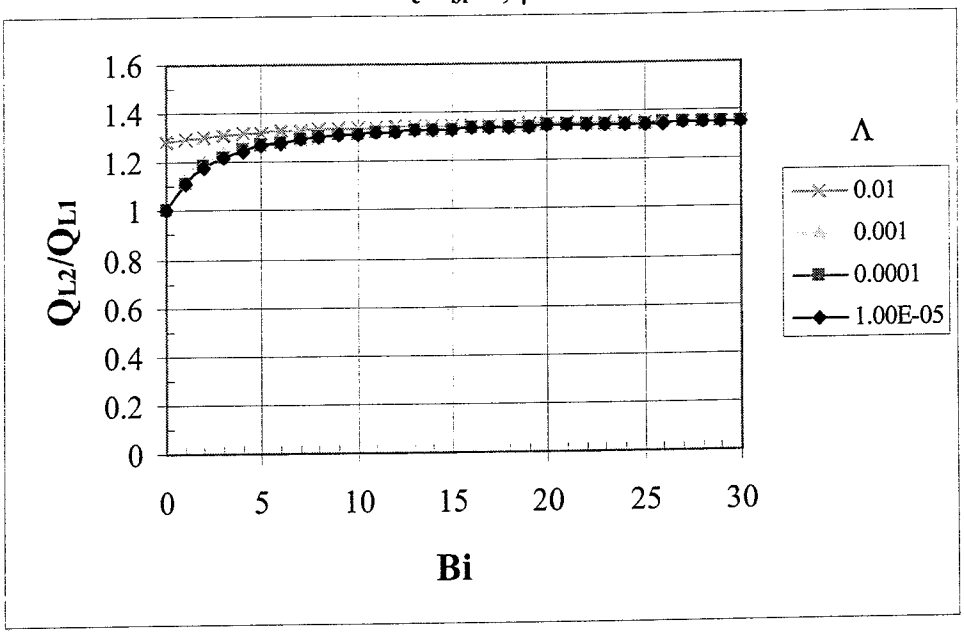

(f) Influence of γ and Biot Number
T_e/T_{bf}=6, Λ=10^{-3}

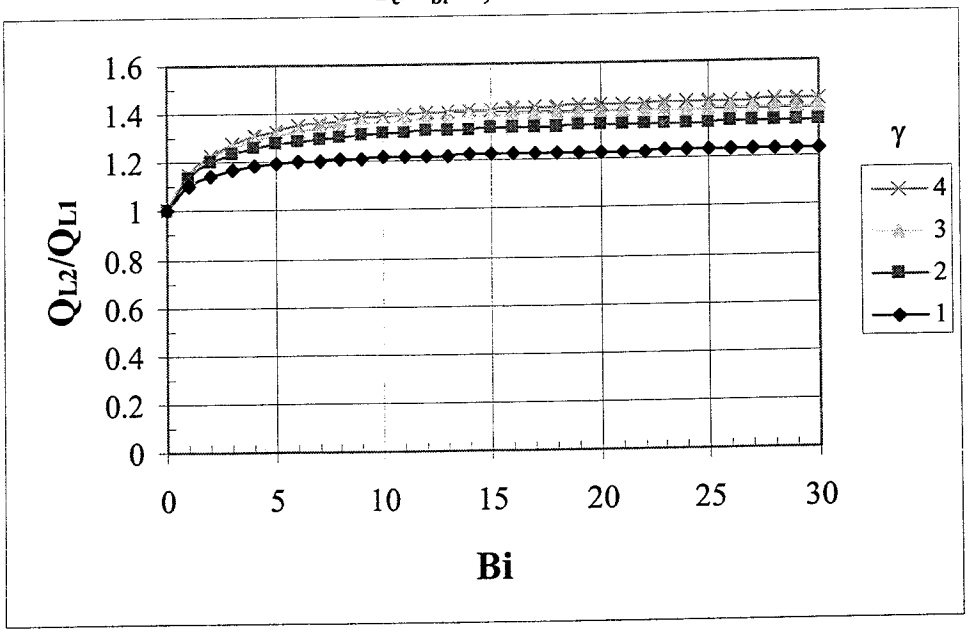

(g) Influence of Environmental Temperature and γ
$\Lambda=10^{-3}$, Bi=5

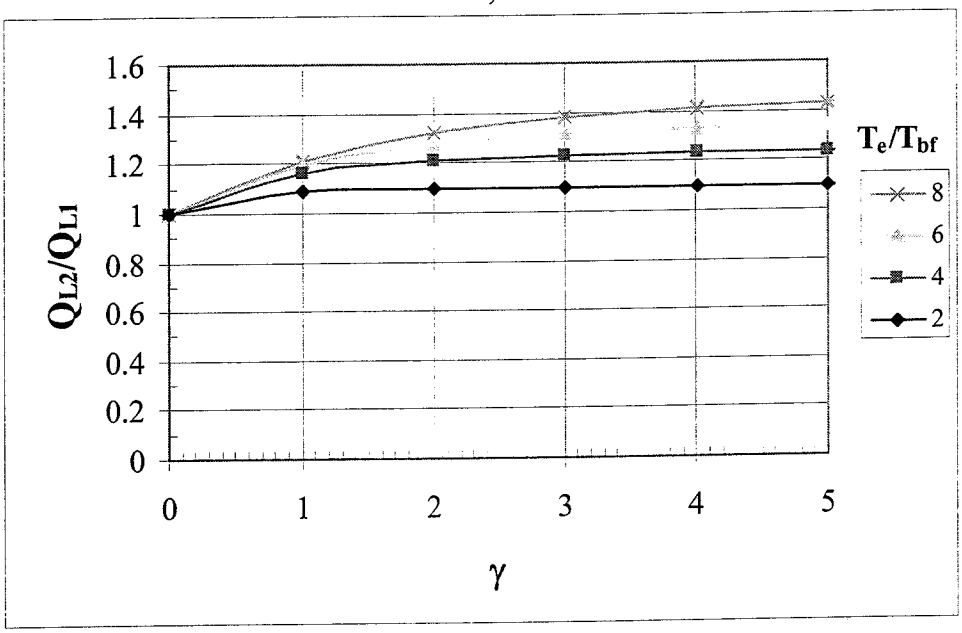

(h) Influence of Λ and γ
$T_e/T_{bf}=6$, Bi=5

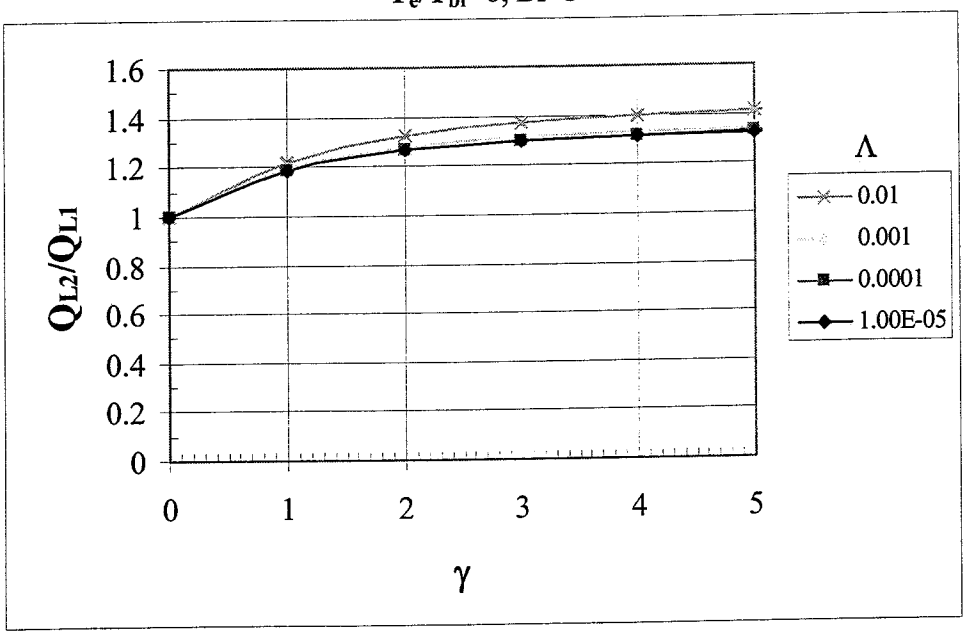

(i) Influence of Biot Number and γ

$T_e/T_{bf}=6$, $\Lambda=10^{-3}$

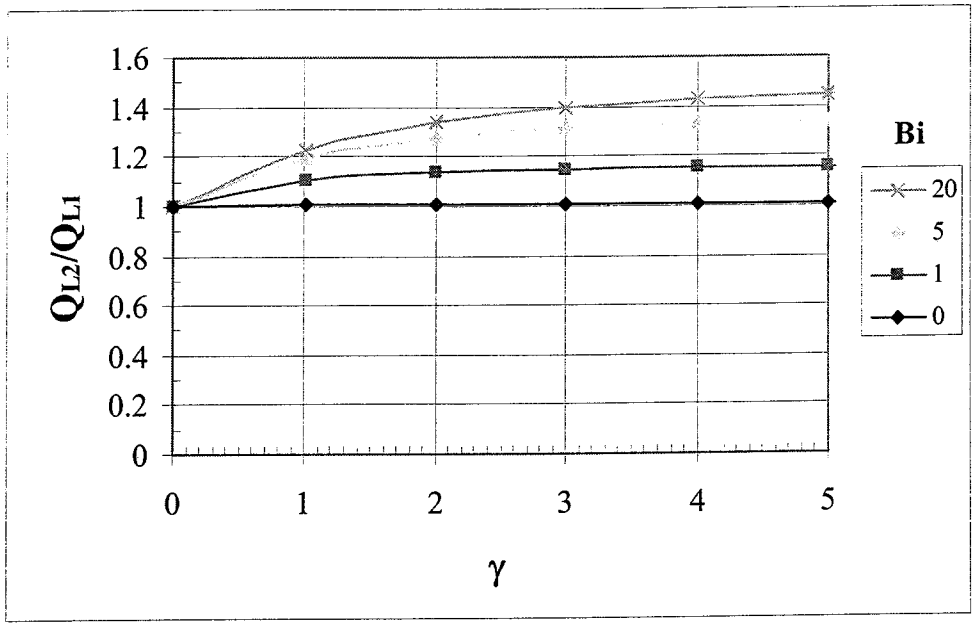

APPENDIX E

PARAMETRIC STUDY OF THE RATIO OF DIMENSIONLESS MASS FLOW RATE PARAMETER, β, FOR MODELS II AND I

Figure E1. Parametric Study of the Ratio of Dimensionless Mass Flow Rate Parameter, β, for Models II and I

(a) Influence of Environmental Temperature and Λ
Bi=5, γ=2

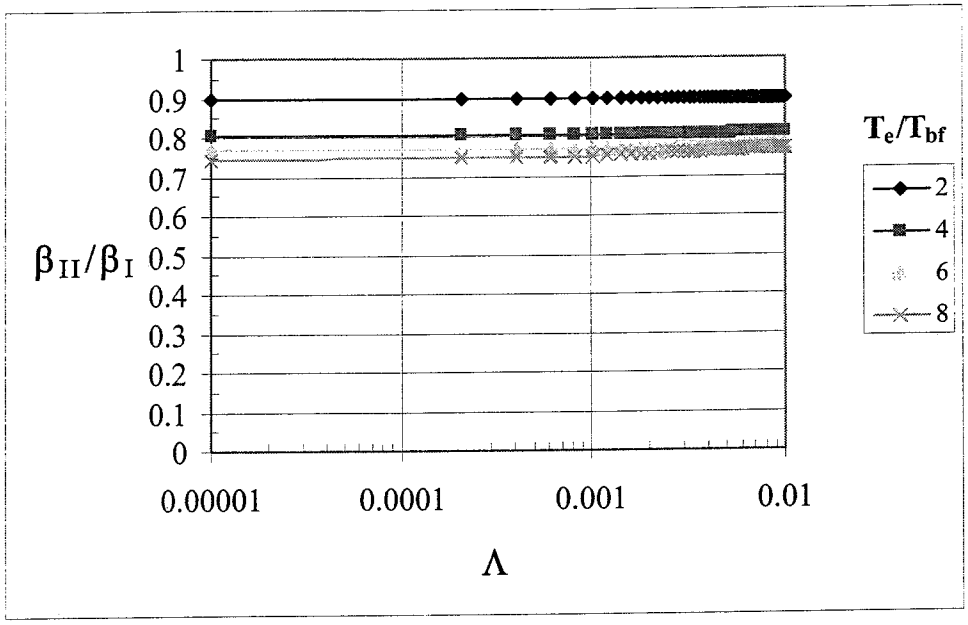

(b) Influence of Biot Number and Λ
T_e/T_{bf}=6, γ=2

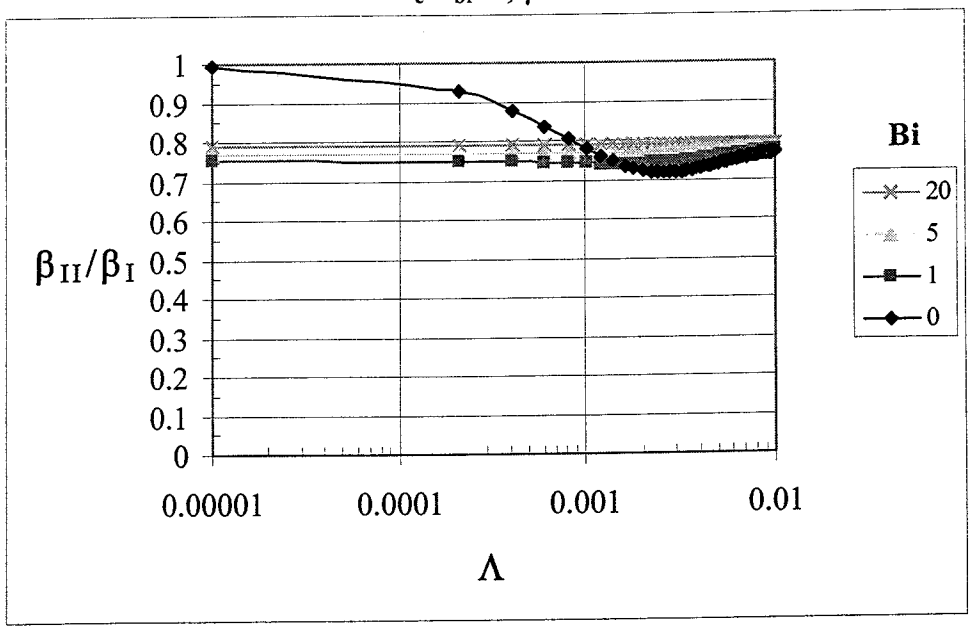

(c) Influence of γ and Λ
T_e/T_{bf}=6, Bi=5

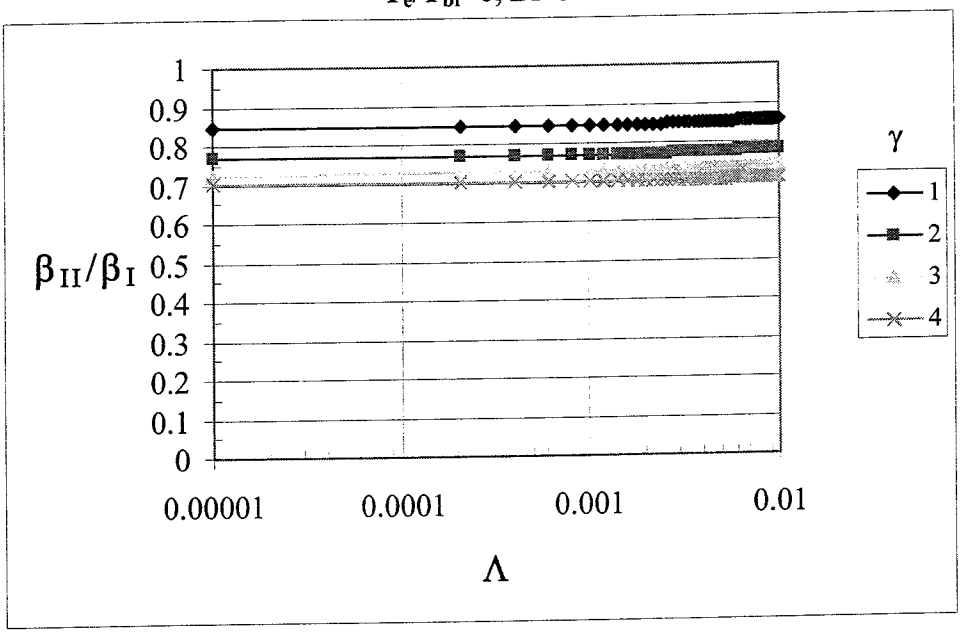

(d) Influence of Environmental Temperature and Biot Number
$\Lambda=10^{-3}$, γ=2

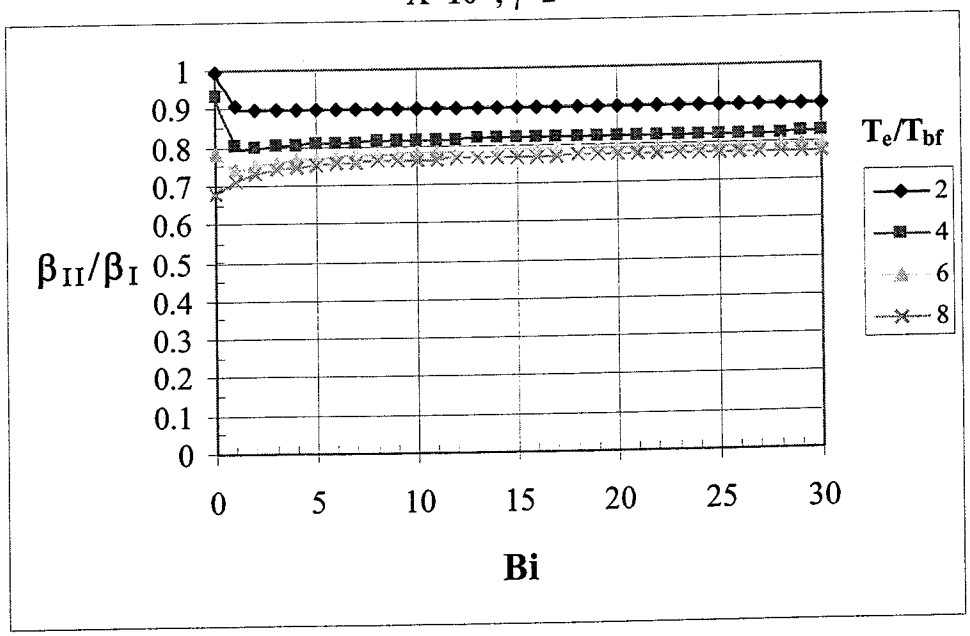

(e) Influence of Λ and Biot Number
T_e/T_{bf}=6, γ=2

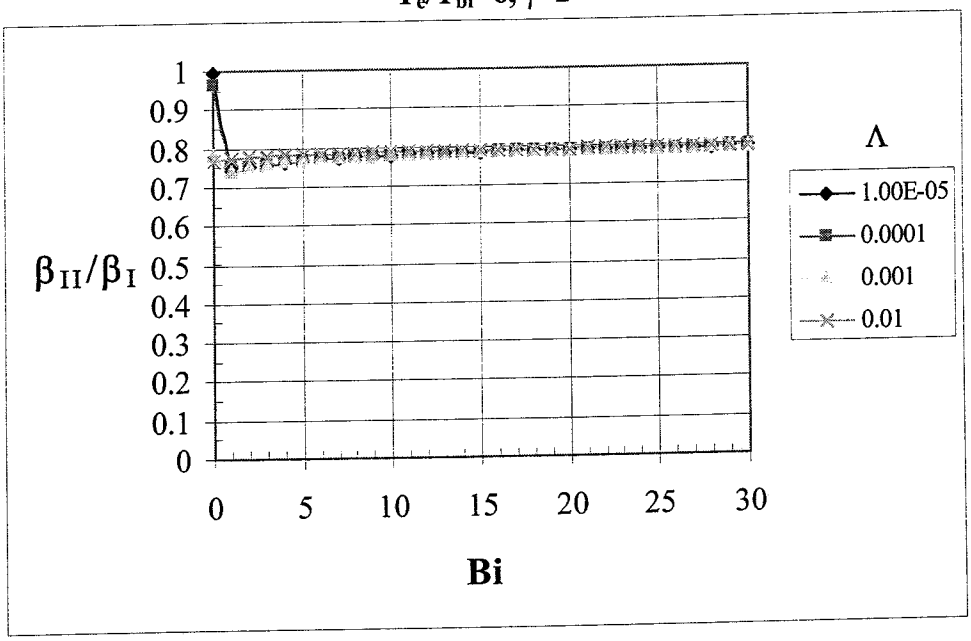

(f) Influence of γ and Biot Number
T_e/T_{bf}=6, Λ=10^{-3}

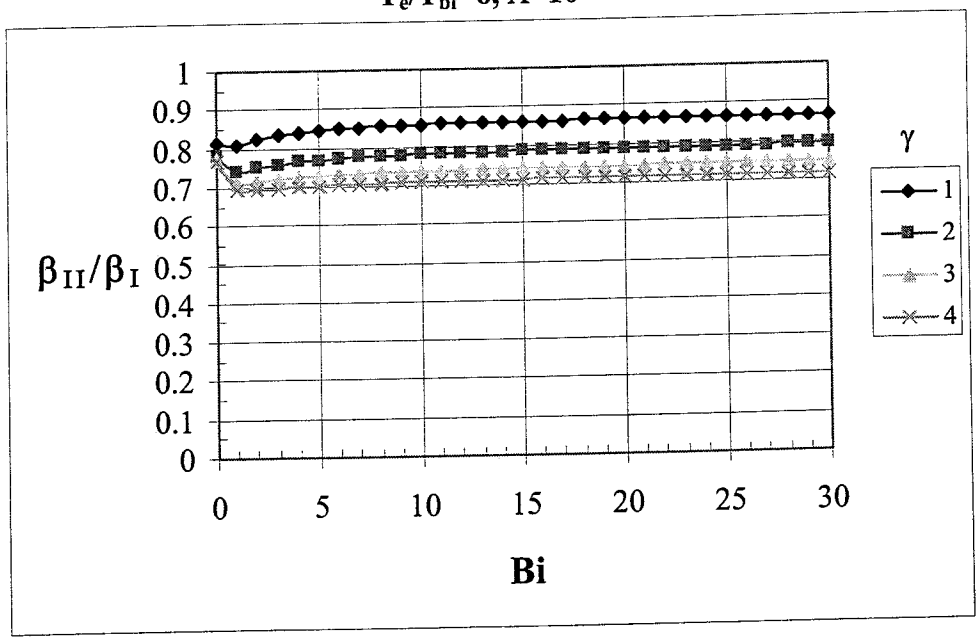

(g) Influence of Environmental Temperature and γ
$\Lambda=10^{-3}$, Bi=5

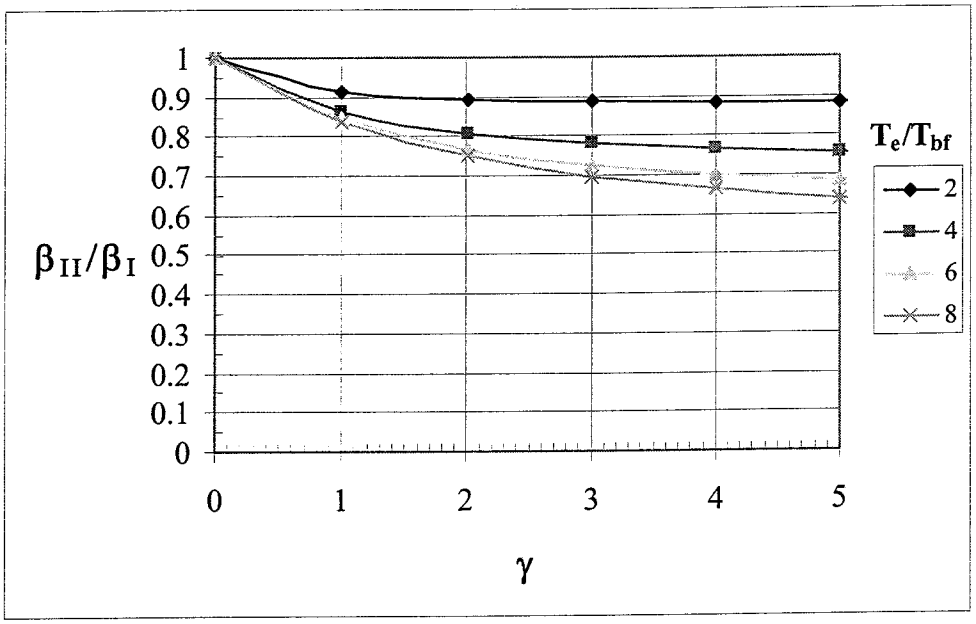

(h) Influence of Λ and γ
T_e/T_{bf}=6, Bi=5

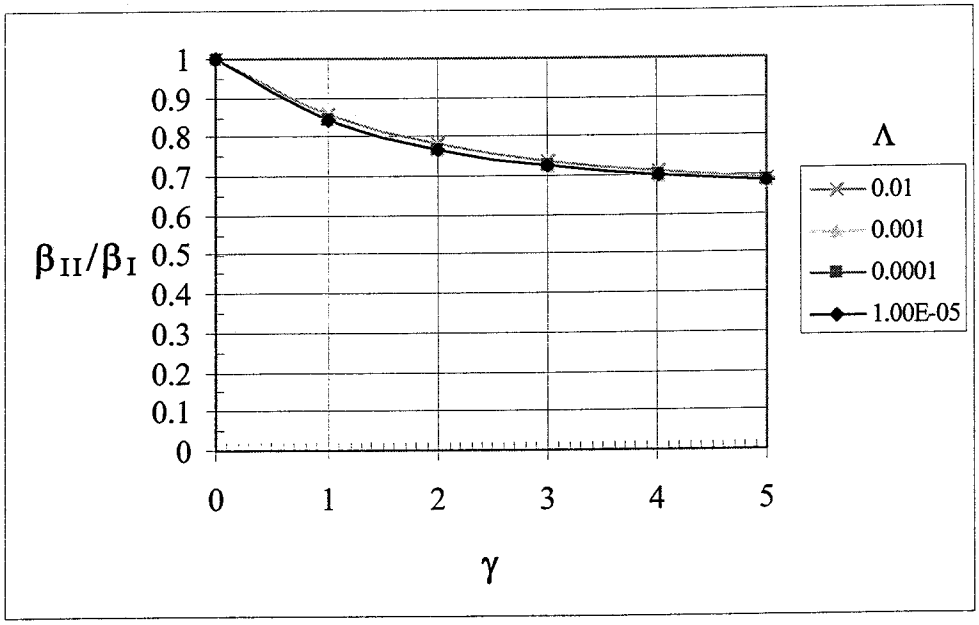

(i) Influence of Biot Number and γ

$T_e/T_{bf}=6$, $\Lambda=10^{-3}$

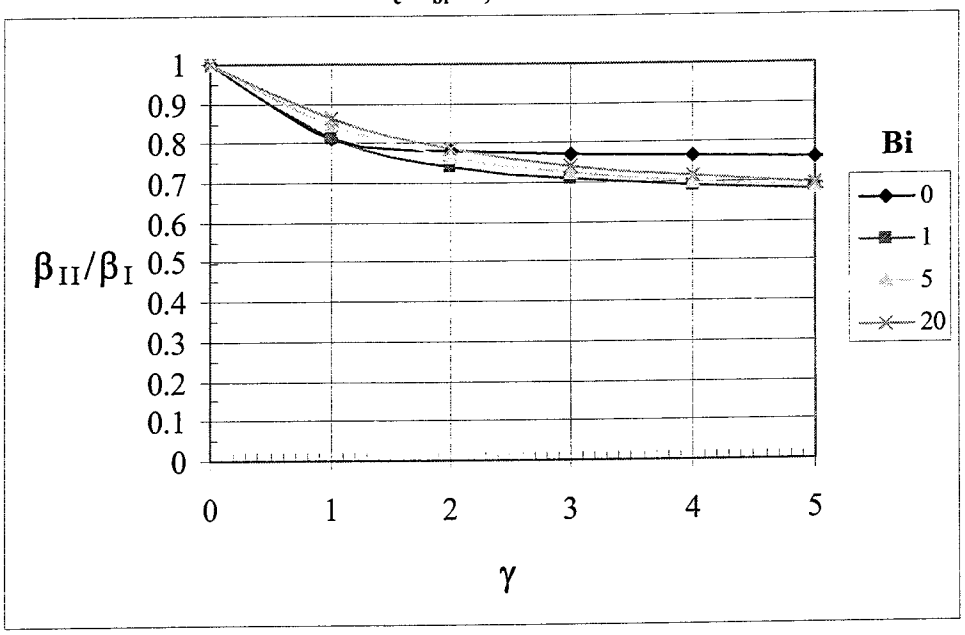

APPENDIX F

MAXIMUM ALLOWABLE ENVIRONMENTAL TEMPERATURE FOR MODEL I AS A FUNCTION OF MATERIAL THICKNESS AND CONVECTION HEAT TRANSFER COEFFICIENT (CROSS-PLOTS)

Figure F1. Maximum Allowable Environmental Temperature for Model I as a Function of Material Thickness and Convection Heat Transfer Coefficient (Cross-Plots)

(a) Aluminum
T_{crit} = 641 K

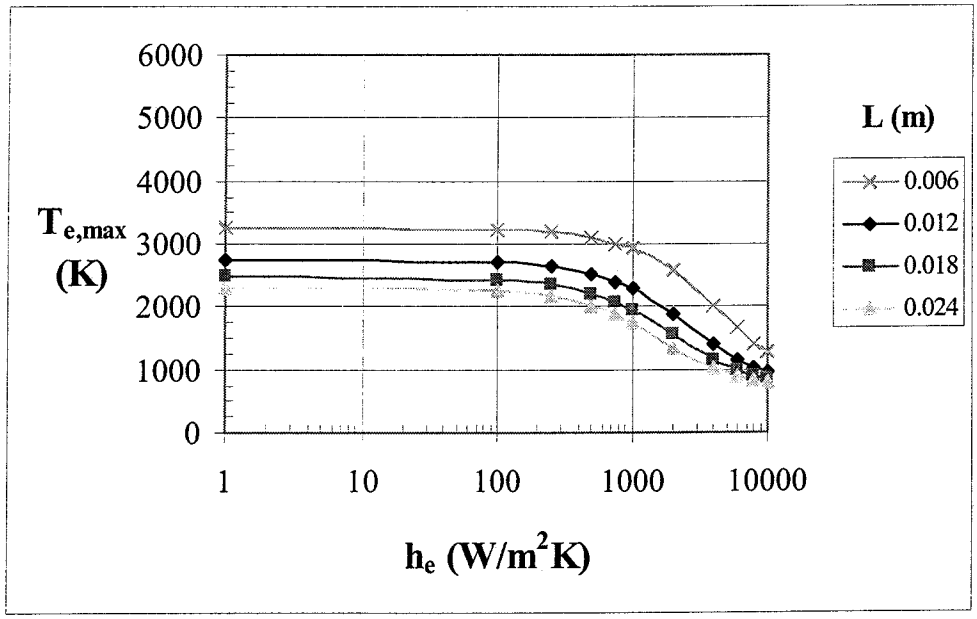

(b) Copper
T_{crit} = 1016 K

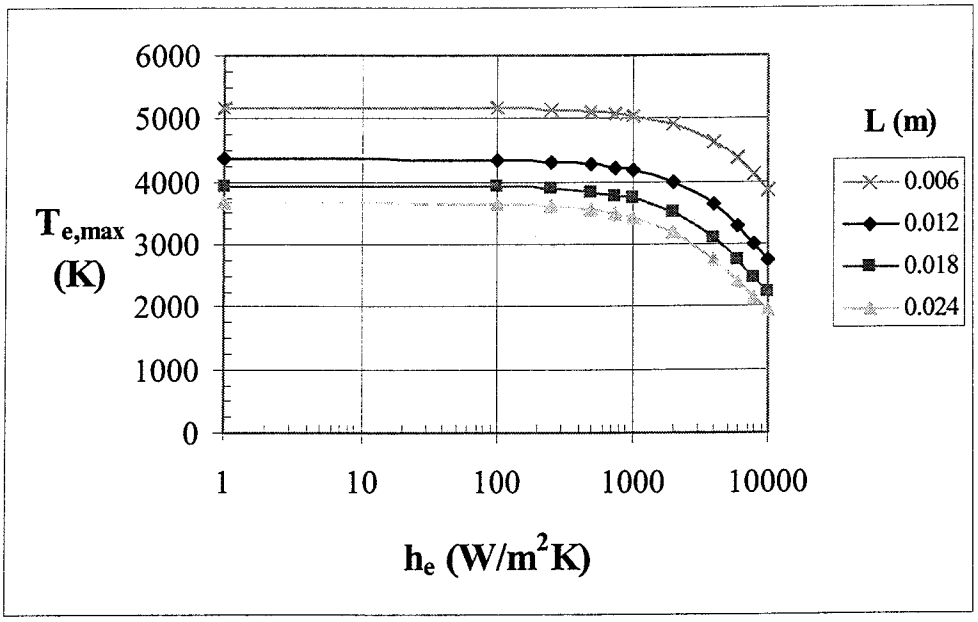

(c) Steel
T_{crit} = 1337 K

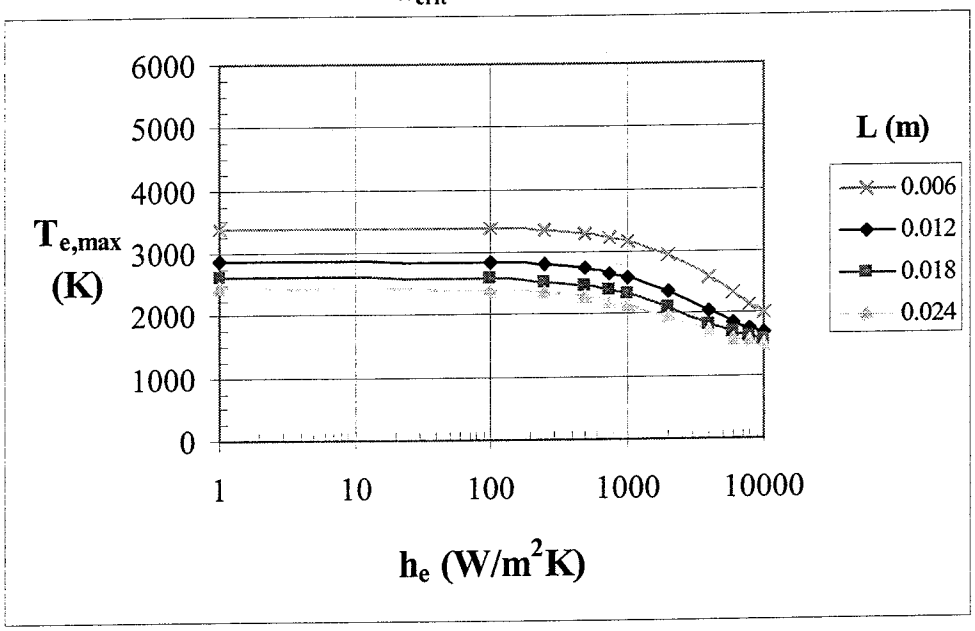

(d) Titanium
T_{crit} = 1464 K

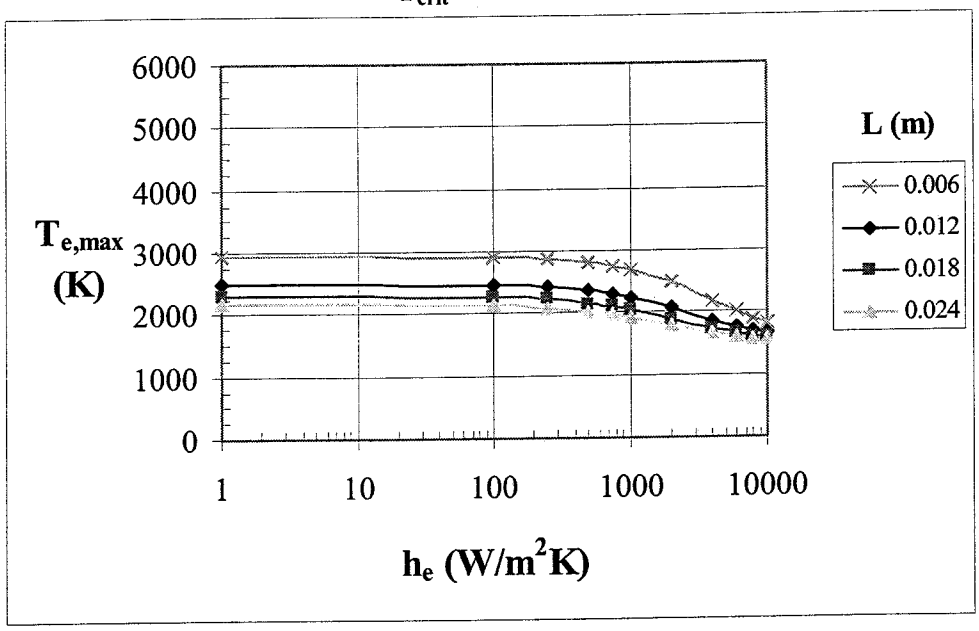

(e) Tungsten
T_{crit} = 2745 K

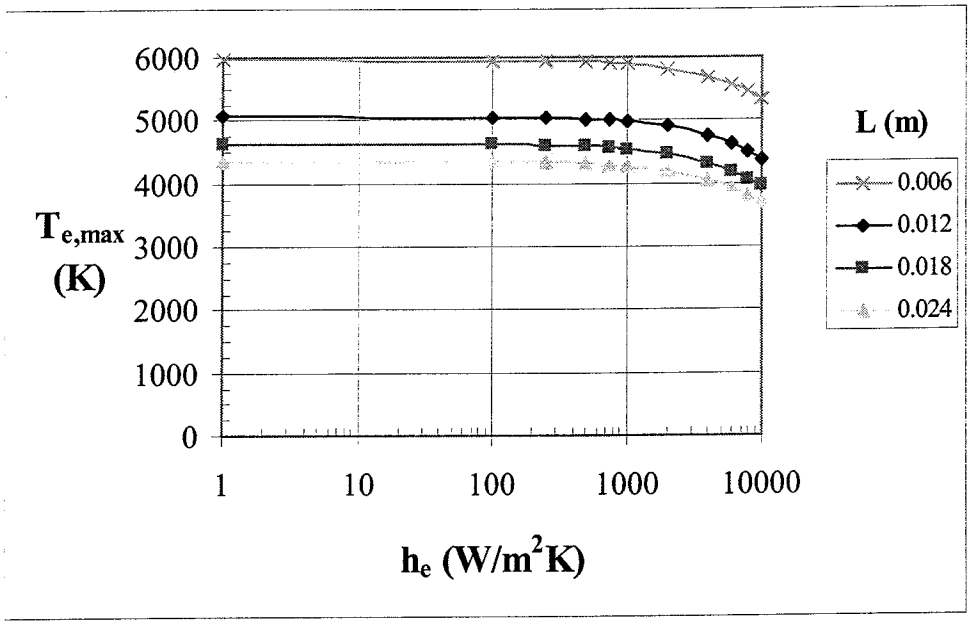

(f) Niobium Carbide
T_{crit} = 2917 K

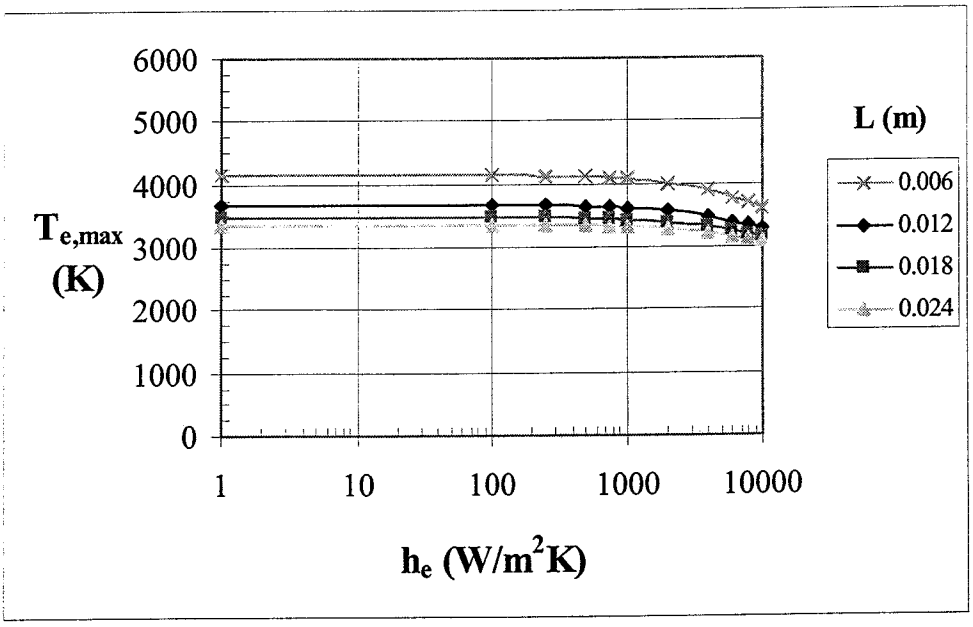

APPENDIX G

PARAMETRIC STUDY OF THE RATIO OF DIMENSIONLESS MASS FLOW RATE PARAMETER, β, FOR MODELS II AND I - SELECTED MATERIALS

Figure G1. Ratio of Dimensionless Mass Flow Rate Parameter, β, for Models II and I as a Function of Channel Diameter and Environmental Temperature

(a) Aluminum
T_{crit} = 641 K

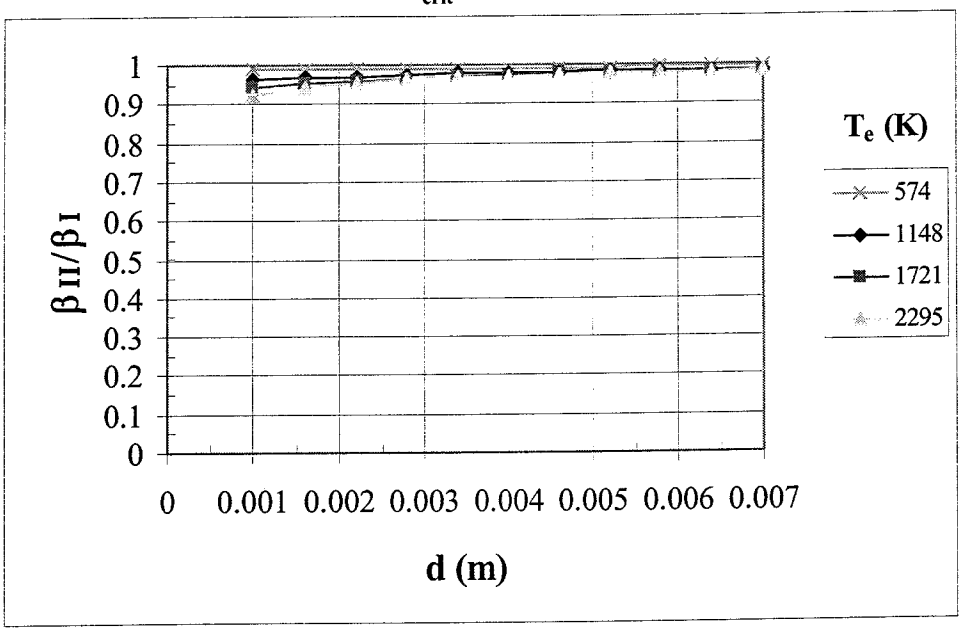

(b) Copper
T_{crit} = 1016 K

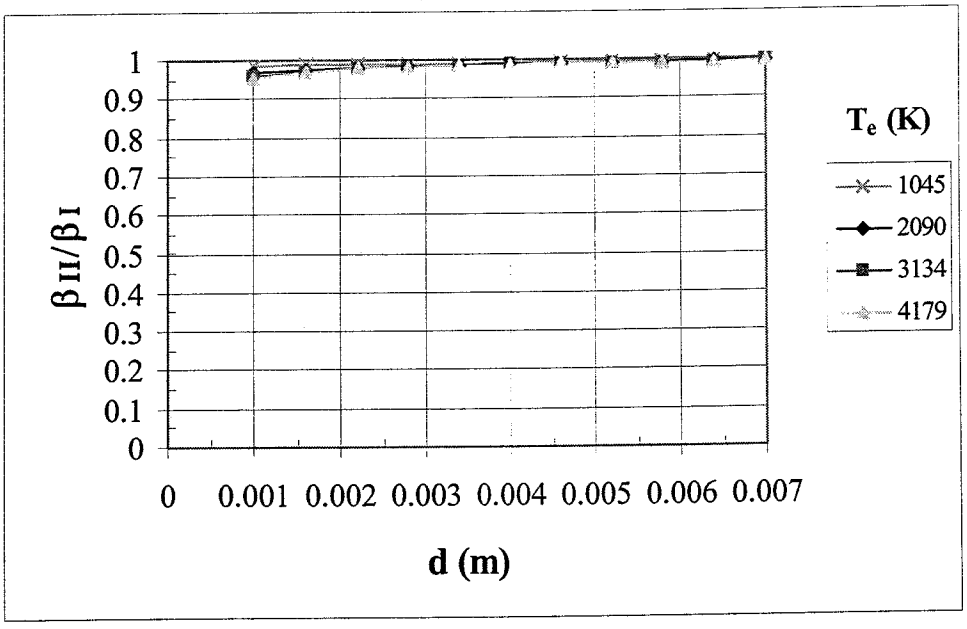

(c) Steel
T_{crit} = 1337 K

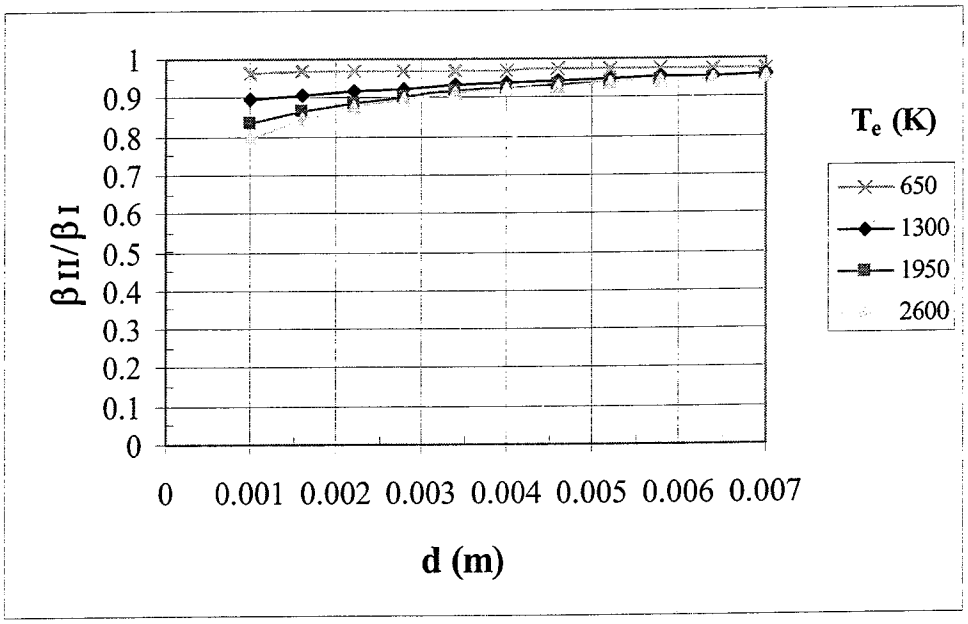

(d) Titanium
T_{crit} = 1464 K

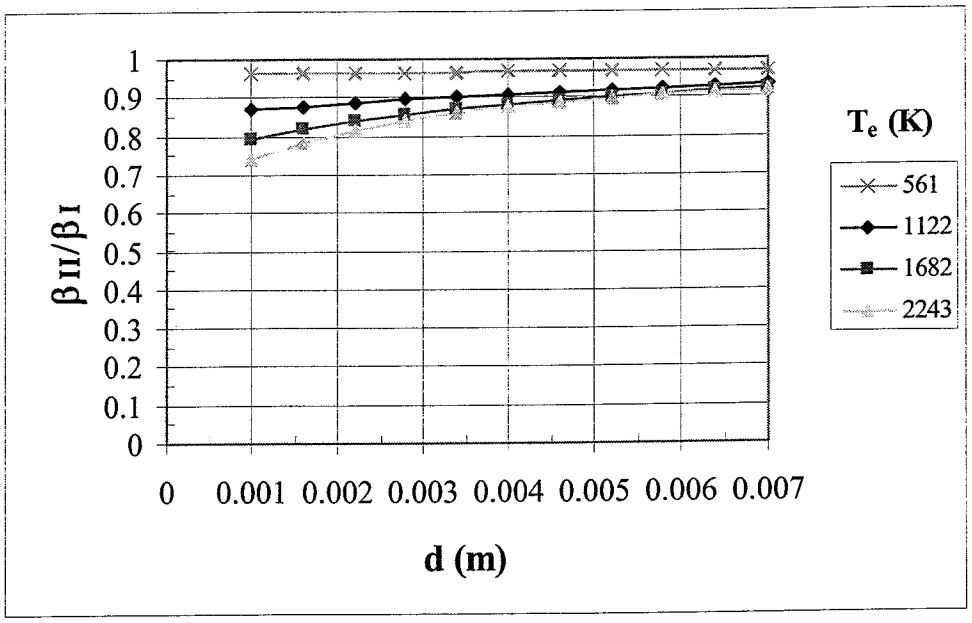

(e) Tungsten
T_{crit} = 2745 K

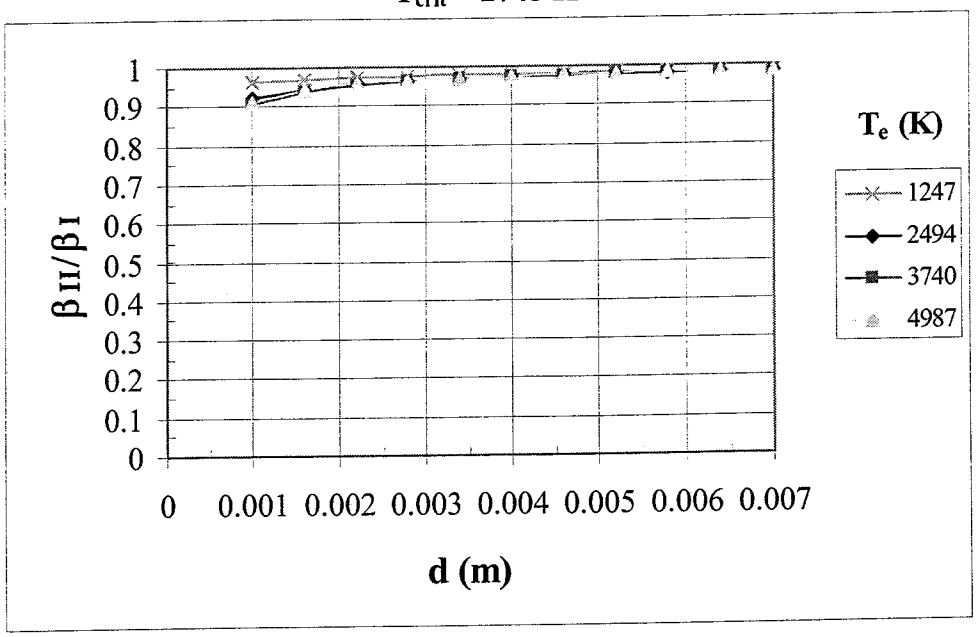

(f) Niobium Carbide
T_{crit} = 2917 K

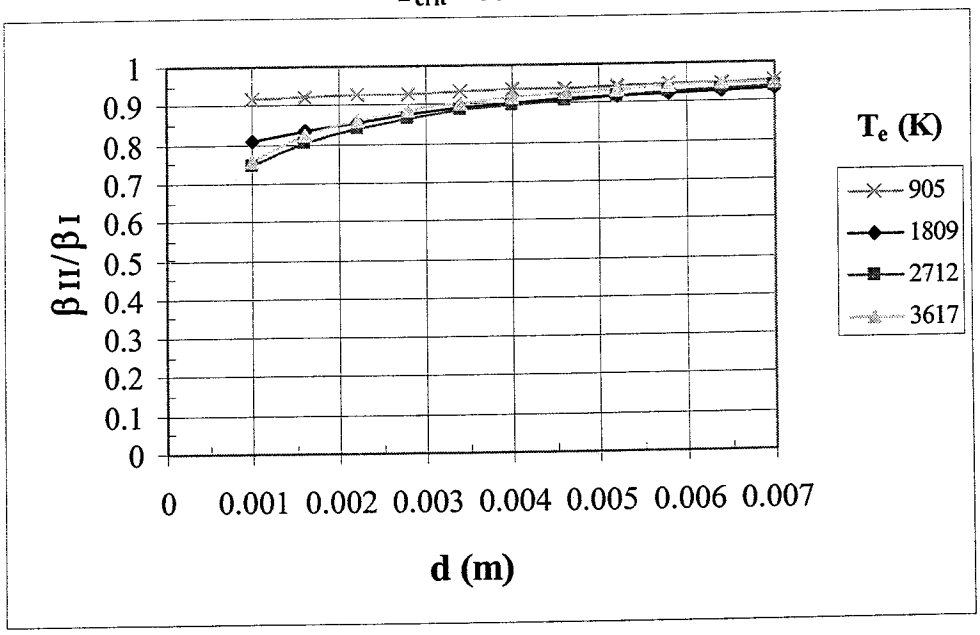

Figure G2. Ratio of Dimensionless Mass Flow Rate Parameter, β, for Models II and I as a Function of Channel Diameter and Material Thickness

(a) Aluminum
T_{crit} = 641 K

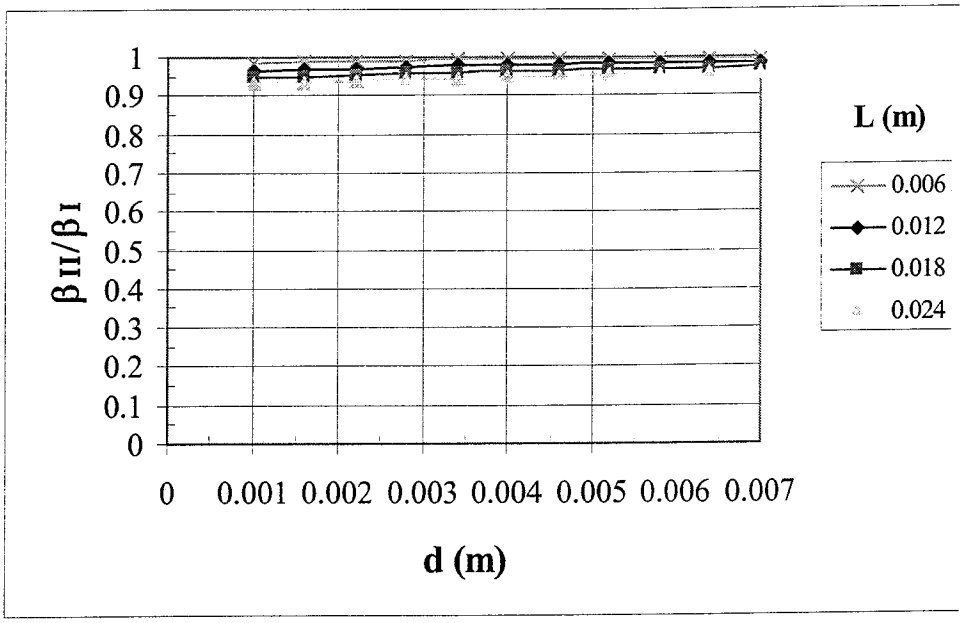

(b) Copper
T_{crit} = 1016 K

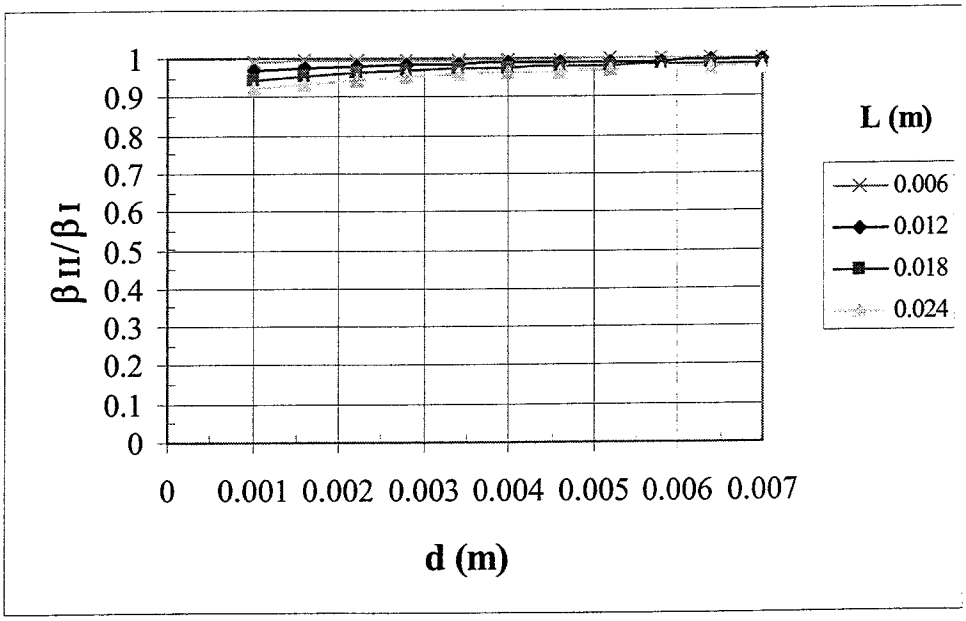

(c) Steel
T_{crit} = 1337 K

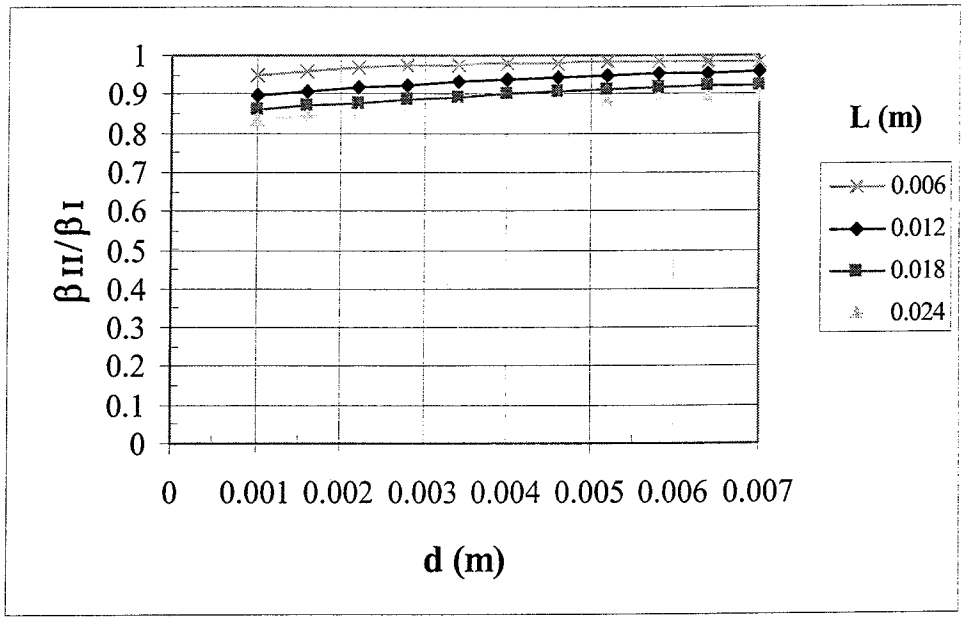

(d) Titanium
T_{crit} = 1464 K

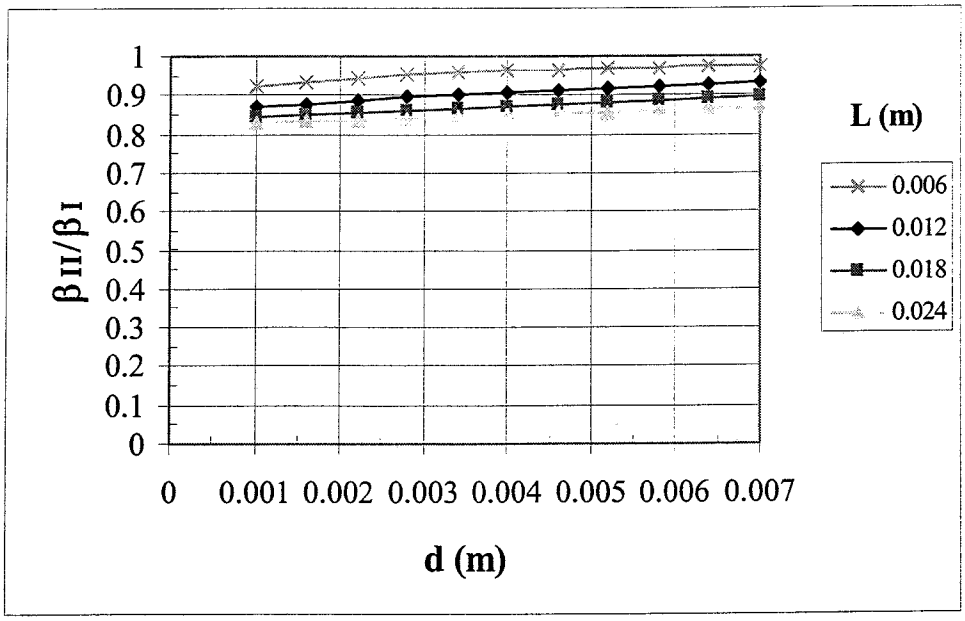

(e) Tungsten
T_{crit} = 2745 K

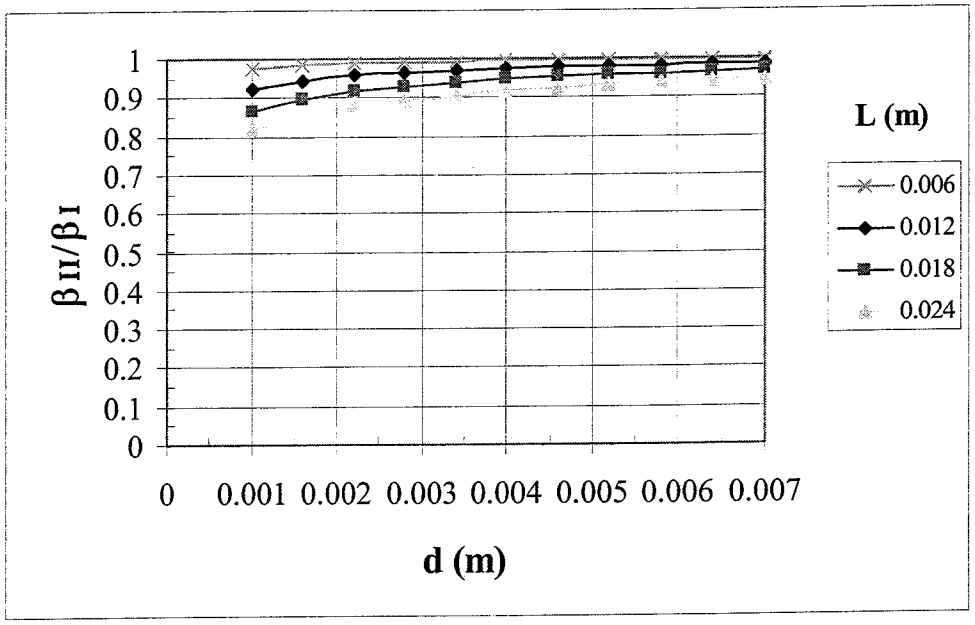

(f) Niobium Carbide
T_{crit} = 2917 K

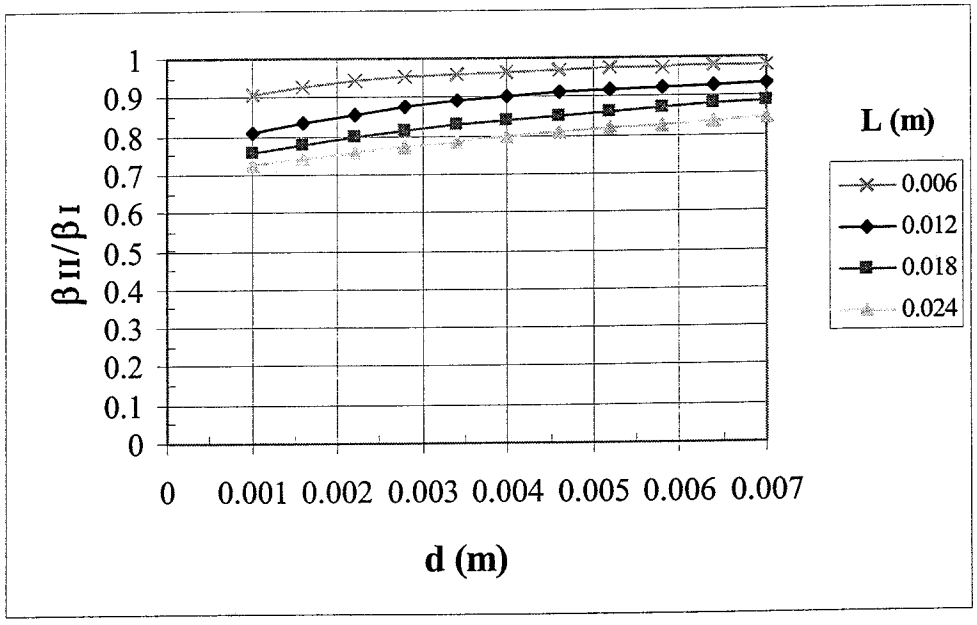

Figure G3. Ratio of Dimensionless Mass Flow Rate Parameter, β, for Models II and I as a Function of Channel Diameter and Convection Heat Transfer Coefficient

(a) Aluminum
T_{crit} = 641 K

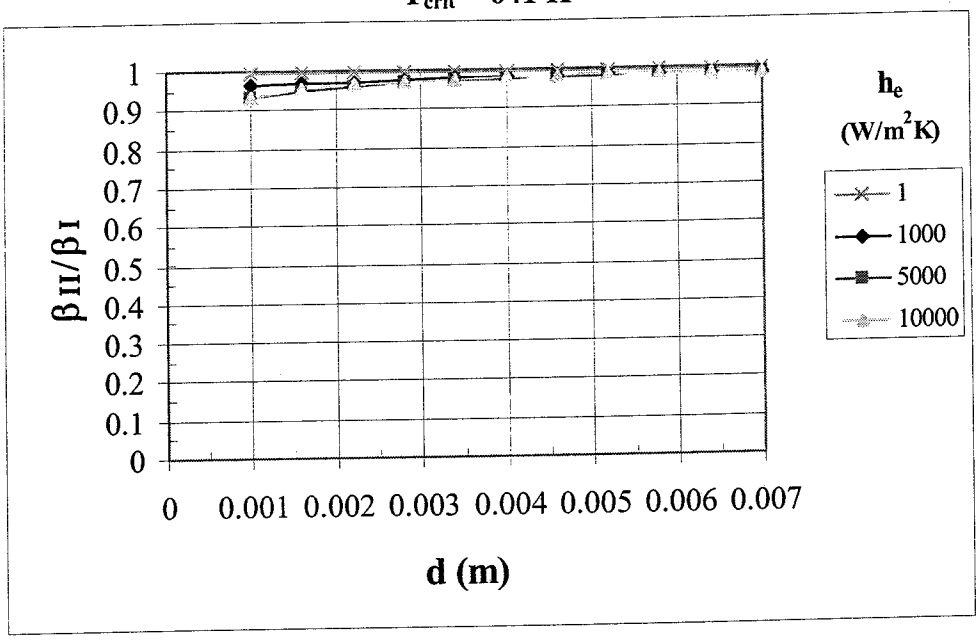

(b) Copper
T_{crit} = 1016 K

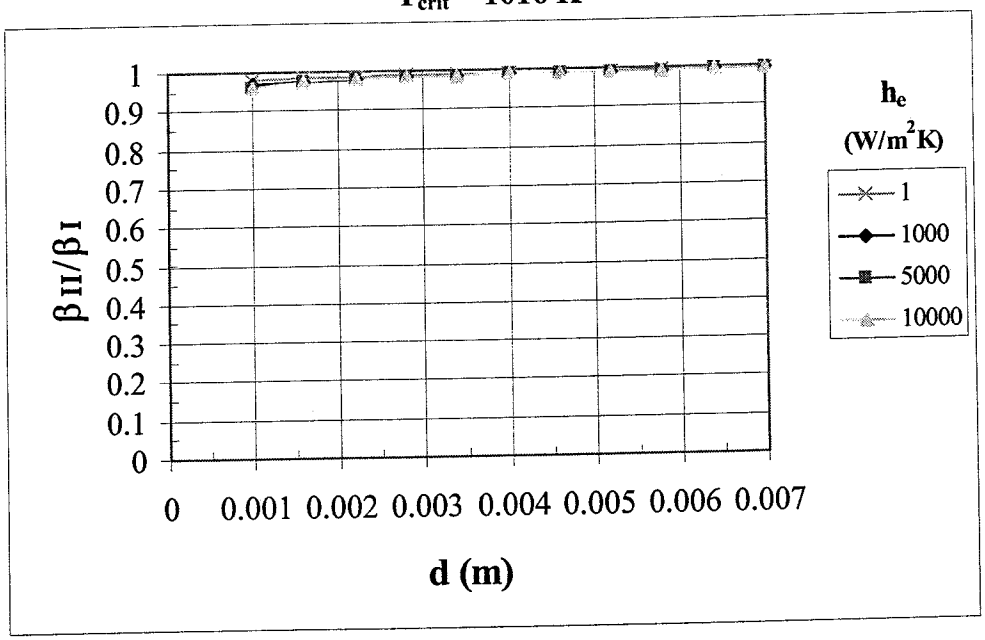

(c) Steel
T_{crit} = 1337 K

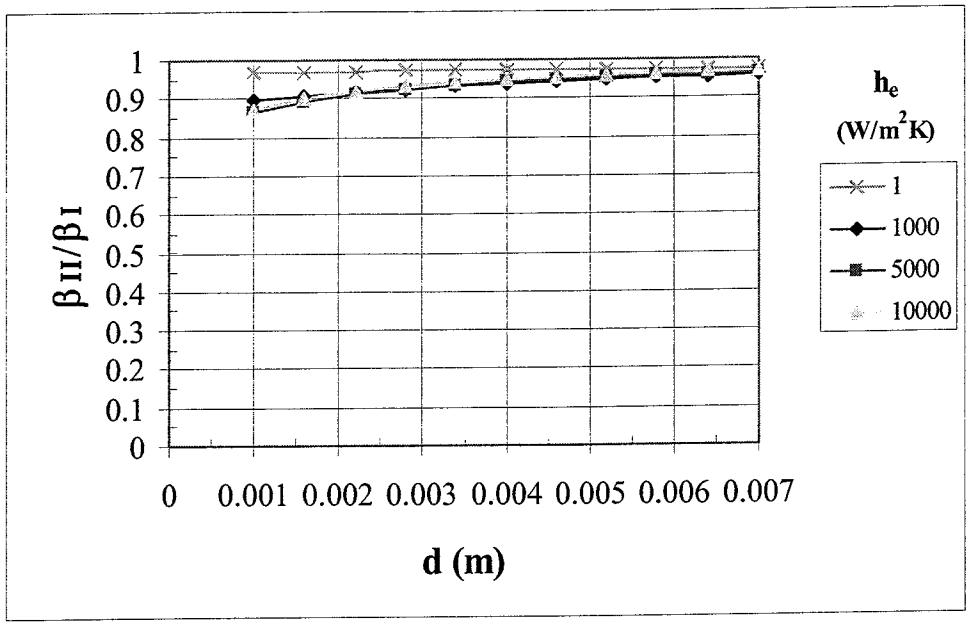

(d) Titanium
T_{crit} = 1464 K

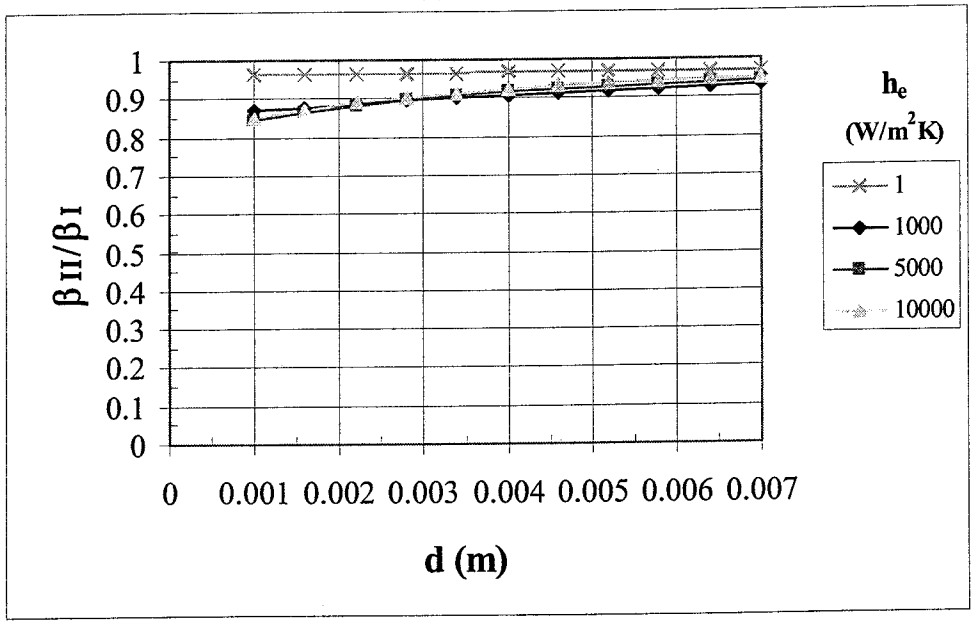

(e) Tungsten
T_{crit} = 2745 K

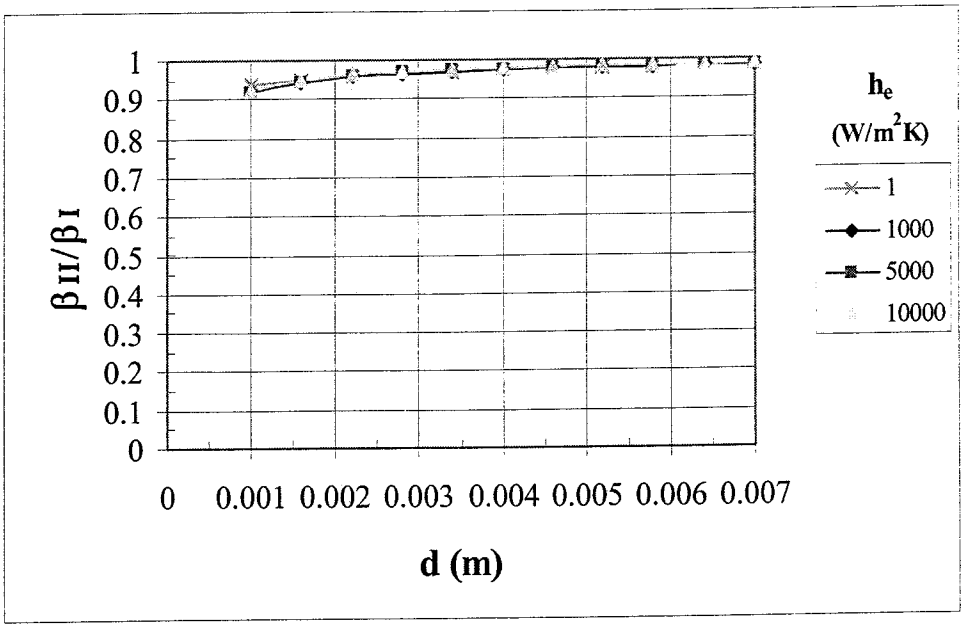

(f) Niobium Carbide
T_{crit} = 2917 K

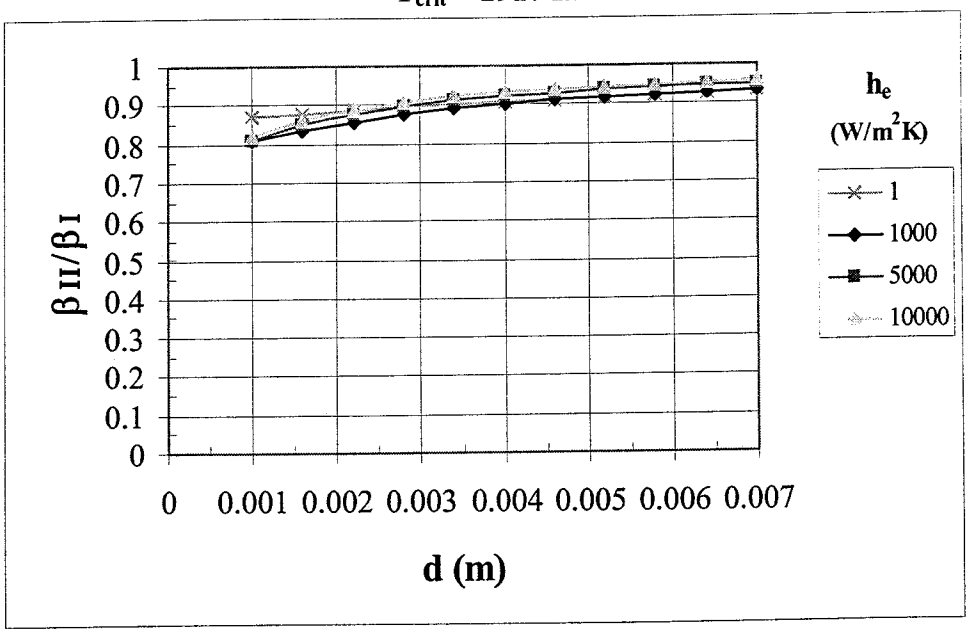

Figure G4. Ratio of Dimensionless Mass Flow Rate Parameter, β, for Models II and I as a Function of Convection Heat Transfer Coefficient and Environmental Temperature

(a) Aluminum
T_{crit} = 641 K

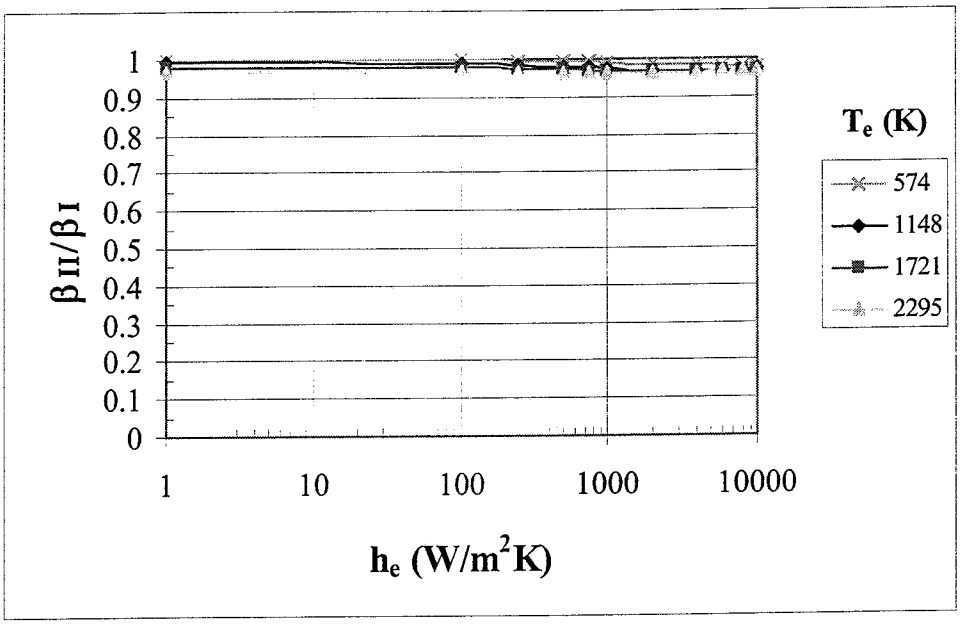

(b) Copper
T_{crit} = 1016 K

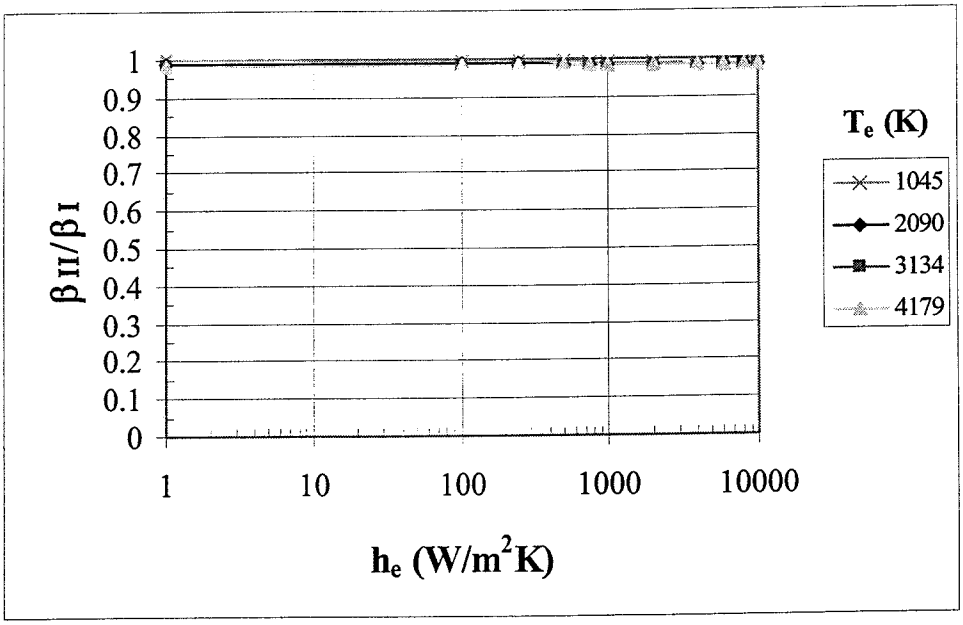

(c) Steel
T_{crit} = 1337 K

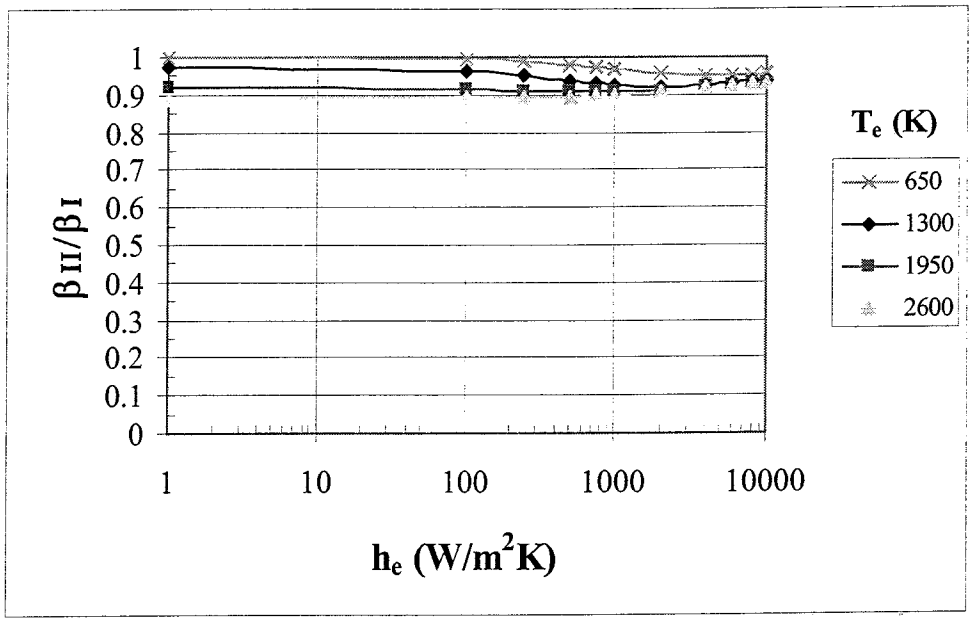

(d) Titanium
T_{crit} = 1464 K

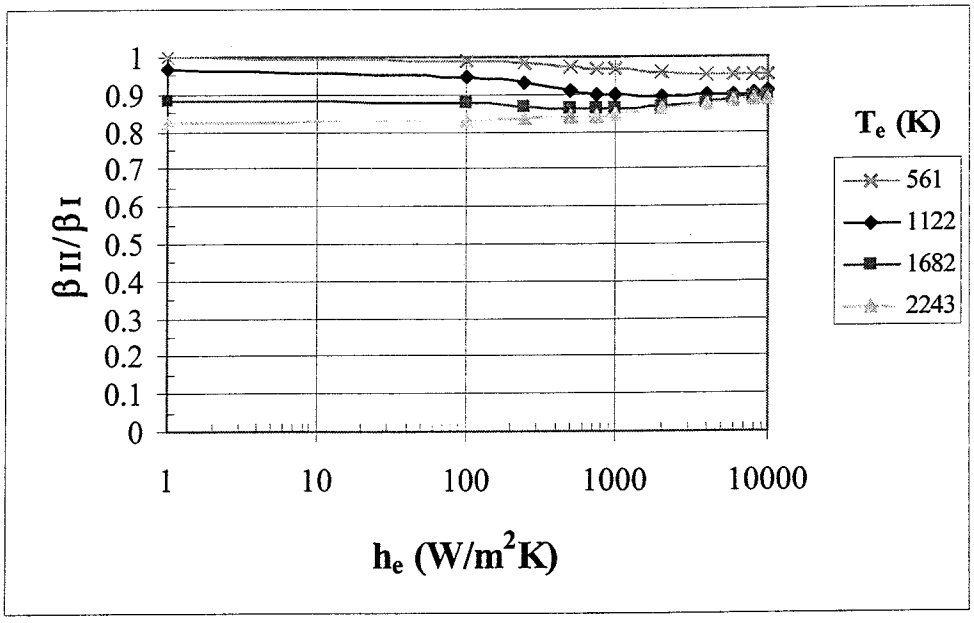

(e) Tungsten
T_{crit} = 2745 K

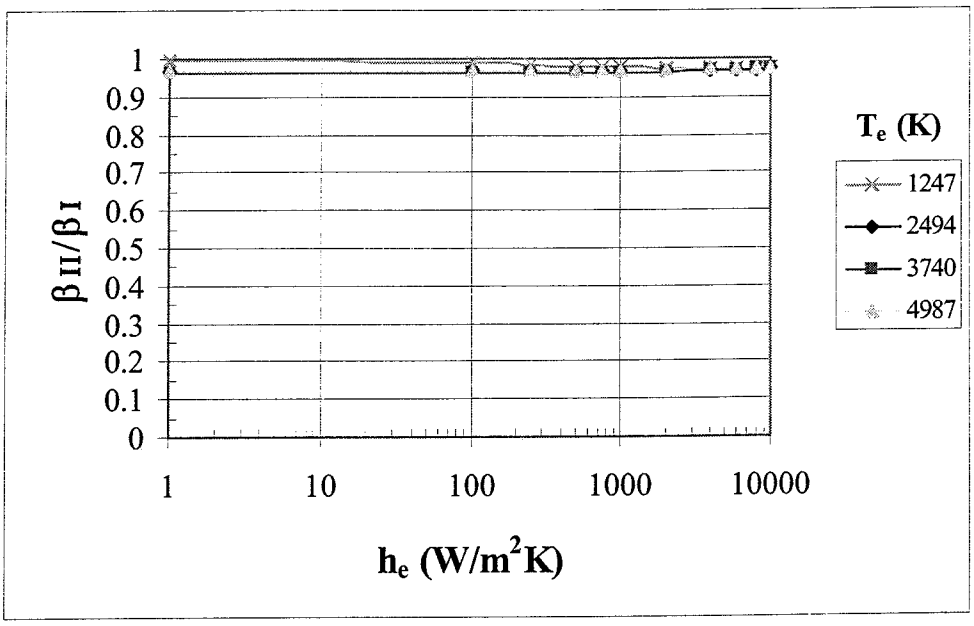

(f) Niobium Carbide
T_{crit} = 2917 K

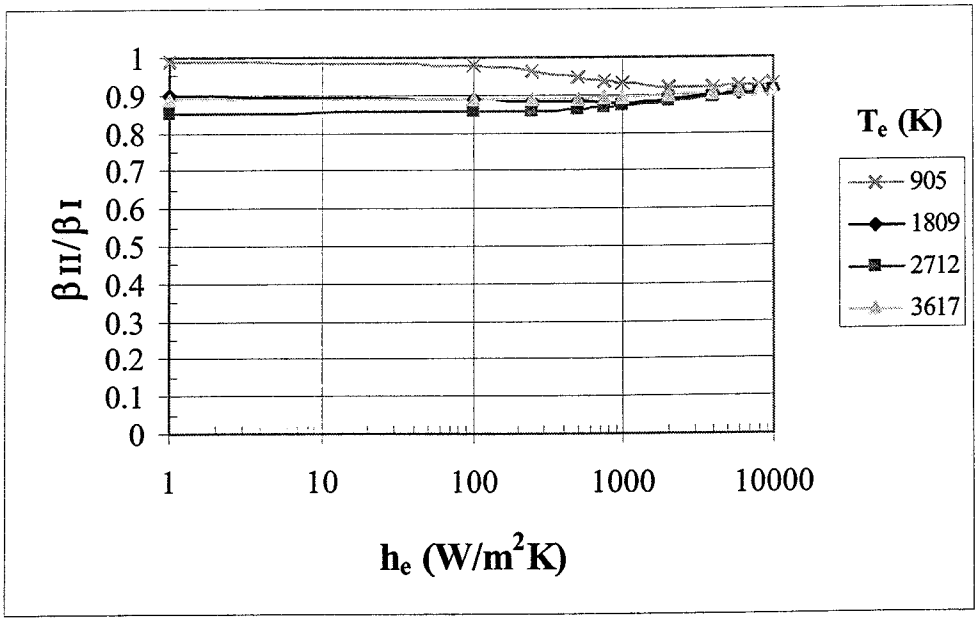

Figure G5. Ratio of Dimensionless Mass Flow Rate Parameter, β, for Models II and I as a Function of Convection Heat Transfer Coefficient and Material Thickness

(a) Aluminum
T_{crit} = 641 K

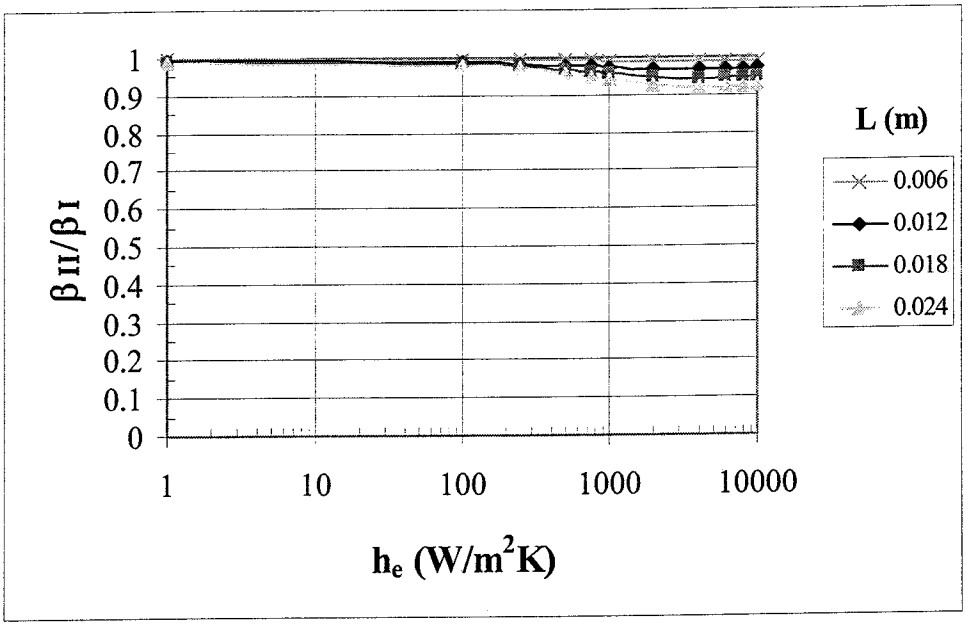

(b) Copper
T_{crit} = 1016 K

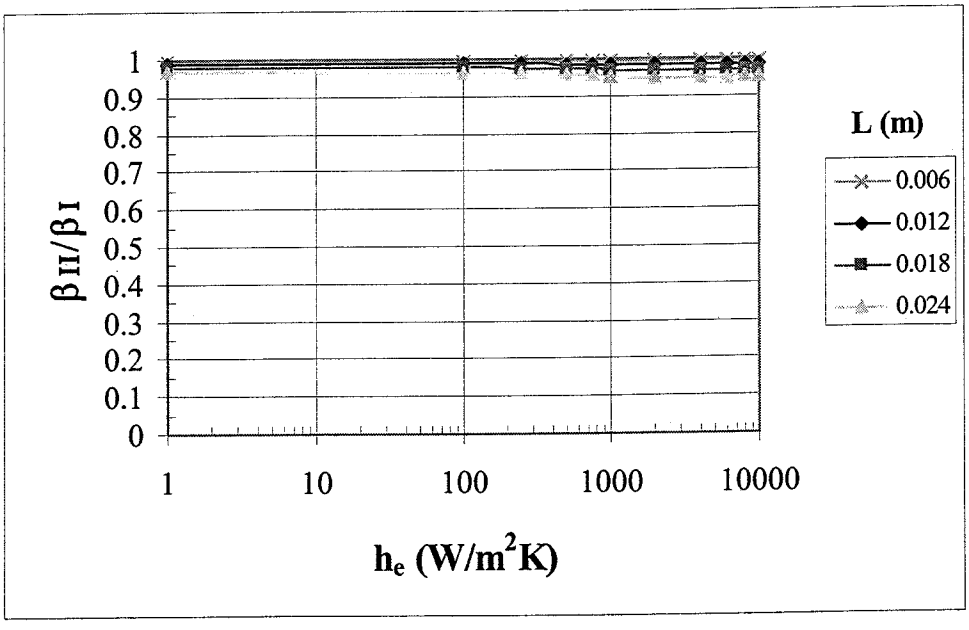

(c) Steel

T_{crit} = 1337 K

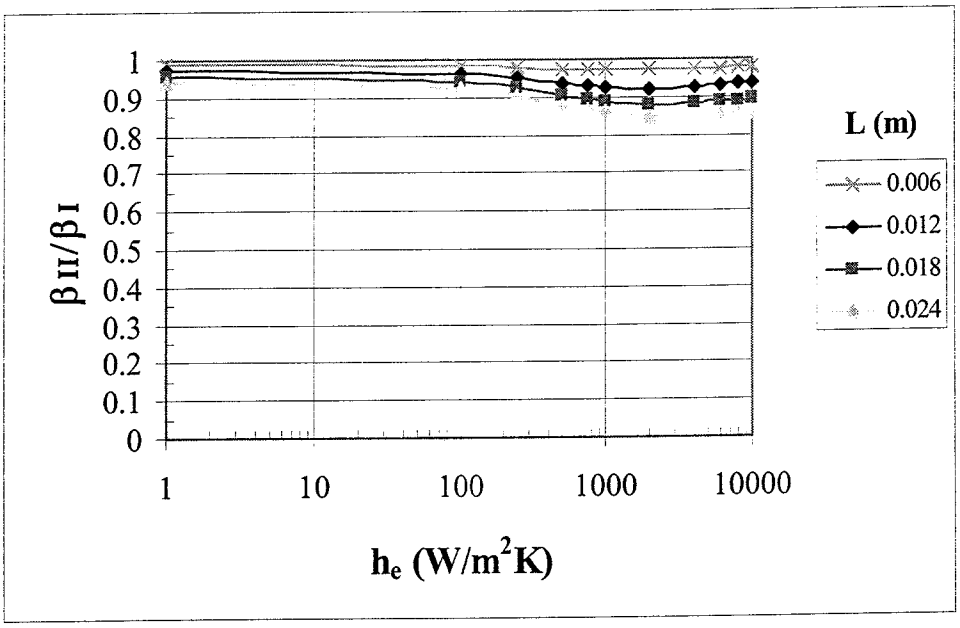

(d) Titanium

T_{crit} = 1464 K

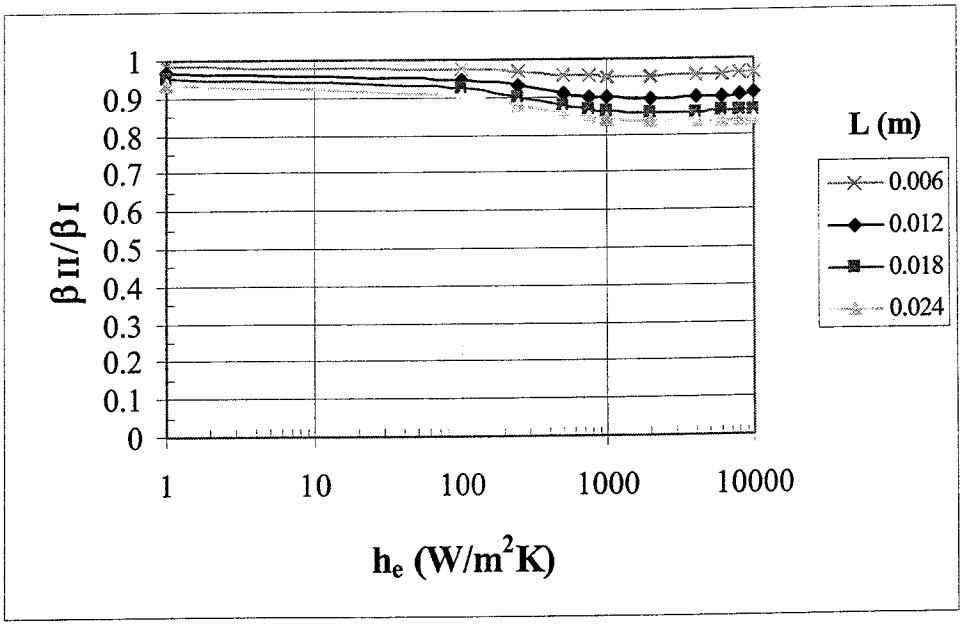

(e) Tungsten
T_{crit} = 2745 K

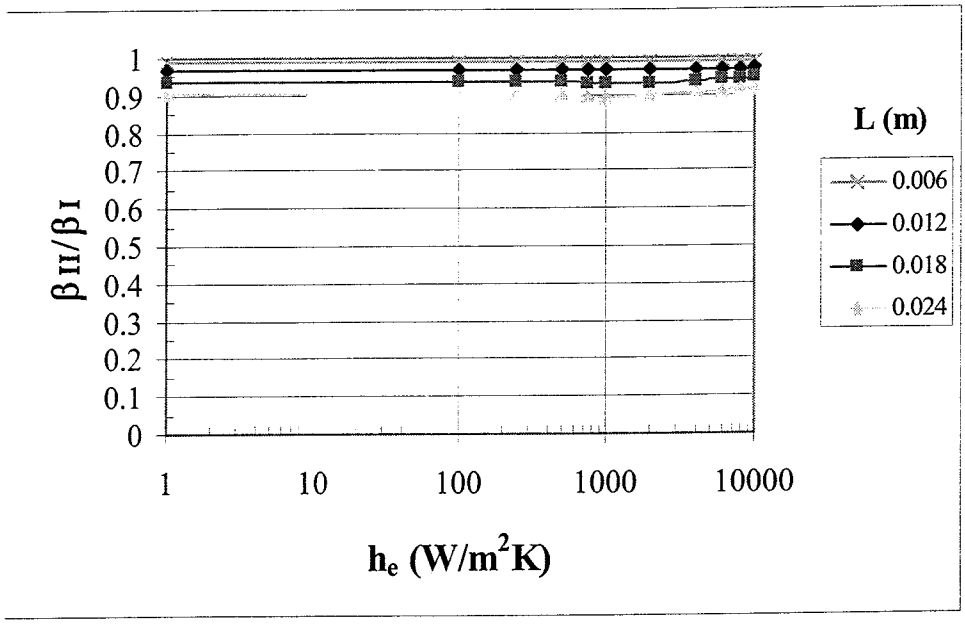

(f) Niobium Carbide
T_{crit} = 2917 K

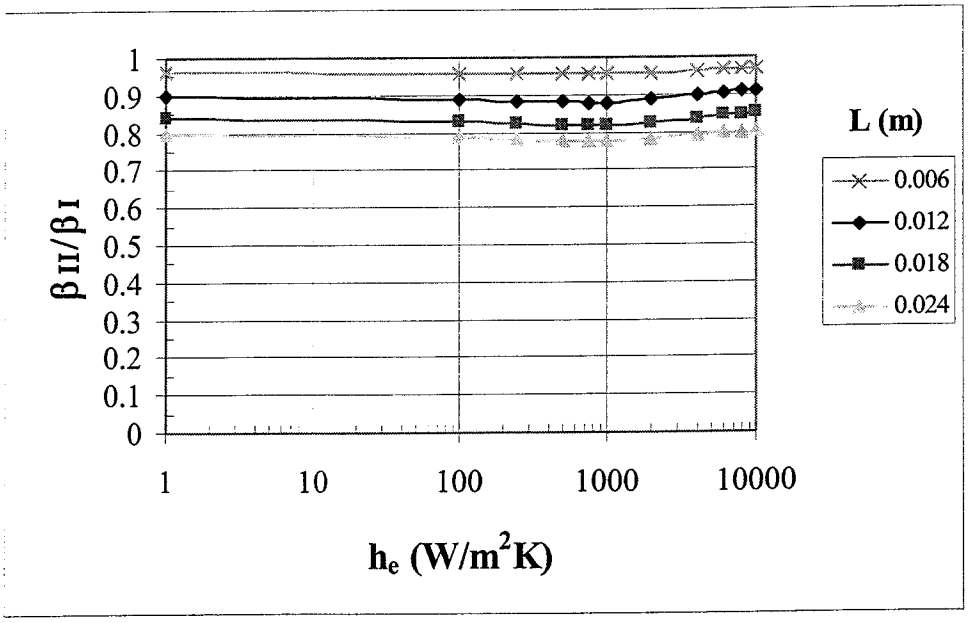

Figure G6. Ratio of Dimensionless Mass Flow Rate Parameter, β, for Models II and I as a Function of Convection Heat Transfer Coefficient and Channel Diameter

(a) Aluminum
T_{crit} = 641 K

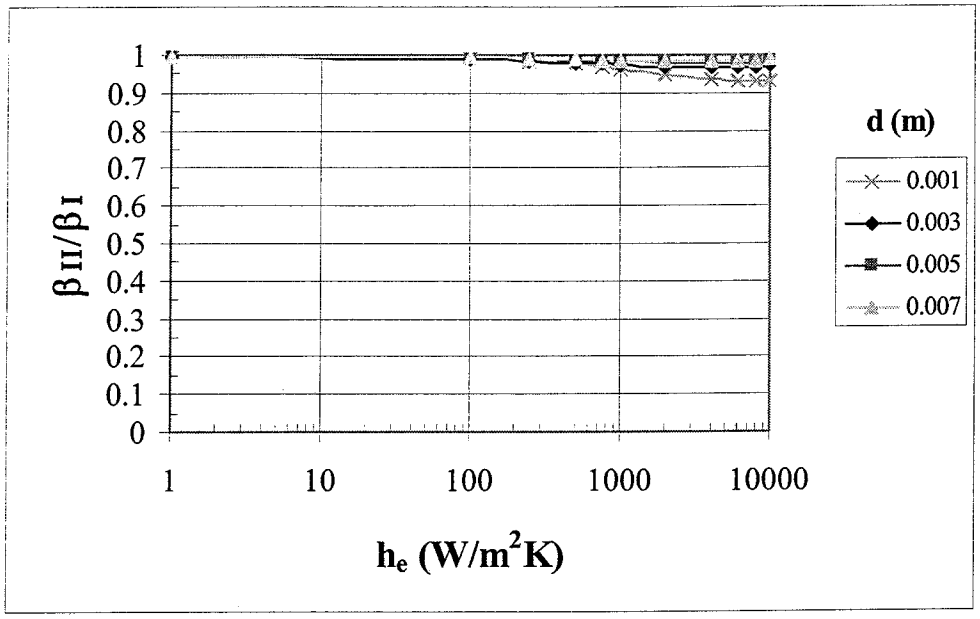

(b) Copper
T_{crit} = 1016 K

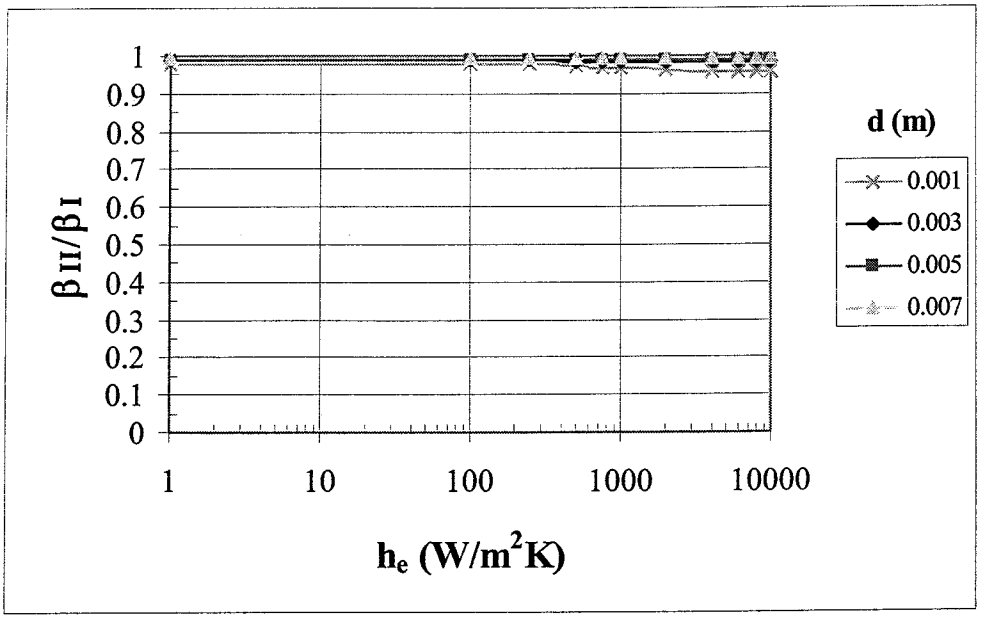

(c) Steel
T_{crit} = 1337 K

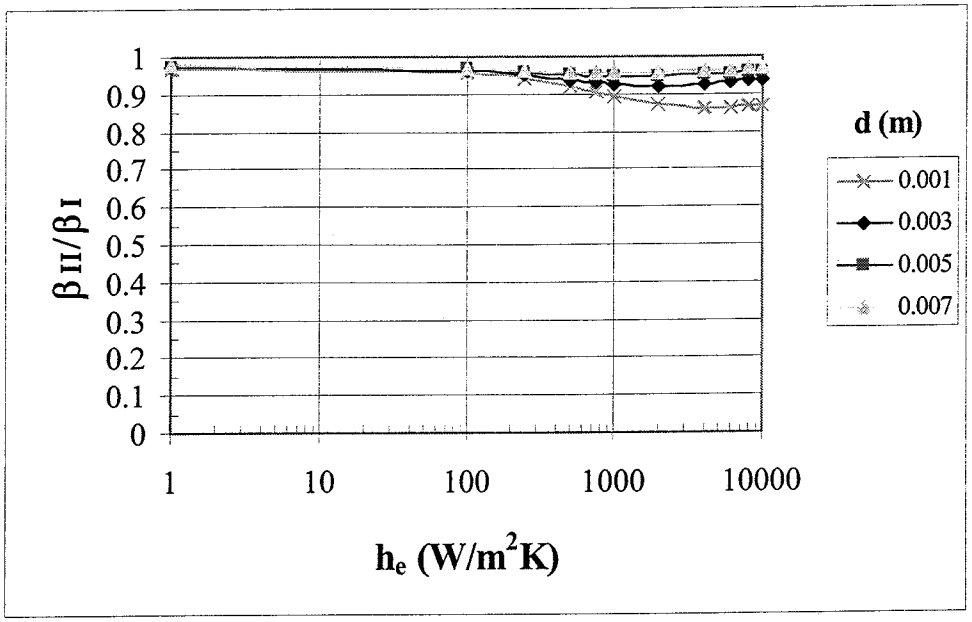

(d) Titanium
T_{crit} = 1464 K

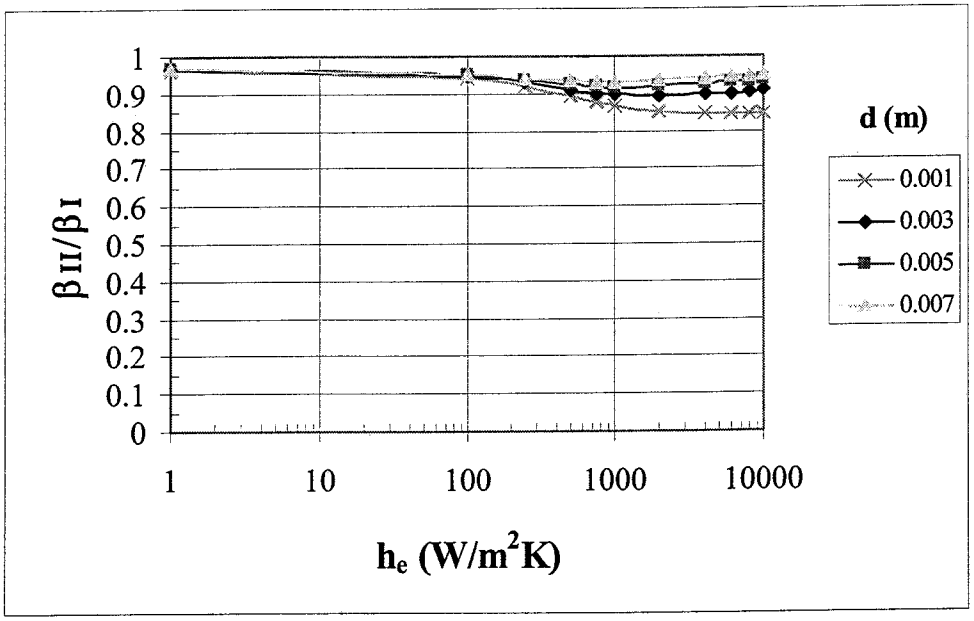

(e) Tungsten
T_{crit} = 2745 K

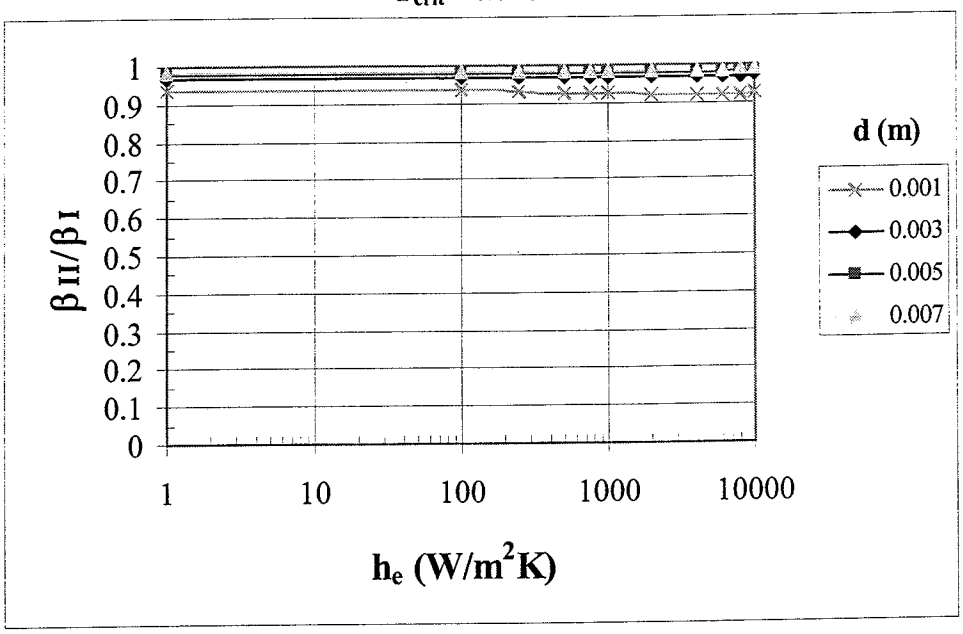

(f) Niobium Carbide
T_{crit} = 2917 K

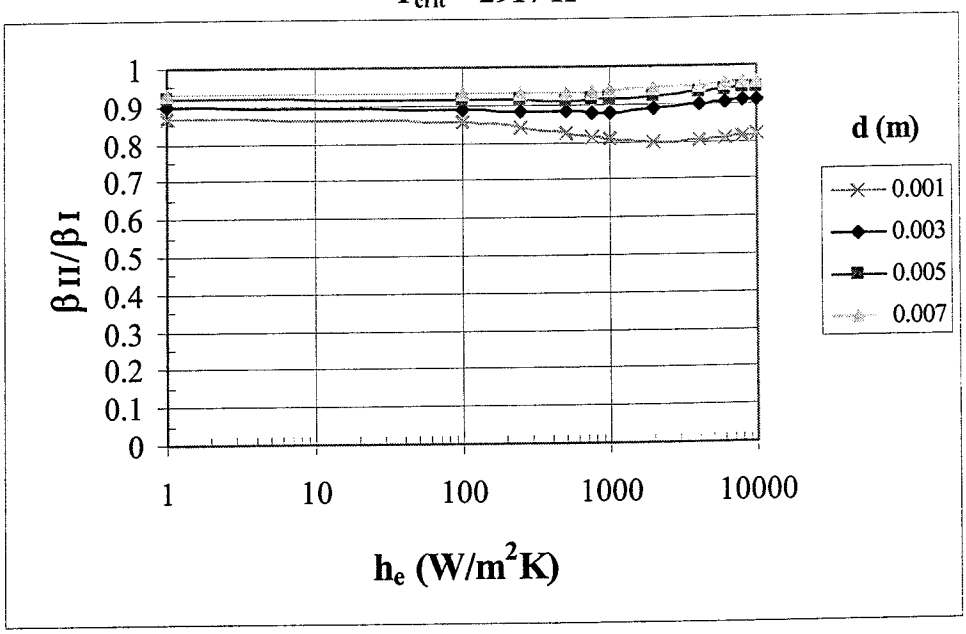

Figure G7. Ratio of Dimensionless Mass Flow Rate Parameter, β, for Models II and I as a Function of Material Thickness and Environmental Temperature

(a) Aluminum
T_{crit} = 641 K

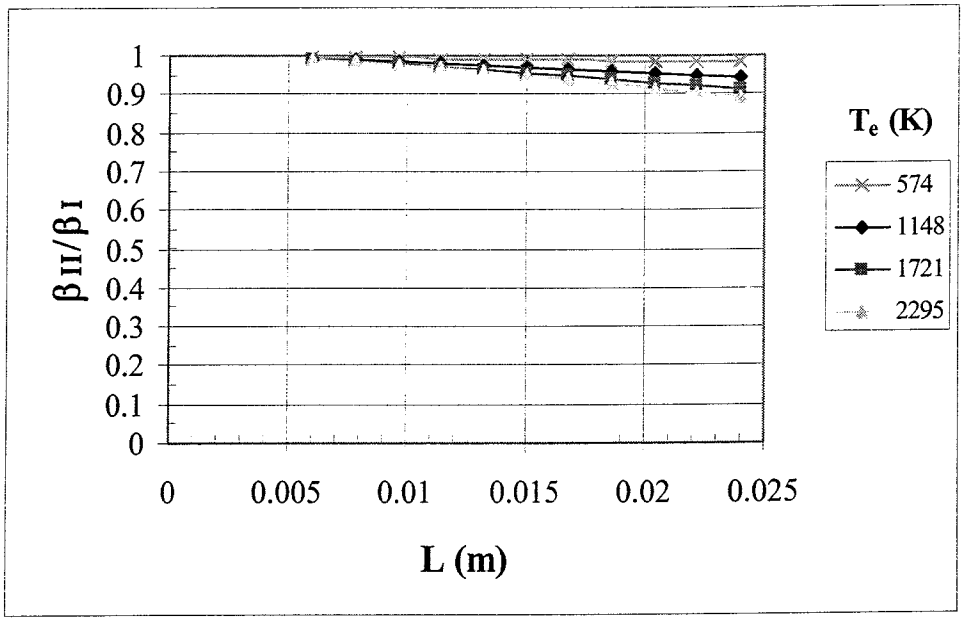

(b) Copper
T_{crit} = 1016 K

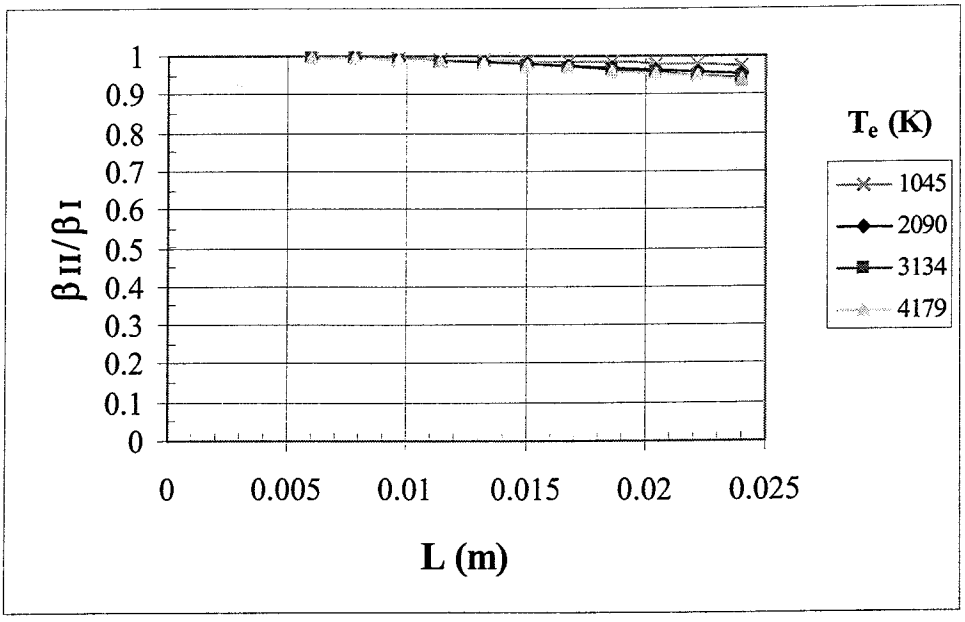

(c) Steel
T_{crit} = 1337 K

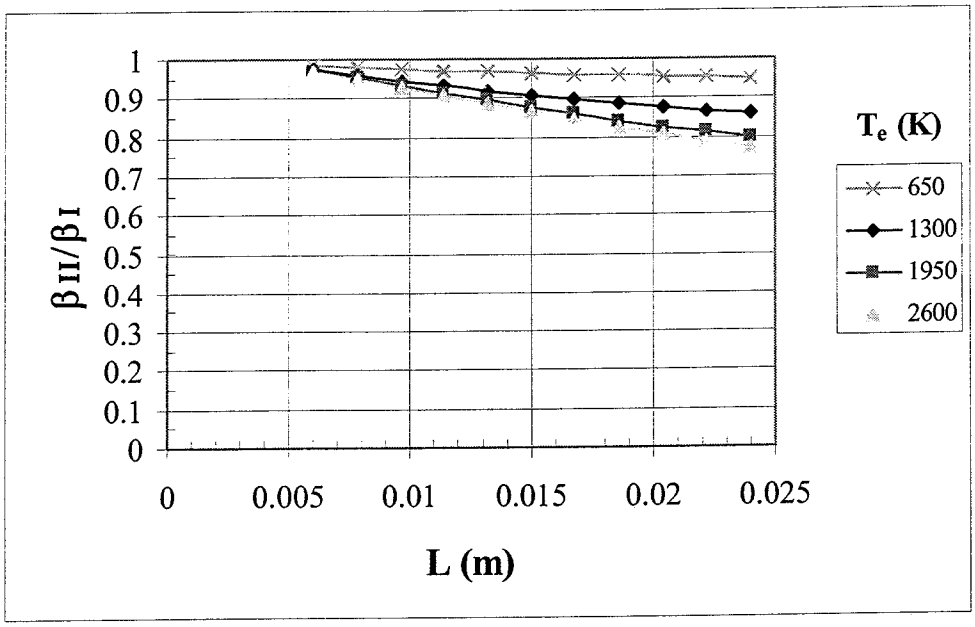

(d) Titanium
T_{crit} = 1464 K

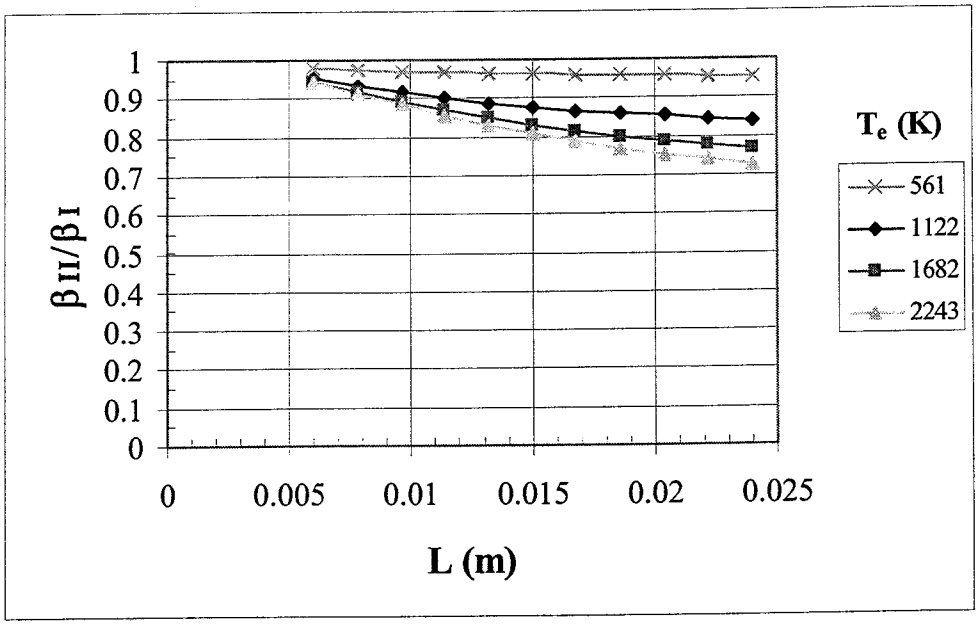

(e) Tungsten
T_{crit} = 2745 K

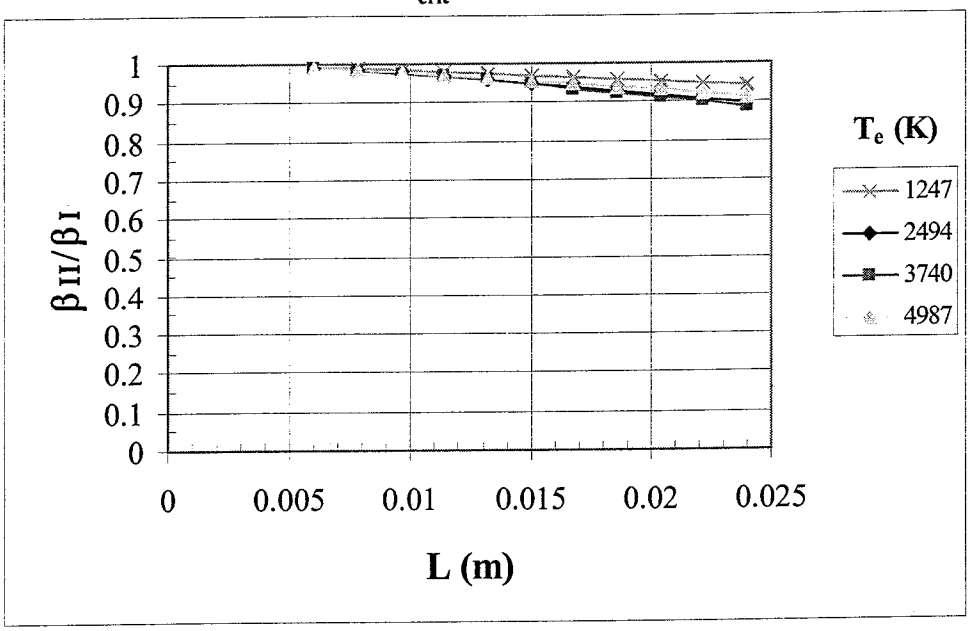

(f) Niobium Carbide
T_{crit} = 2917 K

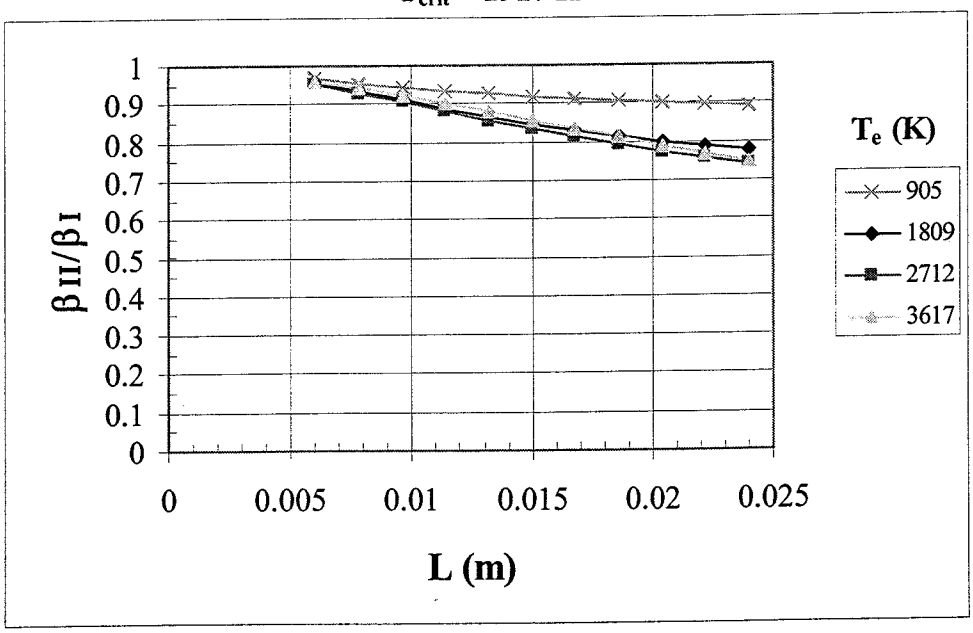

Figure G8. Ratio of Dimensionless Mass Flow Rate Parameter, β, for Models II and I as a Function of Material Thickness and Channel Diameter

(a) Aluminum
T_{crit} = 641 K

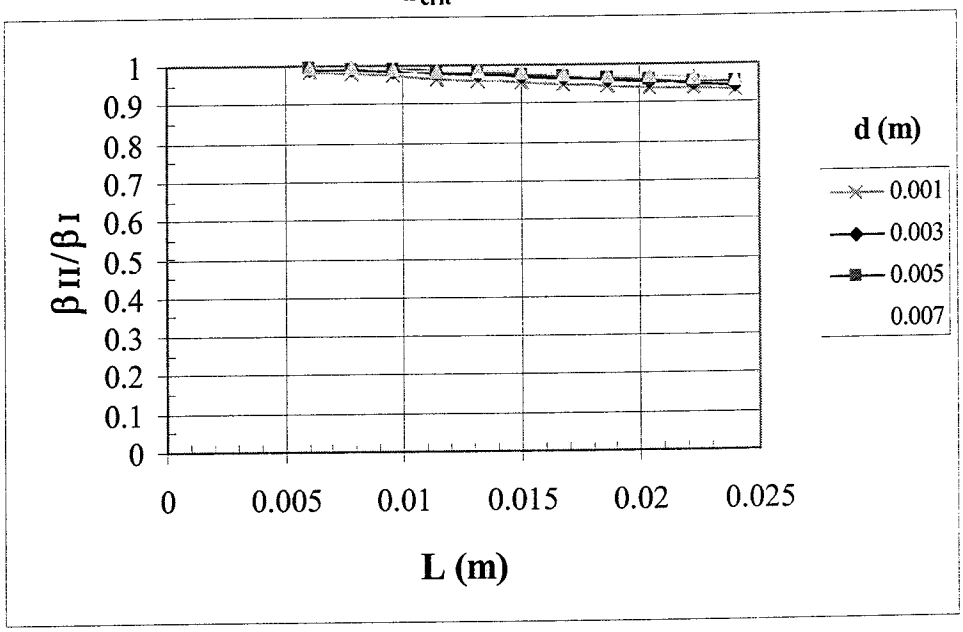

(b) Copper
T_{crit} = 1016 K

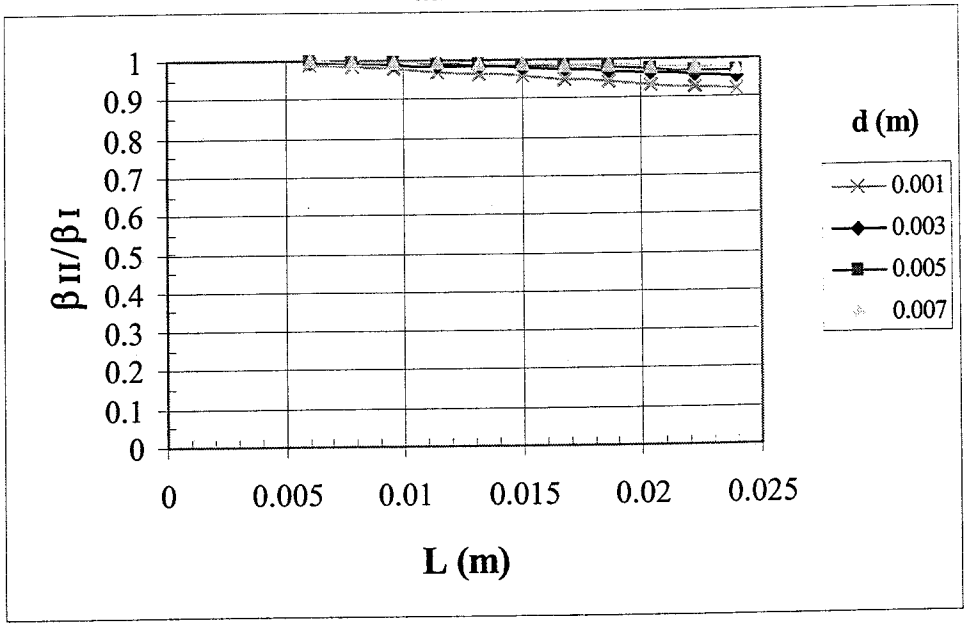

(c) Steel
T_{crit} = 1337 K

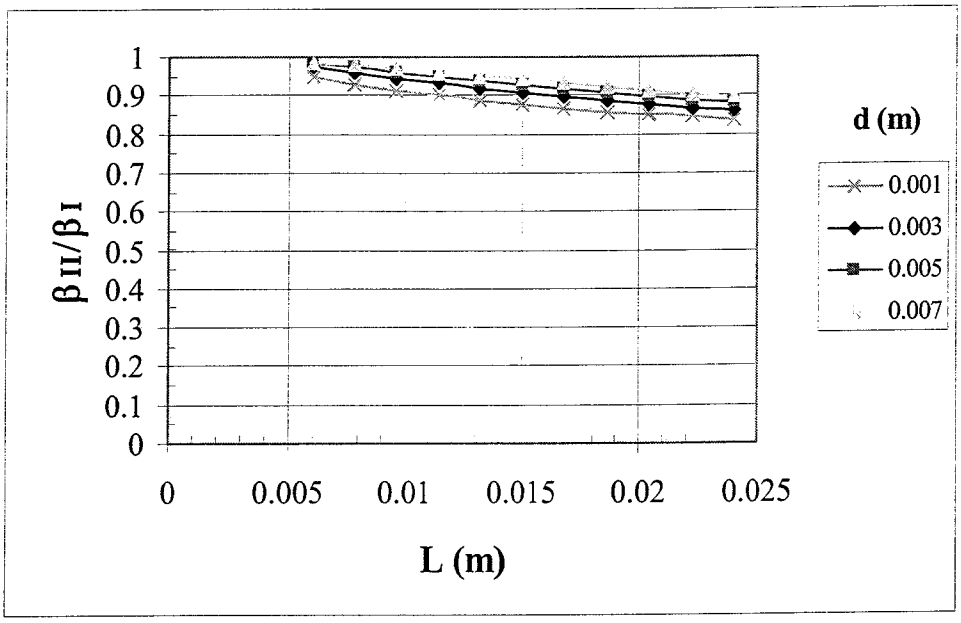

(d) Titanium
T_{crit} = 1464 K

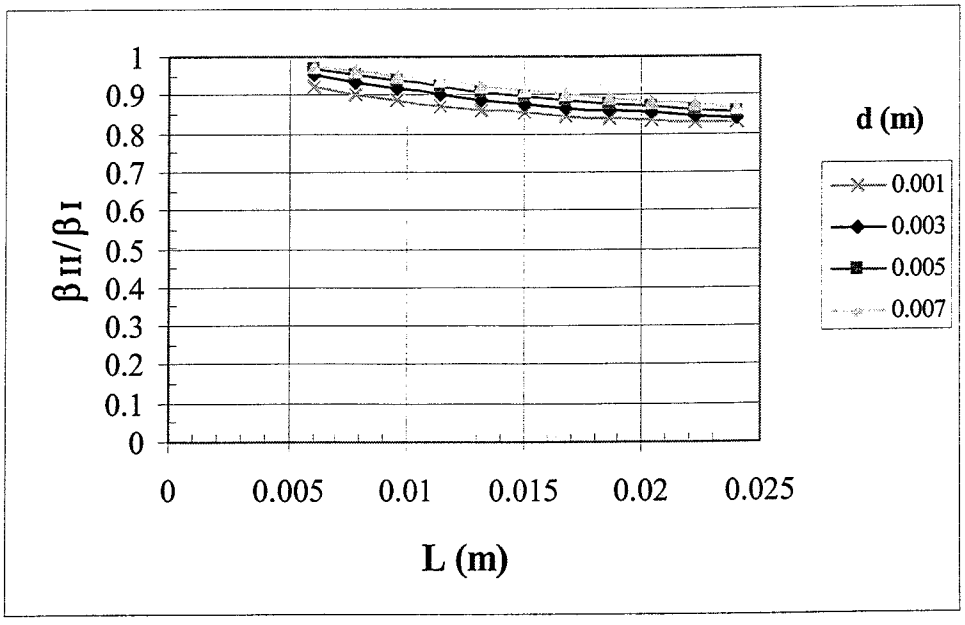

(e) Tungsten
T_{crit} = 2745 K

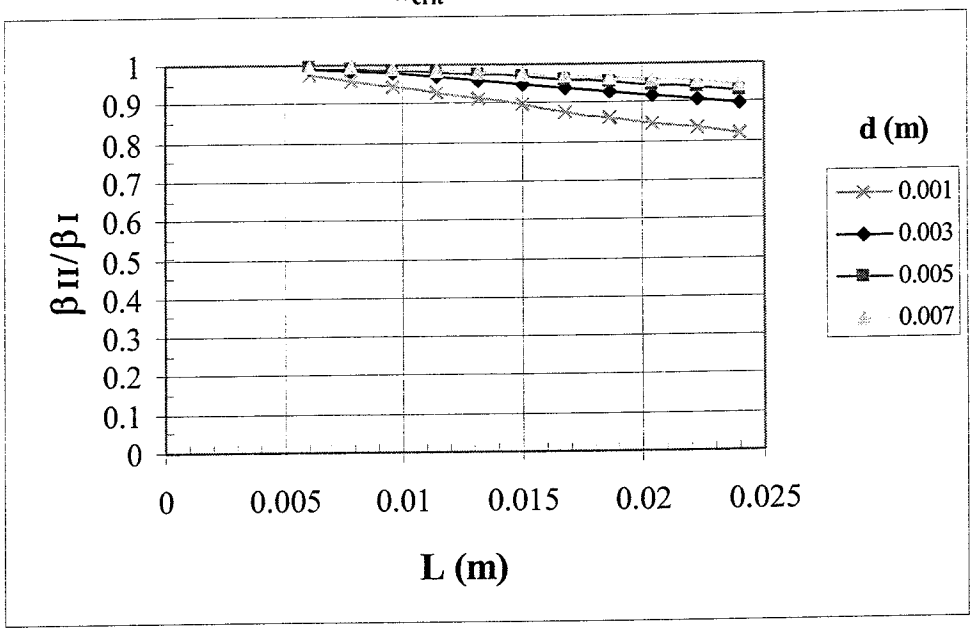

(f) Niobium Carbide
T_{crit} = 2917 K

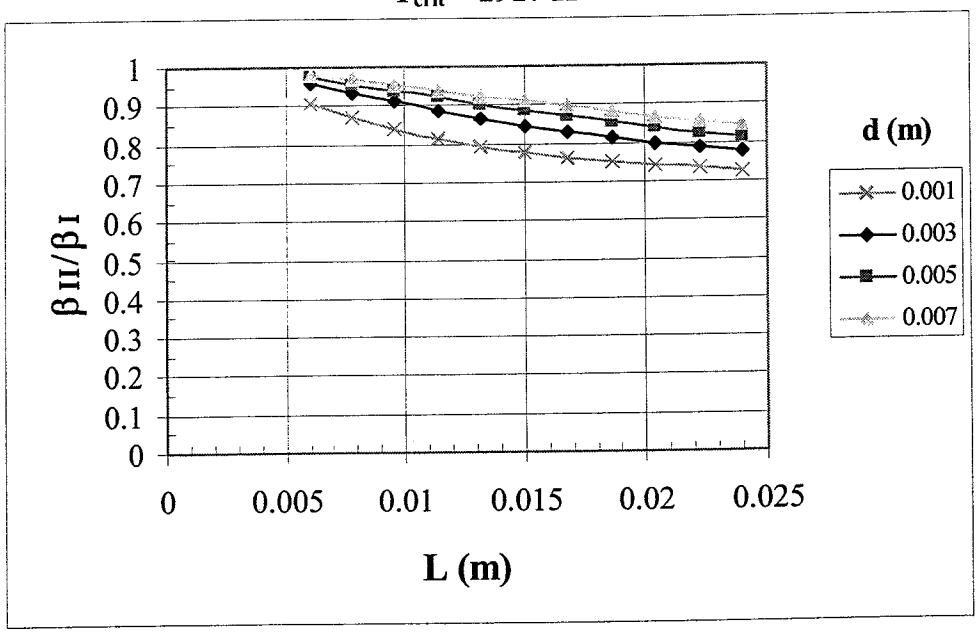

Figure G9. Ratio of Dimensionless Mass Flow Rate Parameter, β, for Models II and I as a Function of Material Thickness and Conduction Heat Transfer Coefficient

(a) Aluminum
T_{crit} = 2641 K

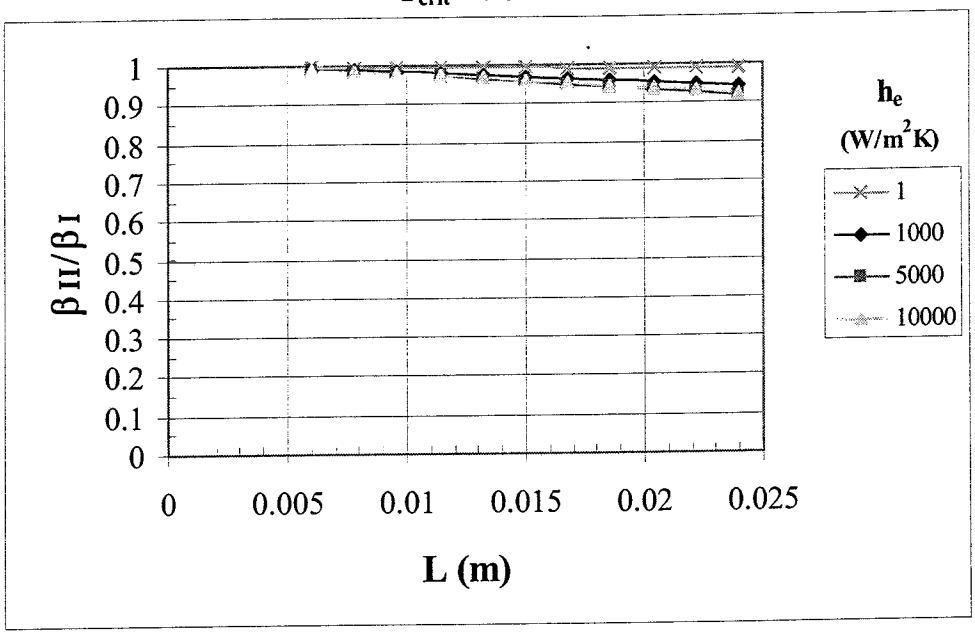

(b) Copper
T_{crit} = 1016 K

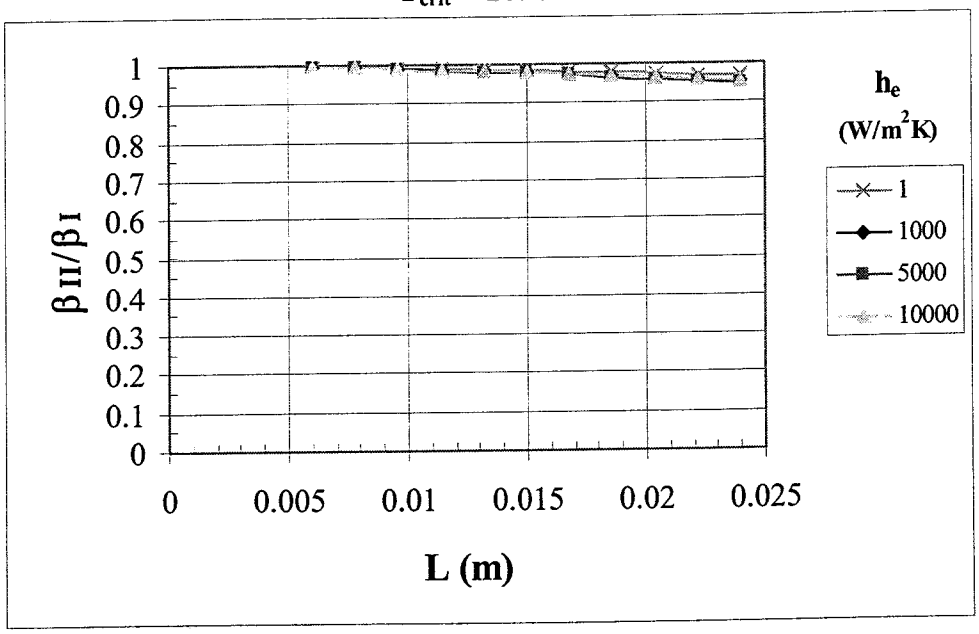

(c) Steel
T_{crit} = 1337 K

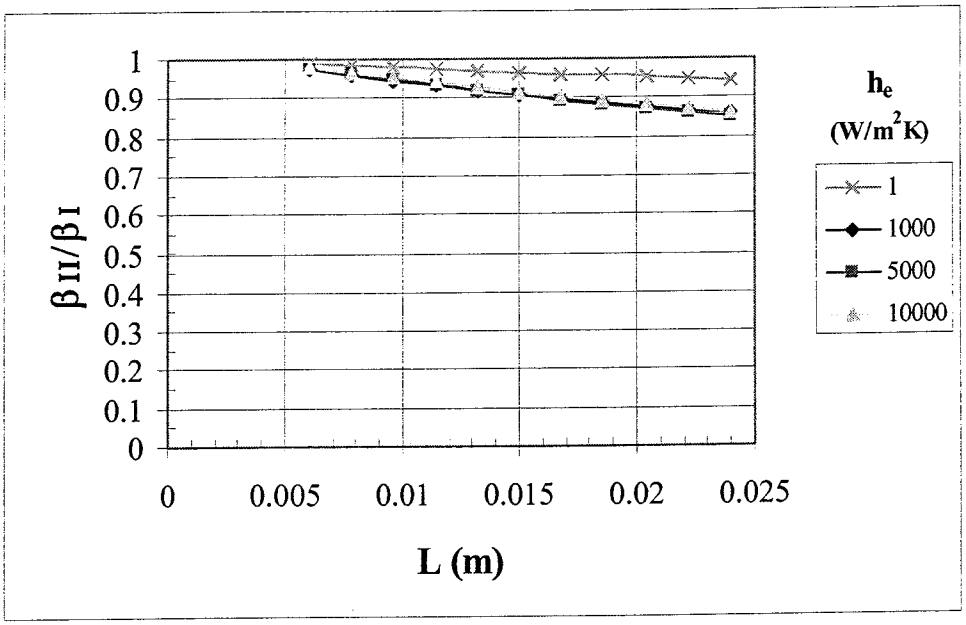

(d) Titanium
T_{crit} = 1464 K

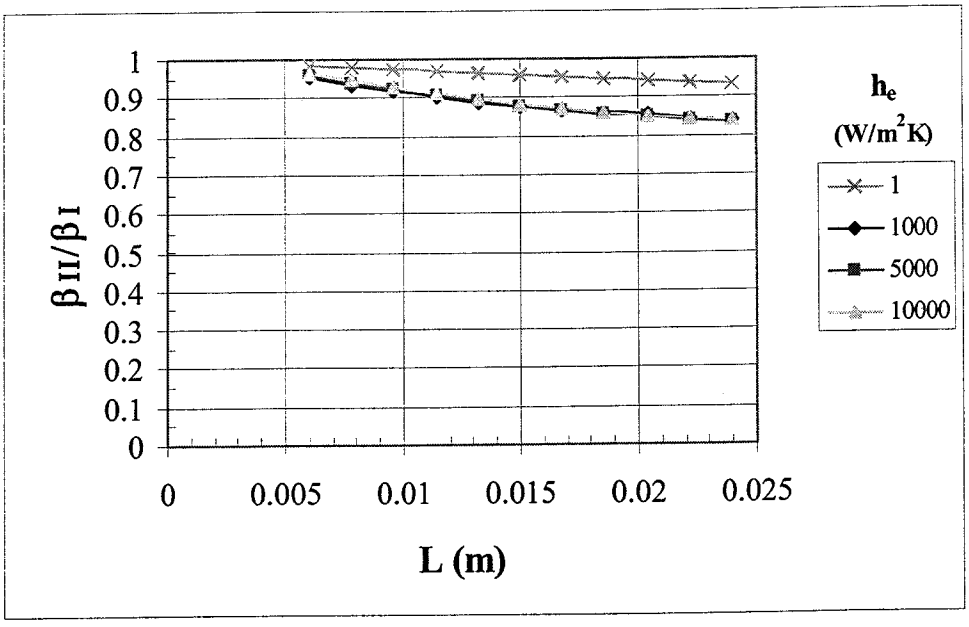

(f) Tungsten
T_{crit} = 2745 K

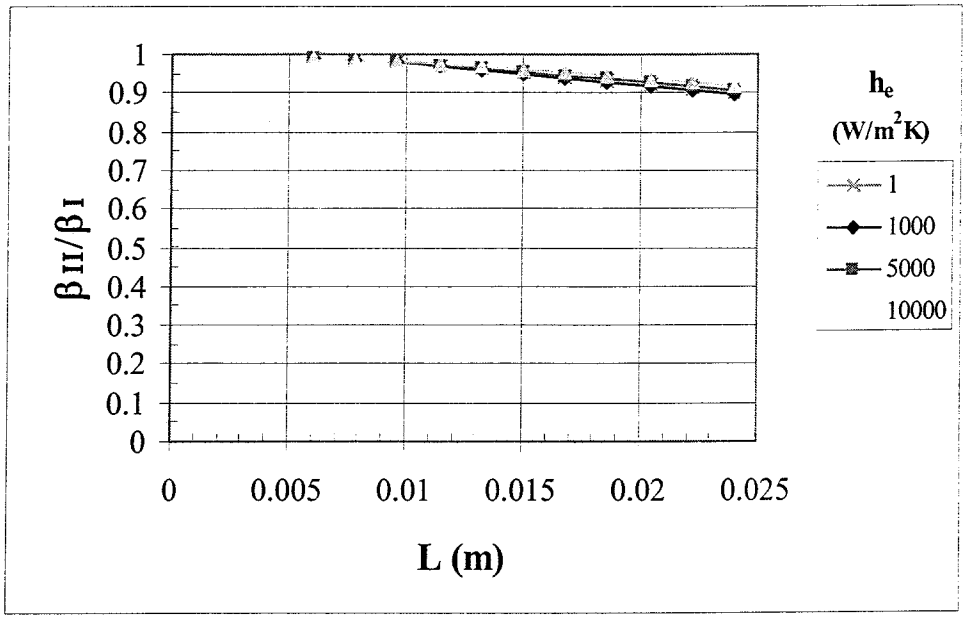

(f) Niobium Carbide
T_{crit} = 2917 K

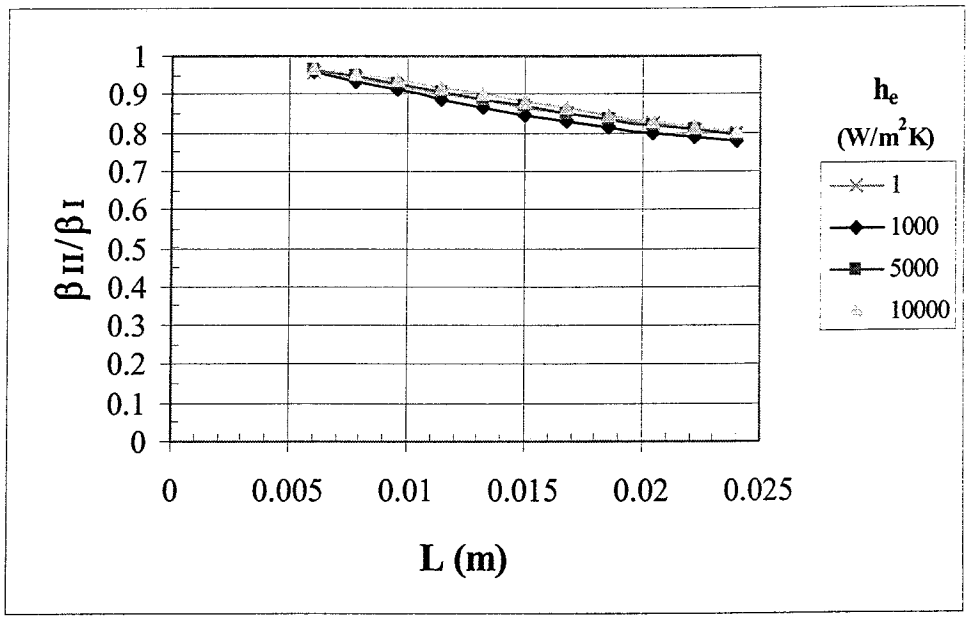

APPENDIX H

PARAMETRIC STUDY OF MASS FLOW RATE PER UNIT AREA FOR MODELS I AND II

Figure H1. Mass Flow Rate Per Unit Area for Models I and II as a Function of Material Thickness

(a) Aluminum
T_{crit} = 641 K

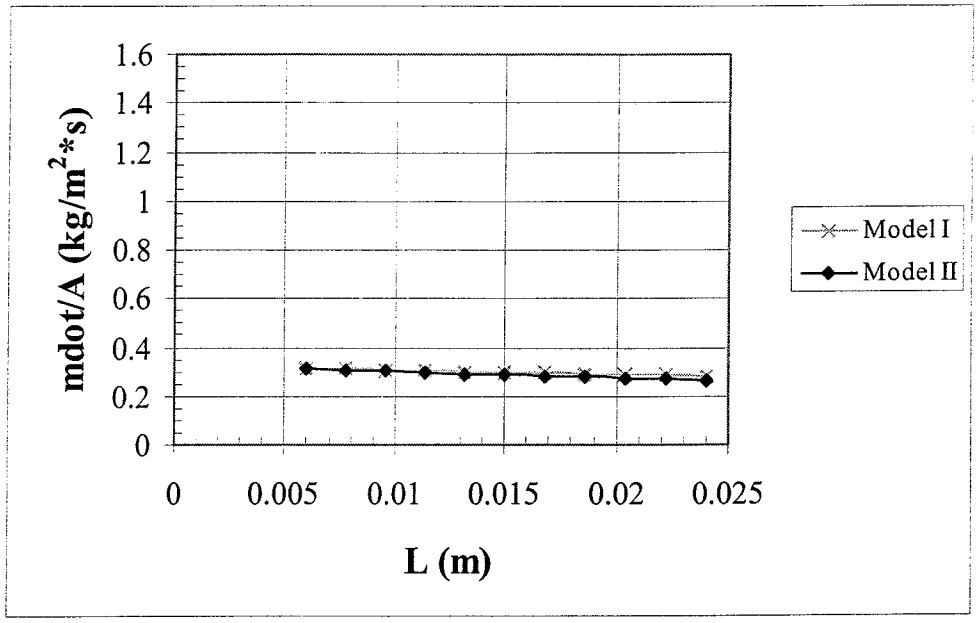

(b) Copper
T_{crit} = 1016 K

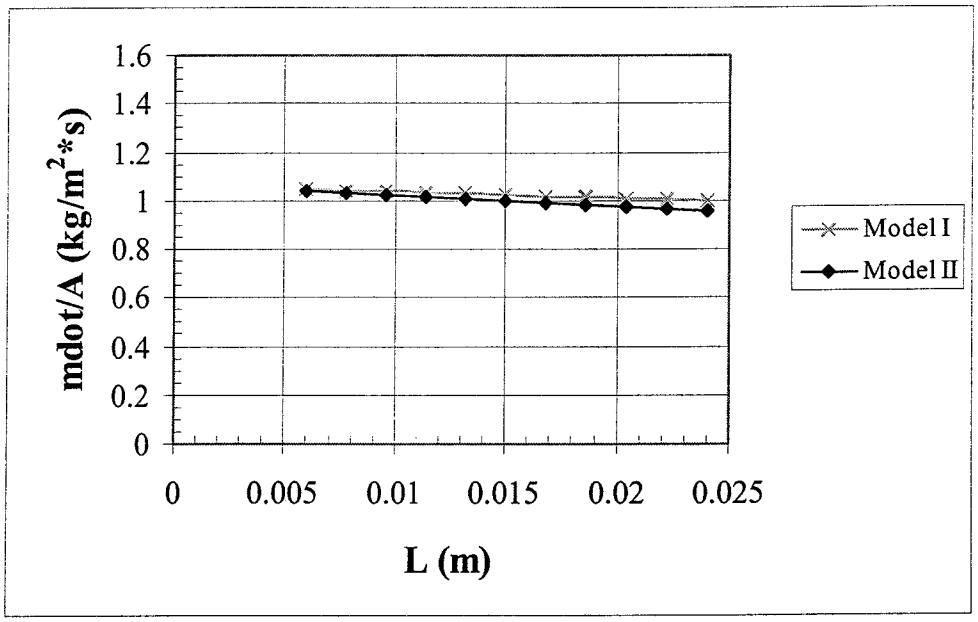

(c) Steel
T_{crit} = 1337 K

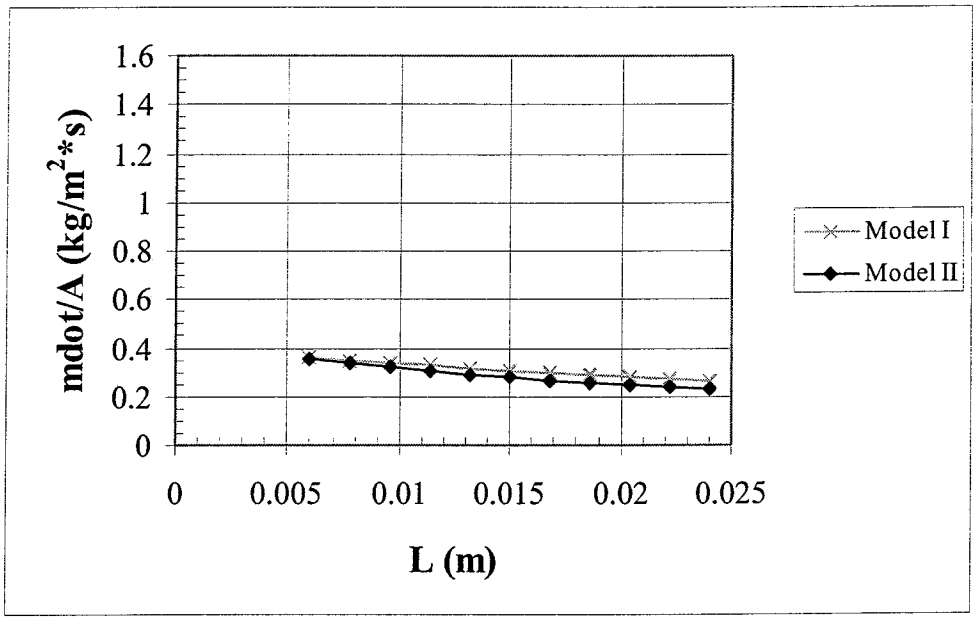

(d) Titanium
T_{crit} = 1464 K

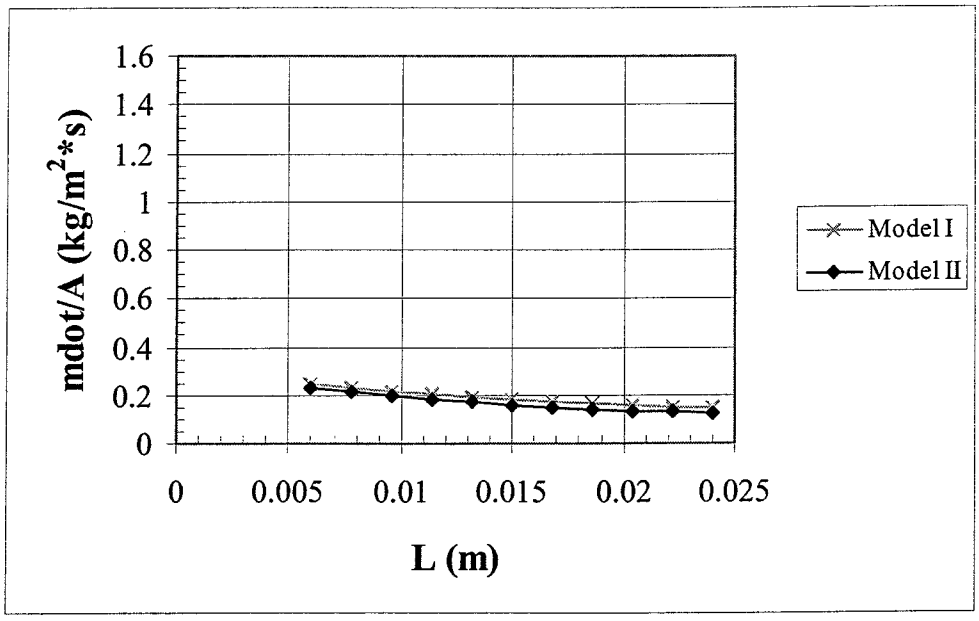

(e) Tungsten
T_{crit} = 2745 K

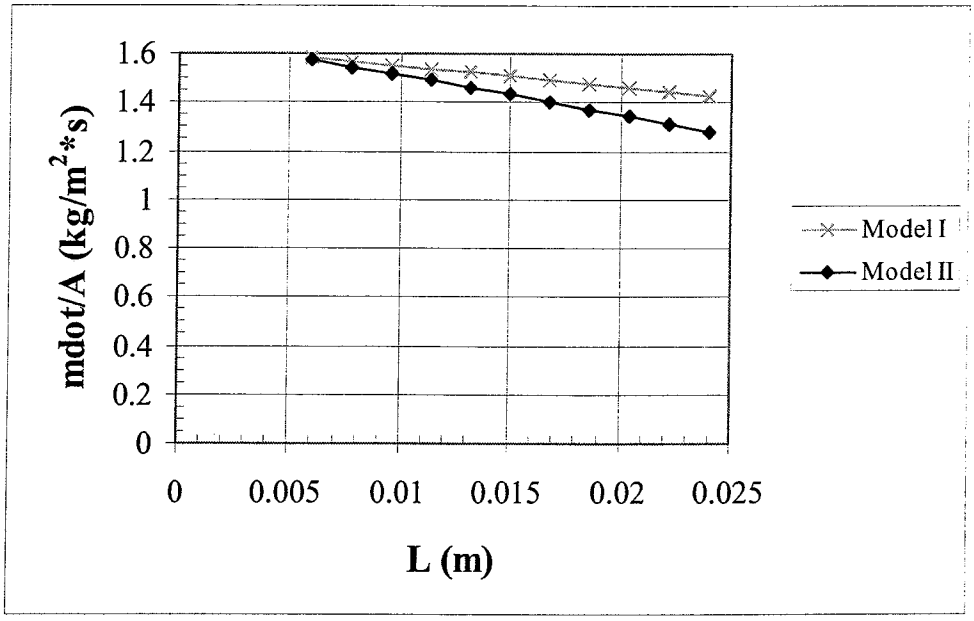

(f) Niobium Carbide
T_{crit} = 2917 K

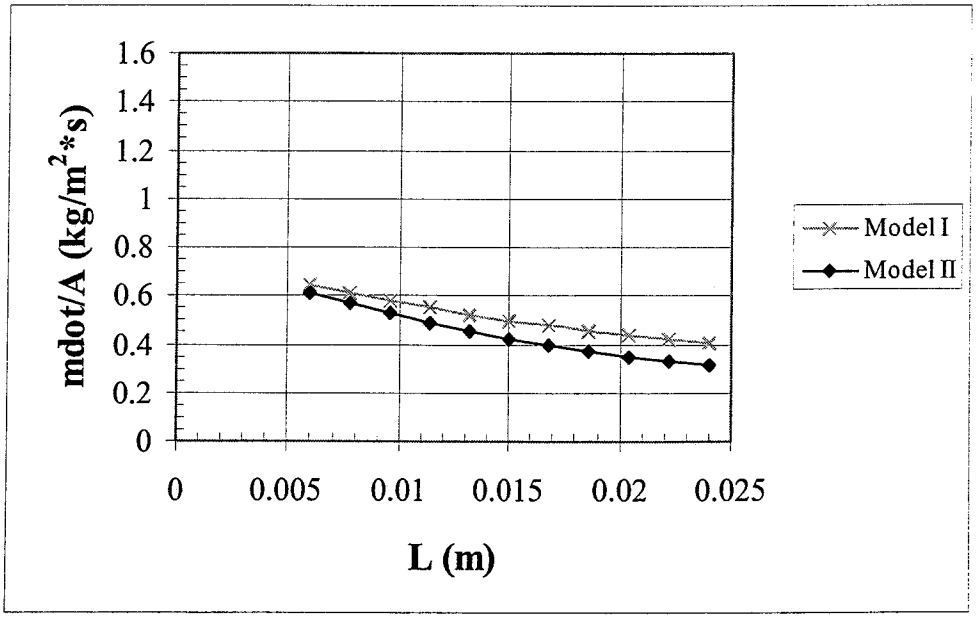

Figure H2. Mass Flow Rate Per Unit Area for Models I and II as a Function of Channel Diameter

(a) Aluminum
T_{crit} = 641 K

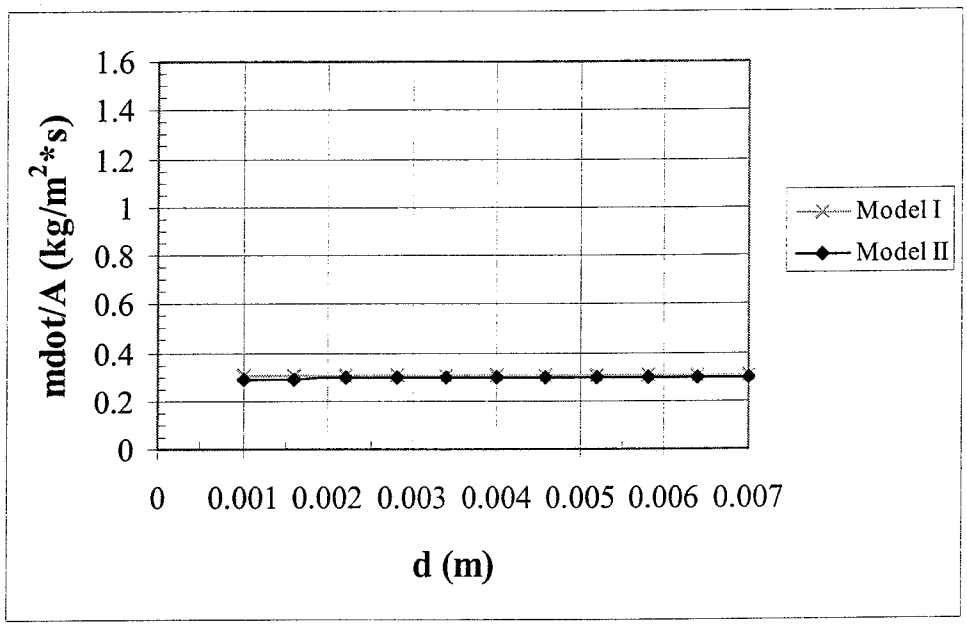

(b) Copper
T_{crit} = 1016 K

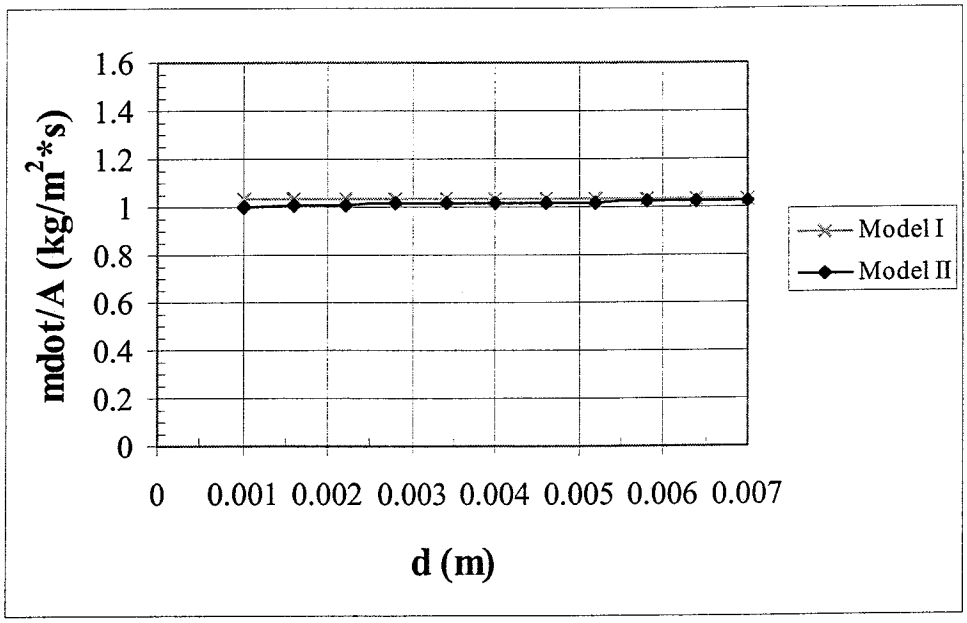

(c) Steel
T_{crit} = 1337 K

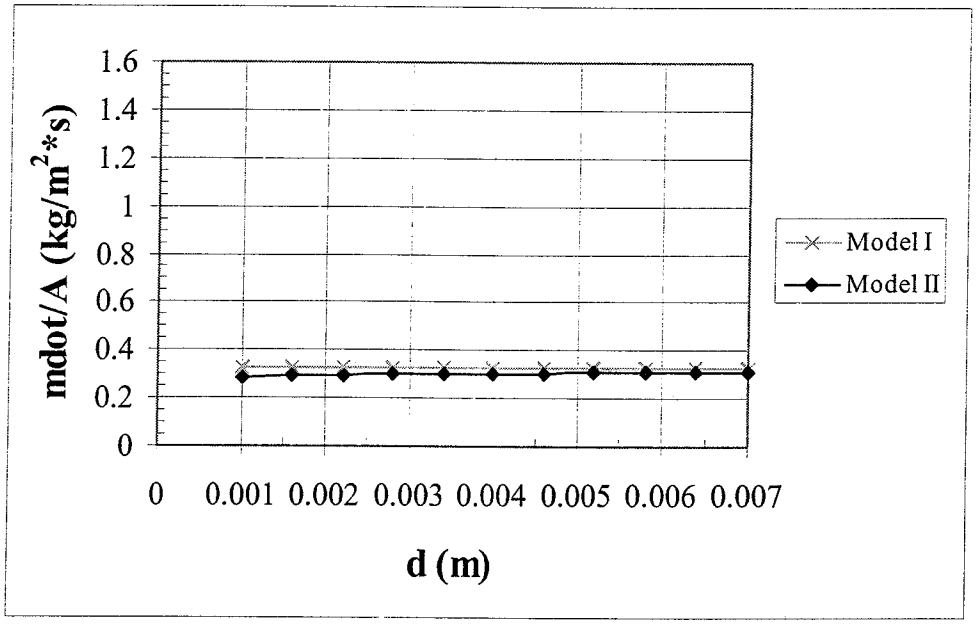

(d) Titanium
T_{crit} = 1464 K

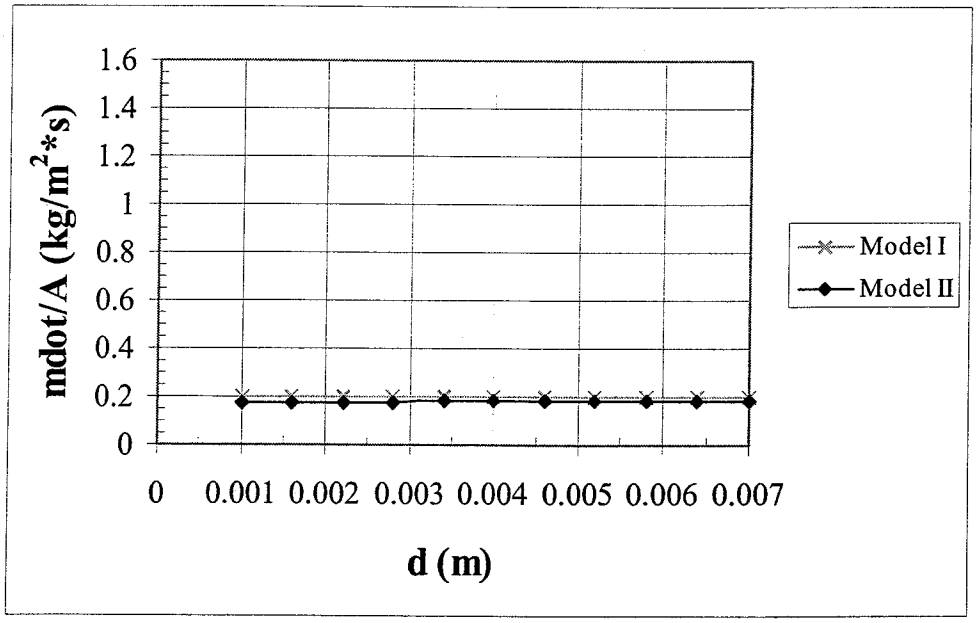

(e) Tungsten
T_{crit} = 2745 K

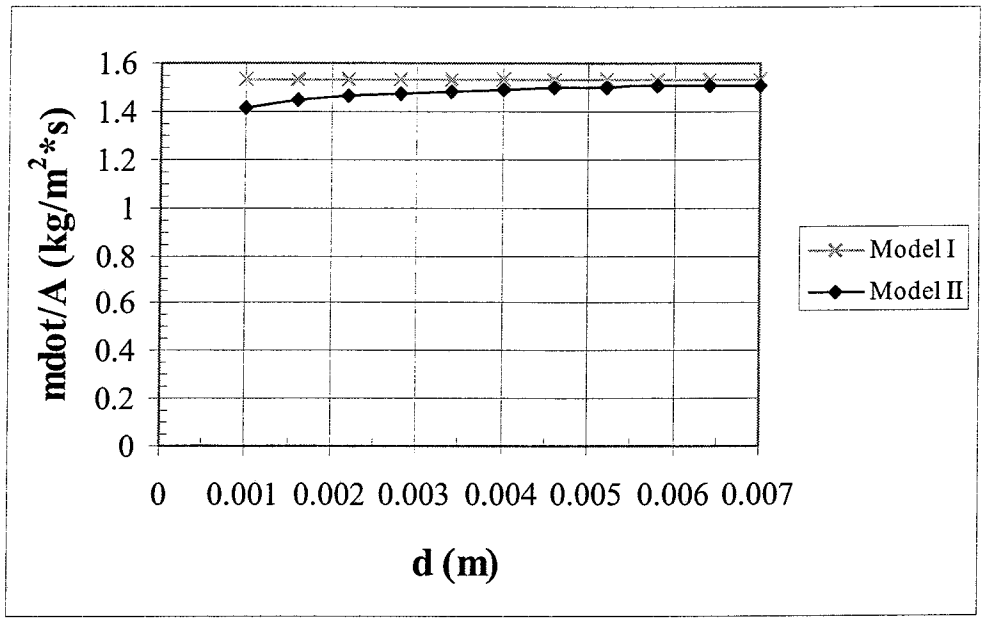

(f) Niobium Carbide
T_{crit} = 2917 K

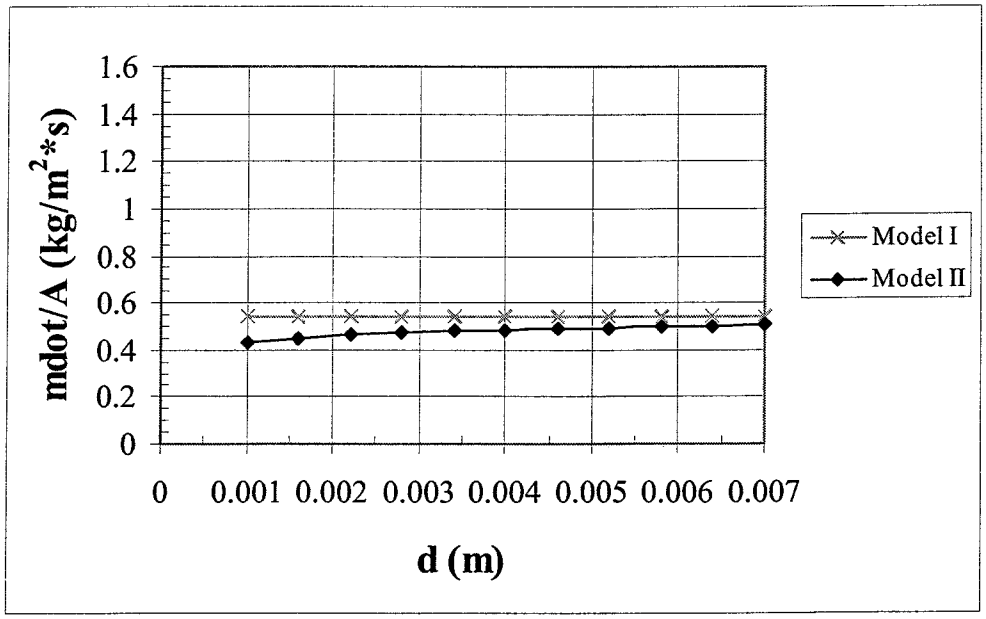

Figure H3. Mass Flow Rate Per Unit Area for Models I and II as a Function of Convection Heat Transfer Coefficient

(a) Aluminum
T_{crit} = 641 K

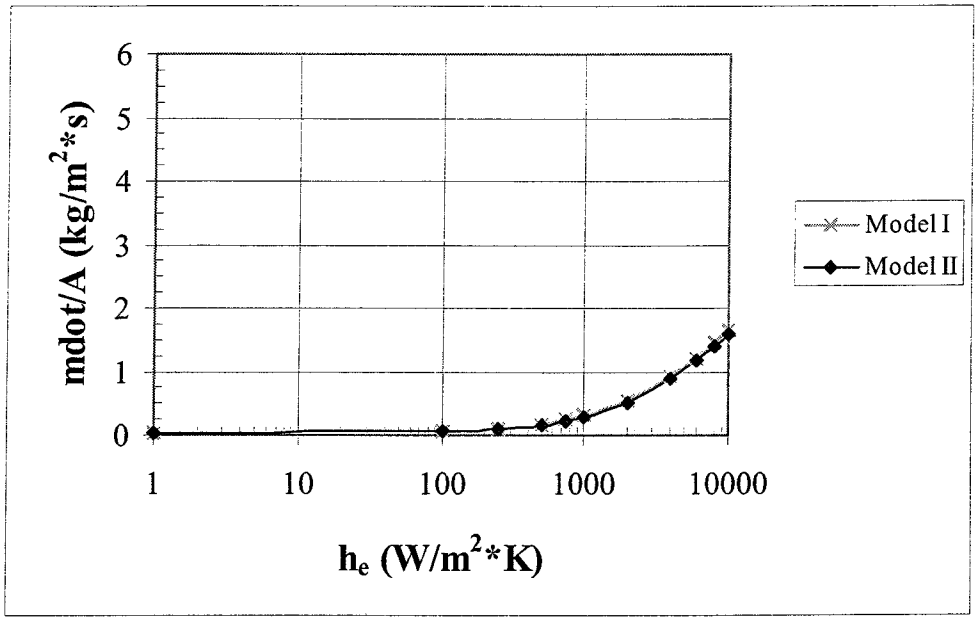

(b) Copper
T_{crit} = 1016 K

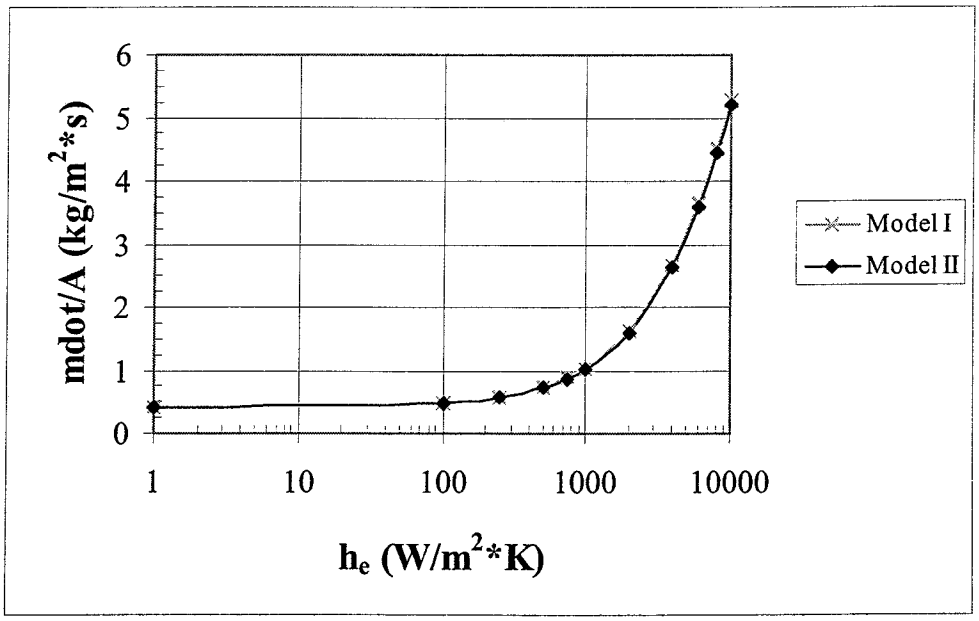

(c) Steel
T_{crit} = 1337 K

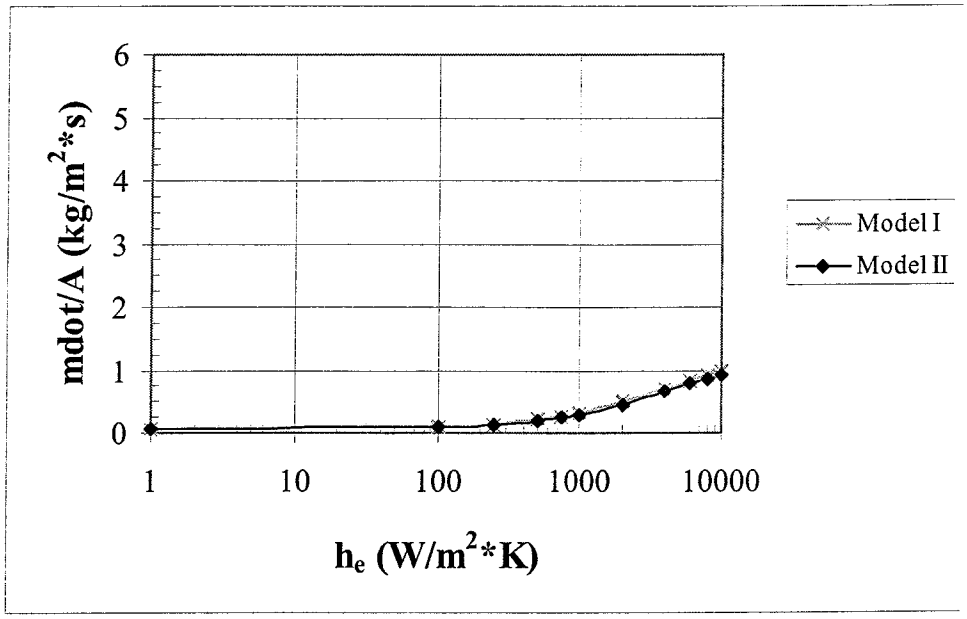

(d) Titanium
T_{crit} = 1464 K

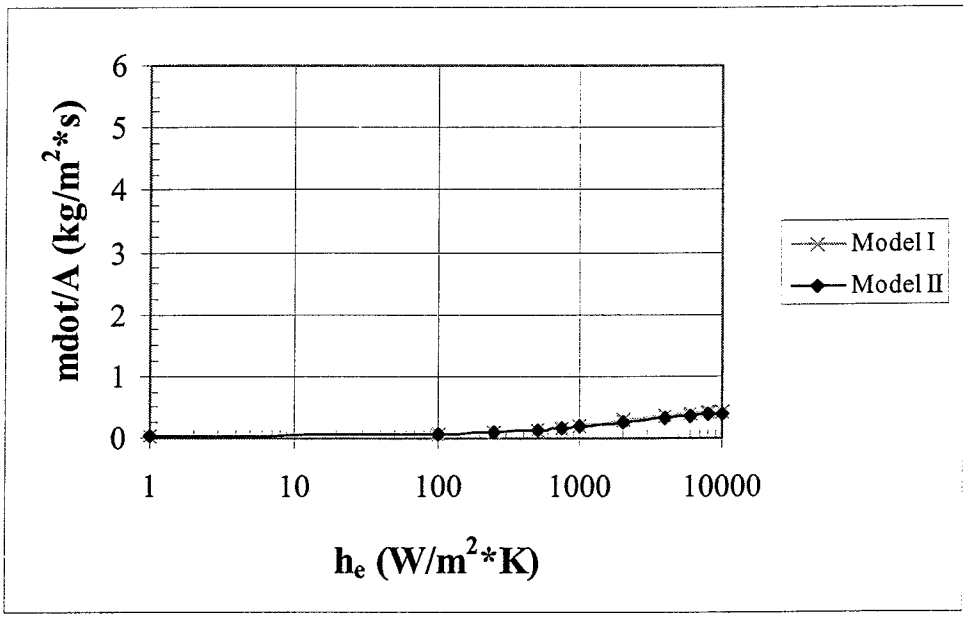

(e) Tungsten
T_{crit} = 2745 K

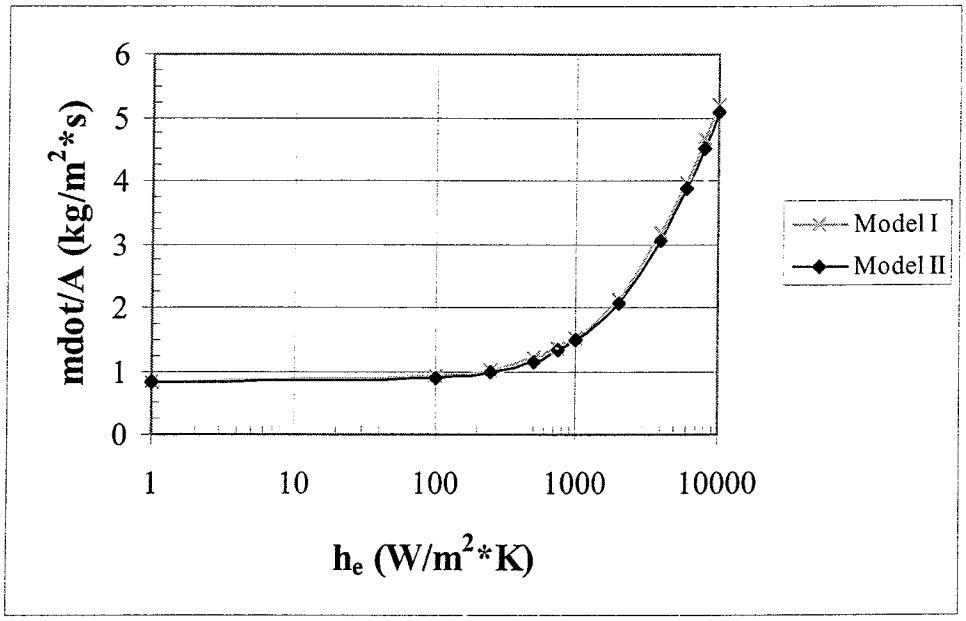

(f) Niobium Carbide
T_{crit} = 2917 K

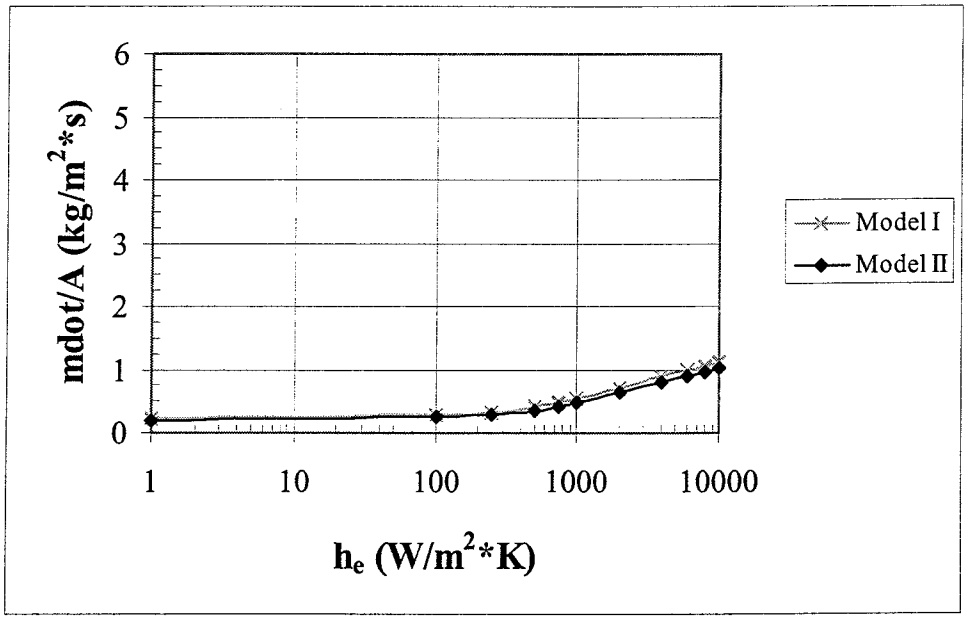

APPENDIX I

COMPUTER PROGRAM DOCUMENTATION

The analytical models have been solved using a computer routine. The source code was developed and programmed in FORTRAN, and is divided into three files: `MAIN.FOR`, `DEC_VAR.INC`, and `INPUT.DAT`. The `MAIN.FOR` file is the program driver. The `DEC_VAR.INC` file contains all of the variable declarations. The `INPUT.DAT` file is the descriptive input deck for the models, and can be adjusted using any text editor.

The `MAIN.FOR` and `DEC_VAR.INC` files have been compiled into an executable file, `DTCTPS.EXE`. This file can be executed either from a Windows environment or from MS-DOS. The `DTCTPS.EXE` file must be located in the same directory as the `INPUT.DAT` file. The program output will be to the screen, and contains both the relevant characteristic input data and the respective Model results. A data output file can be created by using the following command from an MS-DOS prompt: `DTCTPS > OUTPUT.OUT`.

In order to solve Model I and II, a secant iteration scheme was used. Each secant iteration requires two initial guesses that can either be bounded or unbounded, and a numerical convergence criterion. All of these parameters are accessible in the `INPUT.DAT` file. Model II requires extra care in setting the initial guesses, as it has a highly non-linear iterative solution procedure. The default initial values of `xL_2`, `xR_2`, `xL_3`, and `xR_3` should handle most all input conditions, however, they may need to be adjusted for the Model II solution to converge. The need for such adjustments may be indicated by infinite run-times and dubious results. In these situations, either decrease the convergence criteria or define more accurate initial guesses.

All files are presented as follows:

```
      PROGRAM DTCTPS

*=====================================================================*
*=====================================================================*
*  Design of Transpiration Cooled Thermal Protection Systems          *
*  NASA Stennis Space Center                                          *
*---------------------------------------------------------------------*
*  E. Eugene Callens, Jr. & Robert F. Vinet                           *
*  Louisiana Tech University                                          *
*  Ruston, Louisiana                                                  *
*---------------------------------------------------------------------*
*  March 1999                                                         *
*=====================================================================*
*=====================================================================*

c  Variables
      IMPLICIT NONE
      INCLUDE 'DEC_VAR.INC'

c  Equations
      DOUBLE PRECISION EQ1, EQ2
      EXTERNAL EQ1, EQ2

c  Input
      NAMELIST /MISC/ sigma, epsilon, hfg, Cp_liquid, Cp_vapor, Tboil,
     $                Tinitial, Tbf, Te_r, Te_h, hbar_e
      NAMELIST /MATERIAL/ MatName, kw, L
      NAMELIST /MODEL2_ONLY/ hbar_v, P, Aw
      NAMELIST /ITER_PAR/ EPS_1, xL_1, xR_1, EPS_2, xL_2, xR_2,
     $                    EPS_3, xL_3, xR_3
      OPEN (8, FILE = 'input.dat', FORM = 'FORMATTED')
      READ (8, MISC)
      READ (8, MATERIAL)
      READ (8, MODEL2_ONLY)
      READ (8, ITER_PAR)

**********************************************************************
*                          STEADY STATE MODEL I                      *
**********************************************************************

c  Call to the secant iteration to find value of Ts_1
      Falpha_1 = 0.0D0
      CALL SITER (EQ1, xL_1, xR_1, Falpha_1, EPS_1, RESULT_1)
      Ts_1 = RESULT_1

      mDOTperA_1 = ( kw*((Ts_1-Tbf)/L) ) *
     $             ( 1/(hfg + Cp_liquid*(Tboil-Tinitial)
     $             + Cp_vapor*(Tbf-Tboil)) )

**********************************************************************
*                          STEADY STATE MODEL II                     *
**********************************************************************

c  Call to the secant iteration to find value of alpha (& Beta_2)
      Falpha_2 = 0.0D0
      CALL SITER (EQ2, xL_2, xR_2, Falpha_2, EPS_2, RESULT_2)
      alpha = RESULT_2
```

```
      mDOTperA_2 = (Beta_2 * (kw * Tbf)) / (L * hfg)

*************************************************************************
*                          STEADY STATE MODEL III                       *
*************************************************************************

c  Set Ts at 20 K above Boiling Temp. at Stnd. Atm. Conditions
      Ts_3 = 393
      mDOTperA_3 =(((sigma*epsilon)*((Te_r**4)-(Ts_3**4))) + ( hbar_e *
     $            (Te_h-Ts_3))) * (1/(hfg+Cp_liquid*(Tboil-Tinitial)))

*************************************************************************
*                                OUTPUT                                 *
*************************************************************************

      WRITE(*,*) '*******************************************************'
      WRITE(*,*) '* ', MatName, '*'
      WRITE(*,*) '*                                                     *'
      WRITE(*,25) '*', 'kw      = ', kw,      'W/m*K',    '*'
      WRITE(*,27) '*', 'L       = ', L,       'm',        '*'
      WRITE(*,26) '*', 'Te_r    = ', Te_r,    'K',        '*'
      WRITE(*,26) '*', 'Te_h    = ', Te_h,    'K',        '*'
      WRITE(*,26) '*', 'Tbf     = ', Tbf,     'K',        '*'
      WRITE(*,28) '*', 'hbar_e  = ', hbar_e,  'W/m^2*K',  '*'
      WRITE(*,28) '*', 'hbar_v  = ', hbar_v,  'W/m^2*K',  '*'
      WRITE(*,27) '*', 'P       = ', P,       'm',        '*'
      WRITE(*,29) '*', 'Aw      = ', Aw,      'm^2',      '*'
      WRITE(*,*) '*-------------------------------------------------*'
      WRITE(*,32) '*', 'MODEL I  ', '*'
      WRITE(*,33) '*',    'Ts_I       = ', Ts_1,       'K',         '*'
      WRITE(*,34) '*',    'mdot/A_I   = ', mDOTperA_1, 'kg/m^2*s',  '*'
      WRITE(*,32) '*', 'MODEL II ', '*'
      WRITE(*,33) '*',    'Ts_II      = ', Ts_2,       'K',         '*'
      WRITE(*,33) '*',    'Tve_II     = ', Tve_2,      'K',         '*'
      WRITE(*,34) '*',    'mdot/A_II  = ', mDOTperA_2, 'kg/m^2*s',  '*'
      WRITE(*,32) '*', 'MODEL III', '*'
      WRITE(*,33) '*',    'Ts_III     = ', Ts_3,       'K',         '*'
      WRITE(*,34) '*',    'mdot/A_III = ', mDOTperA_3, 'kg/m^2*s',  '*'
      WRITE(*,*) '*******************************************************'

25    FORMAT (1X, A, 1X, A, F6.1, 1X, A, 29X, A)
26    FORMAT (1X, A, 1X, A, F6.1, 1X, A, 33X, A)
27    FORMAT (1X, A, 1X, A, F6.4, 1X, A, 33X, A)
28    FORMAT (1X, A, 1X, A, F7.1, 1X, A, 26X, A)
29    FORMAT (1X, A, 1X, A, F10.8, 1X, A, 27X, A)
32    FORMAT (1X, A, 1X, A, 41X, A)
33    FORMAT (1X, A, 14X, A, F6.1, 1X, A, 16X, A)
34    FORMAT (1X, A, 14X, A, F8.4, 1X, A, 7X, A)


      STOP
      END


*************************************************************************
*  EQUATION 1:  Steady State Model I of Ts equation (set equal to zero)*
*************************************************************************
      DOUBLE PRECISION FUNCTION EQ1(Ts_1)
      IMPLICIT NONE
      INCLUDE 'DEC_VAR.INC'
```

```
      EQ1 = (((sigma*epsilon*L)/kw)*((Te_r**4)-(Ts_1**4))) +
     $      ((hbar_e*L)/kw)*(Te_h - Ts_1) + Tbf - Ts_1

      END

************************************************************************
*    EQUATION 2:  Steady State Model II (iteration on alpha)           *
************************************************************************
      DOUBLE PRECISION FUNCTION EQ2(alpha_iter)
      IMPLICIT NONE
      INCLUDE 'DEC_VAR.INC'

c  Equations
      DOUBLE PRECISION EQ3
      EXTERNAL EQ3

      alpha = alpha_iter

C  Calculate values
      gamma = (hbar_v * P * (L**2)) / (kw * Aw)
      lambda2 = (-alpha + SQRT( (alpha**2)+4*gamma ) )  / 2
      lambda3 = (-alpha - SQRT( (alpha**2)+4*gamma ) )  / 2

c  Call to the secant iteration to find value of QL2
      Falpha_3 = 0.0D0
      CALL SITER (EQ3, xL_3, xR_3, Falpha_3, EPS_3, RESULT_3)
      QL2 = RESULT_3

      Tve_2 = (C1 + ( (alpha/(alpha+lambda2)) * C2*EXP(lambda2) )
     $      + ( (alpha/(alpha+lambda3)) * C3*EXP(lambda3) )) * Tbf
      Hbf = (hfg + Cp_liquid*Tbf*((Tboil/Tbf) - (Tinitial/Tbf)))/hfg
      Hv_2 = (Cp_vapor*Tbf*((Tve_2/Tbf) - (Tboil/Tbf)))/hfg
      Beta_2 = QL2/(Hbf+Hv_2)

      EQ2 = ((gamma/alpha) * (hfg/(Cp_vapor*Tbf))) - Beta_2

      END

************************************************************************
*    EQUATION 3:  Steady State Model II (iteration on QL2)             *
************************************************************************
      DOUBLE PRECISION FUNCTION EQ3(QL2_iter)
      IMPLICIT NONE
      INCLUDE 'DEC_VAR.INC'

      QL2 = QL2_iter

c  Calculate values
      C3 = ((alpha+lambda3)*QL2)
     $        / (lambda3*(EXP(lambda3)*(alpha+lambda3)
     $          - EXP(lambda2)*(alpha+lambda2) ) )
      C2 = -C3*((lambda3*(alpha+lambda2))
     $        / (lambda2*(alpha+lambda3)))
      C1 = 1 - C2 - C3

      Ts_2 = (C1 + C2*EXP(lambda2) + C3*EXP(lambda3)) * Tbf

      EQ3 = ((sigma * epsilon * L * (Tbf**3))/kw)*( (Te_r/Tbf)**4
     $      - (Ts_2/Tbf)**4 ) + ((hbar_e * L)/kw) *((Te_h/Tbf)
     $      - (Ts_2/Tbf)) - QL2
```

```
      END

*****************************************************************************
*****************************************************************************
*                          S U B R O U T I N E S                            *
*****************************************************************************
*****************************************************************************
*****************************************************************************
*                                                                           *
*  Robert F. Vinet                                        23 March 1998     *
*___________________________________________________________________________*
*                                                                           *
*                       The Secant Iteration Function                       *
*                                                                           *
*****************************************************************************
*  This scheme uses the Secant Method Iteration for non-linear              *
*  equations as presented in Hoffman's book pg. 101. [Numerical             *
*  Methods for Engineers and Scientists, McGraw-Hill, 1992];                *
*  The two initial guesses can either be bounded or unbounded.              *
*                                                                           *
*---------------------------------------------------------------------------*
*  EQ1 ... EQn  :   adjust what equation is sent into the iterator          *
*                   in the main program                                     *
*  EPS          :   defines the convergence criterion for the               *
*                   independent variable                                    *
*  XL & XR      :   two initial guesses required                            *
*  FALPHA       :   sets value of f(x) to be solved; typically let          *
*                   FALPHA = 0                                              *
*  ------------------------------------------------------------------       *
*  XC           :   intermediate value of the independent variable;         *
*                   a function of the type of iterator used                 *
*  F            :   name of the function to be iterated                     *
*  FL, FR, FC   :   function evaluated at its respected ind. variable       *
*                                                                           *
*****************************************************************************
      SUBROUTINE SITER (F, XL, XR, FALPHA, EPS, RESULT)
      IMPLICIT NONE
      INTEGER COUNT
      DOUBLE PRECISION F, FALPHA, XL, XR, EPS, XC, FC, FL, FR, RESULT
      COUNT = 0
      FR = F(XR)
      FL = F(XL)
      XC = ((FALPHA*(XL-XR)) + (FL*XR) - (FR*XL))/(FL-FR)
      FC = F(XC)
10    IF (ABS(XL-XR) .LE. (2.0*EPS)) GO TO 100
          IF ((FC*FL) .GT. 0) THEN
              XR = XL
              FR = FL
              XL = XC
              FL = FC
          ELSE
              XR = XL
              FR = FL
              XL = XC
              FL = FC
          ENDIF
      XC = ((FALPHA*(XL-XR)) + (FL*XR) - (FR*XL))/(FL-FR)
      FC = F(XC)
      COUNT = COUNT + 1
      GOTO 10
```

```
C100    WRITE(7,*) 'Number of Iterations to Converge = ', COUNT
100     RESULT = ((FALPHA*(XL-XR)) + (FL*XR) - (FR*XL))/(FL-FR)
      RETURN
      END
```

```
c  Input Variables
c-----------------------------------------------------------------------
      DOUBLE PRECISION sigma, epsilon, hfg, Cp_liquid, Cp_vapor, Tboil
      DOUBLE PRECISION Tinitial, Tbf, Te_r, Te_h, hbar_e, kw, L, hbar_v
      DOUBLE PRECISION P, Aw
      CHARACTER*50 MatName

c  Output Variables
c-----------------------------------------------------------------------
      DOUBLE PRECISION Ts_1, Ts_2, Ts_3, mDOTperA_1, mDOTperA_2
      DOUBLE PRECISION mDOTperA_3, Tve_2

c  Intermediate & Working Variables
c-----------------------------------------------------------------------
      DOUBLE PRECISION EPS_1, xL_1, xR_1, Falpha_1, RESULT_1
      DOUBLE PRECISION EPS_2, xL_2, xR_2, Falpha_2, RESULT_2
      DOUBLE PRECISION EPS_3, xL_3, xR_3, Falpha_3, RESULT_3
      DOUBLE PRECISION gamma, lambda2, lambda3, alpha, QL2, C1, C2, C3
      DOUBLE PRECISION Hbf, Hv_2, Beta_2
      DOUBLE PRECISION alpha_iter, QL2_iter

c  Define Common Blocks
c-----------------------------------------------------------------------
      COMMON /MODEL2/ alpha, gamma, lambda2, lambda3, C1, C2, C3,
     $                Hbf, Hv_2, Beta_2, QL2,
     $                Ts_2, Tve_2

      COMMON /GENERAL/ sigma, epsilon, hfg, Cp_liquid, Cp_vapor, Tboil,
     $               Tinitial, Tbf, Te_r, Te_h, hbar_e,
     $               kw, L, hbar_v, P, Aw
      COMMON /ITER_VAL/ EPS_1, xL_1, xR_1, EPS_2, xL_2, xR_2, EPS_3,
     $                  xL_3, xR_3
```

```
  $MISC
sigma      = 5.67E-8
epsilon    = 1.D0
hfg        = 2257.E3
Cp_liquid  = 4217.D0
Cp_vapor   = 2060.D0
Tboil      = 373.D0
Tinitial   = 298.D0
Tbf        = 393.D0
Te_r       = 1148.D0
Te_h       = 1148.D0
hbar_e     = 1000
  $

  $MATERIAL
MatName    = 'Aluminum'
kw         = 155.8D0
L          = 0.012
  $

  $MODEL2_ONLY
hbar_v     = 300.D0
P          = 0.012
Aw         = 0.000036D0
  $

  $ITER_PAR
EPS_1      = 1D-5
xL_1       = 1.11111111D0
xR_1       = 9.99999999D0
EPS_2      = 1D-5
xL_2       = 0.00111111D0
xR_2       = 0.00999999D0
EPS_3      = 1D-5
xL_3       = 0.00111111D0
xR_3       = 0.00999999D0
  $


c  Define the Variables
c  ---------------------------------------------------------------------
c  sigma      - the Stefan-Boltzman Constant [W/m^2*K^4]
c  epsilon    - emissivity of the surface
c  hfg        - latent heat of vaporization [J/kg]
c  Cp_liquid - specific heat at constant pressure of the coolant liquid
c               [J/kg*K]
c  Cp_vapor   - specific heat at constant pressure of the coolant vapor
c               [J/kg*K]
c  Tboil      - boiling temperature of the coolant fluid [K]
c  Tinitial   - initial temperature of the coolant fluid [K]
c  Tbf        - backface temperature of the wall [K]
c  Te_r       - radiative temperature of environment [K]
c  Te_h       - equivalent temperature of environment due to convection
c               [K]
c  hbar_e     - convection heat transfer coefficient of environment
c               [W/m^2*K]
c  MatName    - text description of material [characters <= 50]
c  kw         - thermal conductivity of wall material [W/m*K]
c  L          - thickness of wall [m]
```

```
c  hbar_v     - convection heat transfer coefficient of vapor [W/m^2*K]
c  P          - perimeter of one channel [m]
c  Aw         - area of one node of channel and surrounding wall [m^2]
c  EPS_1      - convergence criterion supporting surface temperature
c               iteration in Model I
c  xL_1       - initial iteration guess supporting surface temperature
c               in Model I
c  xR_1       - initial iteration guess supporting surface temperature
c               in Model I
c  EPS_2      - convergence criterion supporting alpha iteration in
c               Model II
c  xL_2       - initial iteration guess supporting alpha iteration in
c               Model II
c  xR_2       - initial iteration guess supporting alpha iteration in
c               Model II
c  EPS_3      - convergence criterion supporting QL2 iteration in
c               Model II
c  xL_3       - initial iteration guess supporting QL2 iteration in
c               Model II
c  xR_3       - initial iteration guess supporting QL2 iteration in
c               Model II
```

```
*****************************************************
* Aluminum                                          *
*                                                   *
* kw      =  155.8 W/m*K                            *
* L       =  .0120 m                                *
* Te_r    = 1148.0 K                                *
* Te_h    = 1148.0 K                                *
* Tbf     =  393.0 K                                *
* hbar_e  =  1000.0 W/m^2*K                         *
* hbar_v  =   300.0 W/m^2*K                         *
* P       =  .0120 m                                *
* Aw      =  .00003600 m^2                          *
*---------------------------------------------------*
* MODEL I                                           *
*               Ts_I        =  453.9 K              *
*               mdot/A_I    =    .3022 kg/m^2*s     *
* MODEL II                                          *
*               Ts_II       =  453.0 K              *
*               Tve_II      =  426.7 K              *
*               mdot/A_II   =    .2948 kg/m^2*s     *
* MODEL III                                         *
*               Ts_III      =  393.0 K              *
*               mdot/A_III  =    .3311 kg/m^2*s     *
*****************************************************
```

REPORT DOCUMENTION PAGE

Form Approved
OMB No. 0704-0188

Public reporting burden for this collection of information is estimated to average 1 hour per response, including the time for reviewing instructions, searching existing data sources, gathering and maintaining the data needed, and completing and reviewing the collection of information. Send comments regarding this burden estimate or any other aspect of this collection of information, including suggestions for reducing this burden, to Washington Headquarters Services, Directorate for Information Operations and Reports, 1215 Jefferson Davis Highway, Suite 1204, Arlington, VA 22202-4302, and to the Office of Management and Budget, Paperwork Reduction Project (0704-0188), Washington, DC 20503.

1. AGENCY USE ONLY *(Leave blank)*	2. REPORT DATE	3. REPORT TYPE AND DATES COVERED
	March 1999	Fi nal Contractor Report

4. TITLE AND SUBTITLE

DESIGN OF TRANSPIRATION COOLED THERMAL PROTECTION SYSTEMS

5. FUNDING NUMBERS

Contract No. 32-4136-58019
NAS13-580 DO 15

6. AUTHOR(S)

E. Eugene Callens, Jr. & Robert F. Vinet

7. PERFORMING ORGANIZATION NAME(S) AND ADDRESS(ES)

Mechanical Engineering
Louisiana Tech University
P.O. box 10348
Ruston, LA 71272-0046

8. PERFORMING ORGANIZATION REPORT NUMBER

9. SPONSORING/MONITORING AGENCY NAME(S) AND ADDRESS(ES)

NASA
John C. Stennis Space Center
Building 1100, Code VA34
Stennis Space Center, MS 39529-6000

10. SPONSORING/MONITORING AGENCY REPORT NUMBER

SE-1999-03-00012-SSC

11. SUPPLEMENTARY NOTES

12a. DISTRIBUTION/AVAILABILITY STATEMENT

Publicly Available

12b. DISTRIBUTION CODE

13. ABSTRACT ***(Maximum 200 words)***

This study explored three approaches for the utilization of transpiration cooling in thermal protection systems. One model uses an impermeable wall with boiling water heat transfer at the backface (Model I). A second model uses a permeable wall with a boiling water backface and additional heat transfer to the water vapor as it flows in channels toward the exposed surface (Model II). The third model also uses a permeable wall, but maintains a boiling condition at the exposed surface of the material (Model III). The governing equations for the models were developed in non-dimensional form and a comprehensive parametric investigation of the effects of the independent variables on the important dependent variables was performed. In addition, detailed analyses were performed for selected materials to evaluate the practical limitations of the results of the parametric study.

14. SUBJECT TERMS

Thermal Protection, Transpiration Cooling

15. NUMBER OF PAGES

166

16. PRICE CODE

17. SECURITY CLASSIFICATION OF REPORT	18. SECURITY CLASSIFICATION OF THIS PAGE	19. SECURITY CLASSIFICATION OF ABSTRACT	20. LIMITATION OF ABSTRACT
UNCLASSIFIED	UNCLASSIFIED	UNCLASSIFIED	UNLIMITED